Design of Porous Boron Nitride Materials for Applications in Adsorption

by

Sofia Marchesini

A Thesis submitted in fulfilment of the requirements for the degree of Doctor of Philosophy and the Diploma of Imperial College London

Chemical Engineering Department

Imperial College London

September 2018

Abstract

Porous boron nitride (BN) recently emerged as a new class of adsorbent material with bond polarity and unprecedented high thermal and oxidative stabilities. These properties make BN an attractive adsorbent for use in a wide range of adsorption applications, especially those operating under extreme conditions. Yet, the number of studies on this fascinating material remain limited and its structure and chemistry still vastly unknown. A full understanding of its formation mechanisms, as well as control of its pore structure and chemistry, are necessary to exploit its full potential.

This thesis presents an in-depth investigation of the effects of synthesis conditions on the formation of porous BN and a detailed characterisation of the material. A novel synthesis method was developed for producing high surface area (>1900 m^2/g) porous BN with tuneable micro- and mesoporosity, without the use of templates, presenting opportunity for scalability. The shaping of porous BN powders into industrially relevant pellet morphologies was achieved with no significant detriment to the desirable textural properties of the material. A way to reduce the hydrolytic instability of porous BN is elucidated and samples with significantly higher water tolerance were produced. Finally, porous BN materials with various pore structures and chemistries were tested for a range of adsorption applications in gas, liquid and vapour phase, identifying adsorption mechanisms and outlining potential ways to improve adsorption performance. Overall, this thesis opens the door to the design and improvement of porous BN, establishing it as a promising adsorbent material.

Publications and Patent

S Marchesini, CM McGilvery, J Bailey, C Petit, “Template-free synthesis of highly porous boron nitride: insights into pore network design and impact on gas sorption” *ACS Nano*, 11 (2017): 10003–10011

RT Woodward, A Jobbe-Duval, S Marchesini, DB Anthony, C Petit, A Bismarck; "Hypercrosslinked polyHIPEs as precursors to designable, hierarchically porous carbon foams" *Polymer* 115 (2017): 146-53

S Marchesini, A Regoutz, D Payne, C Petit; “Tunable porous boron nitride: Investigating its formation and its application for gas adsorption” *Microporous and Mesoporous Materials* 243 (2017): 154-163

Patent: Porous Boron nitride, PCT Application No. PCT/GB2018/050686, filed: 16/05/2018

In preparation or submission:

S Marchesini, R Shankar, C Petit, “Enhancing the hydrolytic stability of porous boron nitride *via* the control of crystallinity, porosity and chemical composition”, Currently being reviewed by industrial partners

S Marchesini, W Xiyu, C Petit, “Adsorption of organics on porous BN materials with tuneable chemistries and pore structures”, In preparation

I hereby declare that this work is my own and that any published work was appropriately referenced.

The copyright of this thesis rests with the author. Unless otherwise indicated, its contents are licensed under a Creative Commons Attribution-Non Commercial 4.0 International Licence (CC BY-NC). Under this licence, you may copy and redistribute the material in any medium or format. You may also create and distribute modified versions of the work. This is on the condition that: you credit the author and do not use it, or any derivative works, for a commercial purpose. When reusing or sharing this work, ensure you make the licence terms clear to others by naming the licence and linking to the licence text. Where a work has been adapted, you should indicate that the work has been changed and describe those changes. Please seek permission from the copyright holder for uses of this work that are not included in this licence or permitted under UK Copyright Law.

Acknowledgements

I would like to express my deepest appreciation to my supervisor, Dr. Camille Petit, for all her help and supervision throughout these four years. Camille always provided prompt, extensive and constructive feedback, allowing me to develop my communication and research skills. She also encouraged me to participate in several national and international conferences and to apply for external funding, which allowed me to learn a lot and present my work to experts in my field. Camille also gave me the opportunity to supervise many undergraduate students, to design their experiments and train them, which taught me a lot. I would like to thank all the students for their help in the lab and all the time spent together!

I would also like to thank my industrial supervisor, Dr. Leslie Bolton from BP and my second supervisor, Dr. Matthew Blunt from University College London. They both provided invaluable feedback and technical suggestions and were always extremely supportive.

I would like to acknowledge the funding and technical support from BP through the BP International Centre for Advanced Materials (BP-ICAM), which made this research possible. BP also allowed me to spend 3 weeks in Hull, hosting me at the Saltend Chemical Park, where I tested some of the materials previously produced for different applications. I would like to thank everyone who helped me with the experiments while I was there. I would also like to acknowledge EPSRC for the funding through the CDT in Advanced Characterisation of Materials (CDT-ACM), which gave me the opportunity to participate in many courses for professional and personal development. I would like to express my gratitude to the CDT-ACM directors, Dr. Neil Curson and Prof. Stephen Skinner, for their technical and pastoral support.

I would also like to acknowledge Dr. Catriona McGilvery, Josh Bailey, Ravi Shankar, Dr. Anna Regoutz and Angus Crake for their help in collecting and analysing results, some of which resulted in peer-reviewed publications.

Some special thanks go to all my friends who supported me throughout these four years, the members of the Petit group, the CDT-ACM group and the other friends from Imperial (thank you Moon group). A special thanks to Rob, who made my PhD experience a lot easier.

Finally, grazie alla mia famiglia; thanks to my family who was extremely supportive and always present, although from another country. This achievement would not have been possible without your encouragement and immense support.

Abbreviations

BN	Boron Nitride
BET	Brunauer-Emmett-Teller
1/2/3-D	One/Two/Three-dimensional
MOFs	Metal Organic Frameworks
COFs	Covalent Organic Frameworks
MOPs	Microporous Organic Polymers
h-BN	Hexagonal Boron Nitride
r-BN	Rhombohedral Boron Nitride
c-BN	Cubic Boron Nitride
w-BN	Wurtzite Boron Nitride
t-BN	Turbostratic Boron Nitride
a-BN	Amorphous Boron Nitride
BNNSs	Boron Nitride Nanosheets
DMF	N,N-Dimethylformamide
NMP	*N*-Methyl-2-Pyrrolidone
IPA	Isopropanol
CVD	Chemical Vapour Deposition
AB	Ammonia Borane
MAB	Tri(methylamino)borazine
CTAB	Cetyl-Trimethylammonium Bromide
P123	Poly(ethylene glycol)-block-poly(propylene glycol)-block-poly(ethylene glycol)
DTAC	D-trimethyl ammonium chloride
BCN	Boron Carbon Nitride
SEM	Scanning Electron Microscopy
SE	Secondary Electrons
BE	Backscattered Electrons
XRD	X-Ray Diffraction
TEM	Transmission Electron Microscopy

FFT	Fast Fourier Transform
STEM	Scanning Transmission Electron Microscopy
BF	Bright Field
DF	Dark Field
DFT	Density Functional Theory
EDX	Energy dispersive X-ray spectroscopy
WDX	Wavelength Dispersive X-ray spectroscopy
HAADF	High Angle Annular Dark Field
ATR	Attenuated Total Reflectance
XPS	X-ray Photoelectron Spectroscopy
FTIR	Fast Fourier Transform
TGA	Thermo Gravimetric Analysis
MS	Mass Spectroscopy
RhB	Rhodamine B
MO	Methyl Orange

Table of Contents

Abstract 2
Publications and Patent 3
Acknowledgements 6
Abbreviations 8
Table of Contents 10
List of Figures 15
List of Tables 21
Thesis Outline 22
Motivation 22
Thesis Content 23
Chapter 1: Literature Review 24
1.1 Adsorption theory 24
1.2 Adsorbent materials 25
1.3 Boron nitride 27
1.4 Synthesis methods leading to high surface area BN materials 30
1.5 Top-down synthesis methods 31
1.5.1 Mechanical exfoliation 31
1.5.1.1 Scotch-tape 31
1.5.1.2 Ball-milling 31
1.5.1.3 Other mechanical devices 31
1.5.2 Combination of sonication and chemical methods 32
1.5.3 Exfoliation via chemical functionalization 33
1.5.4 Exfoliation in acids and molten hydroxides without sonication 34
1.5.5 Thermal method 34
1.5.6 Gas exfoliation 35
1.5.7 Boron nitride nanotube unwrapping 35
1.6 Bottom-up methods 36
1.6.1 Chemical blowing technique 36
1.6.2 Chemical vapour deposition 36
1.6.3 High temperature syntheses with the use of templates 37

1.6.3.1 Hard templates 37
1.6.3.2 Structure directing templates 38
1.6.4 Solvo-thermal reactions 38
1.6.5 Template-free high temperature reactions 39
1.7 3D BN 42
1.7.1 3D BN deriving from top-down methods 42
1.7.2 3D BN deriving from bottom-up methods 42
1.8 BN water stability 43
1.9 Applications of porous BN 44
1.9.1 Gas sorption 44
1.9.2 Water cleaning 52
1.9.3 Catalyst or catalyst support 63
1.10 Conclusions and knowledge gaps from the literature 63
1.11 Research aim and objectives 64
1.11.1 Objective 1: To produce porous BN materials with high surface area and tuneable porosity 64
1.11.2 Objective 2: To evaluate and improve BN robustness and recyclability 65
1.11.3 Objective 3: To test BN for different adsorption applications 65
Chapter 2: Methods 66
2.1 Porous BN powder synthesis 66
2.2 Porous BN pellet preparation 67
2.3 Characterisation techniques 67
2.3.1 Structure 67
2.3.1.1 Pore structure and surface area: Nitrogen sorption isotherms at -196 ºC 67
2.3.1.2 Micro/nano-scale morphology: SEM 69
2.3.1.3 Crystalline structure: X-ray diffraction 70
2.3.1.4 Nano-scale morphology and crystalline structure: Transmission electron microscopy 72
2.3.1.5 3D imaging: Scanning TEM tomography 73
2.3.2 Chemistry 74
2.3.2.1 Surface chemistry: X-ray photoelectron spectroscopy 74
2.3.2.2 Bulk chemistry: Fourier transform infrared spectroscopy 75
2.3.2.3 Thermal decomposition: thermogravimetric analysis 75
Chapter 3: Understanding the Synthesis of Porous BN and its Controlling Parameters 76

3.1 Introduction 76
3.2 Materials synthesis 77
3.2.1 Study of the effect of precursor type and molar ratio on porous BN 77
3.2.2 Study of the effect of intermediate preparation on porous BN 78
3.2.3 Study of the effect of temperature on porous BN 79
3.2.4 Study of the effect of ramp rate on porous BN 80
3.3 Effect of precursor type and molar ratio on porous BN structure and chemistry 80
3.3.1 Analysis of chemical features 80
3.3.2 Analysis of structural features and morphology 81
3.4 Effect of intermediate preparation on porous BN structure and chemistry 84
3.4.1 Porous BN synthesised from urea and boric acid precursors 84
3.4.1.1 Analysis of chemical features of BN 84
3.4.1.2 Analysis of structural features and morphology of BN 86
3.4.1.3 Analysis of chemical features of intermediates 88
3.4.1.4 Analysis of crystalline structure and thermal decomposition of intermediates 89
3.4.1.5 Analysis of chemical and structural features of side-product of reaction ..95
3.4.2 Porous BN synthesised from melamine and boric acid precursors 95
3.4.2.1 Analysis of pore structure of BN 96
3.4.2.2 Analysis of chemical and structural features of intermediates 97
3.5 Effect of synthesis temperature on porous BN structure and chemistry 98
3.5.1 Analysis of structural features of BN 98
3.5.1.1 Analysis of chemical features of BN 99
3.6 Effect of ramp rate on porous BN structure and chemistry 100
3.7 Conclusions 101
Chapter 4: Tuning Porous BN Surface Area and Pore Structure 102
4.1 Introduction 102
4.2 Materials synthesis 103
4.2.1 Multiple N-precursor synthesis 103
4.2.2 Preparation of the reaction intermediates for the synthesis of single N-precursor BN 104
4.2.3 Preparation of the reaction intermediates for the synthesis of multiple N-precursors BN 104
4.2.4 Synthesis of porous BN using single or multiple N-precursors 105

4.2.5 Formation of pellets 105
4.3 Results and discussion 105
4.3.1 Structural properties and morphology 105
4.3.2 Chemical properties 113
4.3.3 Pelletisation of porous BN 115
4.4 Conclusions 116
Chapter 5: Evaluating and Enhancing Porous BN Hydrolytic Stability 117
5.1 Introduction 117
5.2 Materials synthesis 118
5.2.1 Preparation of the reaction intermediates for the synthesis of BN 118
5.2.2 Synthesis of porous BN using single or multiple N-precursors 118
5.3 Stability tests 119
5.3.1 Exposure to aqueous solutions 119
5.3.2 Exposure to moisture: Water vapour sorption 119
5.3.3 Exposure to organic solvents 119
5.3.4 Exposure to high temperature oxidising and non-oxidising environments 120
5.4 Results and discussion 120
5.4.1 Water stability evaluation 120
5.4.2 Water stability enhancement 125
5.4.2.1 High-synthesis temperature BN 125
5.4.2.2 Water stability evaluation for high temperature BN 129
5.4.3 Organic solvent stability evaluation 132
5.4.4 Thermal and oxidative stability evaluation 133
5.5 Conclusions 134
Chapter 6: Testing Porous BN for Gas and Liquid Separations 135
6.1 Introduction 135
6.2 Materials testing 136
6.2.1 Gas sorption 137
6.2.1.1 Low pressure gas sorption 137
6.2.1.2 High pressure gas sorption 137
6.2.1.3 Heat of adsorption calculation 138
6.2.1.4 Temperature swing adsorption 138
6.2.2 Organic vapour sorption 139
6.2.3 Dye sorption 139

6.2.4 Oil spills cleanup 140
6.3 Results and discussion 140
6.3.1 Gas sorption 140
6.3.1.1 Low pressure gas sorption 140
6.3.1.2 High pressure gas sorption and heat of adsorption 141
6.3.2 Organic vapour sorption 143
6.3.3 Water cleaning 146
6.3.3.1 Dye sorption 146
6.3.3.2 Oil spills cleanup 150
6.4 Conclusions 151
Chapter 7: Conclusions and Future Plans 153
7.1 Findings and achievements 153
7.2 Future plans 154
7.2.1 To produce stable BN materials via control of structure and chemistry 154
7.2.2 To structure porous BN into valuable products. 154
7.2.3 To scale-up the synthesis of porous BN 155
References 156
Appendix 1 168
Appendix 2 171
Appendix 3 173
Exposure to water via sonication and full evaporation 173
Low temperature BN after humidity exposure 174
High temperature BN 177
High temperature BN after humidity exposure 179
High temperature BN after water exposure 180
Appendix 4 181
Rights and Permissions 184

List of Figures

Figure 1-1 Boron nitride allotropes classified based on their hybridisation state and on their dimensionality. 27
Figure 1-2 (a) h-BN or few-layer BNNSs with unit cell and dimensions; (b) Stone-Wales defects; (c) vacancies (V indicates vacancies, N refers to nitrogen vacancies and B to boron vacancies; the numbers indicate the amount of boron or nitrogen vacancies). 29
Figure 1-3 (a) Amorphous BN; (b) Turbostratic BN structure composed of h-BN layers randomly stacked on top of each other with larger d-spacing compared to h-BN; 29
Figure 1-4 Schematic representation of 2D h-BN sheets forming a 3D h-BN graphitic material with low surface area; BNNSs composed of less than 10 h-BN layers (L) and exhibiting high surface area; t-BN composed of h-BN layers lacking of stacking order and with the presence of a large amount of pores. 30
Figure 1-5 Gas exfoliation of h-BN into BNNSs.[64] 35
Figure 1-6 Templating method to produce mesoporous BN from zeolite template.[72] 37
Figure 1-7 3D BN foams and monoliths prepared *via* (a)[98] top-down and (b,[102] c[103]) bottom-up methods. 43
Figure 2-1 Schematic of tubular furnace set-up with flow meter and bubblers. 66
Figure 2-2 X-ray diffraction principle with Bragg's equation. 71
Figure 2-3 Crystalline structure with the different d-spacings for crystalline h-BN materials. (Unit cell dimensions from [97]) 72
Figure 2-4 Schematic for the principles of XPS analysis with equation. 74
Figure 3-1 Synthesis schematic for porous BN samples prepared from different nitrogen and boron precursors. 78
Figure 3-2 (a) FTIR spectra and (b) images of BN samples produced using different precursors and diverse molar ratios. 81
Figure 3-3 (a) XRD patterns for all samples and (b) Nitrogen sorption isotherms at -196 °C for the purest porous BN samples, as determined by chemical analysis (open symbols represent desorption),(c) pore size distributions and (d) textural parameters derived from nitrogen gas sorption analysis. Error bars represent standard deviation calculated from 3 repeats. 82

Figure 3-4 SEM images for porous BN sample:(a) BN-U5, (b) BN-M0.5, (c,d) BN-U50. (e) TEM images for BN-U5 and (f) BN-U50. 83
Figure 3-5 (a) typical FTIR spectrum for a porous BN sample (BN-U5-phys mix); (b) proposed representative structure of BNNS (from porous BN); (c-e) XPS high resolution fitted core level spectra for N 1*s*, B 1*s* and O 1*s* for a typical BN sample (BN-U5-phys mix);(f) XPS relative atomic percentages for all porous BN samples. 85
Figure 3-6 (a) XRD patterns for porous BN samples; (b) Nitrogen sorption isotherms at -196 °C (open symbols represent desorption);(c) typical high-resolution TEM image for porous BN (BN-U5-phys mix);(d) SEM image for a typical porous BN sample (BN-U5-0). 87
Figure 3-7 FTIR spectra for urea and boric acid intermediates dried for different lengths of time, as well as precursors. 88
Figure 3-8 (a-d) High resolution core level XPS spectra for 2 intermediates and a physical mixture of urea and boric acid for (a) B *1s*,(b) N *1s*,(c) O *1s* and (d) C *1s*. Peak fitted high resolution core level XPS spectra of INT-U5-0 for (e) B *1s*, (f) N *1s*, (g) C *1s*, (h) O *1s*. 90
Figure 3-9 XRD patterns for all samples. The dotted lines represent values from reference patterns for urea [173]and boric acid[174] 91
Figure 3-10 TGA thermal decomposition curves under nitrogen gas flow for precursors and intermediates for urea and boric acid. 92
Figure 3-11 Mass spectroscopy data deriving from thermal decomposition or urea and boric acid intermediates under nitrogen gas flow. 93
Figure 3-12 (a, b)XPS high resolution core level spectra with peak fitting for B 1*s* and N 1*s* for intermediates deriving from urea and boric acid mixtures,(c,d) intermediates treated at 250 ℃ under nitrogen,(e,f) porous BN derived from the same intermediate treated at 1050 ℃ under nitrogen. 94
Figure 3-13 (a) XRD pattern and (b) FTIR spectrum for outlet side-powder produced during BN synthesis. 95
Figure 3-14 Nitrogen sorption isotherms at -196 °C for samples prepared with and without dissolution of the precursors (open symbols represent desorption). 96
Figure 3-15 (a) FTIR spectra and (b) XRD patterns for melamine and boric acid precursors and intermediates. 97
Figure 3-16 (a) N_2 sorption isotherms and (b) textural parameters deriving from the same for BN-U5 samples treated at different temperatures. Three different batches of BN-U5 (~ 3 g each) were synthesised and mixed together before heat-treatment. 98

Figure 3-17 (a) XRD patterns and (b) d-spacing calculated from XRD patterns using Bragg's equation for BN-U5 samples treated at different temperatures. 99
Figure 3-18 Relative atomic percentages deriving from XPS analysis for porous BN (BN-U5) synthesised at 1050 ºC and post-treated at different temperatures under nitrogen. 99
Figure 3-19 (a)Nitrogen sorption isotherms at -196 °C for porous BN samples (BN-MU1:5) produced at different ramp rates; (b) average textural parameters (over > 3 repeats) deriving from nitrogen sorption analysis. 100
Figure 4-1 (a) Schematic of traditional single N-precursor synthesis and (b) the multiple N-precursor synthesis. 104
Figure 4-2 Typical XRD patterns for: (a) h-BN commercial powder and (c) porous BN (BN-U5 sample).Typical high resolution SEM images with FFT's diffraction patterns for: (b) exfoliated h-BN and (d) porous BN (BN-U5 sample). Scale bars in Figures (a, c) are 10 nm. 106
Figure 4-3 SEM images for all porous BN samples synthesised from single N precursors: (a) BN-M0.5;(b) BN-U5; (c) BN-B2; melamine-based multiple N-precursors: (d) BN-MU0.25:5; (e) BN-MU0.5:5; (f) BN-MU1:5; and urea-based multiple N-precursors: (g) BN-BU0.5:5;(h) BN-BU1:5; (i) BN-BU2:5;(j) BN-BU3:5; (k) BN-BU4:5; (l) BN-BU8:5. Scale bar represent 800 nm. 107
Figure 4-4 STEM images in bright field mode collected for single N-precursor BN: (a-c) BN-U5 and multiple N-precursor: (d-f) BN-MU1:5. The particles in Figures a and d were used for the tomography reconstruction. 108
Figure 4-5 (a, d) Images of mesoporosity in boron nitride samples collected with dark field STEM images: (a) a single N-precursor (*i.e.* urea, BN-U5 sample); (d) multiple N-precursor (*i.e.* urea and melamine, BN-MU1:5 sample). (b, e) 3D tomography reconstructions of the 2 samples; (c, f) 3D reconstructions of the pores. Scale bars represent 100 nm. 109
Figure 4-6 Tunable micro- and mesoporosity of boron nitride: (a, c) N_2 sorption isotherms measured at -196 °C for the BN samples synthesised from: (a) urea, biuret and boric acid mixtures and (c) urea, melamine and boric acid mixtures, all showing a gradual increase in the gas uptake and therefore porosity as more of the secondary N-precursor is added (open symbols represent desorption). (b, d) Bar plots showing the BET equivalent surface areas, total volume of pores, micropore and mesopore volume for samples synthesised from: (b) urea, biuret and boric acid mixtures as well as (d) urea, melamine and boric acid mixtures, exhibiting a gradual microporosity enhancement as more of the additional N-precursor is added (error bars represent standard deviations calculated from at least 3 repeats). 111

Figure 4-7 (a) TGA thermal decomposition patterns under nitrogen for different precursors and (b) precursors mixtures. 113
Figure 4-8 FTIR spectra for all porous BN samples. The dotted lines in the figure indicate the position of the two bands for h-BN (~1350 cm^{-1} B-N stretching mode and ~800 cm^{-1} B-N-B bending mode). 114
Figure 4-9 (a-c) Typical XPS high-resolution core level spectra for B 1*s*, N 1*s*, O 1*s* with peak fitting and (d) relative atomic percentages for all porous BN samples.....114
Figure 4-10 (a) Nitrogen sorption isotherms at -196 °C for porous BN (BN-MU1:5) powder and pellet; (b) powder sample;(c) pellet sample. 115
Figure 5-1 (a,b) Nitrogen sorption isotherms at -196 °C for low temperature BN samples before and after exposure to water (open symbols represent desorption); (c,d) textural parameters deriving from the same. Error bars represent ranges from 2 repeats; (e,f) XRD patterns for low temperature BN before and after water exposure (the peak at ~32° derives from a defective sample holder). 122
Figure 5-2 (a,b) FTIR spectra for low temperature BN (BN-MU1:5) before and after exposure to water; (c,d) Relative atomic percentages from XPS analysis for low temperature BN before and after exposure to water (*via* RhB sorption); (e,f) typical high resolution spectra for boron for low temperature BN (BN-MU1:5) before and after exposure to water. 123
Figure 5-3 Equilibrium water vapour sorption isotherms at 30 ºC for three porous BN samples with different pore structures (open symbols represent desorption).....125
Figure 5-4 (a, b, c) Nitrogen sorption isotherms at -196 ºC for three porous BN samples synthesised at low- and high- temperatures (open symbols represent desorption) and (d) textural parameters deriving from nitrogen sorption for the high-temperature BN.....126
Figure 5-5 Crystalline structure with d-spacing for low and high synthesis temperature BN: High resolution TEM images for (a) low synthesis temperature BN-MU1:5-1050 ºC *vs* (b) high synthesis temperature BN-MU1:5-1500 ºC. Grey scales calculated using imageJ from figures (a) in (c) and (b) in (d). 127
Figure 5-6 (a) Typical FTIR spectra for low and high temperature BN samples (BN-MU1:5); (b) XPS relative atomic percentages for low and high temperature BN (BN-MU1:5). 128
Figure 5-7 (a) Water vapour isotherms at 30 ºC measured with a volumetric analyser (3Flex) on three porous BN samples with different pore structures synthesised at 1500 ºC and (b) a comparison of water vapour isotherms collected for two samples with identical formulations but prepared at different synthesis temperatures (open symbols represent desorption). 129

Figure 5-8 (a,b) Nitrogen sorption isotherms at -196 °C for high temperature BN before and after exposure to water (*via* RhB sorption) (open symbols represent desorption) and (c,d) textural parameters deriving from the same; (e,f) XRD patterns for high temperature BN before and after exposure to water. 131
Figure 5-9 (a-c) FTIR spectra for high temperature BN before and after exposure to water (*via* RhB sorption) and regeneration: (d) XPS relative atomic percentages for all samples before and after RhB sorption and regeneration. 132
Figure 5-10 Nitrogen sorption isotherms at -196 °C for low temperature porous BN (BN-MU1:5) before and after exposure to ethanol and n-heptane (no desorption performed for 2 of the samples); the inset shows the surface areas deriving from BET analysis for all samples. 133
Figure 5-11 TGA analysis for low temperature porous BN under (a) nitrogen and (b) air. . 133
Figure 6-1 Gas sorption at low pressure: (a) CO_2, CH_4 and N_2 bar plots with maximum sorption capacities at 25 ºC and 1 bar for low temperature porous BN samples;(b) CO_2 sorption capacity *vs* micropore volume for low and high temperature porous BN; (c), Low pressure isotherms at 25 °C and up to 1 bar for BN-MU1:5 for CO_2, CH_4 and N_2, (d) gravimetric CO_2 sorption and desorption cycles with temperature swing desorption between 30 ºC and 120 ºC (1 bar) on BN-MU1:5. 141
Figure 6-2 (a) High pressure CO_2 and N_2 sorption on porous BN powder and pellet (BN-MU1:5);(b) CO_2 and N_2 sorption on porous BN-MU1:5 at different temperatures;(c) entropy and heat of adsorption for CO_2. 142
Figure 6-3 Organic solvents selection for vapour sorption. 144
Figure 6-4 (a) Nitrogen sorption isotherms at -196 °C for three low temperature porous BN samples (b); Typical vapour sorption isotherms (for methylcyclohexane) measured at 25 ºC for the same three porous BN samples; (c, d) Vapour sorption isotherms for different organic solvents *vs* absolute pressures for two porous BN samples synthesised at low temperature (open symbols represent desorption); (e) Equilibrium vapour sorption capacity in mg/g for porous BN samples at 0.6 P/P_0. 145
Figure 6-5 (a) Vapour sorption capacity at 0.6 P/P_0 *vs* BET surface areas calculated from nitrogen sorption analysis for three low temperature porous BN samples and one high temperature sample; (b) Vapour sorption capacity at 0.6 P/P_0 *vs* micropore volume derived from nitrogen sorption analysis for the same four BN samples. 146
Figure 6-6 Dye sorption tests for porous BN samples with different pore structures for the removal of two different dyes: Methyl Orange (MO) and Rhodamine B (RhB).(a,c)

Concentration of dye *vs* time,(b,d) UV-Vis spectra for the best performing samples and (e) dye removal performance before and after recycling the samples for the two best porous BN samples for RhB (BN-MU1:5) and MO (BN-U5). 148
Figure 6-7 (a) RhB removal capacity *vs* time for *porous* BN samples synthesised at high temperature (1500 ºC);(b) UV-Vis absorption spectra for RhB solutions collected at different times from a sorption experiment performed with BN-MU0.25:5-1500 ºC. 149
Figure 6-8 Crude oil (CrudeA) sorption from water using porous BN (BN-MU1:5)..... 151

List of Tables

Table 1-1 Summary of literature papers in which BN was tested for gas sorption with brief synthesis description, BET equivalent surface area in m^2/g, remarks and references. 47

Table 1-2 Summary of literature papers in which BN was tested for liquid separations and water cleaning with brief synthesis description, BET equivalent surface area in m^2/g, remarks and references. Tests performed at ambient temperature and pressure. 55

Table 3-1. Summary of synthesis conditions for all porous BN samples produced from intermediates. 79

Table 3-2. Textural parameters from nitrogen sorption isotherms at -196 °C. 87

Table 3-3 Textural parameters derived from nitrogen sorption isotherms at -196 °C 96

Table 3-4 XPS relative atomic percentages for porous BN samples synthesised from different ramp rates. 101

Table 4-1 Textural parameters derived from N_2 sorption isotherms at -196 °C for all porous BN samples. ± indicates the standard deviation from at least 3 repeats, % indicates the percentage of micropores. * For BN-MU1:5 the highest surface area achieved is represented here, while the average of at least 3 repeats is ~ 1750 m^2/g. 110

Table 5-1 Elemental atomic and weight percentages for porous BN sample BN-MU1:5 synthesised at low and high synthesis temperatures deriving from EDX analysis. 129

Table 6-1 Naming system for porous BN samples with molar ratios, synthesis temperatures and average surface areas. 137

Table 6-2 Gravimetric crude oil (with different viscosities) sorption capacities for three BN samples with different pore structures. 150

Thesis Outline

Motivation

Adsorbent materials have demonstrated enormous success in a wide variety of different fields ranging from water and air purification to catalysis, separations and many more.[1-4] Adsorbents are large surface area materials capable of efficiently adsorbing and retaining molecules of liquid or gases on their surface. Owing to the success of these materials it is widely believed that they hold the potential to address some current world challenges, such as the sequestration of carbon dioxide from emission sources, significantly reducing greenhouse gas emissions, or the separation of complex chemical mixtures such as hydrocarbons from crude oil, circumventing distillation and significantly lowering industrial energy consumption. In fact, separation processes account for more than half of the energy consumed in industry as they are mostly performed *via* energy demanding methods, such as distillation; adsorbent materials open the door to separation by size-exclusion or chemical affinity by physisorption.[5]

The continuous development of adsorbents means that materials with improved performance are constantly sought. Porous boron nitride (BN) is a novel class of adsorbent material, which offers a range of promising properties such as the presence of a bond-polarity, and extremely high thermal and oxidative stabilities.[6] However this material remains relatively underutilised and is not yet widely investigated. The progress of porous BN therefore requires further research, such as the improvement of its textural properties and the elucidation of mechanisms of formation and material limitations. The improvement and understanding of this material represents the overarching motivation of the work discussed herein.

Thesis Content

The thesis is structured into seven chapters. It opens with a thesis outline describing the context and the motivation for this research project. The first chapter presents the theory of adsorption, BN structures and properties and reviews the different synthesis methods employed to produce high surface area BN materials. It also includes a comparison of publications in which porous BN materials were tested for adsorption in gas or water cleaning applications. At the end of chapter 1, the knowledge gaps from the literature were identified and the objectives for this thesis outlined. Chapter 2 describes the bottom-up synthesis method employed to produce porous BN materials in this project. It also describes the characterisation techniques used with backgrounds and parameters selected. Chapter 3 presents a study on the effect of different reaction variables on the chemical and physical features of the porous BN materials produced. This study allowed for a deeper understanding of the synthesis mechanisms for producing BN as well as to produce porous BN materials with different structures and chemistries. Chapter 4 describes a new method of synthesis for producing porous BN materials. This method enables us to obtain porous BN with record high surface areas and tuneable micro- and mesoporosity Chapter 5 presents an evaluation of the stability of porous BN materials in aqueous solutions and water vapour and explains the decomposition mechanisms. It also provides a method for improving the hydrolytic stability of the material, while still maintaining a relatively high surface area. Chapter 6 describes the tests performed for screening potential applications for porous BN materials. Studying BN materials exhibiting different pore structures and chemistries, we could identify the mechanisms of adsorption. Finally, the overall conclusions from this research project are presented in Chapter 7, where a way forward for further future development is also proposed.

Chapter 1: Literature Review

The aim of this project is to synthesise porous BN materials for adsorption applications. As such, this literature review begins with an overview of the fundamentals of adsorption theory and a review of the key adsorbent materials. Subsequently, the literature review focuses exclusively on BN including, but not restricted to, the most relevant synthesis methods employed for producing high surface area BN materials. These areas have been chosen to cover the motivation for investigating porous BN for adsorption-based applications. An in-depth review of the pertinent papers in the literature, in which porous BN has been employed for adsorption, is presented to provide insights into the previous uses of this material. Furthermore, with the presence of water/moisture typically being present in the envisioned adsorption applications, an additional section is dedicated towards investigating reports of the stability of porous BN in such environments.

1.1 Adsorption theory

Adsorption is the phenomenon of adherence of molecules of fluids to the surface of a material.[7] The adsorbed fluids are named adsorbates, while the substrate material is known as adsorbent. Adsorption can be classified by the type of interaction between adsorbent and adsorbate, *i.e.* physisorption or chemisorption. Physisorption involves weak interactions (London dispersion forces or van der Waals forces), while chemisorption concerns the formation of chemical bonds. It must be noted that physisorption is more common than chemisorption and generally exhibits low specificity, while with chemisorption, specific molecules can be selectively adsorbed.[7] Only a single layer of molecules of adsorbate can be chemisorbed and, because of the chemical bonds, regeneration of the adsorbent requires a larger amount of heat. On the other hand, physisorption may involve the formation of multiple layers of molecules (a multilayer) adsorbed onto the adsorbent's surface. Additionally, physisorption is not energetically activated, so thermodynamic equilibrium is quickly reached and increased temperatures are not favourable, while chemisorption often requires an activation energy, so reaching thermodynamic equilibrium can be slow and increased temperatures can result in enhanced adsorption.

Adsorption is employed for many industrial applications, for instance to store molecules of gases more efficiently or to separate chemical mixtures. As adsorption is a surface phenomenon, efficient adsorbent materials must have high surface areas and well-defined pore structures, in order to selectively adsorb specific target molecules. Therefore, in-depth characterisation of adsorbent's textural properties is required and is usually done using nitrogen sorption analysis to produce isotherms. This analysis allows for the quantification of micro- and mesopore contents and to estimate the surface areas of adsorbent materials (using the Brunauer-Emmett-Teller (BET) analysis).[8] Pores can be classified into three main groups: micro- meso- and macro- pores, depending on their dimensions. Micropores exhibit a width of less than 2 nm, mesopores between 2 and 50 nm and macropores larger than 50 nm. The nitrogen isotherms obtained represent the amount of probing gas (nitrogen) adsorbed onto the surface of the material at specific relative pressures. Based on their shapes, nitrogen sorption isotherms can be classified into different types (IUPAC classification)[9] which are related to different types of porous or non-porous materials. In nitrogen isotherms, a desorption step is also usually performed by lowering the pressure. In mesoporous adsorbents, during the desorption step, hysteresis loops are present because of capillary condensation. The desorption hystereses can be classified based on their shapes, which can be correlated to the pore structures.[9]

1.2 Adsorbent materials

Adsorbent materials should exhibit a variety of properties: a high specific surface area (generally in large excess of 100 m^2/g) in order to accommodate as much adsorbate as possible; a "rich" chemistry and a well-defined pore structure in order to selectively accommodate the adsorbate and enhance the adsorption; chemical, thermal and mechanical stability so they can be reused without modification of their properties and loss of efficiency.

A high specific surface area can be obtained either by creating materials with a large amount of pores (*e.g.* porous carbon) or by developing materials at the nanoscale (*e.g.* graphene).[10] In nanomaterials the surface-to-volume ratio is very high, which increases their reactivity and adsorption capabilities. One such example of a nanomaterial with high surface area is graphene. Graphene is a 2D material which has been highly studied for its many possible applications, including adsorption [11].

Porous materials can be broadly divided into crystalline (*e.g.* metal organic frameworks (MOFs), covalent organic frameworks (COFs), zeolites) [12-14] or amorphous structures (*e.g.* activated carbon, certain types of microporous organic polymers (MOPs)).[15] Crystalline materials exhibit a well-defined pore structure, given by their crystallographic arrangement. Amorphous materials, on the other hand, have broader pore size distributions because the porosity is related to their chemical structure. However, the theoretical surface areas achievable are often higher than in crystalline materials as they are not crystallographically constrained.[16]

Zeolites are a well-studied class of crystalline microporous adsorbents. They are aluminosilicate minerals which can occur naturally and exhibit a well-defined pore structure and, for this reason, they are often defined as molecular sieves. They exhibit high mechanical and thermal stability. However, zeolites are often sensitive to water vapour and can exhibit low selectivity to adsorbates.[17-18]

Another class of porous crystalline materials are MOFs. MOFs are composed of metal clusters and organic linkers which allow for the production of well-defined pore structures and incredibly high surface areas.[19] However, MOFs often display limited stability in water or at high temperatures and their use is limited by their high cost.[20]

A relatively new class of crystalline adsorbents are COFs. COFs are organic crystalline structures formed from light elements joined by strong covalent bonds.[14] They exhibit high versatility which is achieved by changing their building blocks. This allows for tuning of their pore structure and chemistry. However, research on these materials is still at an early stage.[14]

A widely studied class of amorphous adsorbents are activated carbons. These materials are generally cheap to produce as they can be synthesised from readily available precursors and they exhibit high surface areas (up to over 3000 m^2/g) and good chemical stability (*i.e.* resistant to water vapour and acidic and alkali conditions).[21-22] However, carbon-based materials present oxidation issues at temperatures above 500 °C.

MOPs are microporous materials composed of light elements without the presence of metals, which can be crystalline or amorphous (*e.g.* hypercrosslinked polymers).[16] Amorphous MOPs can theoretically exhibit higher surface areas than crystalline equivalents, however, the pore structure is much harder to control.

A relatively recent addition to the class of adsorbent materials is boron nitride (BN). BN is a very promising material, similar to carbon but with higher thermal stability and a bond polarity.

It exists in many crystalline forms (as described in more detail in the following section) and it can be produced with high surface areas, either in a crystalline form with high aspect ratio (nanosheets, analogous of graphene), or as a 3D porous material (turbostratic BN, analogous to activated carbon).

This literature review gives an overview of the properties of this fascinating material, focusing on its strengths but also limitations; it describes the main methods to produce BN with high surface areas and gives some examples of applications in adsorption.

1.3 Boron nitride

Boron nitride (BN) is a non-oxide ceramic which consists of an equal number of boron and nitrogen atoms. BN is similar to elemental carbon because it has the same number of electrons between the neighbouring atoms and it exists in different crystalline forms: hexagonal (h-BN), rhombohedral (r-BN), cubic (c-BN), wurtzite (w-BN), turbostratic (t-BN) and amorphous (a-BN).[23] The hexagonal lattice form can also be obtained in different morphologies at the nanoscale, such as 2D nanosheets (boron nitride nanosheets, BNNSs), 1D nanotubes (boron nitride nanotubes, BNNTs)[23] or 0D fullurene[24] (Figure 1-1). The first 2 crystalline forms, h-BN and r-BN, are formed from sp^2 hybridized atoms, while c-BN and w-BN are formed from sp^3 hybrids, as a result, c-BN and w-BN are analogous to the carbon forms of diamond and lonsdaleite, respectively, *i.e.* they are rare because of the extreme conditions that their synthesis requires.

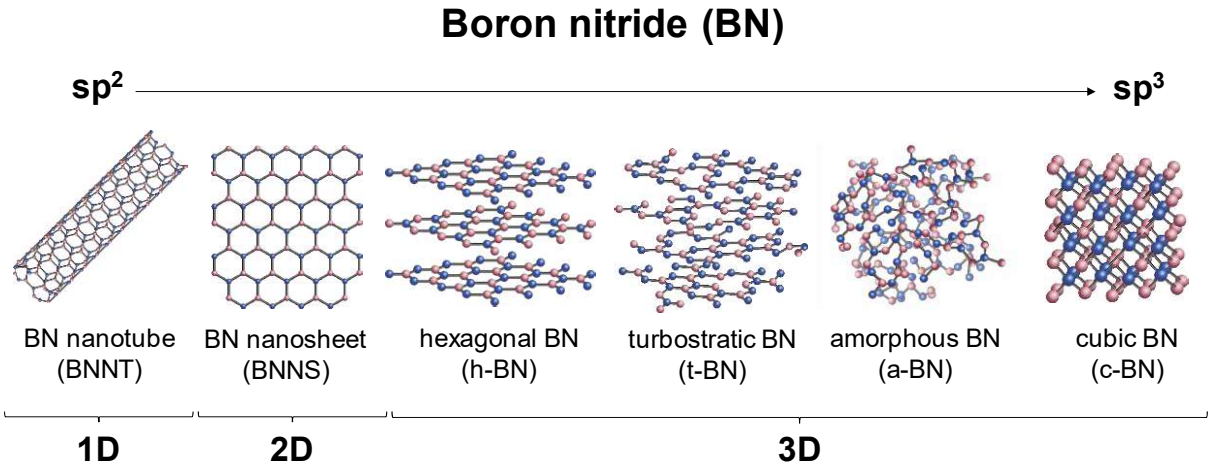


Figure 1-1 Boron nitride allotropes classified based on their hybridisation state and on their dimensionality.

h-BN consists of boron and nitrogen atoms forming a 2D honeycomb structure, with the 2D layers bound together by weak van der Waals forces. The spacing between layers is about 0.333 nm, which is very similar to that observed in graphite (Figure 1-2).[25] The atomic layers in h-BN exhibit predominantly an AA' stacking pattern, which means that each B atom in one layer eclipses with a N atom of the upper (or lower) layer, due to electrostatic interactions, also called "lip-lip" interactions.[26] A few papers have demonstrated that even if AA' is the most common form of stacking, h-BN can also exhibit AB stacking.[27] h-BN exhibit a high melting point (3000 °C), high temperature stability (stable up to 1100 °C in air),[28] large thermal conductivity (300-2000 W/mK), a negative coefficient of thermal expansion (a/b axis: $-2.9 \times 10^{-6}/K$, c axis: $4 \times 10^{-6}/K$), low density (2.3 g/cm^3), high mechanical strength, a low coefficient of friction (< 0.3) and good resistance to oxidation.[23] h-BN is a also wide band-gap semiconductor-insulator (5.6 eV).[26] Like any crystalline material, h-BN (and BNNS) can exhibit some structural defects (Figure 1-2b,c). The type and extent of these defects are typically related to the material itself but also to the methods used to synthesise it. Contrary to graphite, Stone-Wales defects, which consist of pentagon or heptagon fused rings on BNNSs, are thermodynamically unfavourable due to the requirement of the formation of B-B or N-N bonds. On the other hand, the most common defects in BNNSs are vacancies or point defects (Figure 1-2c). These defects often exhibit a well ordered triangular shape, because of the atomic structure of h-BN (Figure 1-2c). [26]

BN, however, can also be obtained in non-crystalline forms, such as amorphous (a-BN) which is completely disordered and formed from sp^2 hybridised atoms, and turbostratic (t-BN) which is formed from 2D h-BN layers randomly orientated on top of each other and with a larger interplanar spacing compared to fully crystalline h-BN (Figure 1-3).

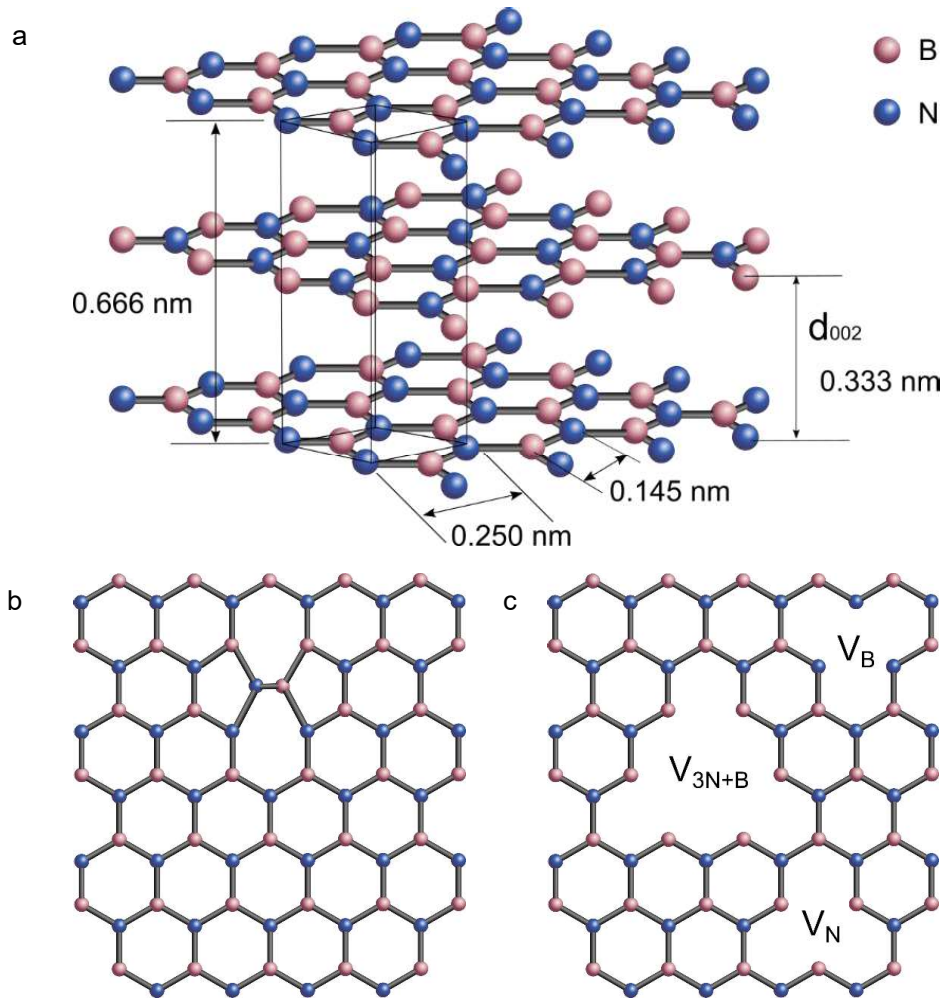


Figure 1-2 (a) h-BN or few-layer BNNSs with unit cell and dimensions; (b) Stone-Wales defects; (c) vacancies (V indicates vacancies, N refers to nitrogen vacancies and B to boron vacancies; the numbers indicate the amount of boron or nitrogen vacancies).

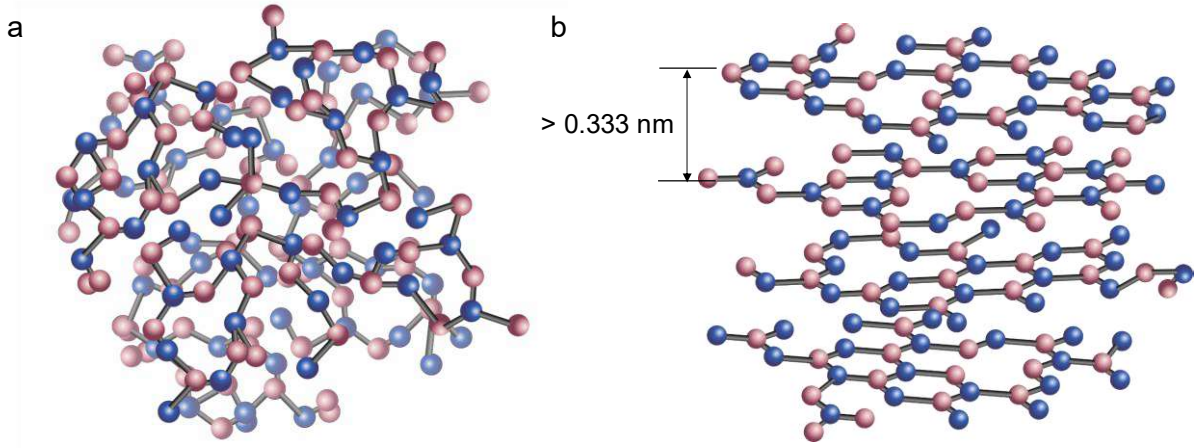


Figure 1-3 (a) Amorphous BN; (b) Turbostratic BN structure composed of h-BN layers randomly stacked on top of each other with larger d-spacing compared to h-BN;

1.4 Synthesis methods leading to high surface area BN materials

There are two main routes to obtaining high surface area BN: (i) producing a material with a large aspect ratio (*e.g.* nanosheets or nanotubes), or (ii) producing a material with a large amount of pores (porous BN). BNNSs, similarly to graphene, fall into the first class and have a theoretical surface area of 2630 m^2/g.[29] Porous BN, however, falls into the second class and is usually a disordered turbostratic and amorphous material, with the 2D h-BN layers randomly tilted between one another. It exhibits stacking and vacancy defects, low crystalline order and usually a large amount of impurities. The stacking defects generate micro- and mesopores within the BN structure (Figure 1-4). The surface area for porous BN is theoretically higher than in a nanosheet configuration, as it is not limited by the crystallographic arrangement of the material.

Here, the main synthesis methods leading to high surface area BN materials are reviewed (with the exception of the methods used to produce nanotubes). Methods can be broadly classified into top-down and bottom-up approaches. Top-down methods involve the exfoliation of h-BN crystalline materials in order to increase the surface areas of the materials, often leading to BNNSs. Bottom-up methods, instead, involve the synthesis of porous BN or BNNSs starting from chemicals containing boron and nitrogen. It must be noted that bottom-up methods can lead to a variety of different BN structures, depending on synthesis conditions. However, only the methods leading to relatively porous BN materials are reviewed here.

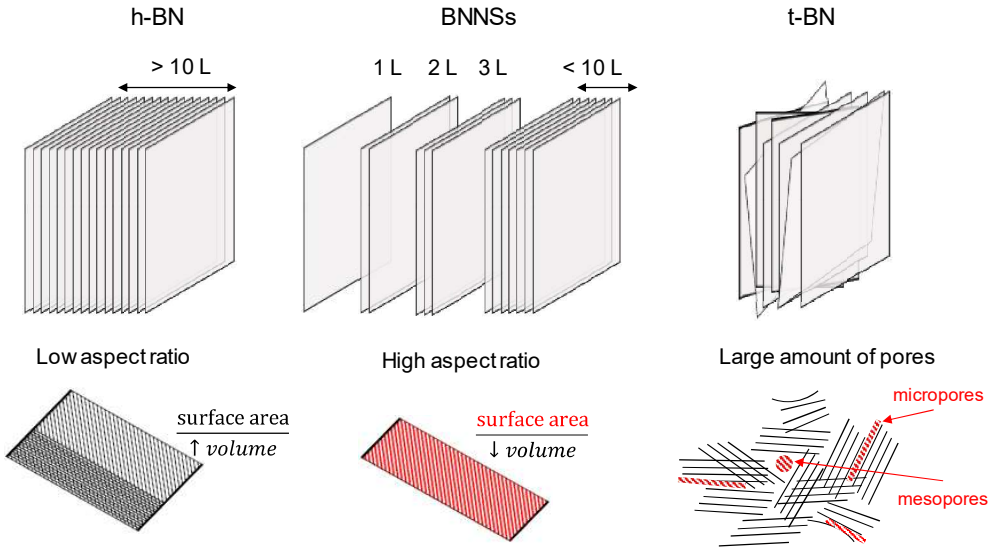


Figure 1-4 Schematic representation of 2D h-BN sheets forming a 3D h-BN graphitic material with low surface area; BNNSs composed of less than 10 h-BN layers (L) and exhibiting high surface area; t-BN composed of h-BN layers lacking of stacking order and with the presence of a large amount of pores.

1.5 Top-down synthesis methods

1.5.1 Mechanical exfoliation

In mechanical exfoliation methods, shear forces play a central role in the production of BNNSs by peeling apart h-BN layers. However, it must be noted that when solvents are employed in the exfoliation, other forces can assist in the exfoliation of h-BN layers, as described in section 2.5.2.

1.5.1.1 Scotch-tape

BNNSs can be produced in small quantities employing the scotch-tape method, which uses an adhesive tape to peel the h-BN layers from the bulk material.[30] This method allows for well-ordered and clean samples, composed of a maximum of 10 layers to be obtained.[31] Scotch-tape was also used in combination with other exfoliation methods such as high-energy electron beam [32] or reactive ion etching.[33] Although the scotch tape method generally maintains the crystallinity and the original lateral sizes of h-BN, it is only suited for fundamental studies when one wishes to analyse the properties of "pure" BNNSs.

1.5.1.2 Ball-milling

Another mechanical method to produce BNNSs *via* exfoliation of h-BN is ball-milling.[34-38] Ball-milling method produces shear and impact forces that cause h-BN to exfoliate, but also tends to create defects on the surface of the BNNS due to the impact forces of the balls on h-BN.[39-40] In order to minimise the amount of defects, low energy milling in combination with the use of lubricating solvents was reported.[39-40] Ball-milling can also be combined with chemical exfoliation methods, for example, NaOH was employed in the exfoliation, with OH^- ions reacting with h-BN, particularly near defect sites, thereby "cutting" the h-BN sheets.[41]. Recently, this method, combined with the use of NH_4Cl powder and heat treatment, was used to obtain BNNSs with high specific surface areas for adsorption processes.[38] Additionally, milling was used to produce NH_2 functionalised BNNSs in high yields (30 mg/mL), which were used to create BN aerogels with relatively high surface area (273 m^2/g). Overall, ball-milling is a rather straightforward method, however the surface area of the materials remains relatively low and the absence of pores can result in low selectivity.

1.5.1.3 Other mechanical devices

Chen *et al.* reported the exfoliation of h-BN using a vortex fluidic device with N-methyl-pyrrolidone as the solvent.[42] The vortex fluid device is a rotating tube inclined at $\Theta = 45°$ and

the shearing in the film is produced from the interplay between centrifugal and gravitational forces. In this process, impact forces are less intense than ball-milling methods, reducing the number of defects formed. However, the quantities of monolayers obtained remained small.

Hilmi *et al.* pioneered the use of a microfluidizer high-pressure fluid processor to exfoliate h-BN using a solvent mixture of N,N-dimethylformamide (DMF) and chloroform.[43] The high shear forces produced during this process induced exfoliation in high yields (yield of 45 %). The thickness of BNNSs obtained was about 8-12 nm, and the sheets were a few micrometres in width.[43] High-pressure microfluidization proves to be promising for large-scale production, however exfoliation remains inefficient at producing few-layers nanosheets.

1.5.2 Combination of sonication and chemical methods

Liquid exfoliation consists of dispersing h-BN in a solvent and subjecting the mixture to sonication. It is suggested that sonication can trigger exfoliation owing to two synergistic effects: (i) the sonication generates shear forces and (ii) the interactions between the polar solvent and h-BN weakens the van der Waals forces between layers. At the weak sites of h-BN, *i.e.* defect sites and layer edges, sonication can also cause the h-BN layers to break, thereby leading to a decrease in the layers' lateral size.

Several authors reported the exfoliation of h-BN *via* sonication in different solvents. Some examples of organic solvents used are: DMF,[44] 1,2-dichloroethane,[27] isopropanol,[45] dimethyl sulfoxide,[46] *N*-Methyl-2-pyrrolidone (NMP), dimethylacetamide (DMAc), 1,2-dichlorobenzene and ethylene glycol to name but a few.[25, 47] Coleman *et al.*[45] found that the most promising solvents (surface tension close to 40 mJ/m^2) were those that minimise the energy of the exfoliation. Exfoliation of h-BN in solvent mixtures were also attempted: ethanol/water (55:45 v/v)[48] and tert-butanol in water (60 wt%)[49]. However, generally the concentration of BNNSs obtained *via* sonication in organic solvents remained low (up to ~ 1 mg/mL) and only partial exfoliation was achieved.

Lin *et al.* demonstrated that water is also effective at exfoliating h-BN using sonication.[50] In this case it was found that hydrolysis of h-BN contributed to the exfoliation (in addition to polarity effect and shear forces). However, the BNNSs were obtained in relatively low yields (0.05-0.1 mg/mL) and the presence of hydroxyl groups will impact their hydrophilicity.

In an attempt to improve the yields of exfoliation, acids were also employed,[51] for instance methanesulfonic acid was used assisted by sonication and produced BNNSs with

concentrations of 0.2-0.3 mg/mL. The proposed exfoliation method was the protonation of h-BN by methanesulfonic acid, which induced repulsive forces between the BNNSs. A significant improvement in the yields of exfoliation was obtained *via* sonication in ionic liquids (~1.9 mg/mL).[52] However, this method necessitates the use of ionic liquids, which are toxic, as well as solvents such as acetone for the removal of ionic liquids. Other exfoliation methods have been reported: sonication at high pressure,[53] sonication using supercritical CO_2[54] and a controlled lithiation process.[55-56]

Overall, exfoliation using sonication is a relatively easy method to implement as it does not require any specific equipment. However, it leads to non-uniform BNNSs with a wide range of layers and in low concentration. In addition, if the BNNSs were to be extracted from the solution, they would likely re-stack, thereby producing a material with low surface area. Some of the solvents used are toxic and/or exhibit high boiling points, thereby leading to high energy consumption to remove them.

1.5.3 Exfoliation via chemical functionalization

Exfoliation *via* chemical functionalization can be broadly described as occurring in two steps: (i) h-BN is dispersed in a solvent containing an organic molecule (often a polymer) while applying sonication and (ii) the solvent is evaporated and then the functionalized BNNSs can be re-dispersed/exfoliated in different solvents. The first step is made possible owing to interactions between the h-BN surface and the organic molecule. The exfoliation of the BNNSs then occurs owing to the chemical affinity between the organic molecule used to functionalize h-BN and the solvent. The organic molecules help to reduce the "lip-lip" interactions between the different layers.

In 2008, Han *et al.* presented a pioneering study on the exfoliation of single crystal h-BN using a chemical method. They used a dichloroethane solution of a conjugated polymer to exfoliate the crystal into BNNSs through sonication.[57] Lin *et al.* presented an easy chemical method to isolate mono- and few-layer BNNSs from h-BN powder using hydrophilic amine molecules.[58] In that case, the process of functionalization can be explained by the presence of Lewis acid-base interactions between the amino group and the electron deficient boron atom of the h-BN. To extract BNNSs, an appropriate solvent was added, followed by sonication.[58] It was demonstrated that when a similar exfoliation method was employed after ball-milling, functionalisation was more efficient because of the presence of defects.[39] Furthermore, mixed

solvent systems (ammonia solution:IPA) have also been employed in the chemical exfoliation of h-BN.[59]

Overall, the functionalization/exfoliation methods described above enable one to disperse BNNSs in a range of different solvents by carefully selecting the functionalizing compounds. However, this approach requires an extra step compared to exfoliation with organic solvents/water/acids. In addition, it leads to a modification of the BNNS chemistry by adding chemical functionality to the layers. The latter aspect may or may not be desirable depending on the desired applications.

1.5.4 Exfoliation in acids and molten hydroxides without sonication

Exfoliation can also be performed using acids without sonication. Du *et al.* reported an exfoliation in acid to obtain BNNSs with large lateral sizes.[60] Similarly to the oxidation of graphite to produce graphite oxide, they exfoliated the nanosheets starting from h-BN powders using H_2SO_4, $KMnO_4$ and H_2O_2. The nanosheets obtained were crystalline and hexagonal in phase and with no impurities or oxidation. The mechanisms of exfoliation included an intercalation step, followed by the formation of nanoparticles in the interlayer spacing and finally the *in-situ* release of gases, which caused the h-BN layers to peel apart. Štengl *et al.* reported a similar exfoliation method.[53] Despite being efficient, exfoliation in acid requires the nanosheets to be washed afterwards to eliminate acid residue. Furthermore, this method is environmentally unfriendly because of the chemicals used.

In 2013 Li *et al*. first reported an exfoliation method using molten hydroxides.[61] Once again, sonication was not applied in this study. They prepared a homogeneous mixture of NaOH and KOH with h-BN powder, which was then heated in an autoclave. They obtained mono and few-layer BNNSs and nanoscrolls (curled BNNSs) with high crystallinity layers.

1.5.5 Thermal method

Solvent-based sonication techniques can generate partially exfoliated h-BN or BNNSs in small concentrations and the other synthesis methods reported above are not always suitable for large scale applications. In this context, Cui *et al.* developed a new top-down method to produce hydroxylated BNNSs in high concentration.[62] Despite h-BN being more oxidation-resistant than graphite, when heated at high temperatures in air, oxygen is incorporated into the h-BN lattice. h-BN was, therefore, heated in air (around 1000 °C) and then dispersed in water (yields for BNNSs suspended in water up to ~ 65 %). Single-layered sheets with large lateral sizes

were obtained, which contained oxygen, hence the name BNO. After BNO was formed, it was functionalised using isocyanate, to demonstrate its reactivity, due to the –OH groups present.[62] A similar exfoliation method was also reported by Yu *et al.*[63] Although this method produces BNNSs in high yields, the sheets are chemically changed. Moreover, the incorporation of oxygen increases the hydrophilicity of the materials, which is detrimental in some applications.

1.5.6 Gas exfoliation

In 2016, a novel exfoliation technique to produce BNNSs in high-yield was presented.[64] This technique consisted of heating h-BN commercial powder to 800 ºC in air, and then submerging the material into liquid nitrogen until it completely vaporises (Figure 1-5). This strategy assumes that h-BN layers expand when heated, causing a reduction of the "lip-lip" interactions between the h-BN layers. The quenching and gasification causes the 2D sheets to curl and exfoliate. This exfoliation procedure was repeated for 10 cycles and led to BNNSs with 1-5 layers and with a yield of up to 20 wt.%. Interestingly, this is one of the only top-down exfoliation methods in which the surface area of BN was reported and increased from 10 to 278 m^2/g after exfoliation. Although this technique provides improved yields, BNNS surface areas remain relatively low and the production method is energy intensive.

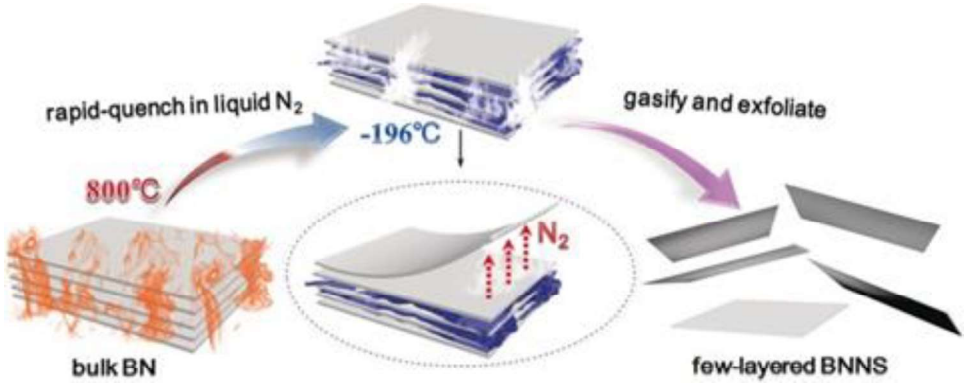


Figure 1-5 Gas exfoliation of h-BN into BNNSs.[64]

1.5.7 Boron nitride nanotube unwrapping

Nanoribbons are folded nanosheets. In 2010, Zeng *et al.* reported the preparation of single and few-layer boron nitride nanoribbons through boron nitride nanotube (BNNT) unwrapping.[65] Erickson *et al.* prepared boron nitride nanoribbons through boron nitride nanotube unwrapping, using alkali metal intercalation.[66] This method obtains highly crystalline boron nitride nanoribbons that are similar to nanosheets, but are semi-conductive. However, in order to use

it as a top-down method to produce BNNSs, it is necessary to first have boron nitride nanotubes as a raw material. The synthesis of BNNTs is not included in this review.

1.6 Bottom-up methods

Bottom-up methods are syntheses that produce BN starting from boron- and nitrogen-containing precursors. The BN produced *via* these methods can be either in the form of BNNSs, a film (usually *via* CVD which is not included in this review), an a-BN/ t-BN material or fully crystalline h-BN, depending on the type of synthesis and conditions used.

1.6.1 Chemical blowing technique

Wang *at al.* reported for the first time a new technique to produce BNNSs in high yield and with large lateral sizes.[67] The authors called this technique "chemical blowing". Typically, they used ammonia borane (BH_3NH_3, AB) as a boron and nitrogen precursor, in a tubular furnace under an argon gas flow. They employed a multiple-step heating procedure during which, the release of H_2 generated the blowing effect. The release starts at low temperatures and forms large bubbles which "become solid" at high temperature, forming BNNSs by collapsing *via* ultrasonic treatment. The yield was high (25 wt.% of the starting precursor) and large area BNNSs were obtained. In another paper by the same authors, a higher yield was reported (40 wt.%) using the same method, but optimizing the various steps, in particular the pre-treatment.[68] This method of synthesis seems really promising to obtain a high yield of BNNSs with large lateral sizes and only a few-layers. The materials obtained could be exploited for fundamental studies. However, the surface area of the nanosheets obtained with chemical blowing is still not very high (~130 m^2/g), and they contain some impurities, likely due to the reaction of AB with oxygen or water. Furthermore, the price of the AB precursor is very high and, therefore, prevents the production of nanosheets in large quantities for industrial applications.

1.6.2 Chemical vapour deposition

BNNSs can also be produced *via* bottom-up methods such as chemical vapour deposition.[69] However, these methods usually produce a large film composed of just a couple of layers of BNNSs. Therefore, this is of more interest for electronic devices or film coatings, rather than the production of high surface area materials. The review for this synthesis method is, therefore, not included here.

1.6.3 High temperature syntheses with the use of templates

Porous BN can be produced from boron- and nitrogen- containing precursors *via* a high-temperature heat-treatment under controlled atmosphere. The porosity can be tuned by the inclusion of a template during high temperature BN synthesis, which is then eliminated post-synthesis or during the synthesis.

1.6.3.1 Hard templates

The hard template method consists of using a solid mesoporous material (such as mesoporous silica) as a template to produce mesoporous materials (such as BN). After BN production, the removal of the template results in templated porosity.

Mesoporous BN was synthesised using a variety of mesoporous templates, for example with the use of a tri(methylamino)borazine (MAB) precursor and silica and carbon templates.[70] The synthesis of BN using the carbon template was more promising than the silica one: the mesoporous BN obtained with the carbon template had a specific surface area of 540 m^2/g, compared to 140 m^2/g for the silica template. Rushton and Mokaya prepared mesoporous BN using silica templates and an ammonia borane (BH_3-NH_3) precursor, heated under a nitrogen/ammonia gas flow, producing a BN with a specific surface area of 327 m^2/g.[71] Zeolite templates were also employed for the synthesis of micro- and mesoporous amorphous BN (Figure 1-6).[72] A double synthesis process was used: firstly a carbonaceous template was prepared by impregnation of the zeolite with propylene before the zeolite was dissolved in acid. Secondly, the carbon template was impregnated with polyborazylene and BN was obtained through ceramization. The carbon template was eliminated by heat-treatment either in ammonia or air. The samples obtained were amorphous and had relatively high specific surface areas (570 m^2/g) and pore volumes (0.78 cm^2/g; volume of micropores: 0.20 cm^3/g). Elemental analysis of the samples indicated almost complete removal of carbon (1 at.%) and the presence of oxygen impurities (14-15 at.%) with traces of boric acid. The absence of crystallinity was attributed to the confinement effect imposed by the template during the crystallites' growth.

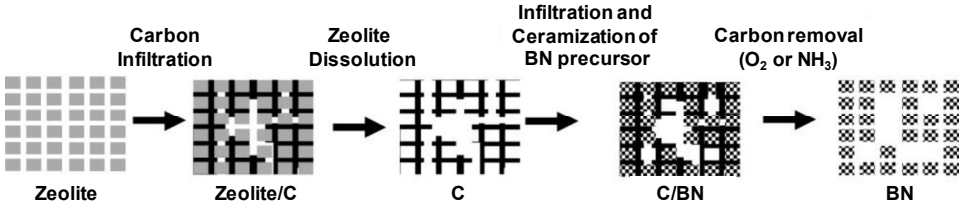


Figure 1-6 Templating method to produce mesoporous BN from zeolite template.[72]

1.6.3.2 Structure directing templates

Structure-directing agents are organic compounds that are mixed with BN precursors, their subsequent elimination during the heating step generates BN with high porosity.

Dibandjio *et al.* prepared mesoporous BN using tri(monomethylamino) borazine (MAB) as precursor and cetyl-trimethylammonium bromide (CTAB) as a structure-directing agent.[73] Mesoporous t-BN was obtained with a specific surface area of 800 m^2/g. Li *et al.* reported the synthesis of highly porous (2078 m^2/g) BN nanoribbons, using boric acid and melamine precursors and a triblock copolymer (P123) as a structure-directing agent.[74] Their heating process consisted of two-steps up to 1300 °C under nitrogen flow. The BN obtained, described as "activated", presented oxygen and carbon impurities and a turbostratic structure with low crystallinity. Other similar templating methods were reported with the use of different structure directing agents: D-trimethyl ammonium chloride (DTAC), [75] cetyl trimethylammonium bromide (CTAB),[76] and 1-butyl-3-methylimidazolium ([Bmim]BF_4) as both template and source of carbon atoms.[77] Han *et al.* reported the synthesis of porous BN with low crystallinity using activated carbon as a template.[78] However, they did not impregnate the carbon with B- and N-precursors. Instead, they placed activated carbon on top of a boron trioxide powder in a furnace, under nitrogen flow (resulting surface area: 67 m^2/g). In a similar way, Vinu *et al*. reported the synthesis of mesoporous BN and boron carbon nitride (BCN) from a mesoporous carbon template.[79]

In general, the template methods as described above enable good control over the pore structure of BN. However, the BNs produced generally contained large amounts of impurities or exhibited lower surface areas than those synthesised using template-free methods. Another disadvantage of templating methods is that they require additional steps to both synthesise and eliminate the template/structuring agent. Furthermore, the elimination of hard templates mostly forms mesopores and no micropores.

1.6.4 Solvo-thermal reactions

Porous BN nanocarpets were prepared by placing precursors (NH_4BF_4 and NaN_3) inside a teflon tube filled with benzene in an autoclave (260 °C, 150 MPa). BN nanocarpets exhibited low crystallinity, a large number of defects and a surface area of 117 m^2/g.[80] The mechanism of formation of BN nanocarpets consisted of three steps: i) BNNSs formed and acted as substrate, ii) BN nanodots grew on the BNNSs, iii) nanorods formed from growth of the nanodots. Another solvothermal reaction was reported in which the same precursors and sulfur

were made into pellets, heated in an autoclave and washed. In this case hollow spheres of BN were obtained and exhibited surface area of 210 m^2/g.[81]

The main advantage of solvo-thermal reactions is the low temperature required during the synthesis of porous BN, which is advantageous in the reduction of production costs. However, the materials produced exhibited relatively low surface areas and a large amount of chemicals were required, some of which are toxic.

1.6.5 Template-free high temperature reactions

Template-free syntheses are typically solid-state reactions between a boron precursor (*e.g.* boric acid or boron oxide) and a nitrogen precursor (*e.g.* melamine or urea). In some cases ammonia gas was employed as nitrogen source.[25] Boron and nitrogen precursors are heat-treated at high temperatures (generally above 800 °C) under an oxygen-free gas atmosphere, and depending on the temperature used, atmosphere, precursors etc.; either h-BN, BNNSs or t-BN can be produced.[25]

Relatively low synthesis temperatures (<~ 900 ºC) often lead to a a-BN/ t-BN material with poor crystalline order and a large amount of oxygen residues (~10/20 wt.%).[82] When the synthesis temperature is increased (~ 1700 ºC), oxygen impurities usually decrease and h-BN with higher crystalline order is produced, however, the material's surface area also decreases.[82-84]

Zhao *et al.*, presented a two-step synthesis of BN nanoplates using a template-free method.[83] The authors employed increasing synthesis temperatures up to 1400 ℃ and observed that the crystallinity of the material increased with increasing synthesis temperature and went from a turbostratic to a hexagonal crystallographic arrangement.

The synthesis temperature clearly has a strong effect on the resulting BN's crystalline structure, impurity content and surface area. However, other synthesis parameters can also affect the chemistry and structure of the BN material obtained. For instance, it was shown that the use of NaCl with melamine and boric acid precursors can promote the crystallisation of h-BN at relatively low synthesis temperature (1050 ºC) by accelerating kinetics of crystallisation, due to the formation of a melt.[85] Similarly, the presence of boron oxide, which melts at high temperatures, was shown to be beneficial in the crystallisation of h-BN, by creating a liquid oxynitride in between BN crystallites, which allows for easier rearrangement at high temperatures.[86] Formation of BN was observed at temperatures as low as 220 ºC and the

amount of oxide residual increased with decreasing urea to boric acid molar ratios.[86] The use of specific precursors, such as a MgB_2 boron source, can also induce crystallisation at relatively low temperatures owing to the specific structure of MgB_2, with Mg atoms placed in between boron sheets, constraining BN growth into ordered BN sheets.[87] The use of a reactive gas atmosphere, such as ammonia or hydrogen, was shown to have a beneficial effect in reducing oxygen and carbon impurities in the final BN material,[88-89] while a post-treatment in air at relatively low temperatures (< 900 ºC) was shown to reduce carbon impurities.[90]

The selection of specific synthesis parameters can also have an effect on BN pore structure. For instance, the use of an excess of nitrogen precursor was shown to increase BN surface area by Nag *et al.*, who reported the synthesis of porous BN at high temperatures with a method involving the reaction of boric acid with urea in different ratios.[91] Therein, the surface area of BN materials could be tuned by the varying of the boric acid and urea molar ratios. Molar ratios of boric acid: urea of 1: x with x= 6, 12, 24, 48 and 72 were used. The mixture was then heated at 900 °C in a nitrogen atmosphere. The overall reaction is: $B_2O_3 + 2NH_3 \rightarrow 2BN + 3H_2O$. The authors determined that the layer thickness (number of layers) decreased with increasing urea concentration and the surface area increased by threefold.[91] However, despite the ability to tune BN surface areas, they remained relatively low (< 1000 m^2/g) and did not permit any control of the pore structure. Similarly, it was demonstrated that increasing the molar ratio of dycianamide to boric acid precursors, the surface area of BN could be increased up to 1900 m^2/g,[92] however, this synthesis also required ammonia gas.

Similar synthesis methods were widely reported in the literature to produce porous BN materials with varying crystallinities, pore structures and chemistries. Recently, Lei *et al.* synthesised oxygen-doped porous BN by dissolving boron trioxide and urea in methanol at room temperature to obtain a white powder.[93] The powder was then heated to 1100 °C under nitrogen/hydrogen gas flow. The BN prepared using this method was made up of 2-6 layers and had good surface areas (536 m^2/g), however it contained oxygen impurities. Typically, when melamine was used instead of urea as a nitrogen source, the microstructure of the BN materials resembled that of whiskers instead of 2D sheets.[90, 94] Li *et al.* reported the synthesis of porous BN whiskers with high surface areas for hydrogen storage and water cleaning.[90] These whiskers were synthesised using boric acid and melamine precursors, which were dissolved in water and heated to obtain a white precipitate that was filtered, dried and used for the reaction. The reaction consisted of three different stages performed in a tubular furnace under nitrogen flow up to 1460 ℃. They also heated up the sample overnight at 550 °C in air

to remove any traces of carbon, resulting in h-BN whiskers with very high specific surface areas of 1687 m^2/g. This represents one of the only studies that reported porous BN with both high crystallinity and high surface area. Clearly, it was shown that reaction parameters used during the formation of BN are fundamental in order to control BN's pore structure.

Interestingly, in most studies the boron- and nitrogen- containing precursors were first dissolved in water or other solvents to prepare an intermediate for the synthesis of BN.[90-91, 93] For melamine and boric acid precursors, the dissolution step resulted in the formation of a melamine diborate compound, with hydrogen bonds between melamine and boric acid.[90, 95] On the other hand, for urea and boric acid the dissolution step was often employed to simply mix the precursors uniformly[91] and its importance remained overlooked until Wu *et al.* recently showed that BN surface area can be directed by re-crystallising urea and boric acid precursors from solvents with different boiling points.[96] This study outlined the fundamental importance of intermediate preparation in tuning the structure and chemistry of the porous BN produced.

The scale-up of a-BN/ t-BN production was also attempted in an early study in 1997 to produce 500 g of material.[97] In this study, tri-calcium phosphate was added to boron oxide and ammonia in order to increase the reactive surface of the boron oxide melt during the high temperature reaction and promote the formation of BN. However, the BN material produced exhibited low surface areas (<20 m^2/g), that, although not discussed, is believed to be related to the use of a gaseous nitrogen precursor, limiting the amount of gases released *in-situ*.

Overall, high temperature syntheses enable the production of relatively large quantities of BN, while keeping the number of synthetic steps low. As a result, high temperature synthesis is one of the more industrially relevant. On the other hand, to obtain highly porous BN, the temperature of the synthesis usually has to be kept relatively low to promote the formation of t-BN, which can suffer from hydrolytic instability, as discussed in detail in Section 2.8. Moreover, t-BN often contains oxygen impurities, which are difficult to avoid at low temperatures. In conclusion, template-free syntheses are highly promising for producing BN materials for applications in liquid and gas separations, where high purity and high crystallinity are not necessary requirements but a high porosity is desirable. Nevertheless, some issues still need to be addressed: control over BN surface area and pore structure needs to be provided, the role of intermediate preparation needs to be clarified and hydrolytic stability needs to be improved.

1.7 3D BN

Three-dimensional (3D) BN materials are defined here as macroscopic 3D foams, pellets, aerogels or monoliths. Although t-BN and h-BN are technically 3D structures at the molecular scale, their macrostructure is usually in a powder form, hence they are not included here. In the recent literature there has been great interest in the production of 3D BN materials for use as adsorbents. The advantage of these materials over powders is that they often exhibit a hierarchical pore structure, allowing for better mass transport, and they are more easily handled.

1.7.1 3D BN deriving from top-down methods

3D BNNS aerogels or monoliths have been prepared by a variety of different techniques and usually exhibited low surface areas and high macropore volumes. In a typical procedure, BNNS aerogels were prepared by exfoliating h-BN to give BNNSs, which were generally functionalised, cross-linked and freeze-casted.[98-100] The resulting 3D BN gels often showed good mechanical properties and elasticity. A low-density BN monolith was prepared by Sudeep *et al.* from h-BN industrial powder *via* cross-linking and lyophilisation.[101]

1.7.2 3D BN deriving from bottom-up methods

3D BN materials can also be prepared *via* bottom-up methods. For instance, Zhao *et al.* described a template-free reaction using ammonia borane and thiourea precursors, mixed and heated to 1200 ºC to give a BN foam.[102] While ammonia borane acted as BN precursor, the thiourea acted as foaming agent, releasing gases during BN synthesis. The resulting material, however, exhibited a low surface area (32 m^2/g). 3D BN foams were also prepared on templates such as nickel foam[103] or a graphene aerogel.[104]A relatively high surface area of 400 m^2/g was reported for the graphene aerogel template and good sorption capacity for oil and dyes.

Some of the structures obtained from top-down and bottom-up methods are shown in Figure 1-7.

Overall, the production of 3D forms of BN is advantageous if the material is to be employed in adsorption or if good mechanical properties are required. However, the materials produced with the methods outlined often exhibit significant macro- and mesoporosity with low micropore volumes and surface areas, making them undesirable for many adsorption applications.

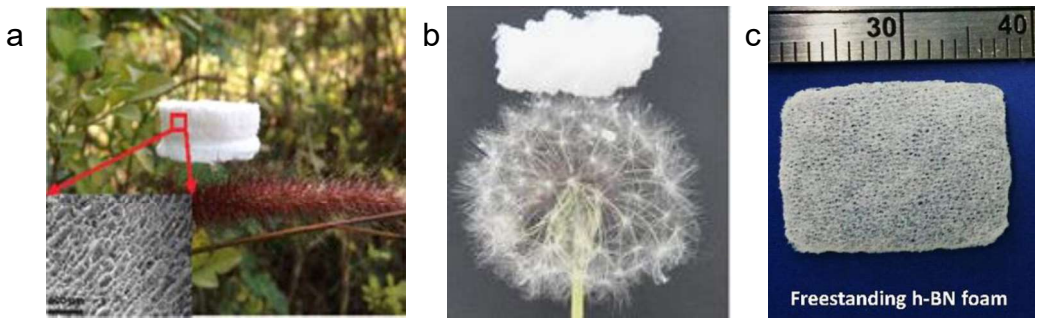


Figure 1-7 3D BN foams and monoliths prepared *via* (a)[98] top-down and (b,[102] c[103]) bottom-up methods.

1.8 BN water stability

The applicability of porous materials depends not only on their desirable textural properties, but also on their durability (*i.e.* chemical, thermal and oxidative stability). Surprisingly, a few studies reported t-BN to be unstable when exposed to water or moisture. Water instability is detrimental in many adsorption applications, such us pollutant removal from aqueous solutions, or gas sorption in the presence of water vapour. Long term storage of materials also requires inert atmospheres or humidity-controlled environments. A brief review of BN water stability studies is therefore presented.

In an early study in 1981 it was observed that BN films deposited *via* CVD from BCl_3-NH_3-H_2 precursors at low temperatures (< 450 ºC) were unstable upon exposure to moisture.[105] In 1994 Cofer and Economy analysed the instability of t-BN and linked it to the degree of crystallinity of the material or its d-spacing.[106] The authors suggested that many BN materials synthesised *via* CVD methods are likely to suffer from moisture sensitivity when not fully crystalline.[106] Therein it was also suggested that larger d-spacings result in weaker bonds between the different BN sheets and usually smaller crystallites, both of which facilitate water to react with BN. When fully hydrolysed, t-BN converted to a denser B_2O_3 material. In 1997 Alkoy *et al.* studied the decomposition of t-BN produced at 900 ºC from boron oxide and ammonia.[97] The authors analysed a t-BN material stored for one year under ambient conditions, *i.e.* in air, and concluded that it had produced an ammonium borate complex ($NH_4B_5O_8 4H_2O$). It was also shown that heating the t-BN material at higher temperatures during synthesis (>1500 ºC) resulted in more crystalline h-BN with smaller d-spacing and it was suggested that this material could exhibit higher stability. However, the surface areas of the materials produced at both low

and high synthesis temperatures were poor (< 20 m^2/g) and a mechanism of decomposition was not proposed.

Hydrolysis was also observed more recently on a ball-milled BN material with a degree of amorphisation due to the mechanical exfoliation.[107] It was proposed that BN reacted with water with the following reaction: $2BN + 3H_2O \rightarrow B_2O_3 + 2NH_3$. In cold water the hydrolysis reaction was slower due to the formation of a glassy boron oxide-type layer, which was insoluble in water below 60 ºC. Surprisingly, more recently a similar hydrolysis reaction was reported on fully crystalline h-BN when sonicated in water for exfoliation.[50] The h-BN edges were "cut" during exfoliation, forming OH groups bound to boron atoms, and releasing ammonia (detected in the water). More recently, Florent and Bandosz produced porous carbon-doped BN and reported the material to be highly unstable in water and moisture.[108] Hydrolysis caused both a loss of surface area and chemical changes. The B-C bonds were reported to be the most unstable sites, although B-N also showed some instability.

In conclusion, it is clear that BN materials suffer from an intrinsic issue of stability in water or moisture. It appears that the instability is higher when the material exhibits lower crystallinity and is almost negligible when the material is fully crystalline. However, despite a number of studies reporting BN to be unstable in water, this issue is not well understood and a solution for overcoming the degradation of porous BN in water is yet to be presented. Many studies reported the utilisation of t-BN materials for aqueous applications (see Table 1-2 in Section 2.9).

1.9 Applications of porous BN

As porous BN is an analogous material to activated carbon but with higher thermal stability and a "richer" chemistry owing to its bond polarity, it is a promising candidate to compete with or surpass carbon-based materials in industrial separations and catalysis. The major studies in which BN has been tested for adsorption applications are summarised in Table 1-1 and Table 1-2. It must be noted that the utilisation of BN materials for adsorption applications is gaining increasing interest in the literature.

1.9.1 Gas sorption

Porous BN materials exhibit high surface areas, high micropore volumes, a bond polarity and high thermal stability, making them potential candidates for a range of diverse gas sorption applications ranging from CO_2 capture,[87-88, 91, 109-111] H_2 storage,[76, 90-91, 93-94] formaldehyde

removal from air,[85, 112] paraffin/olefin separations, [113] *etc*. The context for CO_2 capture stems from reducing greenhouse gas emissions, while H_2 storage is of interest as a renewable fuel, and hydrocarbons separations is beneficial for the chemical industry.

An early effort to synthesise porous BN for gas sorption was made in 1994, preparing t-BN with surface areas up to 712 m^2/g for the adsorption of carbon dioxide and methane.[109] It was observed that the gas sorption capacity did not depend solely on BN surface areas, but also on their pore structures. More recently, a carbon-doped BN material was produced, exhibiting one of the highest CO_2 sorption capacities reported for BN materials.[88] A higher CO_2 affinity was shown on CBN compared to pure BN (capacity of: 3.9 *vs* 1.7 mmol/g at 25 ºC and 1 bar), highlighting the importance of surface chemistry in adsorption.[88] Furthermore, OH and NH_2 functional groups were identified in other studies as responsible for enhancing CO_2 sorption capacity.[110, 114] In general, however, the CO_2 sorption capacity in porous BN materials remains relatively low when compared to other classes of adsorbent materials, such as MOFs,[115] likely due to the weak interactions of CO_2 molecules with BN materials.

Porous BN materials were tested for hydrogen storage applications, for instance, Li *et al.* reported a hydrogen adsorption of 5.6 wt.% at room temperature at a pressure of 3 MPa.[90] The uptake capacity was attributed to: i) large micropore volume and surface area; ii) polarity of the B-N bond; iii) presence of structural defects. Weng *et al.* [94] synthesised porous BN by a similar method and the H_2 adsorption increased with increasing synthesis temperatures up to 2.3 wt.% (at -196 ºC, 1 MPa), but did not directly correlate to BN textural features (*i.e.* surface area and micropore volume). The authors attributed this adsorption behaviour to the presence of inhomogeneities in BN samples with more or less "active sites" for H_2. However, these active sites were not properly defined. Lei *et al.* synthesised oxygen-doped BN with a BET surface area of 536 m^2/g.[93] This BN adsorbed up to 5.7 wt.% of H_2 at 5 MPa and room temperature, and upon lowering the pressure to ambient conditions, 89 % of the hydrogen was recovered. The H_2 sorption/desorption cyclability was also evaluated over 15 cycles with minimal decrease in capacity. Their calculations demonstrated that oxygen impurities have a positive effect on hydrogen adsorption.

Porous BN materials were also tested for paraffin/olefins separation.[113] Porous BN showed higher affinity to paraffins compared to olefins (*e.g.* kinetic selectivity of methane/ethane: 15). The authors suggested that the adsorption mechanism is solely related to dispersion forces, as

the amount of gas adsorbed increased with i) molecular weight of the adsorbates; ii) the boiling point of the adsorbates (higher boiling point compounds are more likely to condense or adsorb).

In general, porous BN materials showed promise for gas sorption applications and were usually synthesised with template-free bottom-up methods. However, the mechanisms of adsorption are not always clear in the literature and their understanding alongside the tuning of porous BN properties may allow for significant improvements in BN gas uptake capacity.

Table 1-1 Summary of literature papers in which BN was tested for gas sorption with brief synthesis description, BET equivalent surface area in m^2/g, remarks and references.

Synthesis method	Surface area [m^2/g]	Species adsorbed (and adsorption capacities) [mmol/g]	Adsorption tests conditions T [°C]	Adsorption tests conditions P [bar]	Remarks	Ref.
Bottom-up template-free: Synthesis from polymeric precursors under dry nitrogen atmosphere. Pyrolysis in vacuum up to 800-1000 °C or under NH_3.	437-712	CO_2: ~0.4-5.5 CH_4: ~1.5	0	1	No correlation between BET surface areas and gas sorption capacities. CH_4/CO_2 selectivity could be correlated to differences in micropore sizes between samples.	109
Bottom-up template-free: Boric acid/urea in different ratios (1:6, 1:12, 1:24, 1:48,1:72) dissolved in water (65 °C). Water evaporated, product heated up to 900 °C under N_2.	927 (for ratio 1:48)	CO_2: 7.3	-80	~0.9 P/P_0 = 0.85	Sorption measured on highest surface area sample	91
		H_2: 2.5	-196	1		
Bottom-up template-free: MgB_2 and NH_4Cl heated up to 1050 °C under NH_3 atmosphere. The product was washed with HCl and water.	236 (highest for 650-750 °C)	CO_2: ~0.4	25	1	MgB_2 promoted crystallisation at low temperatures. Different CO_2 sorption capacities for 2 samples with similar surface areas. Relatively high selectivity of CO_2 over N_2.	87

Bottom-up template-free: Melamine and boric acid (varying molar ratios) were dissolved in water at 90 °C until evaporation. Heat-treatment at 800 °C under Ar. BNC samples obtained (brown colour). Further heat-treated at 800 °C under NH_3 to obtain BN.	1132 (highest for BN) 877 (highest for BCN)	CO_2: 5.6 CO_2: 1.2 CO_2: 1.5 CO_2: 3.9 CO_2: 1.7 (for pure BN)	0 25 25 25 25	1 0.1 0.15 1 1	Highest sorption capacities of CO_2 for BCN compared to BN. CO_2 sorption depending on pore size and chemistry. Pore size less than 0.7 nm preferred for CO_2. Q_{st}= ~27 kJ/mol for BN and 32-35 kJ/mol for BCN. CO_2/N_2 IAST selectivity of 18 for BN, 74 for BCN.	[88]
3D BN foam *via* top-down method: h-BN industrial powder was oxidised, exfoliated and cross-linked using PVA. In-situ free-drying to form PVA/BN sponge.	124 (with 1 wt % PVA)	CO_2: 7.3 CO_2: ~0.9	25 25	50 10	CO_2 adsorption simulations were performed. Strong affinity of CO_2 with the hydroxyl and CH_3 groups in the PVA.	[110]
Bottom-up template-free: Urea/ melamine/ biuret and boric acid precursors mixed in different molar ratios. Synthesis at 1050 °C in N_2.	1924	CO_2: ~ 1.6 CH_4: ~ 0.6 CO_2: ~ 8.0 CO_2: ~ 10.0	25 25 25 10	1 1 20 20	Paper published by our group as a comparison. CO_2 adsorption increases with increasing surface areas. High CO_2 capacity at high pressure. Q_{st}~18 kJ/mol.	[111]
Bottom-up template-free: Melamine: boric acid (1:2 molar ratio) dissolved in water at 85 °C, filtered, washed and dried. Multi stage heating up to 1460 °C. under	1687	H_2: 27.8	25	30	The H_2 capacity increases monotonic with pressure. 83.9 % of the hydrogen could be released when the pressure was lowered to 1 bar.	[90]

N_2. Post-treatment at 550 °C in air overnight.						
Bottom-up template-free: Melamine: boric acid precursors (1:2 molar ratio) dissolved in water at 90 °C until evaporation. Product heated to 1100 °C in NH_3. BN sonicated for 30 min in IPA.	1488 (for synthesis at 1000 °C)	H_2: 11.4	-196	10	The H_2 capacity increases with increasing synthesis temperature (highest H_2 capacity for sample synthesised at 1100 ºC = 1144 m^2/g). The H_2 uptake does not depend on surface area and micropore volume. Sample with highest H_2 uptake has larger total pore volume: 0.9 cm^3/g.	94
Bottom-up template-free: Urea: boron trioxide precursors (5:1 molar ratio) dissolved in methanol, then heated up to 1100 °C under N_2 /H_2. BN with 4 at % oxygen obtained.	536	H_2: 28.3	25	50	89 % of the hydrogen could be released by lowering the pressure to 1 bar. BN reused over 15 cycles. Simulations showed that oxygen-doping resulted in increased H_2 sorption capacity.	93
Bottom-up template: CTAB template, ammonia borane (AB) precursor (CTAB/AB weight ratio varied up to 10) dissolved in ethanol and dried. Heat-treatment at 1150 ºC under NH_3.	1401 (highest CTAB/AB ratio)	H_2: 5.0	-196	1	BN surface areas and micropore volumes increase with CTAB/AB ratio. H_2 sorption measured on the highest surface area sample. Typical isotherm for physisorption of H_2.	76

Bottom-up template-free: Boric acid: dicyanamide (in different molar ratios) dissolved in water and water evaporated. Heated up to 1200 °C under NH_3.	1900 (Dcy/BA = 3:1 and at 800 ° C)	H_2: 12.9 H_2: ~ 6.9	-196 -196	10 1	The H_2 uptake increased with increasing BET surface areas. Similar H_2 capacities as previous reports. [76, 94]	[92]
Bottom-up solvo-thermal: NH_4BF_4, NaN_3 and S mixed and pressed into pellets Heated in autoclave at 320 °C for 20	215	H_2: 20.3	25	100	H_2 capacity increased with increasing BN surface area. Reversible sorption capacity. The authors suggested that the large void spaces (macropores) in the hollow spheres could help to store H_2. Moreover, the B-N bonds on the bent surface of the spheres have an additional dipole moment, increasing interactions with H_2.	[116]
Bottom-up template-free: Urea and boric acid (12:1 molar ratio) dissolved in DI water at 65 ºC until evaporation. Heat-treatment at 900 ºC under N_2.	627	HCHO: 0.6 (with 20 ppm of formaldehyde in air)	25	1	The authors suggested that hydroxyl or amine groups are important in increasing BN interactions and adsorption of HCHO. Adsorption performance decreased during the first 4 runs and then stabilised to 9 mg/g.	[112]
Bottom-up template-free: Melamine and boric acid (1:2 molar ratio) and NaCl were dissolved in water at 80 °C and the water evaporated. Heat-treatment to	364	HCHO: ~12.7	25	1	NaCl promoted crystallization of h-BN at lower temperatures. More crystalline BN exhibited higher stability after regeneration over 15 cycles. NaOH	[85]

1050 °C under Ar. A crystalline BN obtained, further impregnated with NaOH.					impregnated BN showed improved formaldehyde removal capacity. HCHO was converted to less toxic products.	
Bottom-up template-free: Dicyandiamide and boric acid (3:1 molar ratio) dissolved in water until evaporation. Synthesis at 1050 ºC under NH_3. Post-treatment in air at 600 ºC.	1360	N_2: ~ 0.05 CH_4: ~ 0.5 C_2H_4: ~ 2.1 C_2H_6: ~ 3.0 C_3H_6: ~ 4.5 C_3H_8: ~ 5.5	25	1	Molecules with higher molecular weight or higher boiling points are preferentially adsorbed, which is attributed to the fact that adsorption is given by weak dispersion forces (physisorption) and that molecules with higher boiling temperatures prefer to be in a condensed/adsorbed phase. Higher affinity to paraffins compared to olefins.	[113]
Bottom-up template-free: Guanidine hydrochloride and boron trioxide (5:1 molar ratio) dissolved in methanol, mixture pressed into a cylinder by applying 3 tons. Heated to 1050 ºC in N_2.	1114 (pore sizes: 1.06, 1.92, 3.44 and 4.52 nm)	CO_2: 1.7	0	1	OH and NH_2 groups present, promoting NH_3 and CO_2 sorption capacities. Mesopores are beneficial to the adsorption, facilitating access to micropores. H-bonds formed between NH_3 and OH and NH_2 groups.	[114]
		CO_2: 0.8	25	1		
		NH_3: 5.3	25	1		

1.9.2 Water cleaning

A large amount of research is focusing on developing better adsorbent materials for the removal of contaminants from water. Porous BN materials have recently emerged as a promising solution because of their high adsorption capacities of inorganics (*e.g.* metal ions) and organics (*e.g.* dyes, oils and antibiotics) from water and possibility of being regenerated.[117] A full list of the papers is reported in Table 1-2.

Removal of inorganic pollutants

Li *et al.* [90] synthesised a porous BN material with high surface area (1687 m^2/g) which could remove up to 373 mg/g of Cu^{2+} ions from water, exceeding the capacities of other adsorbents such as carbonaceous materials.[117] The high sorption capacity was linked to high surface area and the presence of defect sites. The same authors further improved BN sorption capacity by producing an activated material with a template method (surface area over 2000 m^2/g) for the removal of metal ions from water.[74] Again, Li *et al.*[118] produced fluorinated porous BN, that despite the lower surface area (~1250 m^2/g) compared to their previous works, exhibited higher sorption capacities for metal ions, which was linked to the presence of functional groups (NH_2, OH). 3D BN foams were also tested for the removal of metal ions showing high sorption capacities (Cd^{2+}: 482 mg/g-561 mg/g), which was again attributed to the presence of functional groups (NH_2, OH).[95, 119] Generally, the adsorption mechanisms of BN materials for metal ions were: i) physisorption; ii) chemisorption; iii) electrostatic interactions; iv) hydrogen bonding; v) ion exchange.[117]

Removal of organic pollutants

Porous BN materials were tested for the removal of oils from water.[120-122] BN could adsorb up to 190 times its own weight in oils, and could be recycled either by burning in air, by washing with solvents or by heating at 600 °C in air. Interestingly, an increase in the d-spacing of the nanosheets was observed after oil adsorption.[120] This highlights the ability of BN to swell when it adsorbs hydrophobic liquids. The uptake of oil could be explained by two different factors: i) physisorption and ii) the capillary effect in the holes and in the interlayer of the nanosheets. Clearly, the oil sorption is not just due to physisorption, but other sorption mechanisms are involved. This was further confirmed by the synthesis of a BN 3D foam with low specific surface area (32 m^2/g) but high adsorption capacity for oil.[121]

A large number of studies (see Table 1-2) presented the use of porous BN for the removal of dyes from water and in this case no swelling of the material was observed. Instead, the mechanisms for dye sorption were associated to: i) π-π stacking interactions between the BN materials and aromatic dye molecules;[80, 123-124] ii) electrostatic dipole-dipole interactions between the polar B-N bond and the highly polar dyes;[123, 125] iii) physisorption due to high micropore volume and surface area of BN,[123, 125] and iv) hydrophobic interactions. The adsorption capacity was also found to be highly dependent upon the pH of the solution, which was due to electrostatic interactions with the polar dyes, which could be weakened by competitive adsorption of protons or hydroxides.[89, 126] For a similar reason, it was also found that OH-functionalised BN showed improved capacities for cationic dyes (*e.g.* methylene blue) when exhibiting a negative surface charge.[127] Porous BN materials showed higher sorption capacities of organics from water compared to some activated carbons.[117] Generally, however, any hydrolytic instability of BN was not reported. In fact, porous BN was often successfully regenerated by heating in air and reused for multiple adsorption and desorption cycles with a loss of efficiency of about 5-15 % after up to 10-15 cycles.[38, 74, 121, 127-128] However, it was mentioned that higher crystallinity confers to the BN material a higher stability when used in dye sorption applications, without linking this statement to hydrolysis.[127]

Another possible application for porous BN is the removal of antibiotics from water, however, although the removal capacity was impressive (over 10 times that of other nanomaterials adsorbents),[129] it was observed that when BN surface area was measured after regeneration, it had decreased significantly.[128] The decrease in surface area was attributed to remnant carbon after regeneration, rather than hydrolysis, which was not considered. The authors attributed the high sorption capacity for antibiotics to: i) high surface areas and pore volumes; ii) the crumpled structure of BN; iii) π-π interactions; iv) Lewis acid-base interactions between amine groups and BN.

Interestingly, in most studies in which BN was tested for adsorption applications, the material was synthesised using bottom-up techniques. However, a paper recently presented a study of adsorption using nanosheets prepared *via* ball-milling (*i.e.* a top-down method).[38] BN and NH_4Cl powders were milled under a nitrogen atmosphere with steel balls. The BNNSs obtained exhibited a high specific surface area (751 m^2/g) and a type IV N_2 adsorption isotherm. The authors tested the nanosheets for adsorption of Lysozyme (a model protein) from water and demonstrated successful recycling of the BN after protein adsorption.

In conclusion, porous BN materials showed promise in water cleaning applications, from both organic and inorganic pollutants. However, the instability of porous BN materials in water was not assessed, although the materials were often regenerated and tested for multiple sorption cycles, showing a relatively low decrease in performance.

Table 1-2 Summary of literature papers in which BN was tested for liquid separations and water cleaning with brief synthesis description, BET equivalent surface area in m^2/g, remarks and references. Tests performed at ambient temperature and pressure.

Synthesis method	Surface area [m^2/g]	Species adsorbed (and adsorption capacities)	Remarks	Ref.
Bottom-up template-free: Guanidine hydrochloride and boron trioxide (5:1 molar ratio) mixed in methanol. Then heat-treated up to 1100 °C under N_2/H_2 gas flow.	1427	Engine oil: 29000 mg/g Congo red: 782 mg/g Methylene Blue: 313 mg/g Basic Yellow: 556 mg/g	Shift in the (002) peak from XRD for BN after oil sorption, indicating an increased d-spacing because of oil intercalation. Ethanol generated a smaller enlargement of the interlayer spacing. No swelling or capillary effects occur in dye sorption from water.	[120]
Bottom-up template-free: Melamine: boric acid (1:2 molar ratio) dissolved in water at 85 °C, filtered, washed and dried. Multi stage heating up to 1460 °C under N_2. Post-treatment at 550 °C in air overnight.	1687	Methyl orange:298 mg/g Cu^{2+}: 373 mg/g	Methyl Orange (MO) contains aromatic rings, which can have electrostatic interactions with BN. 100 mg of BN used in 250 mL solution (40 mg/L) of MO. ~88 wt % removal within 5 min. BNNSs can be regenerated in air at 350 ºC.	[90]
Bottom-up template: Melamine and boric acid (1:2 molar ratio) dissolved in water 0.1 M HNO_3 solution (pH=6.5). P123 added as a structure directing agent. Product calcined at 546 °C and then	2078 (Pore sizes: 1.3,	Cr^{3+}: 352 mg/g; Co^{2+}: 215 mg/g Ni^{2+}: 235 mg/g Ce^{3+}: 282 mg/g Pb^{2+}: 225 mg/g	Study compared to previous.[90]Activated BN exhibits improved sorption capacity. BN was regenerated at 400 ºC in air and reused over 6 cycles for tetracycline removal from water, showing ~14 % decrease in removal capacity.	[74]

heated at 1300°C under N_2. "Activated BN" with many impurities obtained.	2.7 and 3.9 nm)	Tetracycline: 305 mg/g Methyl Orange: ~400 mg/g Congo red: ~ 350 mg/g		
Bottom-up solvo-thermal: NaN_3 and NH_4BF_4 (1:4 molar ratio) mixed and ground in glovebox. Powder placed inside a teflon tube with benzene and hot-pressed in autoclave at 260 °C and 150 MPa. Finally, powder filtered and dried. 3D nanocarpets obtained with low crystallinity and large number of defects.	117	Methylene blue: 272 mg/g	2 mg of BN added to 5 mL methylene blue solution (10 mg/L), 99 % removal within 10 s. The authors proposed that π-π stacking interactions help in the adsorption of methylene blue on BN. In another experiment the selectivity of BN for methylene blue over $CuSO_4$ was shown.	80
Top-down mechanical exfoliation: h-BN and NH_4Cl (1:30 weight ratio) ball-milled for 7 h under N_2. Powder calcined at 400 °C under N_2/H_2 flow to remove NH_4Cl. BNNSs obtained.	751	Lysozyme: 312 mg/g	4 mg of BNNSs used for removal of Lysozyme from water (10 mL solution with 60 mg/L concentration) and showed 99 % removal in 180 min. BNNSs regenerated *via* heating in air showed 90 % removal capacity after 10 cycles.	38
3D BN from bottom-up: Ammonia borane and thiourea (1:12 molar ratio heated under N_2 up to 1200 ºC. Thiourea acted as foaming agent. 3D BN foam obtained.	32	Methylene blue: ~500 mg/g ... Methyl orange: 384 mg/g Pump oil: 115000 mg/g Tetrachloromethane: 190000 mg/g	Although the foam exhibited low surface area, it showed good sorption capacity for organic solvents. It was proposed that solvents could be stored in the bubble volume more than being adsorbed on the surface. BN regenerated at 400 ºC in air after methylene blue sorption, slight decrease in capacity (~7 %).	121

Bottom-up solvo-thermal: Procedure taken from Lian et al.[116] NH_4BF_4, NaN_3 and S made into pellets. Heated at 320 ºC in autoclave and washed. BN hollow spheres produced.	210	Polychlorinated biphenyls	Excellent removal capacity of aromatic pollutants at trace levels from water.	[81]
Bottom-up template-free: *BN nanoparticles*: Melamine and boric acid (1:1 molar ratio) sintered at 200 ºC and then 300 ºC under N_2, pulverised, heated at 1400 ºC under N_2. *BN nanosheet*: Urea and boric acid (12:1 molar ratio) dissolved in water at 65 ºC until evaporation. Heated at 900 ºC under N_2. Washed in DI water.	50-120	Brilliant Green Methyl Orange Max adsorption not calculated.	High crystallinity for both materials. Dye sorption greatly affected by pH due to surface charges and adsorption sites: *e.g.* Brilliant green removal capacity was higher with pH > 7, as the dye is positively charged and if H^+ are present there is competitive adsorption.	[126]
Bottom-up template-free: Melamine and boric acid (molar ratio of 1: 2) dissolved in water at 90 °C. Cooled to room temperature to form a precipitate ($C_3N_6H_6 \cdot 2H_3BO_3$), filtered and dried. Heated at 1000 °C under NH_3. Ag nanoparticles added.	670	Rhodamine B: 308 mg/g (on BN/Ag) Rhodamine B: 431 mg/g (on BN)	Ag nanoparticles added due to SERS (surface enhanced Raman spectroscopy) activity but do not contribute to adsorption. BN/Ag stable at 400 ºC	[130]
Bottom-up template-free: Synthesised from reference[120]. Guanidine hydrochloride and boron trioxide (5:1 molar ratio) mixed in methanol Heated at 1100 °C in N_2/H_2.	1427	Antibiotics: CTC: 1170 mg/g TC: 284 mg/g CIP: 206 mg/g NOR: 174 mg/g	The surface area of BN was measured after regeneration by heating in air and decreased to 940 m^2/g. It was suggested that residual carbon is responsible for the decrease. 10 % decrease in performance for CTC removal after 10 cycles	[128]

Bottom-up template-free: Melamine and boric acid (1:3 molar ratio) dissolved in water at 85 ºC. Hot solution then frozen by liquid nitrogen and dried using freeze dryer. Heated to 1000–1300 ºC under N_2	515 (at 1100 °C) (Pores sizes: 1.4, 1.7, 2.7 nm)	Methylene blue: 107 mg/g.	Fast adsorption of methylene blue: BN (50 mg) in methylene blue solution (200 mL, 20 mg/L), 98 % of dye removed in 2 minutes. High adsorption linked to high surface area, negative charge of BN and fiber morphology with many micropores on the external surface favouring adsorption.	[125]
3D BN from bottom-up: Formaldehyde, dicyandiamide and boric acid in a reflux device at 85 °C. Polymerised at 180 °C, heated up to 1200 °C under NH_3.	1406 (at 1100 ºC)	Salad oil: 5000 mg/g Rhodamine B: 554 mg/g Cd^{2+}: 561 m/g	BN sponge recycled after oil sorption by heating under NH_3 and little/no decrease in adsorption capacity observed. Continuous adsorption setup for Rhodamine B performed. 90 % of RhB could be removed by ethanol. The authors suggest that BN is stable. Sorption of other oils evaluated: cyclohexane, pentane, hexane amongst others. -OH and -NH_2 groups present in BN.	[119]
3D BN from bottom-up: Ammonia borane and CTAB with polyHIPE foam templates (PS, PAN and PEHA). Heated at 1150 °C under NH_3.	180	Used engine oil: ~18000 mg/g Dichlorobenzene ~ 14000 mg/g Toluene ~ 16000 mg/g Cyclohexane: ~5000 mg/g Ethanol: ~ 14000 mg/g	3D BN foam is highly hydrophobic: ~144º contact angle.	[122]
Bottom-up template-free: Melamine and boric acid (1:1 molar ratio) mixed in water. Heated at 900 °C in N_2/H_2. BN	964 (2 nm average	Rhodamine-B: 210 mg/g Methylene blue: 13973 mg/g	The pH of the dye solutions was adjusted to maximise dye adsorption. Good adsorption capacity for antibiotics. BN recycled after methylene blue adsorption by treatment in air at	[89]

with little/no oxygen atoms observed from XPS.	pore diameter)	Sulfamethoxazole 330 mg/g	400 ºC; capacity still 80 % after 10 cycles. Adsorption tests performed at different temperatures to study the thermodynamics of adsorption confirmed physisorption occurred. Adsorption given from micropores, surface area, defects, non-covalent π-π interactions between BN and dye's aromatic rings.	
Bottom-up template-free: Urea and boron trioxide 10:1 molar ratio) dissolved in methanol until evaporation. Heated at 1000 °C in N_2\H_2 atmosphere.	1156	Basic Yellow: 424 mg/g Congo Red: 718 mg/g	12 % decrease in adsorption capacity after 15 cycles. Dye sorption attributed to surface area, hierarchical pore structure, π-π interactions, electrostatic attractions.	[123]
Bottom-up solvo-thermal: NH_4BF_4, NaN_3 and S mixed and pressed into pellets Heated in autoclave at 320 °C for 20	215	Basic Yellow: 192 mg/g Methylene blue: 116.5 mg/g	BN preferentially adsorbs aromatic organic compounds over heavy metal ions from water. Regeneration can be performed by heating in air at 300 ºC.	[116]
3D BN from bottom-up: CVD deposition of borazine precursor onto carbon aerogel template at 900 °C in Ar/H_2 atmosphere. Post-treatment heating under oxygen at 600 ºC to remove carbon. BN aerogels obtained with BNNSs and BNNTs.	1051	Cyclohexane: 160000 mg/g	BN could be regenerated after burning the oil in air. However, some residual carbon was present, making the material black after regeneration.	[131]
Bottom-up template-free: Melamine and boric acid (1:9 molar ratio) mixed in acetone and dried. Heat-treated at 300 °C. Pellets of BN made using 3 t.	2	Engine oil: 56800 mg/g Chloroform: ~35000 mg/g Toluene: ~25000 mg/g	Large amounts of oxygen and carbon present and very low surface areas.	[132]

3D BN foam from bottom-up: Functionalised h-BN was cross-linked and lyophilisation was performed to give a 3D monolith.	Non porous	Used engine oil: ~ 2000 mg/g	Macroporous solid monolith with low surface areas. Regeneration *via* burning of the oil in air. OH groups present.	[133]
Bottom-up template-free: Urea and boron trioxide (5:1 molar ratio) mixed in methanol, stirred and dried. Heated to 1100 °C in N_2/H_2. Used to produce membranes with PVDF.	1427	Methylene blue and pharmaceuticals.	The pharmaceuticals and dyes used in the adsorption tests have high polarity and can interact with BN *via* dipole-dipole interactions or π-stacking.	[124]
Bottom-up template-free: Urea and boric acid (3:1 molar ratio) were dissolved in methanol, mixed, dried and then heated at 900 °C under N_2.	1320	Polychlorinated biphenyls	Simulations were performed and indicated π-π, hydrophobic and electrostatic interactions between BN and polychlorinated biphenyls.	[134]
Bottom-up CVD with template: Carbon nanotube film used as a template. Precursors: B, MgO, Fe_2O_3 , NH_3 CVD process at 1200 ºC. Calcination in air at 650 °C to eliminate the template. Freestanding BNNS film obtained.	N/A	Oil/water emulsions separation through filtration	High hydrophobicity of BNNSs attributed mostly to the roughness of the material.	[135]
Bottom-up template-free: Urea and boric acid (48:1) dissolved in water, heated to 900 °C in N_2. BN ground and washed with water.	126 (3.8 nn pores)	Perfluorooctanesulfonate (PFOS): ~57 mg/g Perfluorodecanoate: (PFDA): ~90 mg/g	Adsorption attributed to electrostatic interactions. h-BN regenerated *via* heating in air at 600 ºC and showed good sorption recyclability after 3 cycles.	[136]

3D BN foam from bottom-up: Silica aerogel template, nitrogen and boric acid precursors, CVD at 1700 °C under N_2. 3D foam soaked into PMMA solution to prepare a composite.	166	Chloroform: ~45000 mg/g Hexane: ~20000 mg/g Acetone/ethanol: ~2500 mg/g	Super hydrophobic PMMA/BN foam. High adsorption attributed to high porosity, capillary effects and lipophilicity. Regeneration through burning of the oils. Efficiency ~98/99 % after 30 cycles.	[137]
Bottom-up template-free: Melamine and boric acid (2:1 molar ratio) dissolved in water until evaporation. Multi stage heating up to 1560 ºC under NH_3. Activation using H_2SO_4/HNO_3 aqueous solution and sonication. Sonication for 30 min at room temperature and stirring in water at 80 ºC for 2 h.	1045-1104 (Pore sizes: 1.4, 3.9 nm)	Methylene Blue: 392 mg/g Neutral red: ~190 mg/g Methyl Orange: ~100 mg/g	High degree of crystallinity which confers to h-BN a higher stability compared to t-BN. Activation creates NH_2/OH groups and defects on the surface, which enhance adsorption. Higher temperature (10-30 ºC) increased adsorption. Activated BN is negatively charged. High sorption of cationic dyes (*e.g.* methylene blue) and low sorption of anionic dyes (*e.g.* methyl orange). Electrostatic interactions are key in adsorption.	[127]
3D BN foam from bottom-up: Triethanolamine and boron trioxide (2:3 molar ratio) mixed in a hydrothermal reactor at 200 ºC to obtain a gel. Melamine and boric acid (1:2 molar ratio) dissolved in water to produce melamine diborate crystals. Gel and melamine diborate mixed (1:1), heated at 1100 ºC in N_2.	344	Methylene Blue: 408 mg/g Congo Red: 308 mg.g Gasoline: ~18000 mg/g Cr^{3+}: 453 mg/g Ni^{2+}:173 mg/g Cd^{2+}: 482 mg/g	BN can adsorb both anionic and cationic dyes. BN can be regenerated after dye sorption *via* heating at 500 ºC in air: ~72/89 % capacity after 10 cycles.	[95]
Bottom-up template-free: Melamine and boric acid (1:6 molar ratio) dissolved in water and dried in vacuum. Heat-treated	627	Methylene Blue: 631 mg/g	Porous BN can selectively adsorb methylene blue from a mixed solution with $CuSO_4$, attributed to strong π-π interactions. Regeneration was	[138]

up to 1100 °C in N_2. A post-synthesis treatment in HCl/water was performed to remove residual boron oxide.			performed at 600 °C in air and allows for the retention of 88% of the capacity after 5 cycles.	
Bottom-up template free: Melamine and boric acid (1:2 molar ratio)[90] dissolved in water. Multi-stage heat-treatment up to 1088 °C under N_2. Fluorinated BN (F-ABN) was then produced by dissolving NH_4BF_4 in water and bubbling nitrogen through it to carry the vapour into a reaction chamber heated at 250 °C.	1250 for F-ABN ($0.7\ cm^3/g$ pore volume) ~1.3 nm and ~3.9 nm pores	Cr^{3+}: 387 mg/g on F-ABN or Cr^{3+}: 149 mg/g on ABN	Higher sorption capacity of Cr^{3+} compared to previous work by the same group.[74] High sorption capacity attributed to: i) high surface area and large amount of pores; ii) bond polarity for B-N; iii) structural defects and functional groups, which are more abundant in F-ABN. Adsorbent recycled *via* acid elution and wash with NaOH solution. After 10 cycles 56 % removal capacity retained.	118
Bottom-up template-free: B powders mixed with catalyst (formed from $CoFe_2O_4$ and CoO) in different molar ratios heated to 1400 °C under NH_3.	197	Pump oil: 7800 mg/g Malachite Green: 324 mg/g Methylene Blue: 233 mg/g Cu^{2+}: 679mg/g Pb^{2+}: 537 mg/g Cd^{2+}: 107 mg/g	Despite the relatively low surface area the BN spheres exhibit high adsorption capacity. This was related to the radial orientation of the nanosheets, with a lot of edges available at the surface. The large d-spacing also allow for molecules to intercalate.	139

1.9.3 Catalyst or catalyst support

A catalyst support must present a high surface area, high oxidation resistance, chemical inertness, and high thermal conductivity to avoid hot spots and sintering of the metal particles. Catalyst supports should also avoid any reaction with water.[140] BN exhibits most of the required properties listed above and it was demonstrated that t-BN powder with low crystallinity can be used as a support for catalysts.[140-143] t-BN demonstrated a very high thermal stability and weak interactions between the support and the metal particles.[143]

Although BN materials were usually considered inert, it was recently demonstrated that h-BN or t-BN materials have catalytic properties and were used in oxidative dehydrogenation reactions,[144-147] opening the door to a whole new range of applications. However, catalysis deviates from the purpose of this thesis, and is, therefore, not discussed here in detail.

1.10 Conclusions and knowledge gaps from the literature

The number of papers in which porous BN or BNNSs were produced with high surface area and tested for adsorption applications remains relatively low (< 100 publications). Several synthesis or production methods have been explored with relative success, with each technique offering a different set of strengths and weaknesses.

Most of the papers in which BN was used for adsorption applications employed bottom-up synthesis methods. This is because top-down methods do not always provide the required energy to overcome lip-lip interactions in h-BN, leading to BNNSs in low yield. BNNSs produced *via* top-down methods are often crystalline in the 2D plane but lack tunable pore structures and significant surface areas, thus far. Moreover, exfoliated BNNSs are often obtained in solution and they tend to re-stack together when dried.

Bottom-up methods, on the other hand, can produce large quantities of t-BN, BNNSs or h-BN. Among the bottom-up synthesis methods, the template-free method is often preferred as it involves fewer chemicals and synthesis steps and is, therefore, more industrially relevant. However, in template-free methods it is hard to control the pore structure and surface area of the BN materials produced. In addition, the formation of porous BN *via* this route is not well-understood, in part due to the lack of understanding on the influence of the various synthetic parameters. Moreover, the presence of impurities and the crystallinity of porous BN produced can vary significantly from one work to another. Sometimes, these features are, in fact, not

reported at all. The porous BN produced *via* bottom -up methods exhibits limited crystallinity and a turbostratic nature with a large number of defects, features which are beneficial in adsorption. However, owing to these properties, t-BN was shown to exhibit hydrolytic instability and this issue was often overlooked in the literature.

Finally, the great potential of BN for adsorption was showed in a number of studies, however, there seems to be little understanding of the correlation between adsorption properties and the structure of porous BN sorbents. This understanding is key in order to optimise the chemical and physical features of BN and enhance its adsorption.

With the aim of addressing the knowledge gaps outlined above, the production of porous BN needs to be optimised, evaluating the influence of all the reactions' variables (*e.g.* temperature, heating rate, precursor chemistry and ratio, intermediate preparation) on the chemical and physical features of the material obtained. In addition to probing the effect of reaction variables, predictable and reproducible pathways to porous BN need to be established. A reliable method for the tuning of BN surface area and micro- and mesopore volume is also required. The chemical and physical structure of the porous BN must also be studied in more detail, with focus on the amount of oxygen and carbon impurities present in the porous BN material. Porous BN hydrolytic stability also needs to be evaluated and methods developed to overcome this issue. Finally, it is important to test the porous BN materials for applications in both gas and liquid separations, in order to understand the material's potential in separation, clarify the mechanisms of adsorption and the links between BN physical-chemical features and adsorption capacity.

1.11 Research aim and objectives

The aim of the project is to provide a proof-of-concept for the use of porous BN for liquid and gas separations.

1.11.1 Objective 1: To produce porous BN materials with high surface area and tuneable porosity

This objective aims at providing a better understanding of the relationships between the parameters used during the synthesis and the properties of the porous BN materials produced. This approach will potentially lead to porous BN materials with enhanced surface area and a tailorable porosity.

1.11.2 Objective 2: To evaluate and improve BN robustness and recyclability

The effects of moisture exposure on porous BN structure and chemistry needs to be studied in depth and related to the BN characterisation. This approach will potentially allow one to provide a way for minimising hydrolysis and improving BN recyclability and robustness.

1.11.3 Objective 3: To test BN for different adsorption applications

While Objective 1 focuses on the understanding of the relationships between the synthesis methods and the properties of the nanosheets, Objective 3, which is strongly linked to Objective 1, aims to specifically link the structure/chemistry of the porous BN materials to their adsorption properties.

Chapter 2: Methods

2.1 Porous BN powder synthesis

Porous BN was synthesised from solid precursor mixtures including at least one precursor containing nitrogen (*i.e.* urea, melamine, or biuret) and one precursor containing boron (*i.e.* boric acid or boron trioxide). The precursors were either dissolved in water and recrystallized prior to the synthesis, or simply mixed and ground. The precursor mixtures were then transferred to an alumina boat crucible inside a tubular furnace for pyrolysis. The crucible lid was left partially open (~2 cm), facing the nitrogen inlet. The tubular furnace was a Carbolite Horizontal tube furnace HST 12/600 equipped with a quartz tube of 80 mm internal diameter × 1050 mm length, a schematic representation of the synthesis setup is shown in Figure 2-1. The furnace was sealed with gas tight flanges and thermally insulated with ceramic plugs at both ends of the tube. Nitrogen (zero grade, BOC) was flowed at 250 mL/min for 3 hours prior to the start of the reaction, after which the flow rate was lowered to 50 mL/min, during the reaction. The precursors were then heat-treated under nitrogen gas flow and after heat-treatment the nitrogen was kept flowing while the furnace cooled naturally to ambient temperature. A trap and a bubbler filled with water were used at the outlet tube of the furnace, in order to prevent air from entering the system and to dissolve the ammonia and isocyanic acid produced during synthesis. The resulting BN was stored in a dessicator.

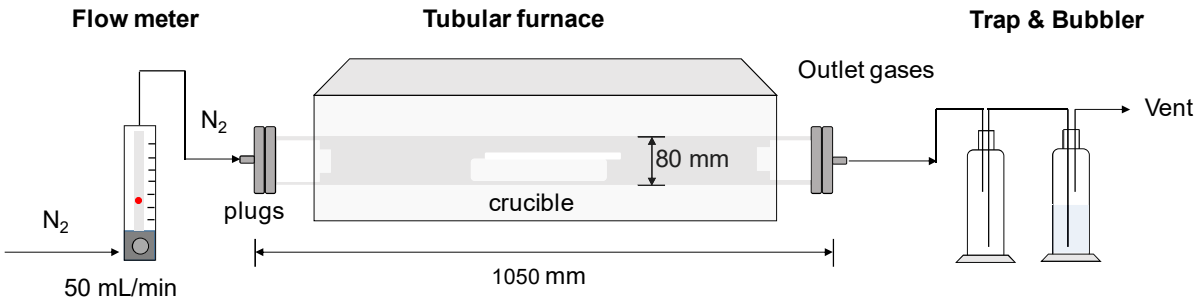


Figure 2-1 Schematic of tubular furnace set-up with flow meter and bubblers.

2.2 Porous BN pellet preparation

Dry porous BN powder (~200 mg) was coarsely ground with a pestle and mortar and was placed into a pellet die (Specac, 13 mm evacuable stainless steel). The die was positioned into a manual press and 5 tonnes of load were applied to form a pellet. The pellet was carefully removed from the pelletizer by inverting the die and applying a small load on its base.

2.3 Characterisation techniques

2.3.1 Structure

2.3.1.1 Pore structure and surface area: Nitrogen sorption isotherms at -196 ºC

Nitrogen physisorption isotherms were measured using a porosity analyser (Micromeritics 3Flex) at -196 °C. Prior to nitrogen sorption analysis the samples were degassed to remove molecules of gases or liquids adsorbed onto the surface. The degas step was performed by heating the samples overnight at 120 °C at roughly 0.2 mbar pressure and degassing them again *in-situ* on the porosity analyser for 4 h down to around 0.003 mbar at 120 °C.

This technique is a volumetric technique, which calculates the amount of nitrogen adsorbed onto the sample by measuring the change in pressure in the chamber.[148] Progressive amounts of nitrogen gas are dosed into the sample chamber and the pressure is monitored until it reaches equilibrium. The free space, which is the volume not occupied by the sample, is calculated at the end of the isotherm measurement analysis by dosing helium into the analysis chamber.[148] The nitrogen isotherms collected can then be used to estimate BET surface areas, total pore volumes, micro- and mesopore volumes and pore size distributions of BN samples.[7]

The equivalent surface areas of the samples were calculated by applying the Brunauer-Emmett-Teller (BET) method to the nitrogen isotherms (1)[8]:

$$\frac{1}{V\left[\left(\frac{P_0}{P}\right)-1\right]} = \frac{1}{V_m C} + \frac{C-1}{V_m C}\left(\frac{P}{P_0}\right) \quad (1)$$

Where:

V: volume of gas adsorbed (derived from the isotherm);

V_m: volume corresponding to the monolayer coverage;

P: equilibrium pressure for the gas (derived from the isotherm);

P_0: saturation pressure (derived from the isotherm);

C; constant.

The Micromeritics software was then used to plot the equation rearranged as (2):

$$\frac{1}{V\left[\left(\frac{P_0}{P}\right)-1\right]}VS\left(\frac{P}{P_0}\right) \quad (2)$$

From this plot V_m and C can be calculated from the intercept ($\frac{1}{V_m C}$) and slope ($\frac{C-1}{V_m C}$) and the BET surface area may then be calculated as follows in equation (3):

$$S_{BET} = \frac{V_m S_{adsorptive} N_{avogadro}}{V_M} \quad (3)$$

Where:

$S_{adsorptive}$: cross sectional area of adsorptive;

V_M: molar volume of the adsorptive at STP (22,414 cm^3/mol);

$N_{avogadro}$: Avogadro constant.

The BET surface area was calculated from the pressure range in which the data points fit a linear data fit and satisfy the following criteria:

- Pressure range V[P_0-P] increases with P/P_0;
- The pressure corresponding to V_m is within the pressure range selected;
- Negative intercepts are not acceptable.

The total volume of pores was calculated from the volume of N_2 adsorbed at $P/P_0 = 0.97$ using equation (4):

$$V_{tot} = \frac{P_{standard} V_{adsorbed} V_M}{RT} \quad (4)$$

Where:

$P_{standard}$: standard pressure (10^5 Pa);

$V_{adsorbed}$: volume of nitrogen adsorbed at $P/P_0 = 0.97$ (derived from the isotherms);

V_M: molar volume of liquid N_2 at 77 K (34.65 cm^3/mol);

R: gas constant;

T: standard temperature.

The micropore volume was determined using the Dubinin-Radushkevich method,[149] which is based on equations (5) and (6):

$$\log(n) = \log(n_{mic}) - D\left(log\left(\frac{P}{P_0}\right)\right)^2 \quad (5)$$

Where:

n: adsorption capacity at P;

n_{mic}: adsorption capacity from the micropores;

D: empirical constant;

P: equilibrium pressure (derived from isotherm);

P_0: saturation pressure (derived from isotherm).

Log(n) is then plotted against $(\log(P/P_0))^2$ allowing for the calculation of a value for n_{mic} from the intercept of the linear range of the plot.

The micropore volume is then calculated from (6):

$$V_{micropore} = \frac{n_{mic}M}{\rho} \quad (6)$$

Where:

M: adsorbate molar mass;

ρ: adsorbate density.

The mesopore volume was calculated by subtracting the micropore volume from the total pore volume. Pore size distributions were estimated using a DFT model for carbon materials with slit pores (using the SAIEUS program provided with the 3Flex porosity analyser). The NLDFT model for carbons with slit pores at 77 K in N_2 (see footnote) was adopted.

2.3.1.2 Micro/nano-scale morphology: SEM

Scanning electron microscopy (SEM) is a technique, which uses the signal generated from an accelerated and focused electron beam onto a conductive sample. The beam (2-40 keV) is generated by an electron gun and accelerated to an anode.[150] The electrons are then focused and scanned through a sample by using a set of electromagnetic lenses (condenser, objective and scan coils). When the primary electron beam hits the sample, different phenomena occur:

- Backscattered electrons (BE): [150] BE are generated from the primary electron beam which is elastically scattered. These electrons have high energy (as the primary electron beam) and are scattered more by heavier elements. Therefore, contrast in BE images depends on the material's composition. Images in BE mode have a lower resolution as the interaction volume of the high energy electrons with the sample is higher compared to other signals, such as secondary electrons;
- Secondary electrons (SE): SE are generated from primary electrons expelling the samples' electrons out of their orbitals. SE have lower energy than BE (~50 eV), therefore only

http://www.nldft.com/

electrons closer to the surface can escape.[150] This gives a better resolution compared to BE imaging mode, as well as a much more pronounced topographic contrast.

- X-rays: X-rays are generated when primary electrons knock electrons out of their inner shells, triggering an electron from an outer shell to move down in energy to replace it. This energy difference is dissipated by generating characteristic X-rays (up to ~10 keV), which can give information about the material's composition as their energy matches with the energy difference between the two atomic orbitals. X-rays can be collected with two different types of detectors: Energy dispersive X-ray spectroscopy (EDX) or wavelength dispersive X-ray spectroscopy (WDX).

For porous BN, the morphology of the samples was evaluated using a scanning electron microscope (SEM, Leo Gemini 1525, Zeiss) in secondary electron mode (InLens detector) at 5 kV. The samples were ground, deposited on carbon tape and coated with 20 nm of chromium to reduce charging in the microscope. The chemical composition and elemental distribution was also measured at 5 kV with an EDX detector.

2.3.1.3 Crystalline structure: X-ray diffraction

X-ray diffraction (XRD) is a non-destructive bulk technique used to characterise the crystal structures of materials. In powder XRD the material is finely ground and each set of crystalline planes constructively diffracts X-rays at specific angles (θ) (Figure 2-2). Crystalline patterns plot the intensity of X-rays diffracted at different angles and they can be used to determine the type of crystalline structure obtained, the spacing between different set of planes (d-spacing), the crystallite sizes and preferential orientations. Bragg's law (7) is then used to calculate the d-spacing:

$$n\lambda = 2dsin\theta \quad (7)$$

Where:

n: integer;

λ: wavelength;

d: spacing between planes;

θ: angle between incident X-rays and crystal lattice.

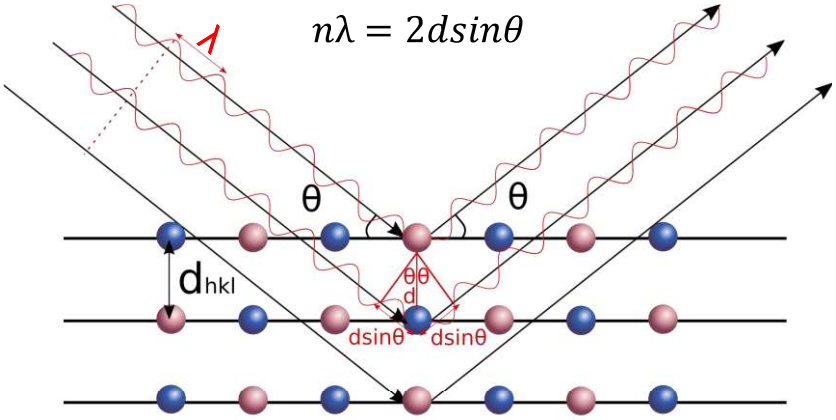


Figure 2-2 X-ray diffraction principle with Bragg's equation.

Powder X-ray diffraction (XRD) was performed using an X-ray diffractometer (PANalytical X'Pert PRO) in reflection mode. The operating conditions included an anode voltage of 40 kV and an emission current of 40 mA using a monochromatic Cu Kα radiation (λ = 1.54178 Å). The XRD detector used was X'Celerator (silicon strip detector). The samples were finely ground before analysis.

For BN materials, XRD was mainly used to identify the type of crystalline structure obtained: hexagonal or turbostratic. While h-BN exhibits the typical graphitic hexagonal pattern with sharp high intensity peaks, t-BN exhibits only two broad low intensity peaks typical for turbostratic materials.[97] This is because the different 2D layers of t-BN are randomly orientated, lacking crystalline order.

The peak position for the (002) peak for h-BN or t-BN is of particular importance as it allows for the calculation of the d(002)-spacing by applying Bragg's equation (Figure 2-3).[151] The interlayer spacing for h-BN is 3.33 Å, and is larger for t-BN materials.[97]

In XRD, different sets of parallel planes are named with Miller indices (h k l) when they intercept the unit cell edges in a/h, b/k and c/l. XRD patterns with two broad low intensity peaks for the (002) and (101) reflections for t-BN, can also indicate the presence of few-layer BNNSs.[152] Nanosheets, similarly to few-layer graphene, lack stacking order due to their exfoliated nature. Therefore, to gain more insight into BN crystalline structure, XRD needs to be coupled with high-resolution transmission electron microscope.

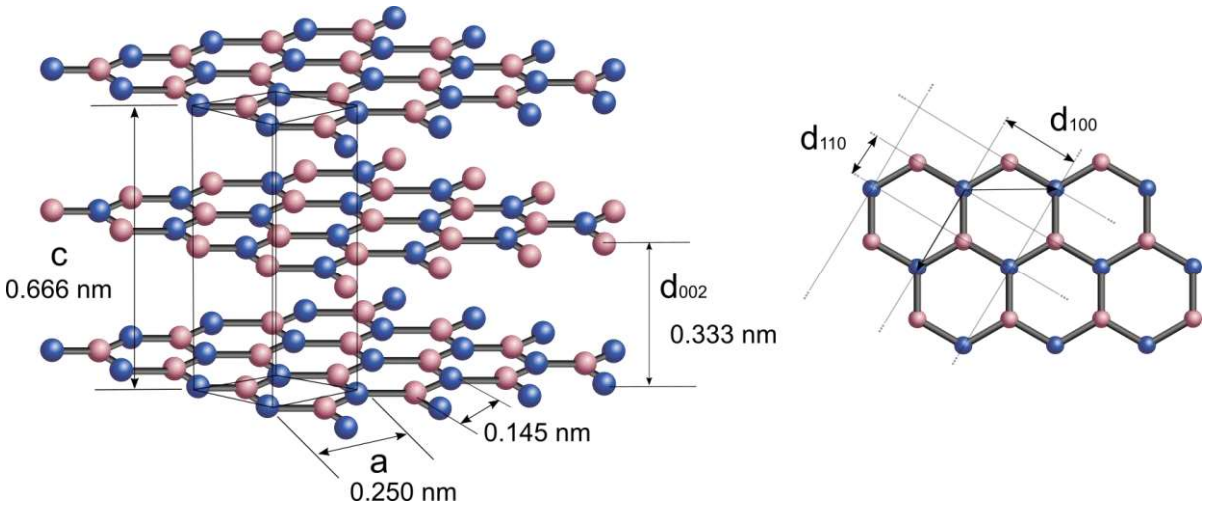


Figure 2-3 Crystalline structure with the different d-spacings for crystalline h-BN materials. (Unit cell dimensions from [97])

2.3.1.4 Nano-scale morphology and crystalline structure: Transmission electron microscopy

Transmission electron microscopy (TEM) is a characterisation technique which uses the information collected from electrons transmitted through the sample, rather than scattered as in SEM. Electrons are again produced from electron guns, with acceleration voltages of ~100-400 kV.[153] Electrons are focused onto the sample by using a set of condenser lenses and apertures and the transmitted beam is then magnified and focused onto a screen to display the image.[154] In order for electrons to be transmitted through the samples, these have to be sufficiently thin, depending on the samples' average atomic number and the acceleration voltage used. Although, theoretically, TEM should be able to image with sub-atomic resolution,[153] the actual resolution cannot reach the wavelength limit and for a Jeol 2100Plus, which was used in collecting most of the images presented in this thesis, the point resolution is 0.23 nm. In imaging mode the contrast is given mainly by thickness, electronic composition and crystalline orientation of the sample.

For porous BN powder samples, the powder was dispersed in ethanol and deposited on a copper carbon holey grid and the microscope was used in imaging mode (not diffraction mode). Fast Fourier transform (FFT) patterns were calculated using ImageJ[155] software on the images collected, which allowed for the identification of any crystalline patterns present. Angus Crake helped in the collection of some of the TEM images presented in Chapter 6.

2.3.1.5 3D imaging: Scanning TEM tomography

Scanning TEM (STEM) is a type of electron microscope equipped with scanning coils to focus and raster the beam across the sample. The microscope can be operated in standard imaging mode by analysing the main transmitted beam signal (bright field, BF), or in dark field mode (DF) in which the detector is not in line with the transmitted beam and collects diffracted electrons. The advantage of DF mode is that the contrast in images is given mainly by atomic number and thickness, limiting the effects due to crystal orientations.[156-157] Electron tomography is a technique which allows for 3D reconstructions of samples by collecting images of the specimen tilted at various angles.[157] STEM tomography was performed on DF images collected with the help of Dr. Catriona McGilvery and the reconstructions were performed with the help of Josh Bailey. The technique was employed to directly visualised pore shape, size and connectivity for mesopores in BN samples with different pore structures.

TEM and STEM imaging were carried out on an FEI Titan 80-300 Cs image-corrected microscope, operating at 80 kV and 300 kV. Sample preparation was performed by dispersing porous BN powder in ethanol and drop-depositing the supernatant on a holey carbon copper grid. STEM images were acquired using a convergence semi-angle of 10 mrad and an inner and outer collection angle to the high angle annular dark field (HAADF) detector of 40 and 196 mrad, respectively. The bright contrast in the STEM images is from regions containing higher atomic number and/or density. For the tomograms, STEM images were acquired every 2° from -54 and +74° and between -70 and +74°. The images were aligned and reconstructed using Inspect3D (FEI Visualization Group). A total of 64 and 62 images were used in each of the final reconstructions. The initial reconstruction was carried out using a weighted back projection algorithm and then reconstructed using 25 iterations of a simultaneous iterative reconstruction technique algorithm. The reconstructed 3D TEM tomography data set was imported into Avizo (FEI Visualization Group, France) as a .rec file.

Image processing steps were taken to remove the noise in the data, thus allowing a more reliable subsequent segmentation. A 3D Median filter was applied with a neighbourhood setting of 26 and 3 iterations, followed by a standard 3D Gaussian filter with a kernel size of 5. Manual verification through all slices confirmed that no major loss of features was encountered using this filtering procedure. A manual threshold was then applied to identify ‘seed’ voxels in the two phases, by first selecting the high grayscale values attributable to the BN material. Subsequently, the remaining unassigned voxels were selected and shrunk by 10 voxels in all directions, allowing for growth towards the true interface in the next step. A typical watershed

segmentation procedure was then followed *via* a gradient mask and inundation process leading to all voxels being assigned as either pore or BN. To account for small numbers of inaccurately labelled pores, a simple threshold procedure was followed within the BN label field to re-label these voxels. No smoothing or simplification was applied on generating the 3D surfaces. To demonstrate the distinct pore morphologies of each of the two samples, a sub-volume was extracted from each 3D dataset and a surface generated for the pore phase.

2.3.2 Chemistry

2.3.2.1 Surface chemistry: X-ray photoelectron spectroscopy

X-ray photoelectron spectroscopy (XPS) is a surface analysis technique, which employs X-rays with a known energy (hν) to irradiate a sample in a vacuum. When the X-rays hit the sample, electrons are knocked out from their orbitals (photoelectrons) with a certain kinetic energy, which depends upon the energy of the light source, the binding energy and a work function as shown in Figure 2-4.[158] The spectra plot binding energy *vs* intensity allow for the gaining of information regarding elements present, chemical states and surface elemental quantification.[158] In order to compensate for the electrons lost in a sample and provide charge compensation, an electron flood gun is used during the analysis.

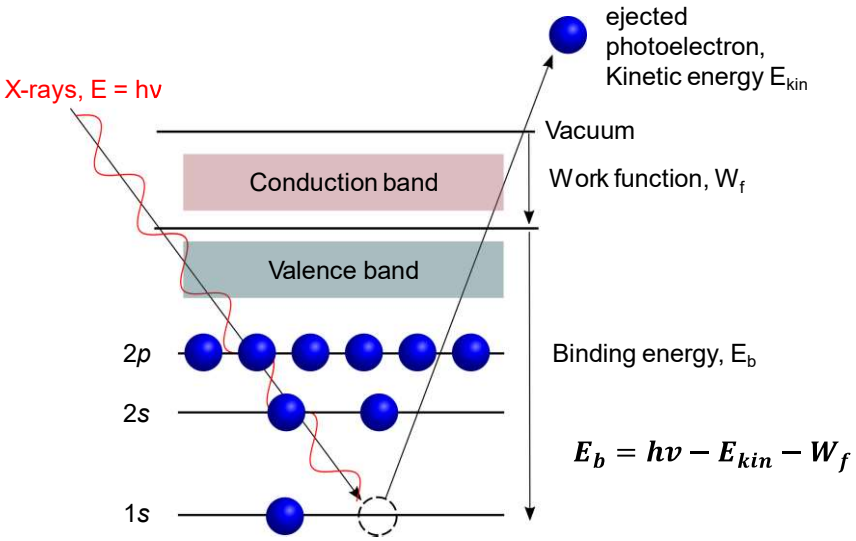


Figure 2-4 Schematic for the principles of XPS analysis with equation.

XPS was performed using a Thermo Scientific K-Alpha$^+$ X-ray Photoelectron Spectrometer equipped with a MXR3 Al Kα monochromated X-ray source (hν = 1486.6 eV). X-ray gun power was set to 72 W (6 mA and 12 kV). Survey scans were acquired using 200 eV pass

energy, 0.5 eV step size and 100 ms (50 ms x 2 scans) dwell times. All high-resolution spectra (B 1*s*, N 1*s*, C 1*s*, and O 1*s*) were acquired using 20 eV pass energy and 0.1 eV step size. The samples were ground and mounted on the XPS sample holder using conductive carbon tape. Thermo Avantage was used for analysis of the XPS data. The XPS spectra were shifted to align the peak for adventitious carbon (C-C) at 285.0 eV.

2.3.2.2 Bulk chemistry: Fourier transform infrared spectroscopy

Attenuated total reflectance (ATR) Fourier transform infrared (FTIR) spectroscopy is a characterisation technique used to determine the chemistry of samples. This instrument emits infrared light of different wavelengths onto a sample and measures the amount of light absorbed. In ATR instruments, a crystal is used to reflect the IR light onto the surface in contact with the sample. The energy absorbed is dissipated in sample with different molecular vibrational modes, which are characteristic of specific chemical bonds. Before analysis the samples were ground in a pestle and mortar and spectra were collected in the range of 500-4000 cm^{-1} using a Perkin-Elmer Spectrum 100 Spectrometer equipped with an ATR diamond crystal. The spectra were collected 8 times and averaged and the background subtracted.

2.3.2.3 Thermal decomposition: thermogravimetric analysis

A thermogravimetric analyser (TGA) is a high accuracy balance used to monitor the mass of a sample during heat-treatment in a controlled atmosphere. The thermal decomposition of samples was analysed with a TGA Netzsch TG209 F1 Libra from ambient temperature to 900 °C (10 °C/min ramp rate) under nitrogen or air gas flow (0.1 L/min). A buoyancy was performed with an empty crucible under the same conditions as used during analysis.

A thermogravimetric analyser coupled with a mass spectrometer (TGA-MS) was used (TGA: Mettler Toledo LMX 1, MS: Hiden Analytical HPR 20 Evolved) to study material's decomposition path as well as gases released during decomposition. In a typical run, the samples were placed in an alumina crucible and heated from 30 to 1050 ºC (10 ºC/min ramp rate), with a 30 minute holding step at 100 ºC.

TGA and TGA-MS were used to both test the thermal and oxidative stability of porous BN samples, as well as to understand the thermal decomposition patterns and gases released during precursor heat-treatment to produce BN.

Chapter 3: Understanding the Synthesis of Porous BN and its Controlling Parameters

Some of the results presented in this Chapter were published in Microporous and Mesoporous Materials. [111]

3.1 Introduction

The heat-treatment of boron- and nitrogen- containing precursors in either template or template-free synthesis methods can lead to porous BN materials.[70, 74, 91] Templating methods use a sacrificial material to enhance the pore volume of BN, while allowing good control over the resulting pore structure of the materials.[72] Typically, templating materials for porous BN include hard templates such as mesoporous silica, carbonaceous materials and zeolites[70-72] or structure-directing compounds such as cetyl-trimethylammonium bromide,[73] or the triblock copolymer P123.[74] However, templating methods present a number of disadvantages, including the removal of solid templates post-synthesis, or the production of porous BN containing many impurities. To try to circumvent these disadvantages, alternative template-free methods which still allow for tailorable pore structures are sought. The template-free synthesis of porous BN usually involves a heat-treatment (500-2000 $^{\circ}$C) of solid nitrogen and boron precursors under either an inert, an ammonia or a nitrogen/hydrogen atmosphere.[85, 90-91, 93-94, 126, 130, 159-162] Although this synthesis method's simplicity presents advantages over templating-techniques, little is known on how to control porous BN structure and chemistry, which is essential in order to tune the material's properties for specific applications. It is, therefore, essential to study the effects of certain synthesis parameters on the structure and chemistry of porous BN materials produced. Furthermore, if BN is to be used in adsorption applications or as a catalyst, it is fundamental to obtain good control over the surface area, as well as the micro- and mesopores ratios. Some preliminary studies have demonstrated the importance of varying synthesis

parameters to control porous BN structure.[91] Nag and co-workers reported that increasing the molar ratio of urea to boric acid increased the surface area of BN by up to 3 times.[91] Interestingly, the nitrogen and boron precursors are often first dissolved in a solvent prior to the synthesis step, the effects of which were overlooked until recently when Wu and coworkers showed that this had a significant impact on BN formation.[163] It was demonstrated that BN surface area could be tuned by recrystallizing urea and boric acid from solvents with various boiling points. This re-crystallization step produced intermediates with different crystalline structures, which had an impact on their decomposition during heat-treatment, resulting in different BN structures.

Therefore, in order to gain a deeper understanding of BN formation in template-free processes, the effect of various synthesis parameters (including type of precursors, molar ratios, intermediate preparation, synthesis temperature and temperature ramp rate) was investigated. By developing a more in-depth insight of template-free synthesis processes, it was hypothesised that a route to greater pore control and improved porous BN structures could be developed (Chapter 5).

3.2 Materials synthesis

3.2.1 Study of the effect of precursor type and molar ratio on porous BN

Porous BN was prepared using a single N-containing precursor: either urea (molecular biology grade, Sigma Aldrich) or melamine (99 %, Sigma Aldrich); and a single B-containing precursor either boric acid (ACS reagent, Sigma-Aldrich) or boron trioxide (99.98 %, Sigma Aldrich). The molar ratios of the N/B-containing precursors (X) were varied. The precursors were dissolved in deionized water at 65 °C for urea or 85 °C for melamine. The water was then allowed to fully evaporate at the same temperature, producing a precipitate which was further dried in the oven (time not recorded) and ground to obtain a white compound named intermediate. Intermediates were then heat-treated at 1050 °C (10 °C/min ramp rate) for 3.5 h under a nitrogen gas flow of 50 cc/min in a tubular furnace to produce BN (Figure 3-1). The samples obtained were named BN-ABX, where A indicates the nitrogen precursor used: M for melamine, U for urea; B indicates the type of boron-precursor used, if boric acid was used no naming was specified, if boron trioxide was used BTriox was indicated; X is the molecular ratio of N-precursor/B-precursor. For example, BN-M0.25 is a sample prepared from a mixture

of melamine and boric acid in an N-precursor/B-precursor molecular ratio of 0.25. The synthesis method and naming systems are summarised in Figure 3-1.

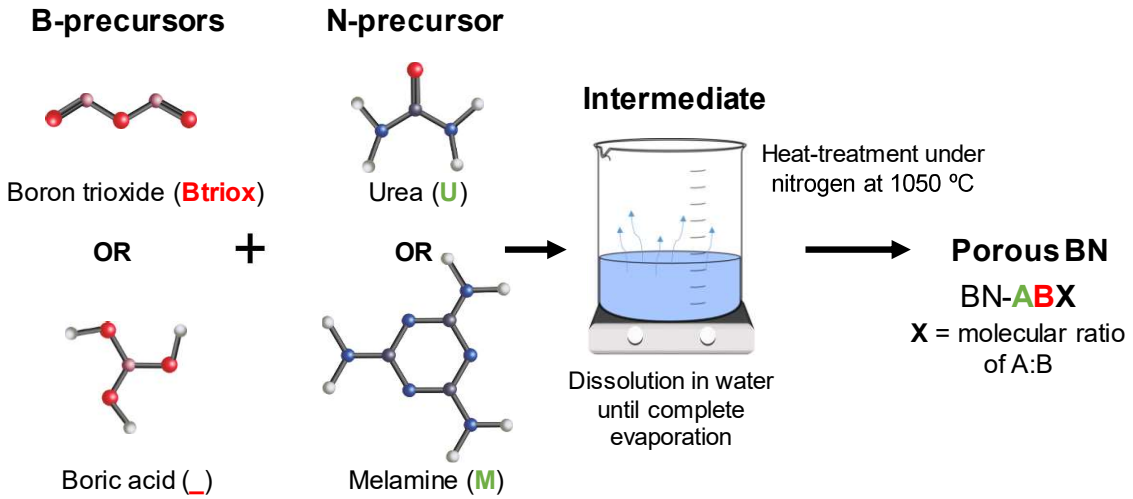


Figure 3-1 Synthesis schematic for porous BN samples prepared from different nitrogen and boron precursors.

3.2.2 Study of the effect of intermediate preparation on porous BN

Urea and boric acid precursors

Urea (9 g) and boric acid (1.85 g) in a molar ratio of 5:1 were dissolved in deionized water (450 mL) at 65 °C and the water then fully evaporated at the same temperature to obtain a white powder called intermediate. This particular molar ratio was selected following on from the results described in section 4.2, as it enables the synthesis of porous BN in relatively good yield. The intermediate powders were then further dried in the oven at 65 °C for different lengths of time (0 h, 50 h, 100 h, 200 h). The samples were then finely ground and named INT-U5-Y where 5 is the molar ratio of nitrogen/boron precursors and Y is the drying time in hours after the evaporation of the water. A physical mixture of urea and boric acid in the same molar ratio was also prepared by mixing and grinding the precursors together without any dissolution step and was named INT-U5-phys mix.

Melamine and boric acid precursors

Melamine and boric acid in a 0.5:1 molar ratio were dissolved in water at 85 °C. This particular molar ratio was chosen following the results obtained in section 4.2. The water was evaporated at the same temperature to again obtain a white precipitate, which was further dried at 85 °C in

the oven overnight and ground to obtain a white compound called intermediate INT-M0.5. A physical mixture of melamine and boric acid in the same molar ratio was also prepared by simply mixing and grinding the precursors together with no dissolution step, and was called INT-M0.5-phys mix.

Porous BN synthesis

The intermediates or physical mixtures were then heated at 1050 °C for 3.5 h under a constant nitrogen gas flow of 50 cc/min, in order to produce porous BN. The nomenclature of the resulting porous BN samples was the same as the intermediates, however named "BN" rather than "INT". The composition and drying times for these porous BN are shown in Table 3-1.

Table 3-1. Summary of synthesis conditions for all porous BN samples produced from intermediates.

Sample	N-precursor	B-precursor	N:B precursors ratio	Drying time after dissolution (h)
BN-U5-phys mix	urea	boric acid	5	NA
BN-U5-0	urea	boric acid	5	0
BN-U5-50	urea	boric acid	5	50
BN-U5-100	urea	boric acid	5	100
BN-U5-200	urea	boric acid	5	200
BN-M0.5-phys mix	melamine	boric acid	0.5	NA
BN-M0.5	melamine	boric acid	0.5	24

3.2.3 Study of the effect of temperature on porous BN

Porous BN (BN-U5-phys mix) was synthesised as described in section 4.2.2., *i.e.* from a physical mixture of urea and boric acid in a molar ratio of 5:1, in a tubular furnace at 1050 ºC (10 ºC/min) for 3.5 h under nitrogen gas flow (50 mL/min), however, the synthesis was scaled-up from ~500 mg to produce ~3 g of BN per batch. The as-synthesised material was fully characterised and placed in a silicon carbide crucible for further heat-treatment in a hot-press at different temperatures (1300, 1550, 1800 ºC) at 10 ºC/min for 3.5 h under nitrogen atmosphere. The hot-press was degassed before heat-treatment to eliminate any air in the chamber.

Samples are named BN-U5-Z, where Z indicates the synthesis temperature used.

3.2.4 Study of the effect of ramp rate on porous BN

Porous BN (BN-MU1:5) was synthesised by physically mixing and grinding B- and N-containing precursors (according to a synthesis procedure described in Chapter 5, details in Appendix 1) and heat-treating them up to 1050 °C at different ramp rates (2.5, 5, 10, 15 °C/min) under nitrogen gas flow (50 cc/min) for 3.5 h. At least 3 samples were produced for each ramp rate and were named BN-MU1:5 -Z , where Z is the ramp rate used during the heat-treatment (°C/min).

3.3 Effect of precursor type and molar ratio on porous BN structure and chemistry

The scope of this section is to analyse the effect of the type of precursor and their molar ratios on porous BN structure and chemistry. The optimisation of these parameters is essential in order to produce porous BN with high surface area and low amounts of impurities.

3.3.1 Analysis of chemical features

Firstly, the chemistry of the powder samples obtained from heat-treatment was analysed using FTIR spectroscopy, to confirm that a BN material was obtained. Figure 3-2a shows the spectra for all samples and highlights the presence of the two main characteristic bands for boron nitride: B-N in-plane stretching mode at ~ 1360 cm^{-1} and B-N-B out-of-plane bending mode at 800 cm^{-1}.[164] However, additional bands are also present for samples produced from less N-precursor in Figure 3-2a, which were identified as boron oxide compounds from a comparison with the FTIR spectrum of B_2O_3. It is hypothesised that the presence of boron trioxide in small quantities is also responsible for the enlargement of the B-N vibrational peaks. It is believed that in the case of nitrogen precursor deficiency, unreacted boron oxide is present in the final product. This is true in the case of: urea/boric acid molar ratio of 0.5 (BN-U0.5), melamine/boric acid molar ratio of 0.25 (BN-M0.25) and melamine/boron trioxide molar ratio of 0.5 (BN-MBTri0.5). This is an indication that an excess of nitrogen atoms is needed in order to ensure the full reaction of the boron precursor to form a BN material and it can be explained because of the high volatility of the nitrogen compounds (which form gases such as ammonia when heated)[165] compared to the boron compounds, which form a viscous fluid.[97] Ammonia

gas reacts with boron oxide melt to form BN in a reaction previously described in the literature: $B_2O_3 + 2NH_3 \rightarrow 2BN + 3H_2O$.[91] Figure 3-2b shows the colour change of BN samples with the use of different precursors and/or molar ratios. In particular, when a large excess of N-containing precursor is used: *e.g.* molar ratio of 1:1 for melamine and boric acid (BN-M1) or melamine and boron trioxide (BN-MBTri1), the samples appeared black, which is a good indication of the presence of a large amount of carbon. In conclusion, in order to minimise carbon and oxygen impurities, the best molar ratio of melamine to boric acid was 0.5, while for urea and boric acid mixtures, this was at least 5. Samples obtained from a mixture of melamine and boron trioxide exhibited either a large amount of carbon impurities (molar ratio of 1), or a large amount of boron oxide impurities (molar ratio of 0.5).

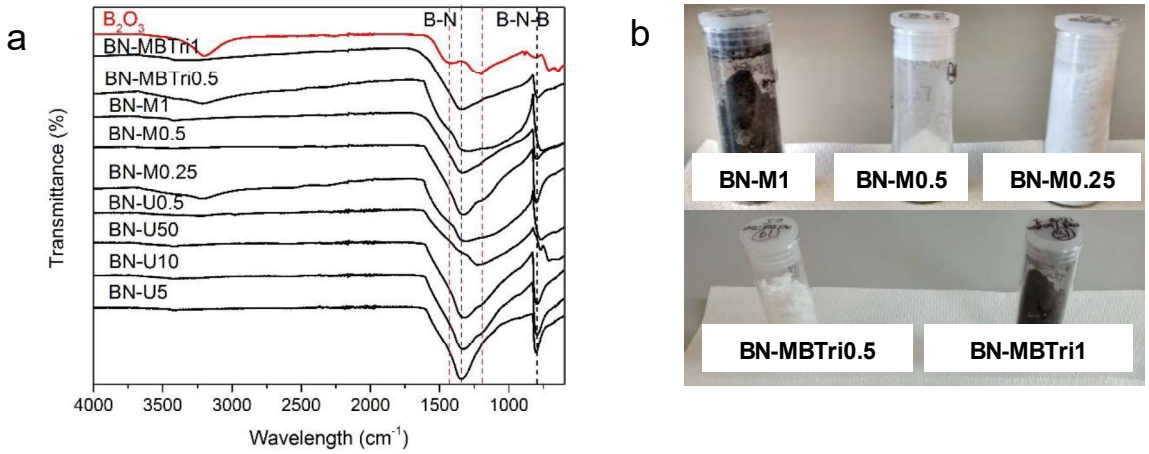


Figure 3-2 (a) FTIR spectra and (b) images of BN samples produced using different precursors and diverse molar ratios.

3.3.2 Analysis of structural features and morphology

The crystalline structure of the porous BN was analysed using XRD. Figure 3-3a shows the crystalline patterns for all powder samples obtained. All samples show low intensity and broad peaks for the (002) and (100) planes for hexagonal BN (JCPDS card no. 34-0421),[166] indicating that some small amounts of h-BN phase is present, indicative of turbostratic BN or BNNSs. However, in the samples prepared with a deficiency of N-containing precursor, an additional peak for B_2O_3 is also present.[82] This is in good agreement with the FTIR analysis (Figure 3-2a), confirming the presence of a large amount of residual boron trioxide after heat-treatment.

In order to use BN as an adsorbent, the material needs to exhibit a high surface area and a large amount of pores. For this reason, the pore structure of materials was characterised with nitrogen

sorption isotherms at -196 ºC, which were collected just for the BN samples which were relatively free of impurities from the previous chemical analysis, *i.e.* BN-U5, BN-U10, BN-U50 and BN-M0.5. The isotherms are shown in Figure 3-3b, the textural parameters deriving from the same analysis were plotted in Figure 3-3d, and the resulting pore size distributions displayed in Figure 3-3c. All samples exhibit a relatively large amount of micropores and some mesopores (Figure 3-3d). In particular, BN-M0.5, obtained from melamine and boric acid, exhibits a larger micropore ratio when compared to the other BN samples, while BN-U5 exhibited a larger mesopores ratio compared to porous BN samples synthesised from urea and boric acid in higher molar ratios. The large uncertainty in the BET surface area of BN-U5 is linked to the intermediate preparation which was not reported here and will be investigated in more detail in section 3.4.

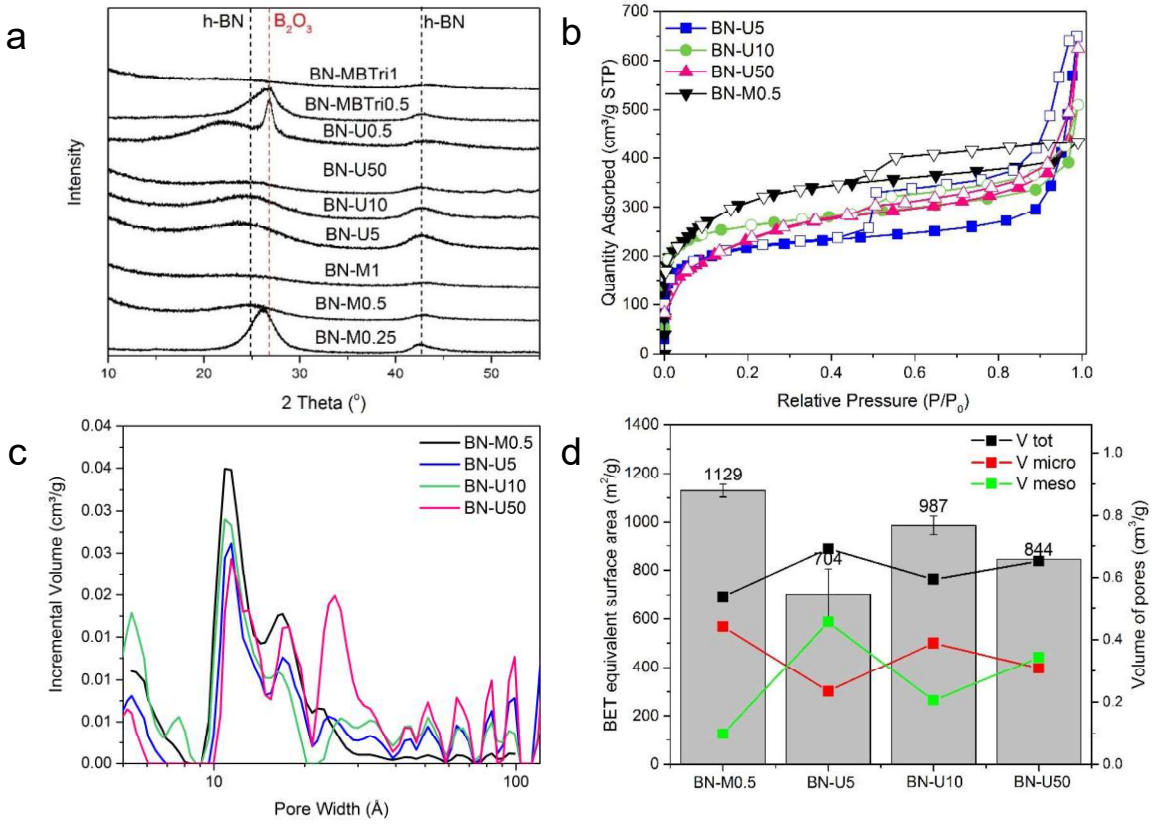


Figure 3-3 (a) XRD patterns for all samples and (b) Nitrogen sorption isotherms at -196 °C for the purest porous BN samples, as determined by chemical analysis (open symbols represent desorption),(c) pore size distributions and (d) textural parameters derived from nitrogen gas sorption analysis. Error bars represent standard deviation calculated from 3 repeats.

The morphology of the different samples produced was analysed *via* SEM and TEM. Images for the representative samples are reported in Figure 3-4. Porous BN shows different morphologies depending on the type of N-containing precursor used and their molar ratios. It

is hypothesised that this is due to the different structures of the precursors used. When urea and boric acid were used, porous BN showed a plate-like structure for low molecular ratios or a more disordered structure with visible macropores (Figure 3-4c) and rods (Figure 3-4d) for high molecular ratios. When melamine and boric acid were employed, the samples exhibited a whisker-like morphology (Figure 3-4b), which was previously reported in the literature.[82] TEM was also used to compare two samples obtained by using different molar ratios of urea to boric acid, which showed a large number of visible mesopores in BN-U5 (Figure 3-4e) and a very thin and crumbled nanosheet for BN-U50 (Figure 3-4f). This is in agreement with what was previously measured using nitrogen sorption isotherms, which showed that BN-U5 exhibited a larger mesopore volume in comparison to samples obtained with larger molar ratios of urea to boric acid. It must be noted that micropores (< 2 nm) are too small to be imaged at this scale.

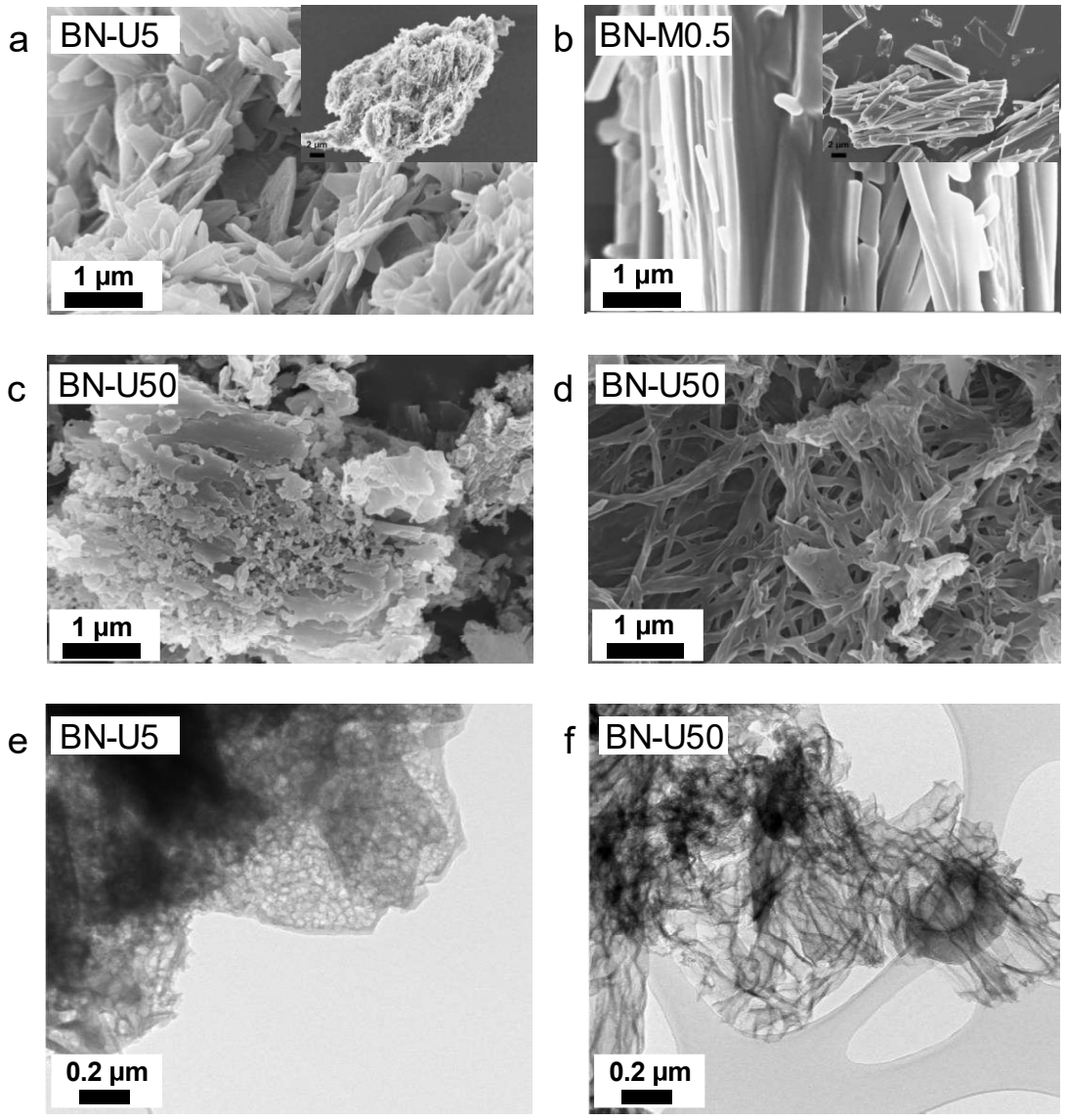


Figure 3-4 SEM images for porous BN sample:(a) BN-U5, (b) BN-M0.5, (c,d) BN-U50. (e) TEM images for BN-U5 and (f) BN-U50.

This preliminary study allowed us to conclude that under these circumstances, in order to obtain the highest purity BN material with relatively high porosity, a mixture of urea and boric acid with molar ratio ≥ 5 has to be used; alternately, if a mixture of melamine and boric acid are employed, a molar ratio of 0.5 produced the most desirable material.

3.4 Effect of intermediate preparation on porous BN structure and chemistry

Boron and nitrogen precursors for both urea and boric acid or melamine and boric acid mixtures are often first dissolved in water to form an intermediate of reaction prior to the synthesis of BN. [90-91, 93] However, the effect of the intermediate preparation on porous BN structure and chemistry is often overlooked. The aim of this section is to understand how this step affects BN pore structure and chemistry, in order to optimise the material's surface area and minimise impurities.

Section 4.4. is divided into two subsections, looking at the effects of intermediate preparations for: i) urea and boric acid or ii) melamine and boric acid precursors mixtures.

3.4.1 Porous BN synthesised from urea and boric acid precursors

3.4.1.1 Analysis of chemical features of BN

In order to understand what effect the dissolution step prior to heat-treatment for urea and boric acid precursors has on BN chemistry, the porous BN samples obtained from the different intermediates were analysed using FTIR spectroscopy. Figure 3-5a shows a typical spectrum for porous BN with the two main characteristic bands for boron nitride B-N in-plane transverse stretching mode at ~1360 cm^{-1} and B-N-B out-of-plane bending mode at 800 cm^{-1}.[164] FTIR spectra did not show any significant variation between samples, indicating no major chemical differences. In order to further understand the chemistry of the materials, XPS analysis was performed (Figure 3-5c-f). As all samples exhibited similar chemical features, the analysis of BN-U5-phys mix is shown as a typical example of these porous BNs. XPS spectra exhibited two characteristic h-BN peaks for the B 1*s* and N 1*s* core level at binding energies of 191.0 eV and 398.5 eV, respectively. These values are in good agreement with the literature: 190.5-191.1 eV for B 1*s* and 397.6-398.7 eV for N 1*s* for boron nitride.[167-168] B 1*s* and N 1*s* spectra also showed another peak at higher binding energies and with lower intensity. These peaks were attributed to shake-up satellite peaks deriving from the presence of sp^2- hybridised BN in the hexagonal phase.[169-171] XPS also highlighted the presence of oxygen in quantities between 10 and 13 at.% (Figure 3-5f). The carbon content, on the other hand, was only between 2 and

4 at.% and was not included in the atomic percentage bar plot as it was attributed to adventitious carbon (*i.e.* not part of the BN structure). It is worth noting, that although not always reported in the literature, porous BN synthesised using similar methods (*i.e.* low synthesis temperatures and oxygen containing precursors), is likely to contain significant oxygen, which can affect BN chemistry as well as the properties of the material when used as an adsorbent. All samples showed a higher content of boron (~52 at.%) compared to nitrogen (~37 at.%). This is due to the higher volatility of the nitrogen precursor. The oxygen content in porous BN was attributed to boronoxynitride BO_xN_y species. Despite being similar to boron trioxide, they do not form a separate phase and cannot therefore be eliminated by simply washing the material in water. This boronoxynitride is richer in boron than nitrogen, with a binding energy for B 1*s* of 192.5 eV.[172]

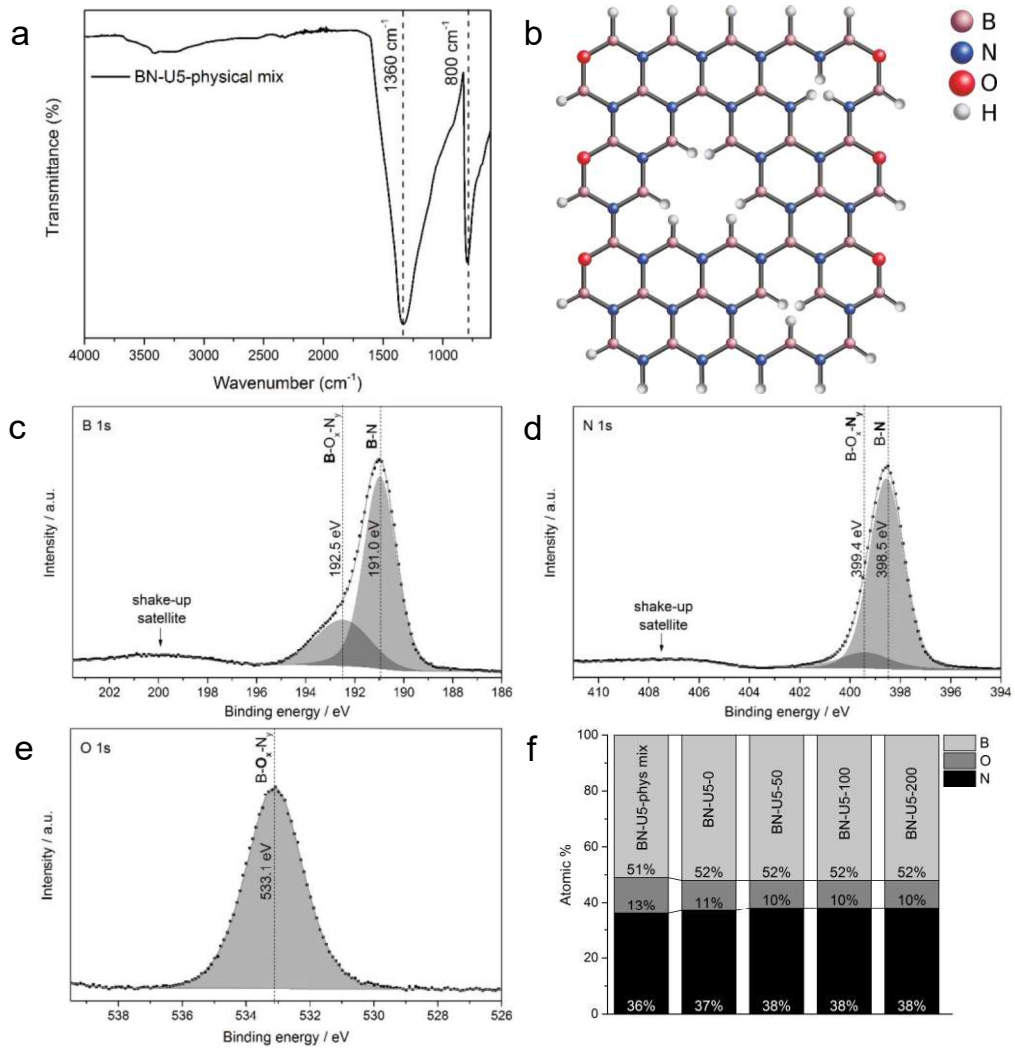


Figure 3-5 (a) typical FTIR spectrum for a porous BN sample (BN-U5-phys mix); (b) proposed representative structure of BNNS (from porous BN); (c-e) XPS high resolution fitted core level spectra for N 1*s*, B 1*s* and O 1*s* for a typical BN sample (BN-U5-phys mix);(f) XPS relative atomic percentages for all porous BN samples.

From FTIR and XPS studies, it can be concluded that the chemistry of porous BN is not affected by the intermediate preparation and that BN exhibited: a) a B/N ratio >1 ; b) oxygen in quantities of about 10 at.% and in the form of a boronoxynitride compound; and c) little/no –OH groups as indicated by the low intensity of the respective band in FTIR. A potential representative structure for the BNNS (from porous BN) is shown in Figure 3-5b.

3.4.1.2 Analysis of structural features and morphology of BN

FTIR and XPS analyses showed that all porous BN samples exhibited similar chemical features. In order to evaluate the structural properties of the material, the samples were analysed using XRD and nitrogen sorption isotherms. The XRD patterns showed the (002) and (100) peaks for hexagonal BN (JCPDS card no. 34-0421)[166] (see Figure 3-6a). The d-spacing for the (002) plane calculated from XRD data, which indicates the interlayer spacing, was larger than the literature value for bulk h-BN (3.3 Å)[25] and increased slightly with the urea/boric acid intermediate drying time from 3.5 Å for BN-0 to 3.6 Å (although the broad peaks do not allow for precise calculations) for BN-U5-200 and BN-U5-phys mix. The large d-spacing, low intensity peaks and the absence of other reflections, indicate that the porous BN obtained exhibited a disordered turbostratic structure, likely with a large amount of defects and impurities.[160] While the chemical features did not visibly change with the change in the intermediate drying time, the XRD patterns point to some structural variation. Further analyses were therefore conducted to gain a greater insight into the BN structure.

To further investigate the porous structure of the BN materials, nitrogen sorption at -196 °C was employed. The isotherms (Figure 3-6b) were of type IV, indicative of the presence of both micropores and mesopores. Type H3/H4 hysteresis indicated that the pores obtained had a slit shape. Table 3-2 summarises all of the textural parameters obtained from nitrogen sorption isotherms for the porous BN samples synthesised from different intermediates. The BET surface area and total volume of pores increased in BN samples synthesised from urea and boric acid intermediates with increasing drying time, up to 1016 m^2/g and 0.869 cm^3/g. Particularly, the amount of micropores increased proportionally with drying time. Porous BN synthesised from a physical mixture of urea and boric acid also exhibited a high surface area.

Since it is clear from the discussion above that the intermediate drying time had an effect on the microscale structure of the resulting porous BN, we then investigated whether this was also the case at the macroscale. The morphology of the samples was characterised with SEM. SEM (Figure 3-6d) showed similar morphology to that previously reported for the same precursors

in Figure 3-4. No major differences were observed between the samples synthesised with different drying times for urea and boric acid mixtures. High-resolution TEM was also employed (Figure 3-6c) showing the typical disordered structure for turbostratic BN, in line with what was observed from XRD patterns. This highlighted the presence of some crystallinity, but with 2D-layers stacked non-uniformly on top of one another. Again, no major differences between the various samples were observed.

Table 3-2. Textural parameters from nitrogen sorption isotherms at -196 °C.

Sample	S_{BET} (m^2/g)	V_{tot} (cm^3/g)	V_{mic} (cm^3/g)	V_{mes} (cm^3/g)	V_{mic}/V_{tot}
BN-U5-0	403	0.625	0.164	0.461	0.262
BN-U5-50	514	0.654	0.212	0.442	0.324
BN-U5-100	695	0.719	0.273	0.446	0.380
BN-U5-200	1016	0.869	0.417	0.452	0.480
BN-U5-phys mix	945	0.852	0.389	0.463	0.457

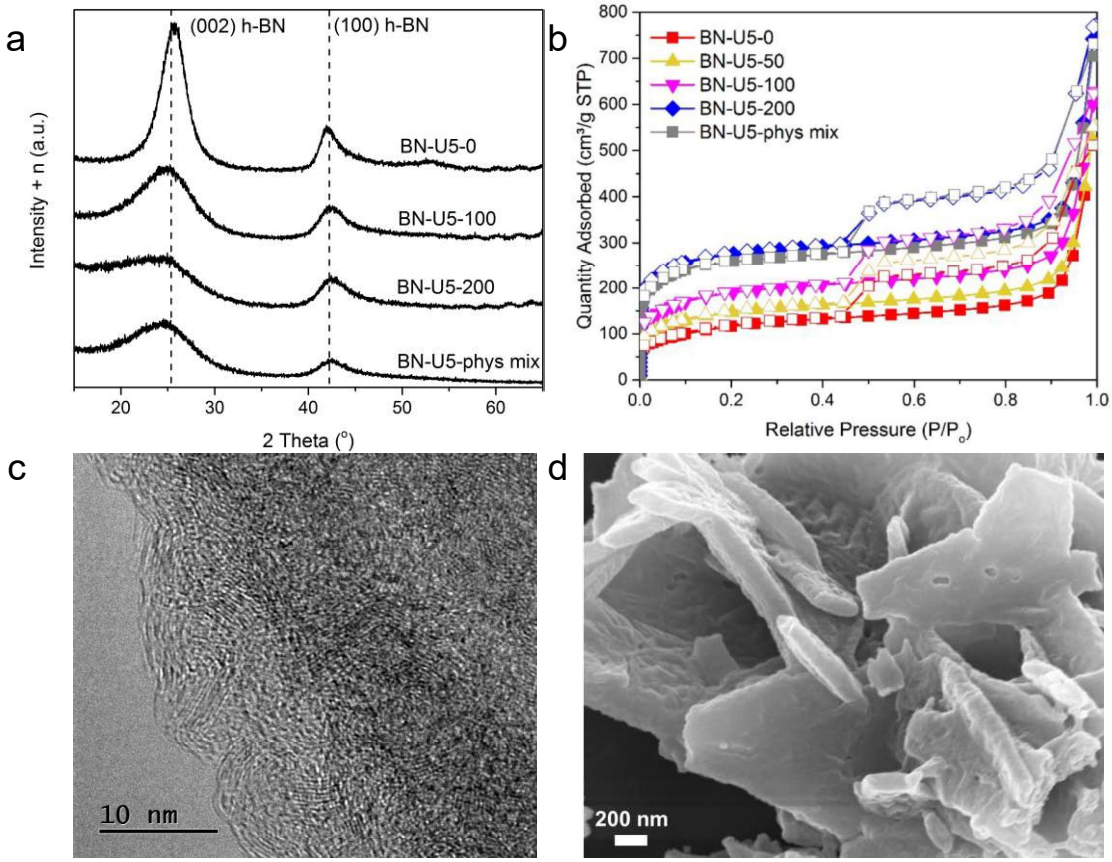


Figure 3-6 (a) XRD patterns for porous BN samples; (b) Nitrogen sorption isotherms at -196 °C (open symbols represent desorption);(c) typical high-resolution TEM image for porous BN (BN-U5-phys mix);(d) SEM image for a typical porous BN sample (BN-U5-0).

3.4.1.3 Analysis of chemical features of intermediates

It was previously observed that the intermediate preparation for urea/boric acid mixtures, had a major effect on BN pore structure. The intermediates were, therefore, studied in order to explain how they affect BN formation. The FTIR spectra of the intermediate were compared to the spectra of the starting precursors (Figure 3-7). No additional bands were present, suggesting no chemical reaction occurred when the two precursors were dissolved and/or mixed together. This was also observed by Wu and coworkers.[163] Only the sample with the lowest drying time (INT-U5-0) exhibited some additional bands, which were attributed to water still present on the sample. This lack of chemical variation was surprising, as the porous properties of BN samples obtained from the urea and boric acid intermediates varied significantly. XPS was, therefore, employed in order to confirm/ disprove what was observed by FTIR for urea and boric acid intermediates.

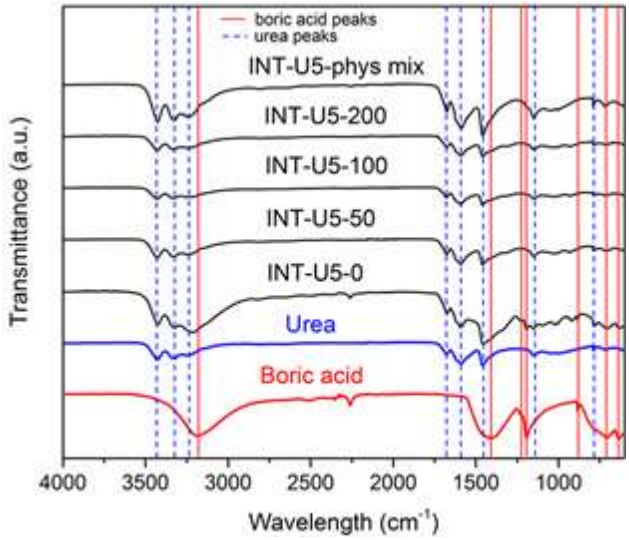


Figure 3-7 FTIR spectra for urea and boric acid intermediates dried for different lengths of time, as well as precursors.

XPS core level spectra of urea/boric acid intermediates (INT-U5-0 and INT-U5-200) and physical mixture (INT-U5-physmix) were compared by overlapping spectra normalised to the O 1*s* peak (Figure 3-8a-d). All peaks are located at similar binding energies and have similar shapes, which confirms that no chemical reaction occurred, as previously inferred from FTIR results. XPS spectra for a typical intermediate sample were also fitted in Figure 3-8e-h. The B 1*s* spectra of the intermediates in Figure 3-8a and e, show a main peak at binding energies of 192.7-192.9 eV, which corresponds to the literature value for boric acid.[172] The N 1*s* spectrum (Figure 3-8b and f) also exhibits one main peak corresponding to urea at binding

energies of 400.0-400.2 eV, which correspond to the experimentally measured value (400.0 eV). However, both N 1*s* and B 1*s* spectra exhibited some additional peaks which were present in the pure urea and boric acid precursor as well, and that probably belonged to impurities. Although these impurities were not identified at this stage, the same peaks appeared in the physical mixture as well as the intermediates, supporting the hypothesis that no reaction occurred. The spectra for the O 1*s* (Figure 3-8c and g) showed two main peaks corresponding to the values measured for urea and boric acid. The C 1*s* spectra (Figure 3-8d and h) exhibited 3 peaks, corresponding to the carbon in urea, some impurity not yet identified, and adventitious carbon (C-C). The peak position did not show any major changes between the samples, however, the element ratios varied. This is indicated by a variation in peak intensities, which showed no significant trend, and was attributed to local heterogeneity in the samples (especially in the physical mixture as this sample is not as uniformly mixed).

3.4.1.4 Analysis of crystalline structure and thermal decomposition of intermediates

Chemical analysis of the intermediate samples formed from dissolution of urea and boric acid precursors did not highlight any major differences between the samples. Hence, XRD was used next to try to elucidate the crystalline structure of the intermediates. XRD patterns for all intermediate samples, as well as starting precursors are shown in Figure 3-9. No new peaks other than those attributed to urea and boric acid were observed, ruling out the formation of a crystalline structure as the intermediate. Owing to the absence of a dissolution step, the physical mixture exhibited a different crystalline structure compared to that of the intermediate samples (higher relative intensity of (110)/(101) reflections for urea). The peak related to boric acid was visible on the XRD pattern of the physical mixture, while this was not the case for the intermediate samples. This is attributed to the fact that boric acid molecules were better mixed in the latter samples. The visible difference in crystallinity (difference in relative intensities) between the various intermediates (and the physical mixture) may have had an impact on the thermal decomposition profile of the samples, which in turn could have influenced the morphology of the resulting materials (Figure 3-9).

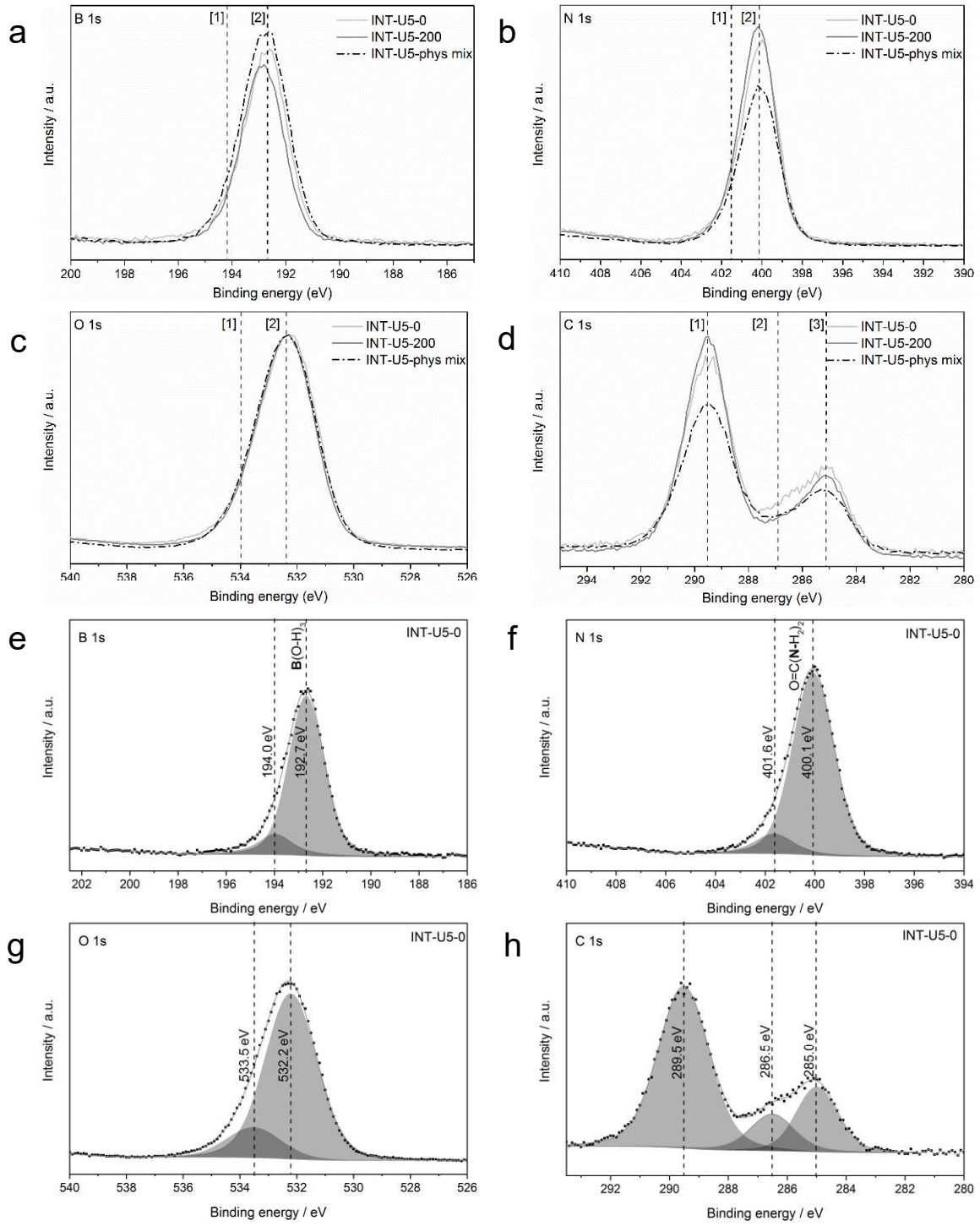


Figure 3-8 (a-d) High resolution core level XPS spectra for 2 intermediates and a physical mixture of urea and boric acid for (a) B *1s*,(b) N *1s*,(c) O *1s* and (d) C *1s*. Peak fitted high resolution core level XPS spectra of INT-U5-0 for (e) B *1s*, (f) N *1s*, (g) C *1s*, (h) O *1s*.

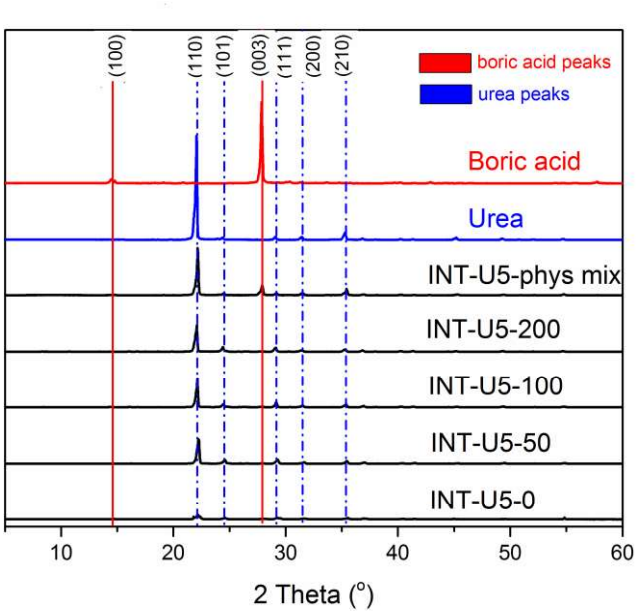


Figure 3-9 XRD patterns for all samples. The dotted lines represent values from reference patterns for urea [173]and boric acid[174].

To investigate this aspect, the intermediates as well as the physical mixture were analysed using TGA-MS. TGA-MS was performed on the intermediates, as well as the physical mixture deriving from urea and boric acid mixtures. TGA curves are shown in Figure 3-10 and demonstrate that urea fully decomposes below 500 °C, in a complex set of reactions previously described in the literature,[165, 175] while boric acid loses some mass but does not fully decompose, forming boron oxide melt and releasing water.[176] When boric acid and urea are mixed together, it is hypothesised that the ammonia released from the decomposition of urea reacts with boron oxide formed from boric acid, producing a boron nitride compound.[91] The material produced is highly affected from the decomposition pattern of the precursors. Between 160 °C and 250 °C the intermediates that were dried for longer displayed a lower mass loss, which could be explained by the formation of a higher quantity of thermally stable B-N bonds at lower temperatures.

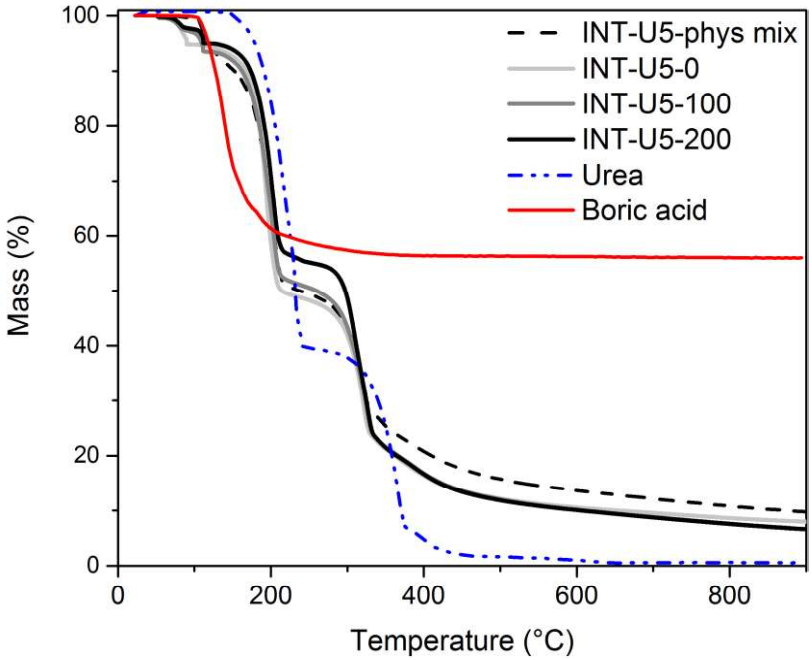


Figure 3-11 TGA thermal decomposition curves under nitrogen gas flow for precursors and intermediates for urea and boric acid.

Mass spectroscopy (Figure 3-12) showed that the major weight losses observed by TGA analysis correspond to the release of four different gases, namely ammonia, carbon dioxide, isocyanic acid and water. Intermediates dried for longer times started releasing ammonia at lower temperatures, which is in agreement with the hypothesis of the formation of a higher quantity of B-N bonds at lower temperatures, and therefore a lower mass loss between 160 °C and 250 °C. The physical mixture shows a slightly different thermal decomposition pattern, with an additional peak in Figure 3-12 for ammonia and carbon dioxide. In summary, it is hypothesised that intermediates dried for longer start releasing gases (*e.g.* ammonia) at lower temperatures. These gases can react with boron oxide to form B-N precursor in larger quantities, resulting in increased thermal stability. The resulting BN exhibited higher porosity as it formed while large amount of gases, which acted as porogen agents, were released. This led to the synthesis of higher porosity BN.

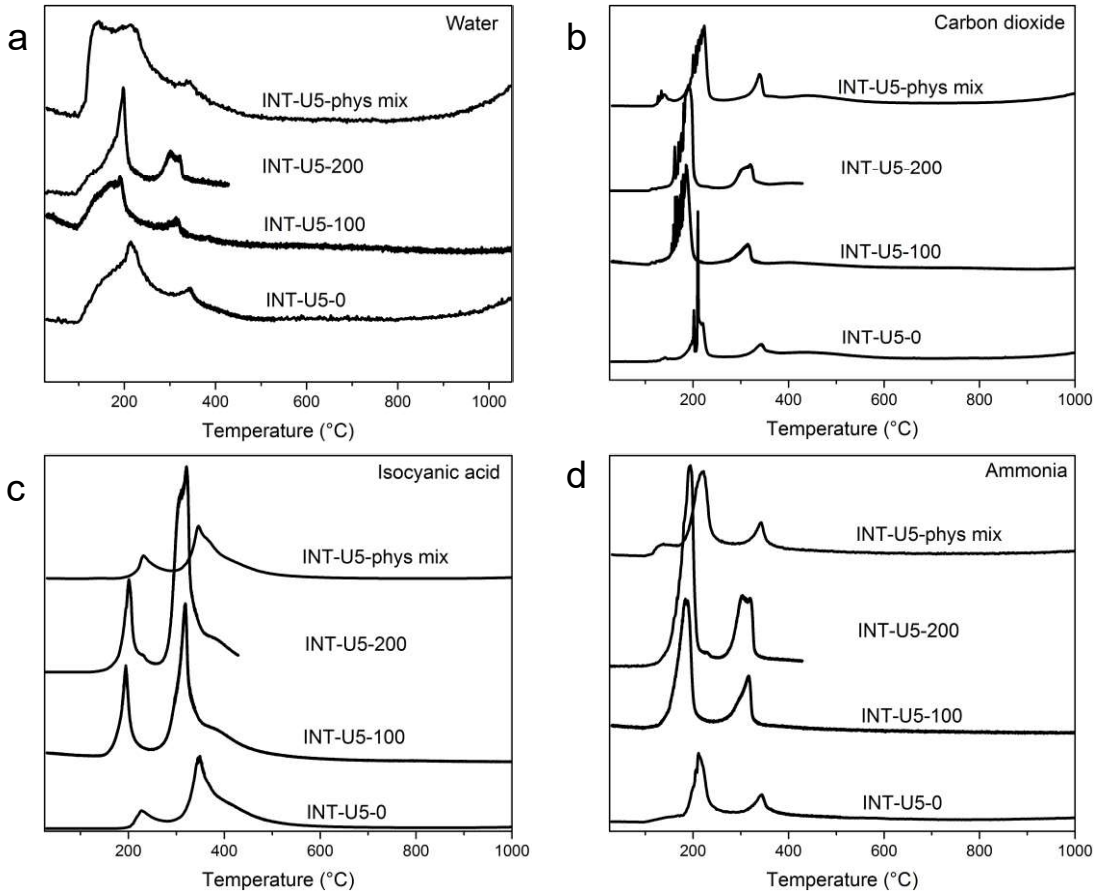


Figure 3-12 Mass spectroscopy data deriving from thermal decomposition or urea and boric acid intermediates under nitrogen gas flow.

To further understand the production of porous BN and to confirm the formation of a BN precursor during the heat treatment of the intermediates below 250 °C, intermediates were heat-treated up to 250 °C (10 °C/min) under nitrogen, cooled and analysed with XPS and FTIR. It must be underlined that at 250 °C the intermediates would be mostly in the form of a melt, potentially containing some amorphous BN, boron oxides and gases. Figure 3-13 shows XPS analysis of INT-U5-0, which is a simple mixture of urea and boric acid precursors as previously discussed and INT-U5-0-250, which is the same intermediate heat-treated at 250 °C. After heating to 250 °C, some changes in the chemistry of the material appeared. In particular, two new peaks appeared at the same binding energies as B-N: ~398.5 eV (B 1*s*) and ~191.0 eV (N 1*s*). The presence of the 2 satellite peaks for both N 1*s* and B 1*s* at higher binding energies are indicative of π-π* transitions, which occur in the hexagonal form of BN, further confirming the formation of B-N bonds.[170]

In particular the B 1*s* peak, which was located at 192.7 eV for boric acid in INT-U5-0, shifted to lower binding energy (192.3 eV) after heating to 250 °C (INT-U5-0-250), which is in line with the hypothesis that some B-OH bonds were substituted by less electronegative NH_2 groups, as previously reported by Gouin et al.[172] in a nitridation of boric acid under an ammonia atmosphere. B 1*s* for boron nitride BN-U5-0 exhibits some boronoxynitride impurities. The N 1*s* peak for INT-U5-0 is located at 400.1 eV for urea, and it shifted to lower binding energy (399.5 eV) when heated at 250 °C. This peak was assigned to NH_2 molecules reacting with boric acid and some boronoxynitride compounds. The C 1*s* and O 1*s* core level spectra for INT-U5-0, INT-U5-0-250 and BN-U5-0 are also reported in Appendix 1 (Figure A1.3). XPS allowed us to confirm that BN began to form at temperatures as low as 250 °C. FTIR spectroscopy further confirmed the presence of B-N vibrational bands at 775 and 1390 cm^{-1}.[172] (Appendix 1, Figure A1.2).

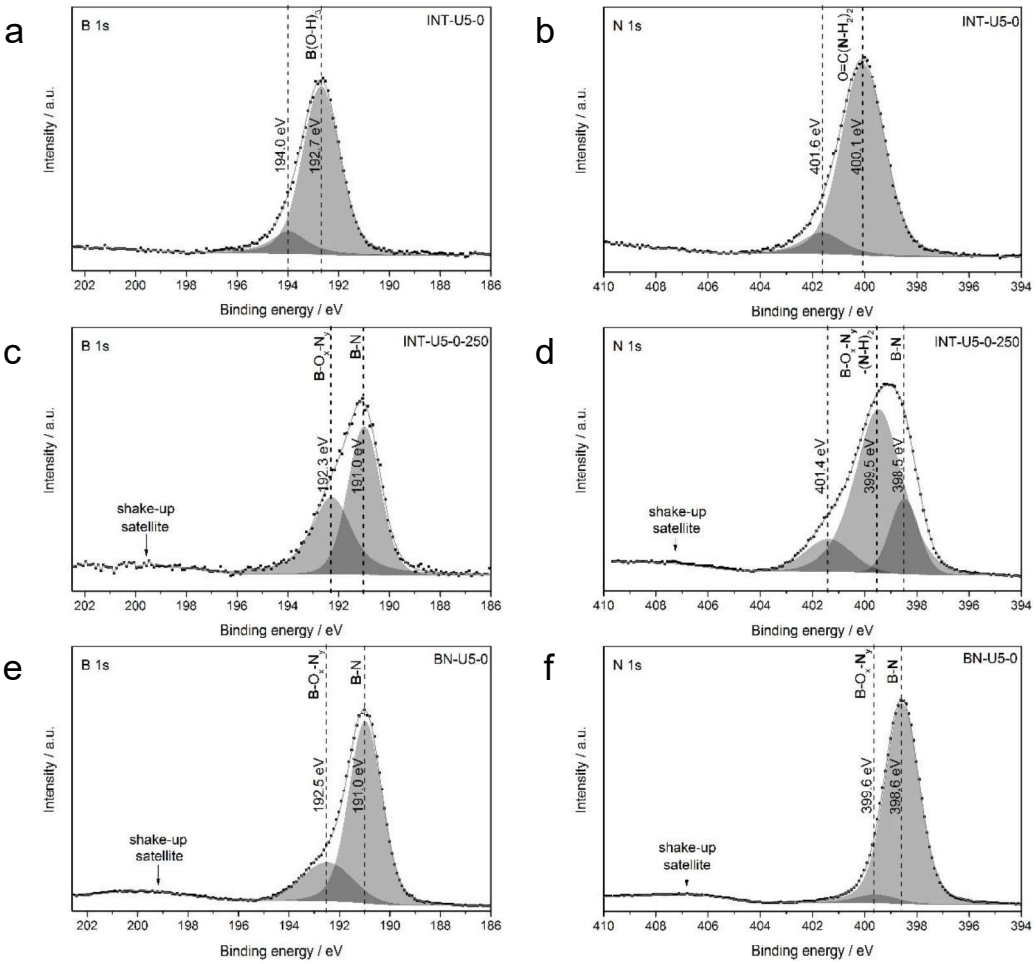


Figure 3-13 (a, b)XPS high resolution core level spectra with peak fitting for B 1*s* and N 1*s* for intermediates deriving from urea and boric acid mixtures,(c,d) intermediates treated at 250 °C under nitrogen,(e,f) porous BN derived from the same intermediate treated at 1050 °C under nitrogen.

3.4.1.5 Analysis of chemical and structural features of side-product of reaction

Finally, the mechanism of reaction for porous BN synthesis proposed, was further confirmed by analysing a side-product of the reaction, which formed in the outlet tube of the furnace during BN synthesis. Formation of this compound is due to the condensation of gases and vapours released during the decomposition of the precursors. The product formed in the outlet tube was analysed in order to gain a deeper insight into its formation mechanism and confirmed the reaction mechanism previously proposed. The XRD pattern in Figure 3-15 showed that the white powder was crystalline and matched well with the crystalline structure of ammonium bicarbonate.[177] In order to further confirm/disprove what was observed of the material's structure, its chemistry was also investigated using FTIR spectroscopy (Figure 3-14b), which were in good agreement with that of ammonium bicarbonate (NIST database). This compound can be formed *via* condensation of ammonia, carbon dioxide and water,[178] which further confirms the release of these gases during BN formation. This may be an issue when scaling-up the reaction as it can occlude the outlet tube and cause pressure build-up inside the furnace. However, precipitation may be avoided by simply heating the outlet in order to avoid condensation.

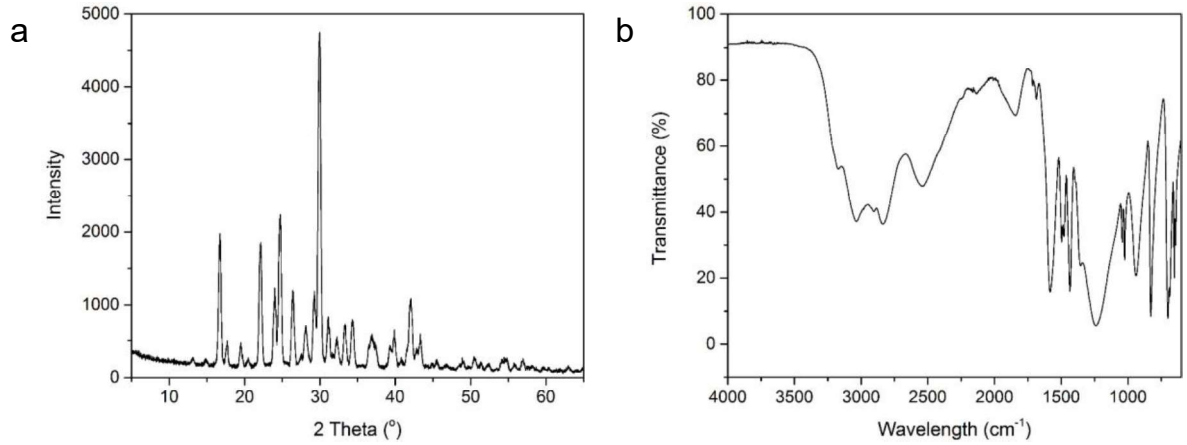


Figure 3-14 (a) XRD pattern and (b) FTIR spectrum for outlet side-powder produced during BN synthesis.

3.4.2 Porous BN synthesised from melamine and boric acid precursors

In the previous section, the effect of the intermediate preparation for urea and boric acid mixtures was studied. To allow for further understanding of porous BN formation, another pair of commonly used precursors, melamine and boric acid, was also investigated. In this section, the effect of the intermediate preparation for mixtures of these precursors is evaluated.

3.4.2.1 Analysis of pore structure of BN

The pore structure of porous BN samples synthesised from a melamine and boric acid intermediate (prepared *via* dissolution of the precursors in water) or physical mixture (no dissolution) was analysed with nitrogen sorption isotherms, shown in Figure 3-15. When no dissolution was performed (BN-M0.5-phys mix), the sample showed low porosity, as indicated by a lower nitrogen adsorption when compared to BN synthesised from melamine and boric acid previously dissolved in water (BN-M0.5). The textural parameters derived from nitrogen sorption isotherms at -196 °C are reported in Table 3-3 and further confirm that BN-M0.5 prepared *via* dissolution of the precursors in water exhibits significantly higher surface area when compared to the sample prepared from a physical mixture (1129 *vs* 190 m^2/g). BN-M0.5 exhibits similar chemical and physical features as previously described in section 4.3 and is, therefore, not characterised here.

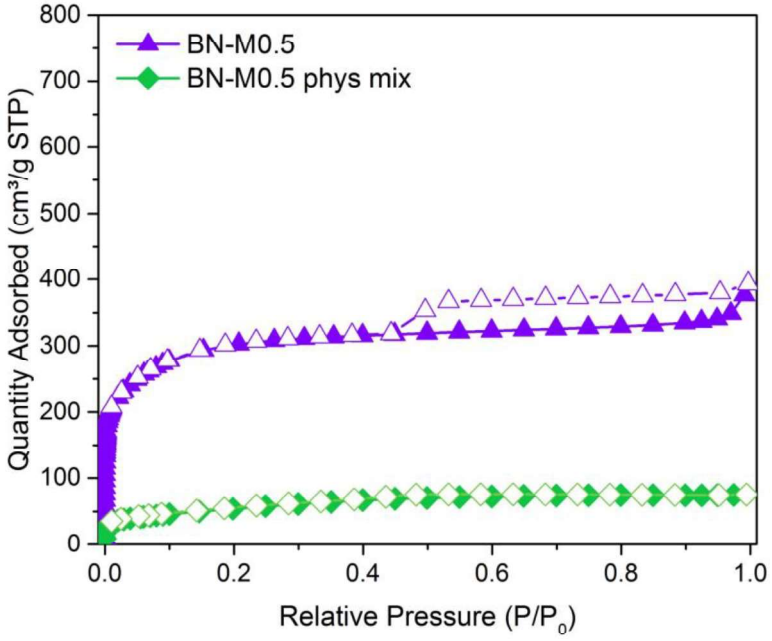


Figure 3-15 Nitrogen sorption isotherms at -196 °C for samples prepared with and without dissolution of the precursors (open symbols represent desorption).

Table 3-3 Textural parameters derived from nitrogen sorption isotherms at -196 °C

Sample	S_{BET} (m^2/g)	V_{tot} (cm^3/g)	V_{mic} (cm^3/g)	V_{mes} (cm^3/g)	V_{mic}/V_{tot}
BN-M0.5	1129	0.539	0.441	0.098	0.818
BN-M0.5-phys mix	190	0.116	0.027	0.089	0.303

3.4.2.2 Analysis of chemical and structural features of intermediates

In order to explain why the dissolution step for melamine and boric acid mixtures had a major effect on BN pore structure, the intermediates samples were characterised. The chemistry and crystalline structures of melamine and boric acid intermediate and physical mixture were investigated using FTIR and XRD, respectively (Figure 3-16). Both analyses showed the appearance of additional peaks in melamine and boric acid intermediates, compared to their physical mixture. The intermediate structure formed was previously described in the literature as a hydrogen bonded melamine diborate compound. [179-180] It is, therefore, hypothesised that the formation of a melamine diborate compound is responsible for the formation of porosity in BN prepared from a melamine and boric acid mixture, possibly making the mixture more conducive to the formation of BN bonds at lower temperatures.

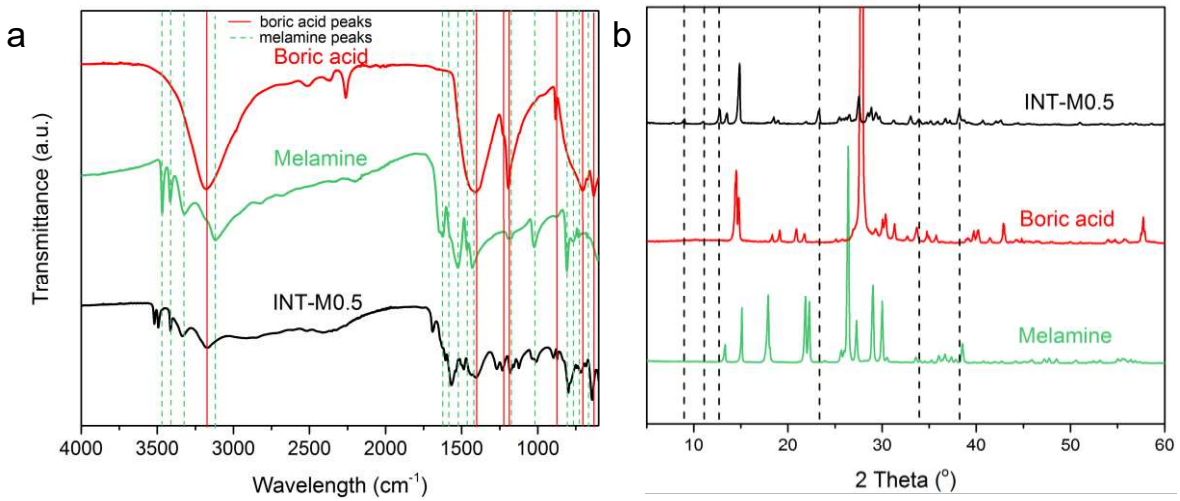


Figure 3-16 (a) FTIR spectra and (b) XRD patterns for melamine and boric acid precursors and intermediates.

In conclusion, the preparation step of the intermediates of reactions *via* dissolution and recrystallization of the precursors in water (for both urea/boric acid or melamine/boric acid mixtures) was of fundamental importance in order to control BN structure and chemistry. However, while boric acid and urea dissolved in water and recrystallised are simple physical mixtures with varying crystalline structures, melamine and boric acid when dissolved in water and recrystallised form a hydrogen bonded compound.

3.5 Effect of synthesis temperature on porous BN structure and chemistry

3.5.1 Analysis of structural features of BN

Porous BN was heat-treated post-synthesis at different temperatures under nitrogen atmosphere as it was thought that this may improve the crystallinity of the material and reduce the amount of oxygen impurities. The effect of this post-synthesis heat treatment on pore structures and surface areas was studied *via* nitrogen sorption, as increased crystallinity is often detrimental to porosity (Figure 3-17). As expected, porous BN surface areas and micropore volumes decreased with increasing heat-treatment temperatures. BN total pore volume remained relatively constant as temperature of the heat-treatment increased and, as a result, the mesopore volume increased with synthesis temperature. This could be explained by the release of oxygen from BN with increasing synthesis temperature, leaving pores in their place. The decrease in micropore volume, instead, could be linked to recrystallisation of porous BN, generating a BN material with higher crystalline order.

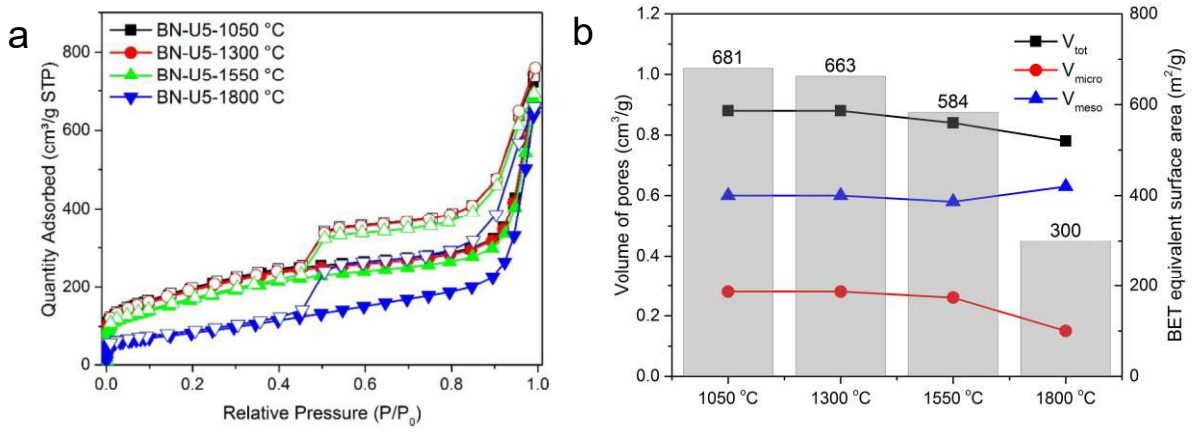


Figure 3-17 (a) N_2 sorption isotherms and (b) textural parameters deriving from the same for BN-U5 samples treated at different temperatures. Three different batches of BN-U5 (~ 3 g each) were synthesised and mixed together before heat-treatment.

In order to confirm whether a BN material with higher crystalline order was produced upon heat-treatment, XRD analysis was employed. XRD patterns for BN-U5 samples synthesised at different temperatures are reported in Figure 3-18a, in which all samples exhibited a turbostratic structure with two broad low intensity peaks. However, as the synthesis temperature increased, the peak position for the (002) reflection shifted to slightly higher angles, indicating a decrease in d-spacing (although because of the broadness of the peaks an accurate calculation was not possible). The full width at half maximum (FWHM) for the (002)

peak decreased with increasing temperatures, indicating that larger crystallites were formed. This suggests the transformation of porous BN to a more ordered structure, closer to a h-BN crystalline material, which exhibits a d-spacing of 0.33 nm,[25] as shown in Figure 3-18b.

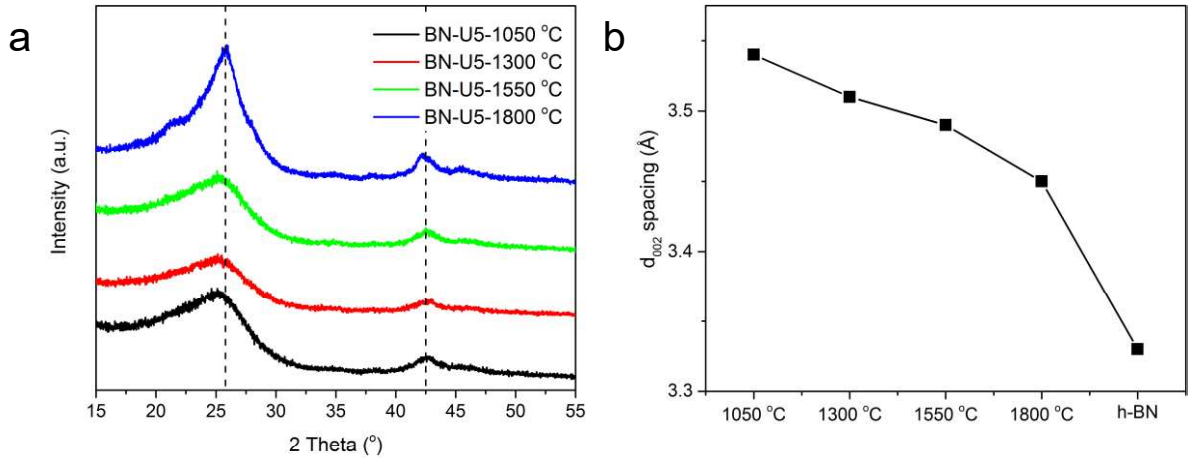


Figure 3-18 (a) XRD patterns and (b) d-spacing calculated from XRD patterns using Bragg's equation for BN-U5 samples treated at different temperatures.

3.5.1.1 Analysis of chemical features of BN

The chemistry of all samples was analysed with XPS. Relative atomic percentages are reported in Figure 3-19 and show little/ no changes with changing synthesis temperature.

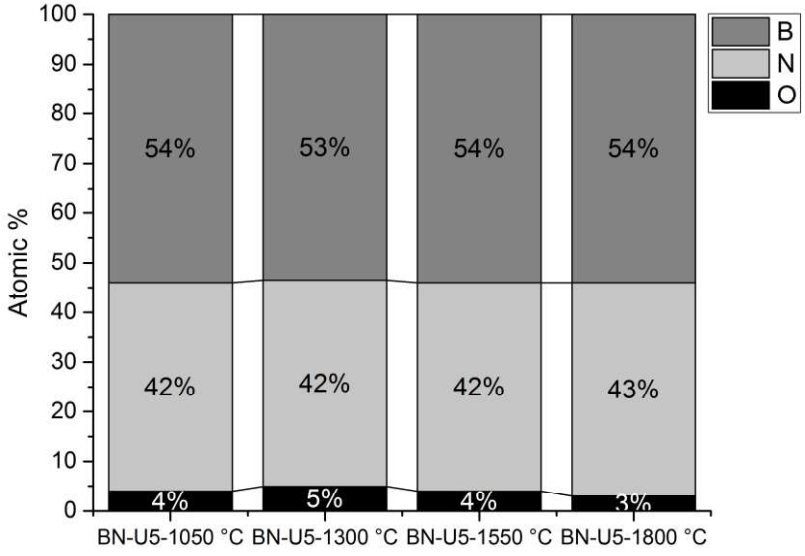


Figure 3-19 Relative atomic percentages deriving from XPS analysis for porous BN (BN-U5) synthesised at 1050 ºC and post-treated at different temperatures under nitrogen.

3.6 Effect of ramp rate on porous BN structure and chemistry

Porous BN synthesis has the potential for scale-up. However, industrial-sized reactors may not offer the capability of heating at high ramp rates, due to limitations in bulk heat transfer. Therefore, it is essential to evaluate the effect of temperature ramp rate on the resulting BN material.

The textural parameters of BN samples produced using different ramp rates were evaluated *via* nitrogen sorption isotherms at -196 °C (Figure 3-20). All of the isotherms exhibit similar shape independent of the ramp rate used and the analysis of the average textural parameters confirmed little/no change in surface areas and volume of pores, indicating that the ramp rate did not have any significant effect on porous BN structure.

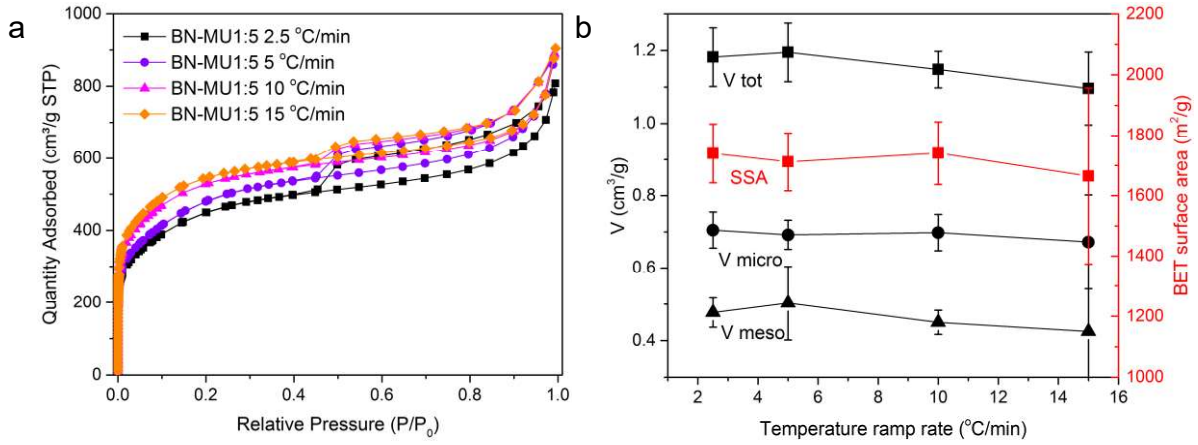


Figure 3-20 (a)Nitrogen sorption isotherms at -196 °C for porous BN samples (BN-MU1:5) produced at different ramp rates; (b) average textural parameters (over > 3 repeats) deriving from nitrogen sorption analysis.

The effect of temperature ramp rates on the thermal decomposition of the precursors was evaluated using TGA analysis (Figure A1.4, Appendix 1). Higher ramp rates affect the decomposition of the precursors in two different ways: i) the precursors start to decompose at higher temperatures; ii) more gases are released at higher temperatures. It was previously shown that the decomposition pathways of the precursors had a significant effect on BN pore structure, however, in this case the two effects could cancel each other out.

The chemistry of porous BN samples was also investigated using XPS analysis (Table 3-4), which showed very similar features and atomic percentages for all elements in porous BN samples synthesised from different temperature ramp rates, indicating that the ramp rate had no effect on BN chemistry.

Table 3-4 XPS relative atomic percentages for porous BN samples synthesised from different ramp rates.

Sample	B 1s	N 1s	O 1s
BN-MU1:5 (15 °C/min)	52	39	9
BN-MU1:5 (2.5 °C/min)	51	41	8

3.7 Conclusions

Porous BN synthesis mechanisms were investigated and the parameters controlling BN formation were elucidated. It was found that an excess of urea is necessary when urea and boric acid precursors are used in the formation of porous BN, while a molar ratio of 0.5 of melamine/boric acid is optimal in order to minimise the amount of resulting impurities when melamine and boric acid precursors are used. The preparation of the intermediate of reaction, formed by dissolution of the precursors in water and recrystallization, also proved to be fundamental for both precursors' mixtures. For melamine-based BN, the dissolution step allowed us to obtain a porous BN material, while the physically mixed equivalent produced a BN material with a low amount of pores. This effect was explained because of the formation of a melamine diborate compound during dissolution and recrystallisation. For urea-based BN, the preparation of an intermediate of reaction also proved important as this could greatly affect the porosity of the BN material obtained. Simply changing the drying time of the precursors produced porous BN with varied BET surface areas (from ~400 to >1,000 m^2/g.) This variation was attributed to differences in the thermal degradation of the intermediates, affecting BN formation. Intermediates dried for longer began decomposing at lower temperatures and, as a result, BN formation occurred during the release of more gases, which acted as porogen agents. Porous BN with high surface areas could also be obtained by simply physically mixing urea and boric acid without any dissolution step.

The synthesis temperature had a great effect on BN pore and crystalline structures. While all BN samples obtained were turbostratic (even at 1800 °C), the d-spacing decreased with increasing synthesis temperatures and the crystallite size increased, pointing towards the formation of a more crystalline BN. Increasing crystalline order resulted in decreased micropore volumes and surface areas of BN samples.

The temperature ramp rate used during BN synthesis had no major effect on BN pore structure and chemistry. Additionally, the results showed relatively good reproducibility, pointing towards the potential for scale-up of the synthesis method.

Chapter 4: Tuning Porous BN Surface Area and Pore Structure

The findings presented here were published in ACS Nano[181] and a patent was filed for this synthesis method (PCT Application Nº. PCT/GB2018/050686).

4.1 Introduction

Tuneable porosity and chemistry, as well as robustness, are key features of porous materials, as they are employed in a wide range of applications such as gas storage, water and air purification, molecular separations, catalysis and drug delivery.[7, 182-185] Porous BN is a promising material because of its excellent thermal stability (up to 1000 °C in air and over 1800 ℃ in inert atmospheres), high thermal conductivity and mechanical resistance as well as catalytic properties.[186-192] However, in order to pave the way to porous BN's commercial viability, a cost-effective and straightforward method to tune the material's pore structure is sought. As alluded to previously, a template-free method is preferred due to the lack of requirement for template removal and/or additional synthesis steps. A few studies were published on the topic, for instance, Nag and coworkers [91] demonstrated that the surface areas of BN could be increased by varying the molar ratios of urea to boric acid. However, the surface areas reported remained relatively low (S_{BET} < 1000 m^2/g). Wu *et al.*[96] produced porous BN with high surface areas (1900 m^2/g), however large excesses of N-precursor were required. In the previous chapter, the importance of the preparation of the intermediates of reaction was also demonstrated, but this approach required long preparation times.[111] Moreover, these studies still lacked of a fundamental understanding of porous BN formation and of a method for tuning the micro/mesoporosity of the material.

In this chapter, a novel synthesis method to produce porous BN with tuneable surface areas, pore and crystalline structures and chemistries was investigated, with potential for scalability.

This approach relies on the use of multiple N-precursors and does not require any washing step. With this method, a greater understanding of the formation of porous BN is reached. Using multiple N-precursors allowed for the release of gases, *i.e.* porogens, over a wider range of temperatures in comparison to a single N-precursor. The proposed precursors were readily available and cheap compounds, containing only N, C, O and H atoms, which either became part of BN structure, or acted as porogens when released as gases. Using this approach, no additional washing step was required as porous BN was produced relatively free of impurities. All samples were characterised with a large number of techniques to provide a deep understanding over porous BN chemistry, structure and pore morphology. In particular, STEM tomography was employed to provide a 3D image of the mesopores of the material. Further analytical techniques were employed to characterise the pore structure from the macro- to the nanoscale. Porous BN pellets were also produced by simply compressing powder samples, without the addition of any binders, with the aim of demonstrating the processability of the material and its mechanical robustness, both essential for industrial applications.

4.2 Materials synthesis

4.2.1 Multiple N-precursor synthesis

Porous BN samples were synthesised *via* a novel multiple N-precursor method shown in Figure 4-1b. For comparison, porous BN was also prepared using the traditional synthesis method, *i.e.* from one N-containing precursor and one B-contaning precursor. This method is called here "Single N-precursor route" and is shown in Figure 4-1 a. The naming system for porous BN samples deriving from the 2 methods is summarized within the schematic in Figure 4-1.

Different N-containing precursors and boric acid as a B-containing precursor were used for the synthesis of porous BN. The N-precursors used were urea (molecular biology grade, Sigma-Aldrich), melamine (melamine 99 %, Sigma-Aldrich) and biuret (biuret, Sigma-Aldrich). The B-precursor used was boric acid (ACS reagent, Sigma-Aldrich). The samples will be referred to as "single N-precursor BN" when prepared from a single N-precursor, while when multiple N-precursors were used the samples will be named "multiple N-precursors BN".

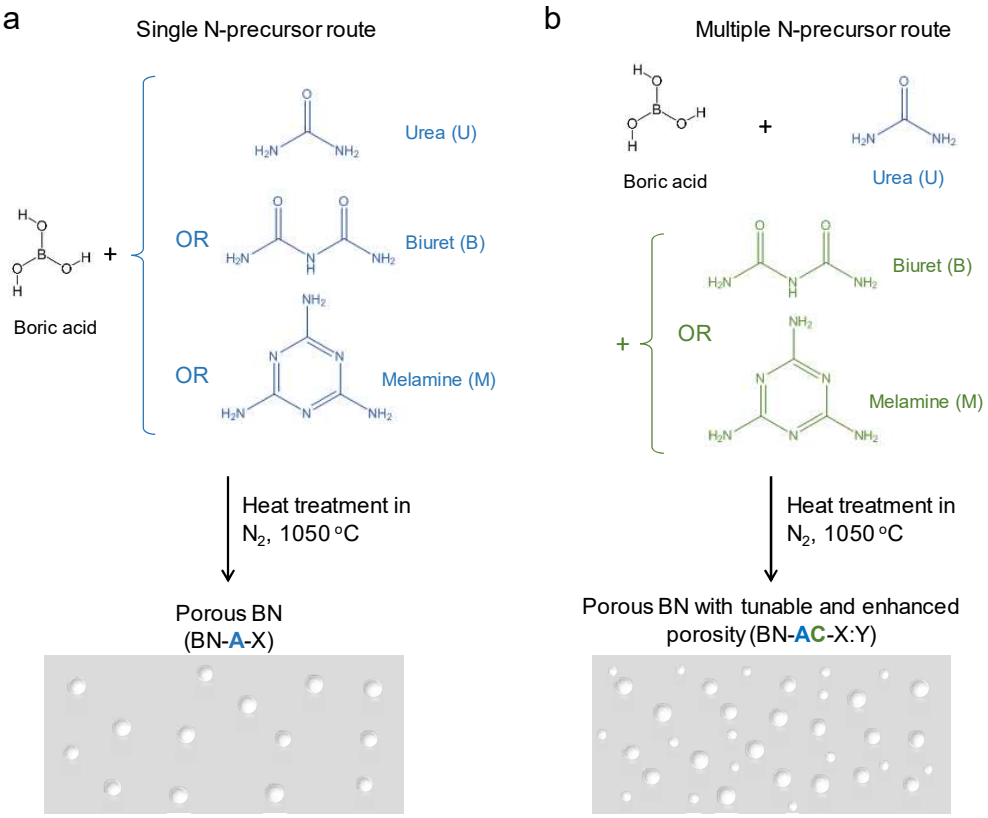


Figure 4-1 (a) Schematic of traditional single N-precursor synthesis and (b) the multiple N-precursor synthesis.

4.2.2 *Preparation of the reaction intermediates for the synthesis of single N-precursor BN*

The intermediates consisted of either a mixture of urea and boric acid, a mixture of biuret and boric acid, or a mixture of melamine and boric acid. In the first two cases, the chemicals were a simple physical mixture of the two precursors. In the latter case, when melamine was used, this was first dissolved with boric acid in water and the water was completely evaporated and the intermediate was further dried overnight at 85 ºC. This step is essential when melamine/boric acid precursors are employed, as discussed in Chapter 4. The molar ratios of urea:boric acid, biuret:boric acid and melamine:boric acid were equal to 5, 2 and 0.5, respectively. These ratios were selected based on previous results (Chapter 4) and because they produced relatively pure porous BN.[86, 90-91, 180]

4.2.3 *Preparation of the reaction intermediates for the synthesis of multiple N-precursors BN*

Either biuret or melamine were used as the N-precursor together with urea. Biuret and melamine both exhibited higher decomposition temperatures than urea, so acted as “secondary”

N-precursors. Typically, the molar ratio of urea to boric acid was kept constant at 5, while the molar ratio of biuret to boric acid was changed between 0.5 and 8 and that of melamine to boric acid between 0.25 and 1. The precursors were simply mixed and ground together prior to heat-treatment, without the need for a dissolution step. The molar ratio of melamine to boric acid was not increased over 1 as an excess of melamine produced a sample with a large amount of carbon impurities.

4.2.4 Synthesis of porous BN using single or multiple N-precursors

The intermediates were placed in an alumina boat crucible and heated up to the 1050 °C (10 °C/min ramp rate) under nitrogen gas flow (50 cc/min during analysis, 3 h at 250 cc/min to purge). The temperature was held at 1050 °C for 3.5 hours and the furnace was then allowed to cool naturally under continuous nitrogen flow. If a single N-precursor was used the samples were named BN-A-X while if multiple N-precursor were used the samples were named BN-AC-X:Y. Where A and AC correspond to the N-precursors used: urea, biuret or melamine (A or C = U, B, M). X and Y correspond to the molar ratios of N-precursor to boric acid. For example, BN-U5 was synthesized from a mixture of urea and boric acid in molar ratio of 5. BN-BU0.5:5 from a mixture of biuret:urea:boric acid in molar ratios 0.5:5:1.

4.2.5 Formation of pellets

Porous BN pellets were prepared from powder samples. BN-MU1:5 ~ 200 mg was coarsely ground and placed into a pellet die and 5 tonnes of load were applied.

4.3 Results and discussion

4.3.1 Structural properties and morphology

A number of techniques were employed in order to provide a complete picture of the porous BN pore shape, size and connectivity ranging from the micro- to the nano-scale. XRD was also used to confirm the formation of an amorphous or turbostratic BN material, as shown in Figure 4-2c. To allow for comparison, a spectrum for h-BN crystalline powder was also provided (Figure 4-2b), which shows the presence of much more well defined peaks of higher intensity, indicative of its highly graphitic structure. All porous BN samples exhibited low intensity and broad peaks at 2Theta 26° and 41° for the (002) and (100) planes of h-BN, respectively.[166] However, these XRD patterns (an example of which is shown in Figure 4-2c) are

indistinguishable between BNNSs or t-BN and so do not confirm the production of t-BN/a-BN. In order to understand if t-BN/a-BN or BNNSs were obtained, TEM was employed together with fast Fourier tranform (FFT) patterns. This is because fully exfoliated BNNSs would also show low intensity and broad peaks, as they lack 3D stacking order. An image for a typical porous BN sample is shown in Figure 4-2d. The sample exhibits a disordered structure with some regions of crystallinity, however no pattern is observed from the FFT, a clear indication of t-BN/a-BN. A TEM image image of a BNNS sample obtained *via* h-BN exfoliation was also collected for comparison (Figure 4-2b), commercial h-BN exfoliated *via* a 6-hour sonication in water). This image shows a more ordered hexagonal pattern, indicating the presence of highly crystalline 2D BNNSs, in agreement with the typical hexagonal pattern obtained in the FFT image.

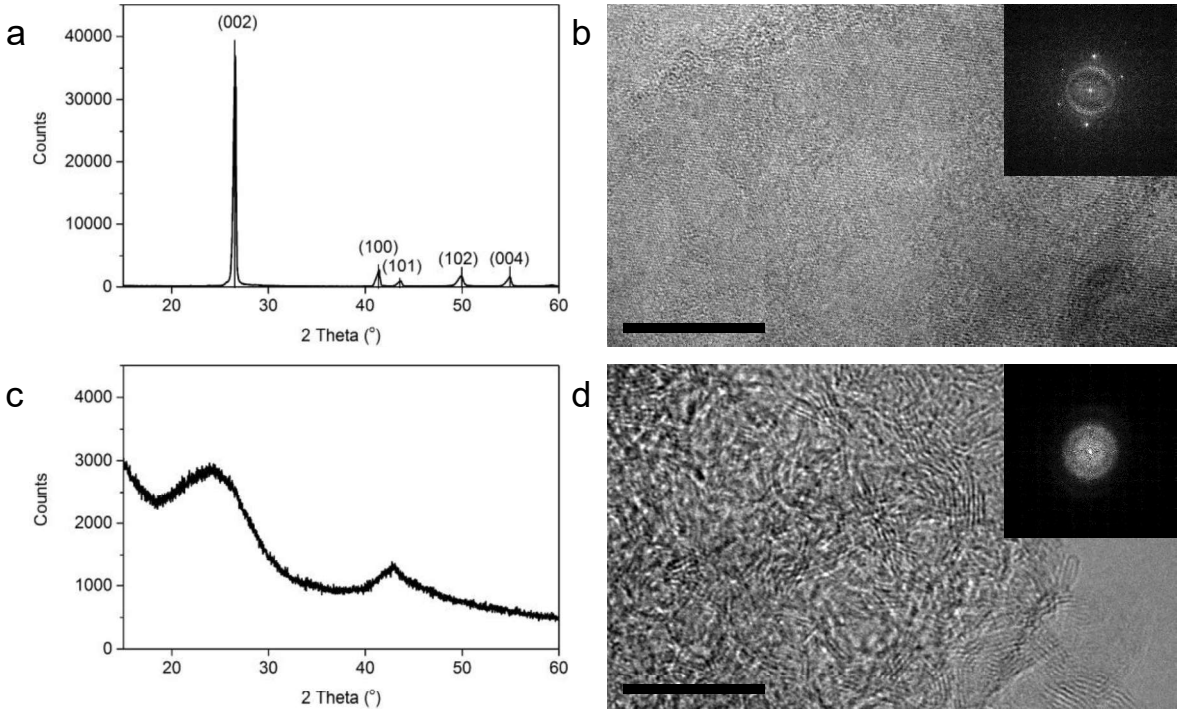


Figure 4-2 Typical XRD patterns for: (a) h-BN commercial powder and (c) porous BN (BN-U5 sample).Typical high resolution SEM images with FFT's diffraction patterns for: (b) exfoliated h-BN and (d) porous BN (BN-U5 sample). Scale bars in Figures (a, c) are 10 nm.

SEM imaging was also employed to visualise the morphology of the samples (Figure 4-3). Urea- or biuret- based samples exhibited a flake-like morphology, as would be expected from 2D nanosheets, while melamine-based BN showed a whisker-like morphology, with no visible macropores (Figure 4-3a-c), in good agreement with observations described in Chapter 4. When two nitrogen precursors were employed (Figure 4-3d-l), the morphology of the resulting

porous BN became more disordered, with a more fibrous structure obtained for melamine-based samples (Figure 4-3l). The different morphologies observed to the various N-precursor BN likely depends on the structure of the precursors.[82] Moreover, when a higher quantity of N-precursor compared to B-precursor is used, this can create some 'turbulences' while BN is forming, because of the higher quantity of gases released. This may result in the formation of a more disordered BN structure.

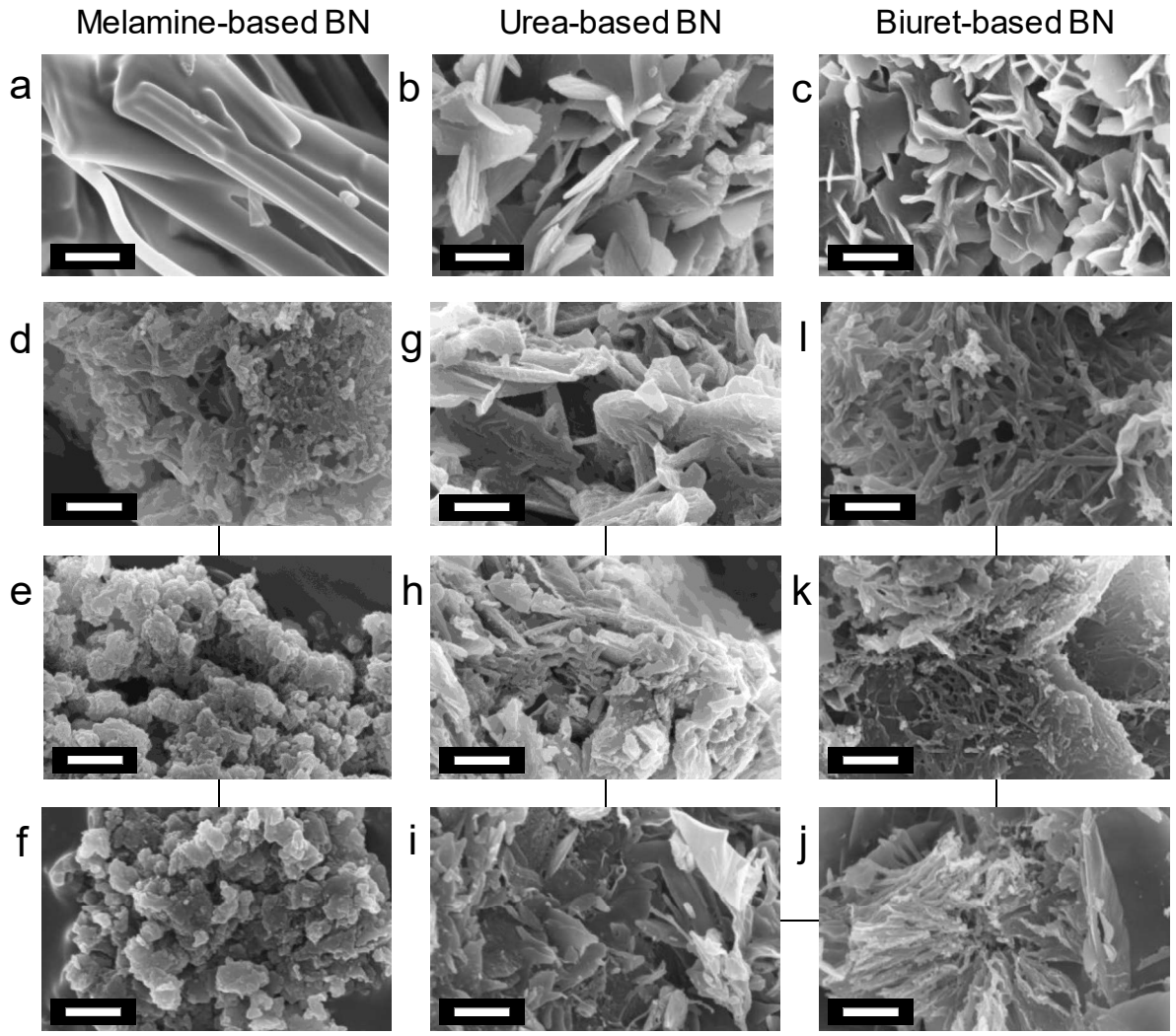


Figure 4-3 SEM images for all porous BN samples synthesised from single N precursors: (a) BN-M0.5;(b) BN-U5; (c) BN-B2; melamine-based multiple N-precursors: (d) BN-MU0.25:5; (e) BN-MU0.5:5; (f) BN-MU1:5; and urea-based multiple N-precursors: (g) BN-BU0.5:5;(h) BN-BU1:5; (i) BN-BU2:5;(j) BN-BU3:5; (k) BN-BU4:5; (l) BN-BU8:5. Scale bar represent 800 nm.

While macropore features can be observed from high resolution SEM images, the mesopores cannot be directly visualised from the images shown in Figure 4-3. Therefore, high resolution

STEM was used to visualise smaller features, particularly mesopores, within two different types of porous BN materials (a single N-precursor BN *vs* a multiple N-precursor BN, Figure 4-4). The porous BN materials exhibit different features, with the presence of what appears to be relatively uniform mesopores in the single N-precursor sample (Figure 4-4a-c) and thinner 2D sheets for multiple N-precursor BN (Figure 4-4d-f). Different particles were imaged within the same sample and showed that the materials were relatively homogenous. In order to visualize the 3D pore structure of these materials, a tomography reconstruction was performed on dark field STEM images collected at various tilting angles. The reconstructed volumes are reported in Figure 4-5. Single N-precursor BN exhibited a sponge-like structure, with regular spherical mesopores of diameters between 10-30 nm (Figure 4-5a-c). The volume percentage of mesopores calculated from the 3D reconstruction of the single N-precursor BN was 45 vol.%. On the other hand, multiple N-precursor BN exhibited smaller mesopores and appeared more like a thin 2D sheet which had crumpled on itself (Figure 4-5d-f). Although it may appear that single N-precursor BN exhibited a larger amount of pores, it must be taken into account that the smaller mesopores and micropores cannot be visualized at this resolution.

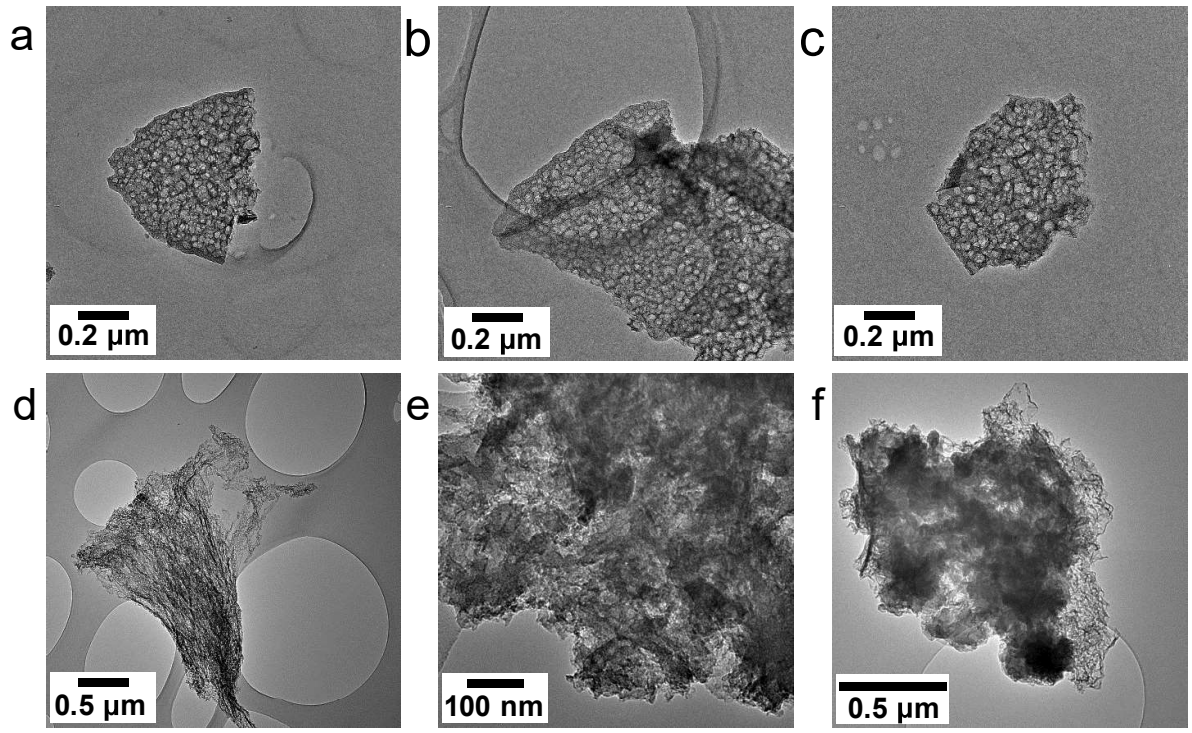


Figure 4-4 STEM images in bright field mode collected for single N-precursor BN: (a-c) BN-U5 and multiple N-precursor: (d-f) BN-MU1:5. The particles in Figures a and d were used for the tomography reconstruction.

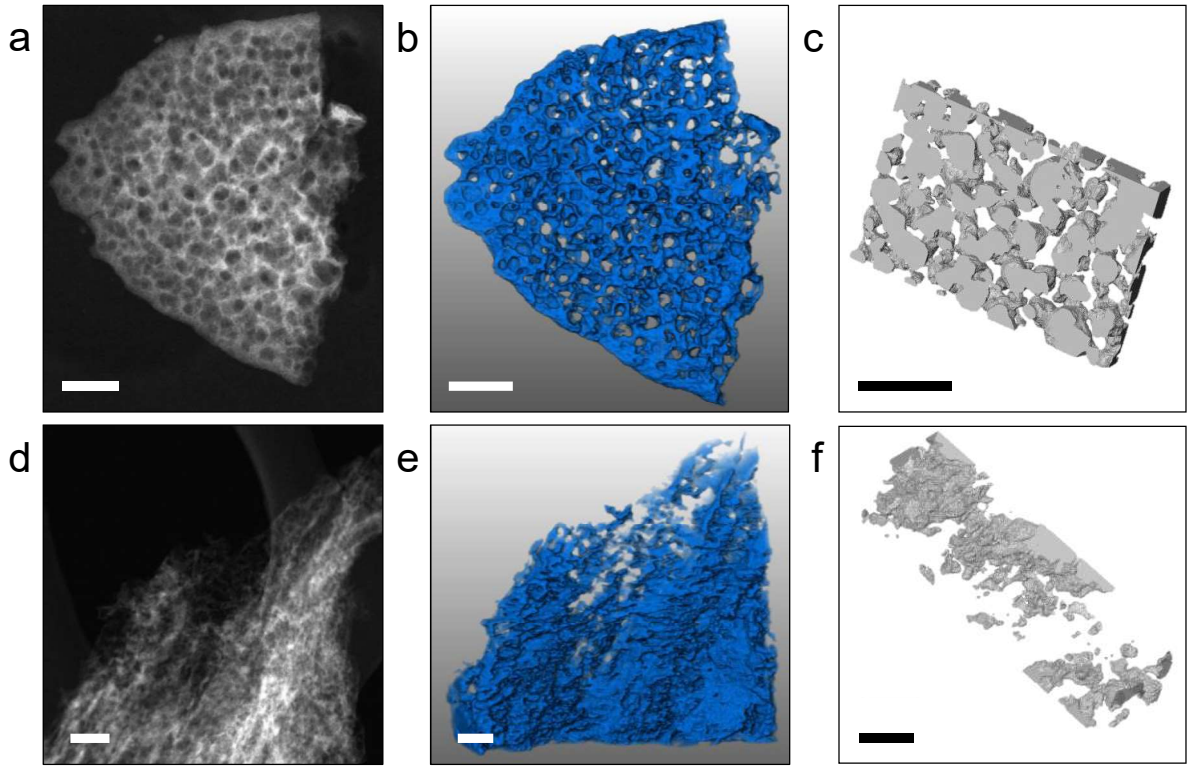


Figure 4-5 (a, d) Images of mesoporosity in boron nitride samples collected with dark field STEM images: (a) a single N-precursor (*i.e.* urea, BN-U5 sample); (d) multiple N-precursor (*i.e.* urea and melamine, BN-MU1:5 sample). (b, e) 3D tomography reconstructions of the 2 samples; (c, f) 3D reconstructions of the pores. Scale bars represent 100 nm.

In order to study smaller pores (*i.e.* micro- and lower range mesoporosity), nitrogen sorption analyses at -196 ºC were employed (Figure 4-6, Table 5-1). All samples exhibited type IV isotherms, indicating the presence of micro- and mesopores (Figure 4-6a,b). When multiple N-precursors were used, porous BN surface areas steadily increased with increasing quantity of the secondary N-precursor. The highest value measured was 1900 m^2/g, amongst the highest surface areas reported for porous BN. As a comparison, the theoretical surface area of a material composed of a single atomic layer BN sheet would be of ~2630 m^2/g.[29] Li *et al.* produced a porous BN material with the highest surface area reported (2078 m^2/g). However, in that case a block copolymer was used as a structure-directing agent, which introduced a large amount of impurities in the material.[185] Weng *et al.*[92] also produced high surface area BN by using dicyanamide and boric acid precursors, however, their synthesis was done under ammonia, a toxic and flammable gas, at 800 °C. Wu *et al.* also reported a high surface area BN which was synthesised by using urea and boric acid mixture in a molar ratio of 30, which was initially dissolved in a methanol/water solution.[96] However, this method required a dissolution step and the use of a huge excess of urea. Moreover, in these studies, no tuning of the

micro/mesoporosity was achieved. Herein, it was demonstrated that not only the surface area could be finely tuned, but also the ratio of micro- and mesopores. For instance, in melamine-based samples, surface areas, volume of micropores and total pore volume all increased when more melamine precursor was used, however, this also led to a decrease in mesopore volume. This increased micro- to mesopore ratio was likely due to the release of increased amounts of gases during heating, enhancing the formation of micropores. For the biuret-based samples, the surface areas and micropore volumes again increased with increasing amounts of biuret, however in this case the volume of mesopores exhibited a more irregular pattern. Adding small quantities of biuret reduced the resulting mesopore volume, while the addition of larger quantities of biuret appeared to have the reverse effect, leading to increased mesopore volumes. This effect was attributed to multiple factors, such as the different morphology of the samples, the amount of gases released and the temperature at which they were released.

Table 4-1 Textural parameters derived from N_2 sorption isotherms at -196 °C for all porous BN samples. ± indicates the standard deviation from at least 3 repeats, % indicates the percentage of micropores. * For BN-MU1:5 the highest surface area achieved is represented here, while the average of at least 3 repeats is ~ 1750 m^2/g.

Sample	$_{BET}(m^2/g)$	±	$V_{tot}(cm^3/g)$	$V_{micro}(cm^3/g)$	$V_{meso}(cm^3/g)$	%
BN-U5	945	73	0.85	0.33	0.53	38.8
BN-B2	936	--	0.59	0.33	0.26	55.9
BN-BU0.5:5	1263	--	1.02	0.46	0.56	45.1
BN-BU1:5	1387	--	0.72	0.53	0.19	73.6
BN-BU2:5	1525	--	0.77	0.58	0.19	75.3
BN-BU3:5	1564	--	0.82	0.60	0.22	73.2
BN-BU4:5	1599	--	0.92	0.64	0.28	69.6
BN-BU8:5	1602	--	1.09	0.54	0.55	49.5
BN-M0.5	1089	26	0.54	0.43	0.11	79.6
BN-MU0.25:5	1345	34	1.09	0.54	0.55	49.6
BN-MU0.5:5	1600	36	1.11	0.64	0.47	58.0
BN-MU1:5	1924*	104	1.20	0.78	0.42	65.0

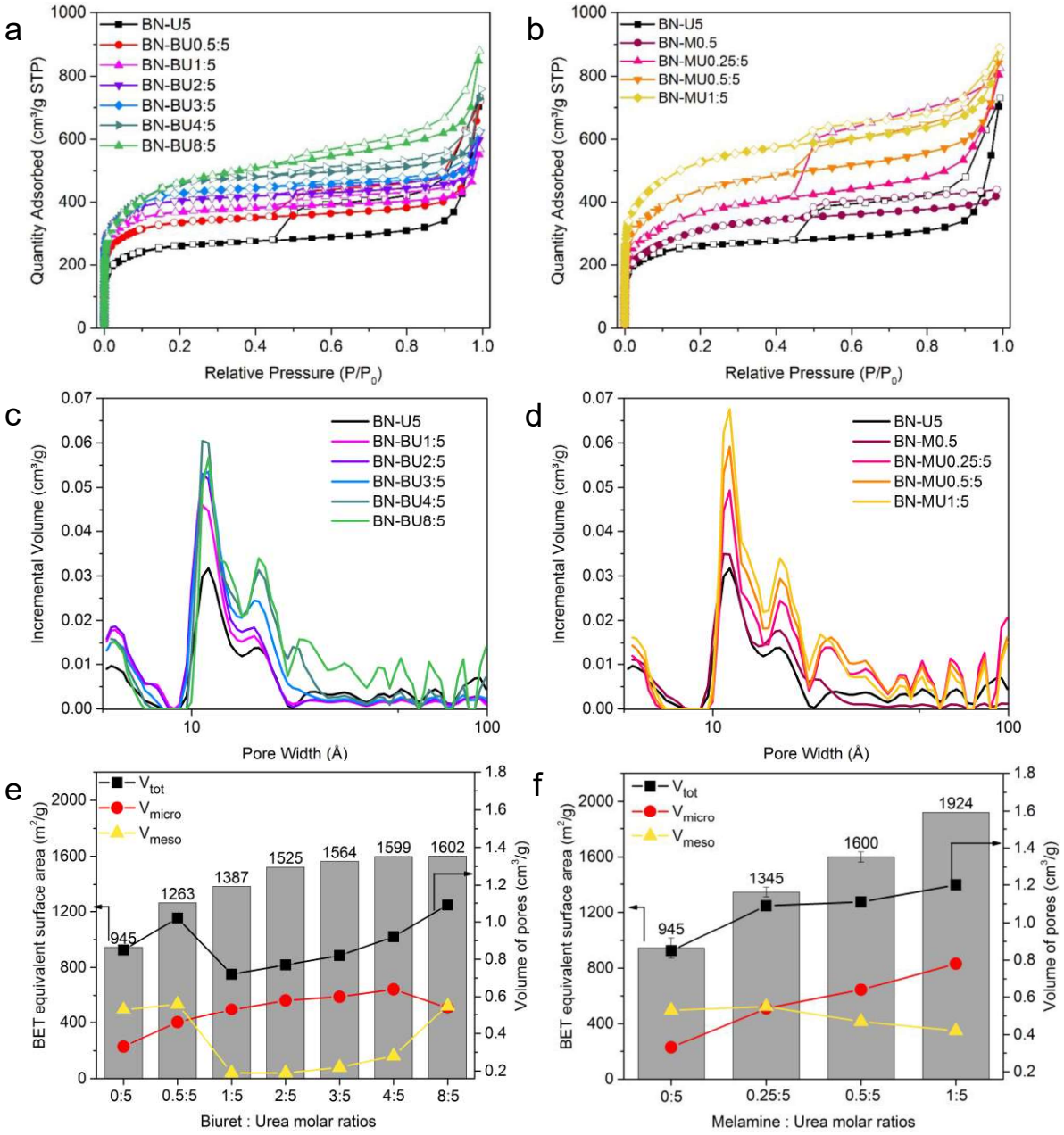


Figure 4-6 Tunable micro- and mesoporosity of boron nitride: (a, c) N_2 sorption isotherms measured at -196 °C for the BN samples synthesised from: (a) urea, biuret and boric acid mixtures and (c) urea, melamine and boric acid mixtures, all showing a gradual increase in the gas uptake and therefore porosity as more of the secondary N-precursor is added (open symbols represent desorption). (b, d) Bar plots showing the BET equivalent surface areas, total volume of pores, micropore and mesopore volume for samples synthesised from: (b) urea, biuret and boric acid mixtures as well as (d) urea, melamine and boric acid mixtures, exhibiting a gradual microporosity enhancement as more of the additional N-precursor is added (error bars represent standard deviations calculated from at least 3 repeats).

In order to explain why BN surface area and micropore volume increased with the use of multiple nitrogen precursors, the thermal decomposition patterns of different precursors and precursors mixtures were analysed. It was hypothesised that the pores were generated from the release of gases during the decomposition of the chemicals and so the variation in porosity may be explained by analysing the temperatures and decomposition profiles of the precursors and their mixtures. It can be observed from Figure 4-7a that among the nitrogen precursors, urea began to decompose at the lowest temperatures (~150 °C), while biuret decomposed at a slighly higher temperature (~190 °C), exhibiting a similar decomposition pattern. Melamine, instead, decomposed in a single step at a much higher temperature (~260 °C). To better understand the formation of porous BN, TGA was also performed on urea and boric acid; or urea, meamine and boric acid mixtures (Figure 4-7b). When a multiple N-precursor mixture was used (MU1:5), decomposition was observed over a wider range of temperatures, with more gases being released at higher temperatures when compared to a single N-precursor mixture (U5). It was, therefore, hypothesised that when urea decomposed, it began to release different gases, including ammonia, which started to react with boron oxide/boric acid, as observed in Chapter 4. When higher temperatures were reached, biuret or melamine then began to decompose, leading to a continued gas release during the formation of BN. These gases could both take part in the reaction and/or simply act as porogen agents. One could argue that the increase in surface area is due to an increase in nitrogen/boron molar ratio, as previously shown by Nag *et al.* [91] for urea and boric acid precursors. However, the highest surface area samples formed using multiple N-precursors exhibited N:B molar ratios of 16 and 22 and when a single N-precursor BN was produced with similar molar ratios, surface areas of only ~900 m^2/g were obtained, less that half that of the multiple N-precursor equivalents. This demonstrated that the use of different N-containing precursors is fundamental to enhance BN surface area and to allow the tuning of its pore structure.

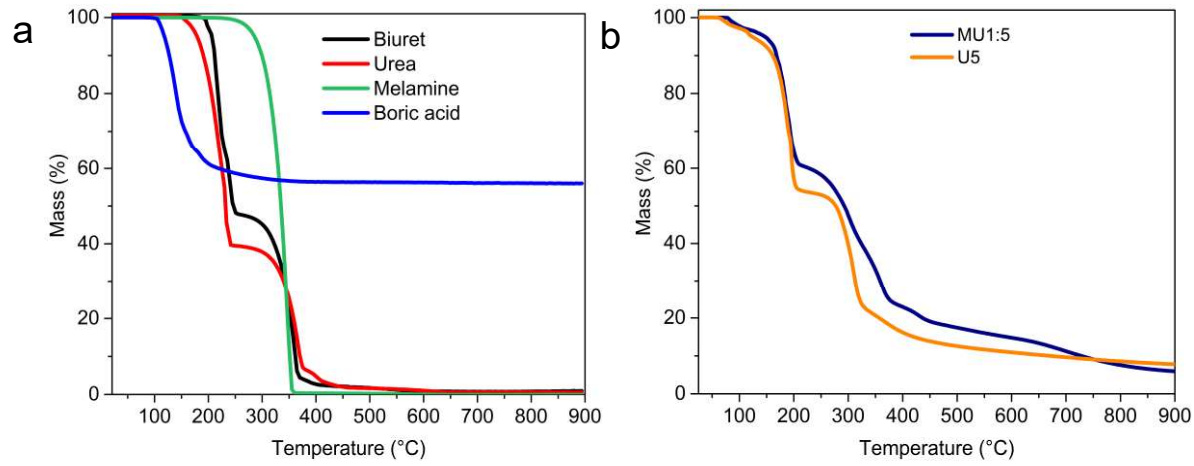


Figure 4-7 (a) TGA thermal decomposition patterns under nitrogen for different precursors and (b) precursors mixtures.

4.3.2 Chemical properties

The chemistry of the samples, both bulk and surface, were analysed as they are critical for adsorption applications. FTIR was performed on all samples and they all exhibited characteristic bands for h-BN (1350 cm^{-1}: B-N in-plane stretching mode; 800 cm^{-1}: B-N-B out-of-plane bending, Figure 4-8).[164] XPS analysis also confirmed the formation of h-BN with the typical B 1*s* and N 1*s* core level spectra for BN at 191.0 eV and 398.6 eV, respectively Figure 4-9. The presence of satellite peaks at higher binding energies was also observed.[169-171] These analyses suggested that some hexagonal phase is present, despite the samples being turbostratic/amorphous. XPS showed that oxygen was also present, as previously observed in Chapter 4,[111] in which it was attributed to a boronoxynitride compound. It is interesting to note that the oxygen content varies quite widely between the different samples, however this variation is likely associated with sample preparation, for example *via* varying degas times prior to XPS analysis, which could leave some adsorbed oxygen species on BN surface. A small carbon content (~2-4 at.%) is observed in all samples, and carbon species are mostly belonging to adventitious carbon and are, therefore, not reported here.

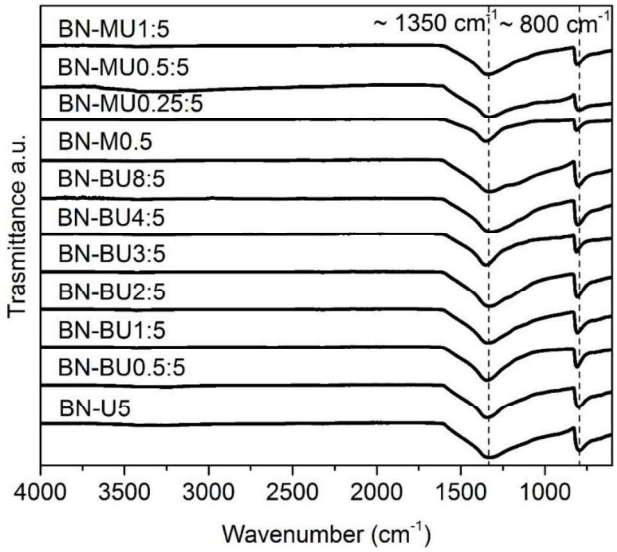


Figure 4-8 FTIR spectra for all porous BN samples. The dotted lines in the figure indicate the position of the two bands for h-BN (~1350 cm^{-1} B-N stretching mode and ~800 cm^{-1} B-N-B bending mode).

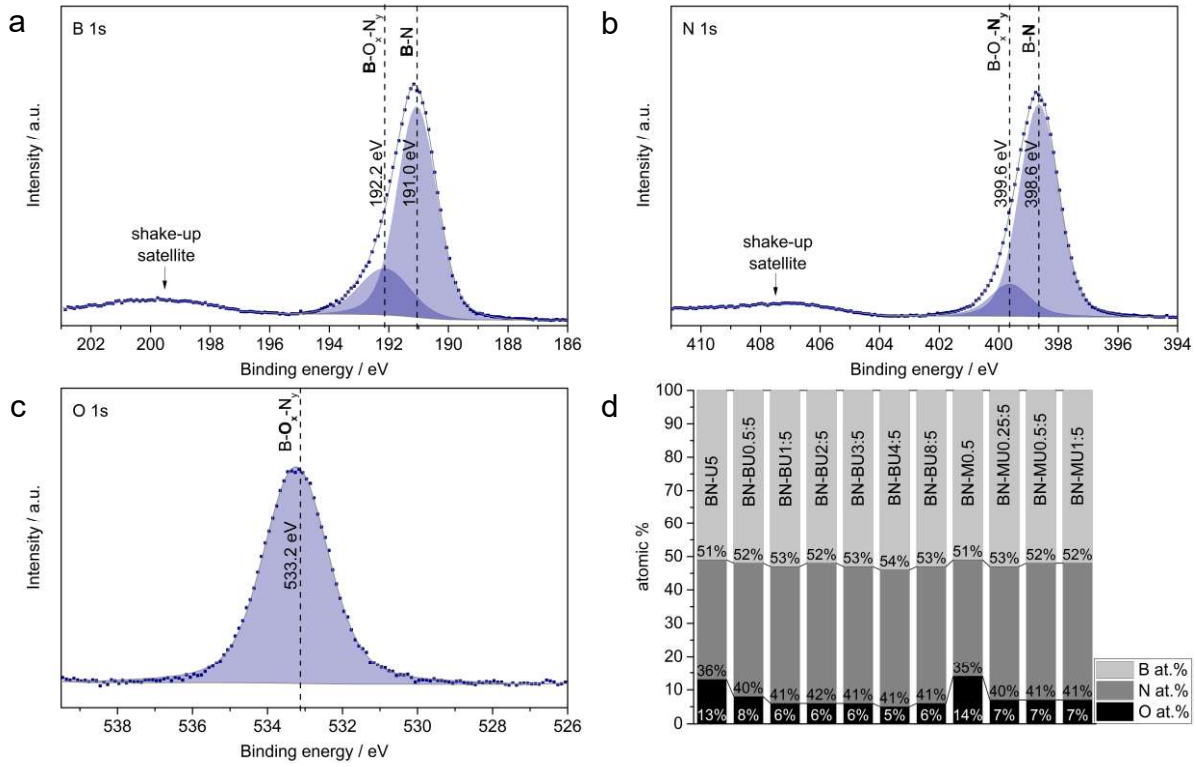


Figure 4-9 (a-c) Typical XPS high-resolution core level spectra for B 1*s*, N 1*s*, O 1*s* with peak fitting and (d) relative atomic percentages for all porous BN samples

4.3.3 Pelletisation of porous BN

In order to be used at industrial scale, powder adsorbents must be formed as pellets or beads to minimise pressure drops and to allow for easier handling. Therefore, the formation of pellets is commonly employed, however, this usually lowers the porosity of the material, due to the 'collapse' of pores upon compression and/or the addition of a low-surface area binder (*i.e.* an 'inactive' component). Porous BN pellets were produced from a multiple N-precursor BN (BN-MU1:5) (Figure 4-10b,c) and their porosity was analysed using N_2 sorption (Figure 4-10a). Suprisingly, the isotherms of the material before and after pelletisation exhibited a similar shape, indicating a limited decrease in the surface area and volume of pores. The average decrease over four repeats were: 16 % for surface area, 19 % for total pore volume and 17 % for micropore volume. This suggests that the porous BN powder exhibited great mechanical stability when compressed and points towards the processability of this material for potential applications in industry.

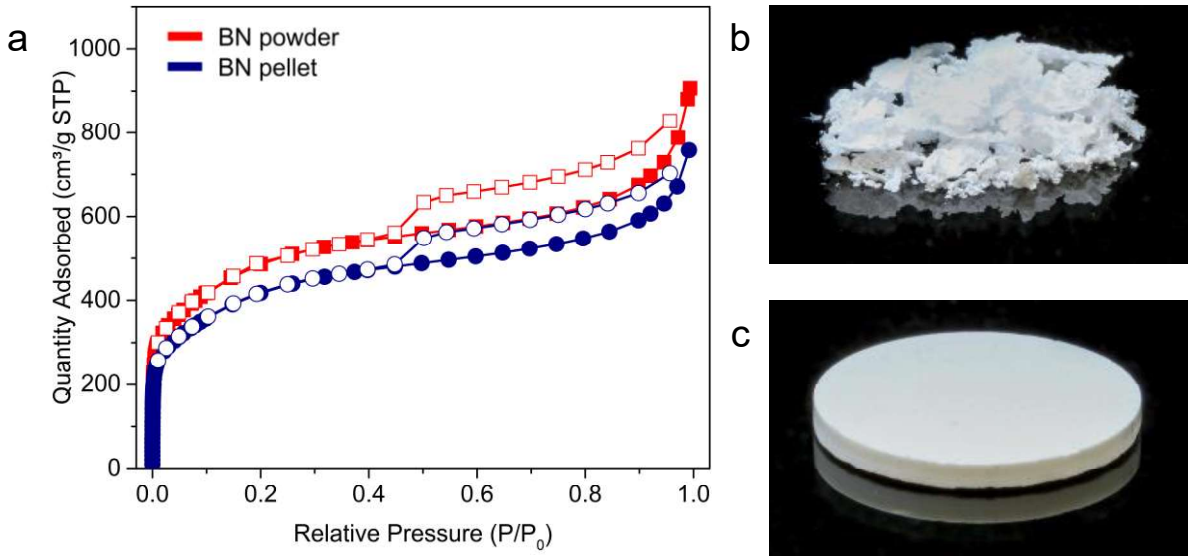


Figure 4-10 (a) Nitrogen sorption isotherms at -196 °C for porous BN (BN-MU1:5) powder and pellet; (b) powder sample;(c) pellet sample.

The surface morphology of porous BN pellets was imaged with SEM (Figure A2.1, Appendix 2) and showed the presence of regions with a large amount of macropores, created during compression of porous BN powder at the junction of different particles and regions in which little/no pores are present.

The microstructure of BN-MU1:5 powder and pellet samples were also compared *via* TEM analysis (Figure A2.2, Appendix 2) and showed no differences between the two samples, although this is not a bulk analysis method. Nevertheless, porous BN (both pellet and powder)

exhibited a d-spacing calculated from TEM images of about 0.35 nm and a disordered structure with a large number of defects, typical for t-BN materials. A typical triangular vacancy is also highlighted in Figure A2.2e, Appendix 2.

4.4 Conclusions

A novel synthesis method based on the use of multiple N-containing precursors was developed. The N-precursors have different thermal decomposition temperatures and act as both porogen agents and nitrogen source, enabling the control of porous BN structure and the production of BN with amongst the record-high surface areas for these materials. A key outcome of this chapter is the tuneability of micro and mesopore volumes in porous BN. Moreover, the pore network was directly visualized using tomography and characterized with a variety of techniques from the nano- to the macro-scale. Finally, porous BN powder was structured into pellets with minimal decrease in porosity, pointing to a good processability of the material.

Chapter 5: Evaluating and Enhancing Porous BN Hydrolytic Stability

Manuscript currently under revision by industrial partners.

5.1 Introduction

Chemical separations and catalysis require the development of robust, recyclable porous materials, opening the door to their long-term utilisation. Porous BN has recently attracted a lot of attention in the scientific community as a promising candidate for many of these applications owing to its excellent thermal stability and high surface areas. However, although a number of studies demonstrate porous BN with good water stability,[90, 120] contrasting reports have been published, leading to questions about the feasibility of using porous BN materials in applications involving even low amounts of water. Li *et al* employed porous BN for the removal of methyl orange (MO) from water and showed that the sorbent could be regenerated by heating in air at 350 ºC for 2 h.[90] In another example, Lei *et al.* reported the adsorption of Congo red (CR) from water using porous BN and its subsequent regeneration at 600 ºC in air, maintaining the original porosity.[120] However, t-BN materials were reported to be unstable upon exposure to water or moisture.[97, 193] According to Cofer and Economy, the instability of t-BN is an intrinsic problem, dependent upon the material's d-spacing.[106] Larger d-spacings led to decreased water stability in comparison to fully crystalline h-BN, which was attributed to weaker bonds between BN sheets, making the material more susceptible to hydrolytic attack.[106] During hydrolysis, BN sees the formation of (-OH) groups at the edges, increasing the material's hydrophilicity and promoting BN decomposition into boric acid and ammonia.[50] Surprisingly, a similar hydrolysis mechanism was also reported for fully crystalline h-BN materials sonicated in water.[50] In this case, hydrolysis was proposed as an exfoliation mechanism to "cut" h-BN sheets. Cut edges contained mostly boron atoms with attached

hydroxyl groups, which was explained with the thermodynamically favourable release of ammonia during hydrolysis. However, the authors did not mention the possibility of full decomposition of BN. Recently, Florent and Bandosz tested the water stability of carbon doped BN,[108] reporting a high sensitivity of the material to water and moisture, resulting in chemical changes and losses in both surface area and porosity. Therein, the B-C bonds were identified as the preferred sites of attack, although the B-N bond was also reported to be unstable. With conflicting reports in the literature, the need for an in-depth evaluation of the stability of porous BN toward hydrolysis is required. The lack of understanding of porous BN's instability in water, is therefore limiting the material's utilisation.

In this chapter, the aqueous stability of porous BN samples synthesised in Chapter 5 was investigated in detail to provide a deeper understanding of the effects of water or moisture on the chemistry and structure of BN materials with different pore structures and to elucidate the hydrolysis mechanisms. Furthermore, a strategy for the enhancement of BN stability in water was also proposed. Porous BN materials with significantly greater stability were produced, while still maintaining high surface areas and good adsorption capacities. The results presented here are key in enhancing porous BN lifetime when used for applications in catalysis and molecular separations, where moisture or water may be present.

5.2 Materials synthesis

5.2.1 Preparation of the reaction intermediates for the synthesis of BN

Intermediates were prepared by simply mixing and grinding B- and N-containing precursors without any dissolution step, using a single and multiple N-precursor method as described in Chapter 5. Three different precursor mixtures were selected for this study, as they allow for the synthesis of porous BN materials with different pore structures. The naming system is described in Chapter 5, but details of the molar ratios for each sample are outlined below:

- Precursor for BN-U5: molecular ratio of urea:boric acid = 5:1;
- Precursor for BN-MU0.25:5: molecular ratio of melamine:urea:boric acid = 0.25:5:1;
- Precursor for BN-MU1:5: molecular ratio of melamine:urea:boric acid = 1:5:1.

5.2.2 Synthesis of porous BN using single or multiple N-precursors

Intermediates were heat-treated at 1050 °C or 1500 °C (10 °C/min) for 3.5 h under constant nitrogen gas flow. The furnace was then allowed to naturally cool under nitrogen to produce

porous BN materials with different pore structures. Porous BN samples synthesised at 1050 °C are named “low temperature BN”, while porous BN synthesised at 1500 °C are named “high temperature BN”.

5.3 Stability tests

Porous BN samples were exposed to water, moisture, or organic solvents (n-heptane or ethanol) regenerated and then fully characterised to evaluate their stability. Porous BN thermal and oxidative stabilities were also evaluated. A description of the tests is outlined below.

5.3.1 Exposure to aqueous solutions

Porous BN was exposed to aqueous solutions of organic dyes in order to investigate the water-stability of the adsorbents. The tests were performed by vigorously stirring porous BN powder (100 mg) in 250 mL aqueous solutions (40 mg/L) of Rhodamine B (RhB) for 4 h, at room temperature. After the dye removal tests, the materials were filtered, dried and regenerated at 600 ºC in air to decompose the dye. In this Chapter, the hydrolytic stability of the material was evaluated by fully characterising chemistry and structure of BN before and after regeneration.

5.3.2 Exposure to moisture: Water vapour sorption

Porous BN samples were degassed at 120 °C at roughly 0.2 mbar pressure and again *in-situ* on the porosity analyser for 4 h down to around 0.003 mbar. Water vapour isotherms were collected at 30 ºC for porous BN samples at up to 90 % relative humidity in a gas/vapour volumetric analyser (3Flex). The timings for the collection of each point were not recorded as the equipment waited for equilibrium to be reached. This test was performed primarily to evaluate the affinity of the samples with water and their water adsorption capacity. However, after water vapour sorption tests, porous BN samples were degassed at 250 ºC in vacuum and characterised to evaluate their stability after exposure to moisture.

5.3.3 Exposure to organic solvents

Low temperature porous BN (BN-MU1:5, 100 mg) was exposed to solvent (n-heptane and ethanol; Analytical grade) by vigorously stirring the powder in 250 mL of solvent overnight (~24 h) at ambient temperature. The material was then filtered, dried and regenerated at 250 °C in vacuum to evaluate its organic solvent stability.

5.3.4 Exposure to high temperature oxidising and non-oxidising environments

Thermal and oxidative stabilities of BN were evaluated by heating the samples (~30 mg) in a TGA apparatus from ambient to 1050 °C (10 °C/min) under nitrogen or air (100 mL/min).

5.4 Results and discussion

5.4.1 Water stability evaluation

Three low temperature BN samples with different pore structures and similar chemistries were exposed to aqueous solutions of RhB dye (dye adsorption capacities for porous BN are discussed in Chapter 7). Here, the hydrolytic stability of porous BN was analysed by fully characterising the samples after regeneration, which was performed at 600 ºC in air. One could argue that if any structural/chemical changes occurred in porous BN, these could be caused by carbon deposits deriving from incomplete decomposition of the dye. TGA analysis was, therefore, performed to evaluate the decomposition of RhB in air. The results from the decomposition analysis (Figure A3.1 Appendix 3) demonstrated that RhB fully decomposed at the selected temperature, leaving no residual carbon. Moreover, XPS analysis was performed on porous BN after regeneration and further confirmed the full decomposition of RhB, as no chlorine was observed in the BN material and the amount of carbon remained similar or lower than in the starting material (~2 at% *vs* ~3 at%, respectively) (Figure A3.1b Appendix 3). The effects of exposure to water on BN's physical and chemical properties were, therefore, analysed.

Firstly, the pore structure and surface area of low temperature BN was characterised before and after exposure to water *via* nitrogen sorption isotherms at -196 ºC. The results for all samples before and after exposure to water (*via* RhB sorption tests) are reported in Figure 5-1a-d. All porous BN samples showed a significant decrease in surface area and micropore volume after water exposure. Interestingly, the percentage of micropores decreased significantly in all porous BN samples, indicating that the micropores are initially most susceptible to degradation. This hypothesis is confirmed as porous BN samples with higher micropore volumes (BN-MU1:5 > BN-MU0.25:5 > BN-U5), showed increased water instability, as indicated by a larger decrease in surface area and pore volume. For instance, highly microporous BN-MU1:5 exhibited a significant decrease in surface area from 1650 to 29 m^2/g after exposure to water. It must be noted that highly microporous BN materials likely exhibit a large amount of defect sites, which are preferential sites of attack and reactivity.

It was previously proposed that the stability of porous BN depends upon the d(002)-spacing.[106] The crystalline structure of porous BN before and after exposure to water was, therefore, analysed with XRD. XRD patterns for all porous BN samples before and after exposure to water are reported in Figure 5-1e,f. All pristine porous BN samples exhibit very similar XRD patterns with the same peak position for the (002) peak between the different samples, indicating that they all exhibit similar d(002)-spacing (~0.35 nm). The absence of other reflections other than the (002) and (100) and the large width and low intensity of the peaks indicate that all samples are turbostratic, as previously highlighted in Chapter 5. After exposure to water and regeneration, all samples showed a higher relative intensity of the (002)/(100) peaks, possibly indicating a preferred orientation of the crystals along the (002) plane. In addition, the peak position for the (002) peak (~25°) shifted to higher angles, indicative of a decrease of the d(002)-spacing and the full width at half maximum (FWHM) decreased, demonstrating an increase in crystallite size (larger number of 2D layers). These three factors together showed that the samples exhibited higher crystallinity after exposure to water, likely as amorphous BN was more readily decomposed in water, resulting in an apparent increase in crystallinity.

While it was demonstrated that water had a detrimental effect on the pore structure of BN materials, it is also important to understand if any chemical changes occurred. All samples were, therefore, characterised using XPS and FTIR analyses. Typical FTIR spectra for low temperature BN before and after exposure to water are shown in Figure 5-2a, b. Prior to exposure to water, the sample exhibits the two characteristic BN bands at ~1360 cm^{-1} (B-N in-plane transverse stretching mode) and ~800 cm^{-1} (B-N-B out-of-plane bending mode),[164] with little/no -OH groups present. After exposure to water, a broader and more intense shoulder for -OH groups was detected together with a small peak at ~1000 cm^{-1}, which was assigned to the B-O bending mode.[194] The relative atomic percentages derived from XPS for low temperature BN samples before and after exposure to water are summarised in Figure 5-2c and d. As expected, the oxygen content increased in all porous BN samples after exposure to water. The high-resolution spectra for B 1*s* for a typical sample before and after water exposure are also shown in Figure 5-2e and f. The boron oxide peak becomes more intense after exposure to water and shifts to higher binding energies, likely indicating an increase in oxygen content. This is an indication that hydrolysis is occurring, causing the oxidation of BN and formation of a larger quantity of boronoxynitride and B-OH groups.[50] Samples with higher micropore volumes and surface areas (BN-MU1:5 > BN-MU0.25:5 > BN-U5) showed higher increases

in oxygen content, indicative of more extensive hydrolysis, in line with the previously described structural changes. The relative nitrogen content decreased in all samples after exposure to water, confirming that a decomposition reaction is occurring, in which water reacts with BN to release ammonia: $3H_2O + 2BN \rightarrow B_2O_3 + 2NH_3$.[50]

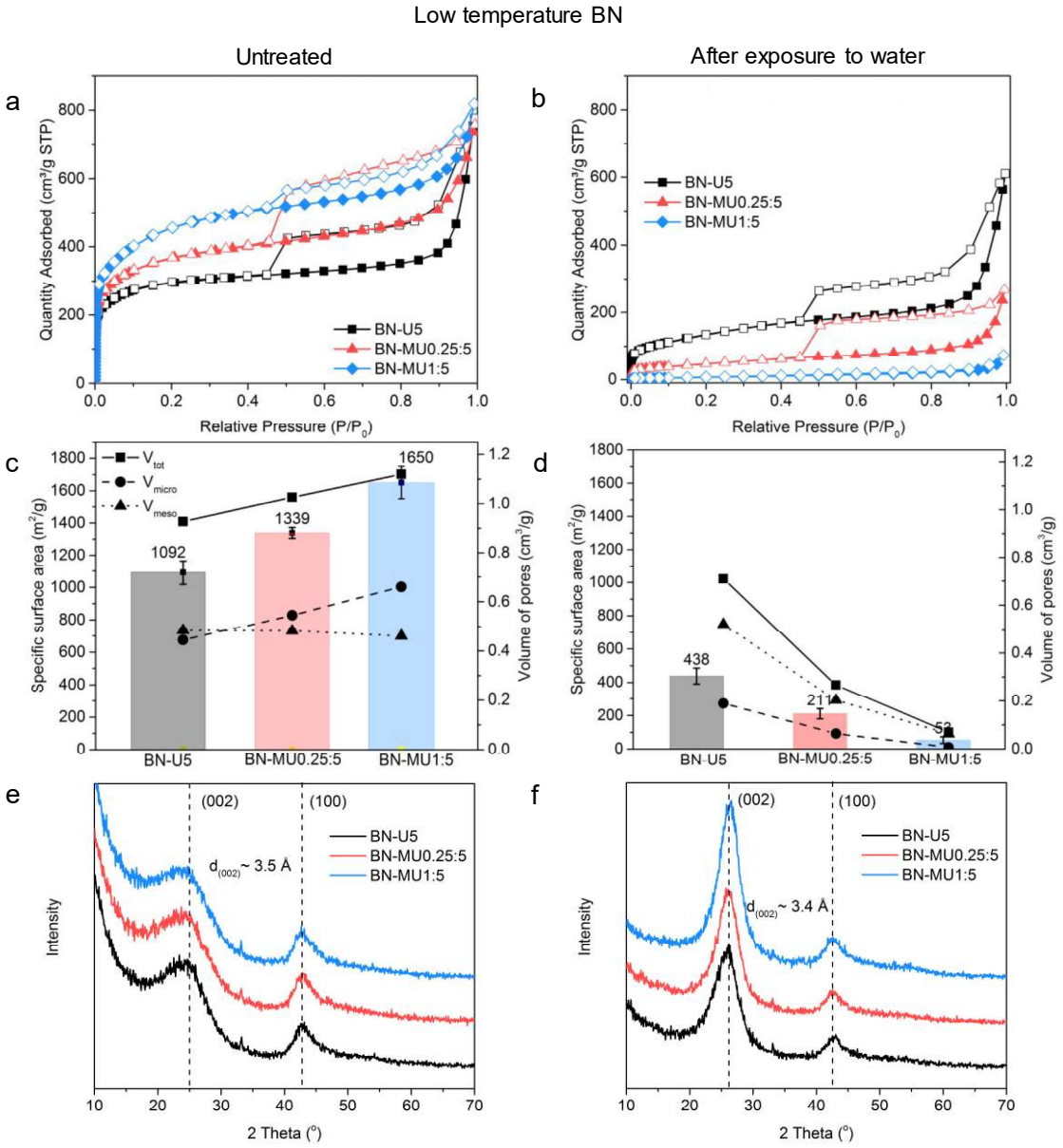


Figure 5-1 (a,b) Nitrogen sorption isotherms at -196 °C for low temperature BN samples before and after exposure to water (open symbols represent desorption); (c,d) textural parameters deriving from the same. Error bars represent ranges from 2 repeats; (e,f) XRD patterns for low temperature BN before and after water exposure (the peak at ~32° derives from a defective sample holder).

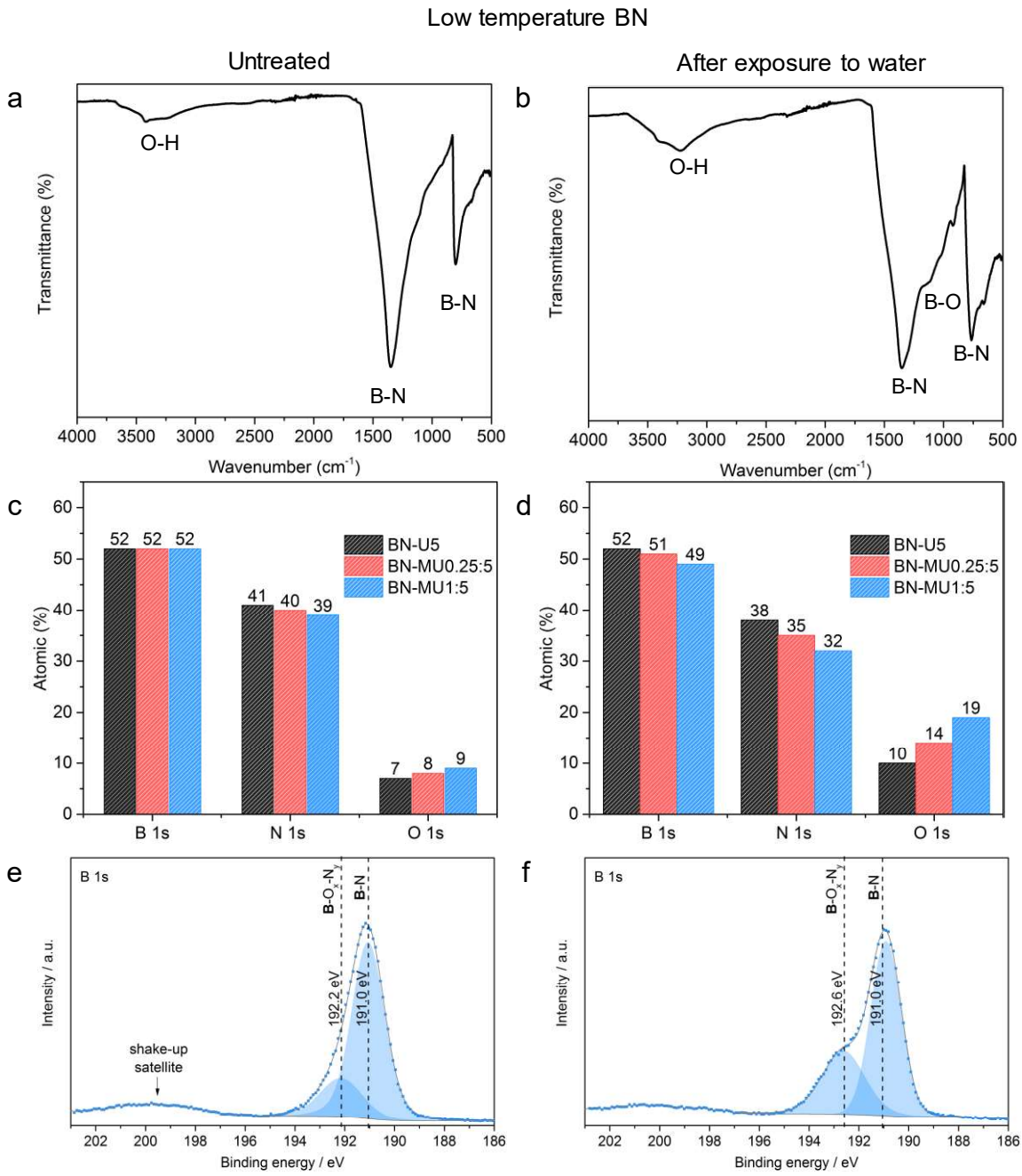


Figure 5-2 (a,b) FTIR spectra for low temperature BN (BN-MU1:5) before and after exposure to water; (c,d) Relative atomic percentages from XPS analysis for low temperature BN before and after exposure to water (*via* RhB sorption); (e,f) typical high resolution spectra for boron for low temperature BN (BN-MU1:5) before and after exposure to water.

Although BN oxidation was demonstrated from XPS analysis, the full identification of B_2O_3 was not possible, which may be due to peak overlap or dissolution of the boron oxide in water. In order to confirm the formation of B_2O_3, porous BN (BN-U5) was sonicated in water for 7 h (to accelerate its decomposition) and was then dried at 65 °C until full evaporation of the water (further details in Appendix 3). The chemistry of the resulting product was characterised with

XPS analysis (Figure A3.2. Appendix 3). The high-resolution B 1*s* and N 1*s* spectra for BN-U5 after exposure to water showed the presence of the two typical peaks for h-BN (at 190.7 eV and 398.4 eV for B and N, respectively).[169-171] However, the peaks corresponding to BN showed decreased relative intensities and it was calculated that roughly 6 mol% of BN remained (Figure A3.2d Appendix 3). The quantity of O atoms increased dramatically from ~12 to ~ 48 at.% and that of N decreased from ~38 to ~ 8 at.%. The high-resolution spectrum for B 1*s* exhibited an additional peak (other than the one belonging to BN) at ~193.5 eV, which was assigned mainly to B_2O_3 but also to some B-O-B and B-OH groups.[195] The high-resolution spectrum for N 1*s* also showed an additional peak at ~402.1 eV, which was attributed to NH_4^+ groups.[196] These observations are in line with the hypothesis of the formation of ammonia (gas) and boron trioxide (dissolved in water and then recrystallised), confirming the mechanism of reaction proposed.

To provide a greater insight into the interactions of porous BN with water, vapour isotherms were collected at 30 ºC for the pristine samples and are reported in Figure 5-3. Samples with higher micropore volume and surface areas showed higher water uptake (BN-MU1:5). All samples exhibited a degree of water sorption from low relative pressures, indicating that porous BN samples may be slightly hydrophilic. If total water uptake was normalised to the material's surface areas, all samples exhibited a similar uptake of 0.2 cm^3/m^2.
Interestingly, at about 30 % of relative humidity (0.3 P/P_0), all samples showed a steeper uptake of water vapour. This could be an indication that BN becomes more hydrophilic, because of the formation of -OH groups, adsorbing more water with increasing relative humidity levels.
All porous BN samples (Figure 5-3) showed incomplete desorption of water upon reduction of pressure, which is also an indication of some structural/chemical changes in the material (due to hydrolysis), or chemisorption.

After water vapour sorption, porous BN samples were degassed at 250 ºC under vacuum and were fully characterised. Some hydrolysis was observed even after exposure to only water vapour (discussed further in Appendix 3), rather than aqueous solutions as in the dye sorption experiments.

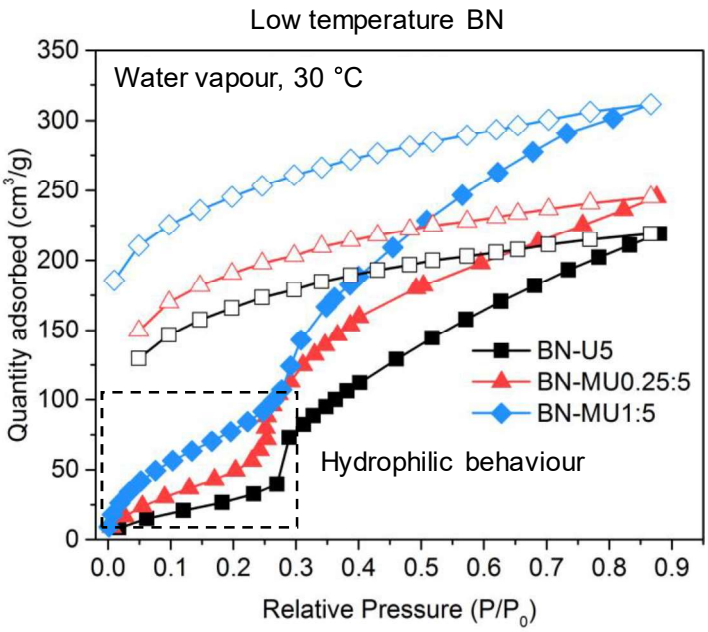


Figure 5-3 Equilibrium water vapour sorption isotherms at 30 ºC for three porous BN samples with different pore structures (open symbols represent desorption).

From this section, it is hypothesised that the water instability of low temperature porous BN is linked to the presence of defects, which are preferential sites for attack; presence of oxygen atoms, which increase the material's hydrophilicity; and textural properties, *i.e.* high surface area and turbostratic nature. A way to mitigate BN instability while still maintaining the material's porosity, would be to produce low-defects BN nanosheets arranged in a disordered manner to produce porosity (house of card configuration), without oxygen impurities. Taking all of these considerations into account, in the following section an approach to improve BN water-stability is presented by synthesising porous BN at higher temperature (1500 °C instead of 1050 °C).

5.4.2 Water stability enhancement

5.4.2.1 High-synthesis temperature BN

Three BN samples synthesised at high temperature (1500 ºC) (namely: BN-U5, BN-MU0.25:5 and BN-MU1:5) were compared to samples synthesised from identical formulations but at lower synthesised temperature (1050 ºC). Firstly, pore structure and surface area of the materials were characterised from nitrogen sorption analysis at -196 ºC (Figure 5-4). As expected, the surface areas and micropore volumes of porous BN samples decreased at high synthesis temperature (as observed in Chapter 4). However, for samples synthesised from

multiple N-precursor mixtures, BET surface areas of around 1000 m^2/g could still be obtained, compared to ~700 m^2/g for single N-precursor BN (BN-U5-1500 ºC). Interestingly, the total pore volume and mesopore volume showed no significant decrease when compared to low-temperature samples, as shown from total uptakes in nitrogen isotherms in Figure 5-4a-c.

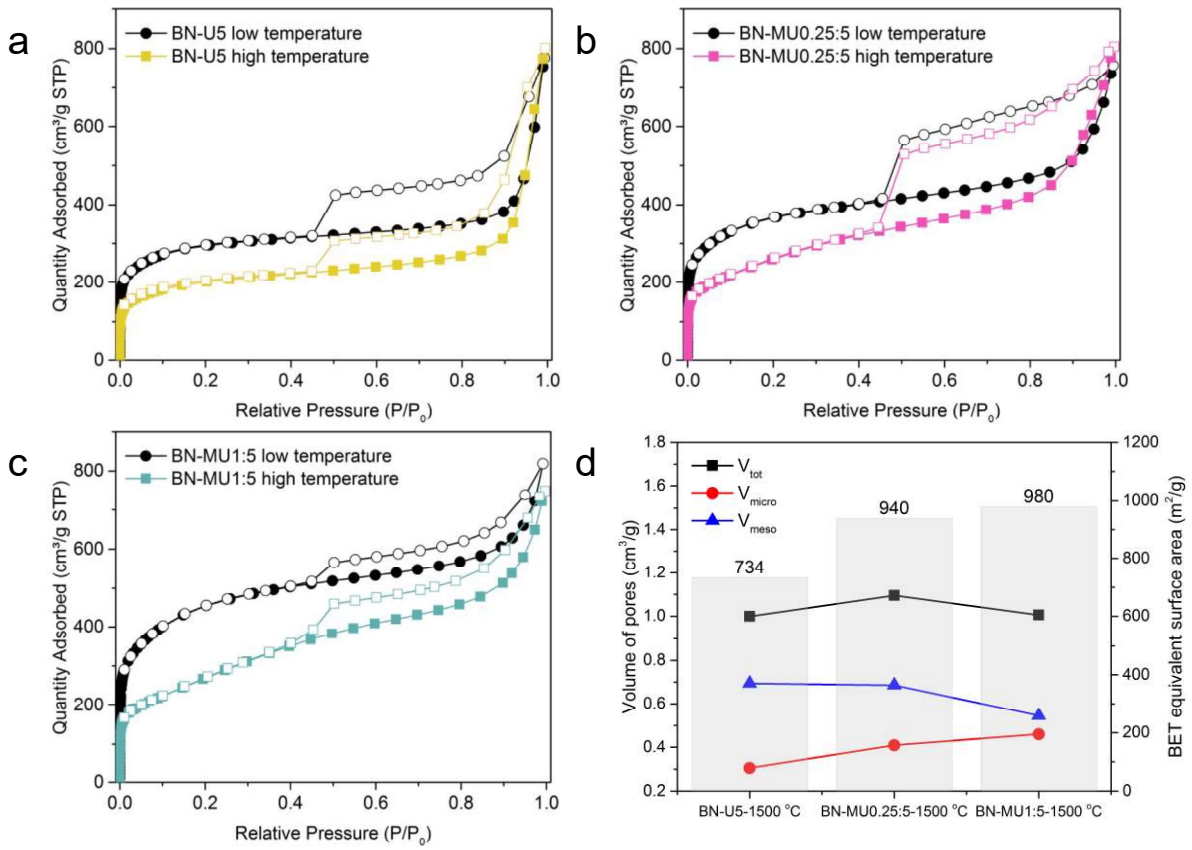


Figure 5-4 (a, b, c) Nitrogen sorption isotherms at -196 ºC for three porous BN samples synthesised at low- and high- temperatures (open symbols represent desorption) and (d) textural parameters deriving from nitrogen sorption for the high-temperature BN.

The crystalline structures of two samples synthesised at low and high temperature were compared using XRD patterns (Figure A3.6 in Appendix 3). Only discreet changes were observed, which indicated that, surprisingly, the samples did not exhibit higher crystallinity. In order to directly observe the crystalline structure of the material, high-resolution TEM was performed on two samples of BN-MU1:5 synthesised at low (1050 ºC) and high temperature (1500 ºC) (Figure 5-5a,b). It can be observed from the images that porous BN exhibits a disordered turbostratic structure at both temperatures, but BN synthesised at higher temperature exhibits regions of higher crystalline order, with a larger number of stacked 2D layers. The d-spacing calculated from the images is 3.5 Å.

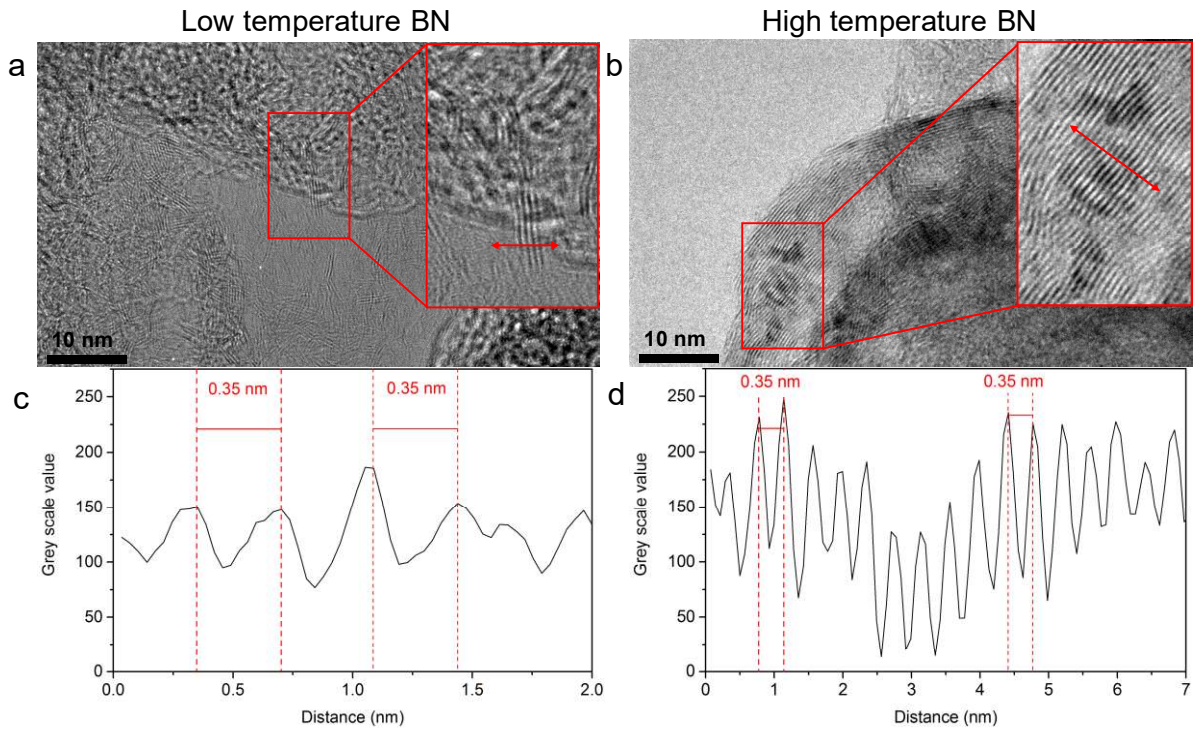


Figure 5-5 Crystalline structure with d-spacing for low and high synthesis temperature BN: High resolution TEM images for (a) low synthesis temperature BN-MU1:5-1050 ºC *vs* (b) high synthesis temperature BN-MU1:5-1500 ºC. Grey scales calculated using imageJ from figures (a) in (c) and (b) in (d).

The morphology of the samples was studied with high-resolution SEM (Figure A3.7 in Appendix 3). The images show similar morphologies for low and high temperature BN (BN-MU1:5), suggesting that synthesis temperature did not have a significant effect on the larger-scale morphology of the samples.

FTIR spectroscopy was used to analyse the chemical features of high temperature BN samples and compared to the low temperature BN. FTIR spectra for different porous BN samples synthesised at high temperature are reported in Figure A3.8 in Appendix 3 and a comparison between low and high temperature BN is shown in Figure 5-6a. The two typical vibrational bands for h-BN are present, namely B-N in-plane transverse stretching mode at ~ 1360 cm^{-1} and B-N-B out-of-plane bending mode at 800 cm^{-1}.[164] Generally, the peaks are sharper and more symmetrical compared to low temperature BN, which may indicate a change in the chemical composition of the samples, such as lower oxide content. In order to quantify the oxygen content in high temperature BN samples, as well as of the percentages of boron and nitrogen atoms, XPS was employed. XPS relative atomic percentages are reported in Figure 5-6b and Figure A3.9b in Appendix 3. XPS spectra for low and high temperature BN were also

compared in Figure A3.9 in Appendix 3. The oxygen content in porous BN synthesised at high temperature decreased from ~10 to 5 at%. This decrease is significant but could be related to oxygen species adsorbed onto the surface before analysis. The exposure to air was minimised by maintaining the samples *in vacuo* prior to XPS analysis and all samples were prepared under the same conditions (this is different from what was observed in Chapter 5, where samples were analysed in different batches).

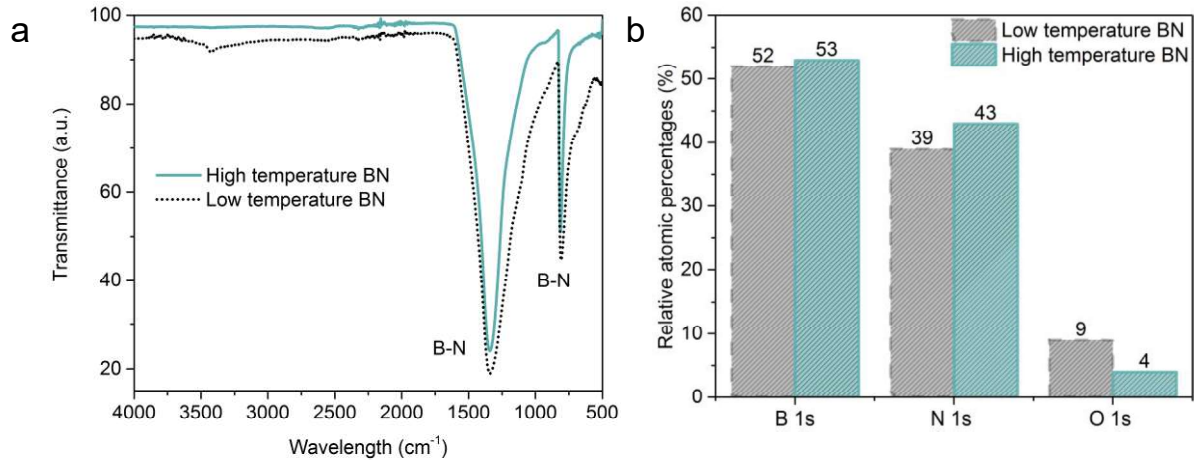


Figure 5-6 (a) Typical FTIR spectra for low and high temperature BN samples (BN-MU1:5); (b) XPS relative atomic percentages for low and high temperature BN (BN-MU1:5).

SEM-EDX was also used to compare two porous BN samples with identical precursor formulations, synthesised at low and high temperatures. While XPS allows for quantification of the surface chemical composition of the samples, SEM-EDX gives an indication of the elemental distribution (with mapping) of bulk composition. The samples were prepared by pressing the powder on the carbon tape to obtain a relatively flat surface for analysis. Two SEM images, as well as elemental mapping and EDX spectra are reported in Figure A3.10 in Appendix 3. To ensure good representation, numerous particles (> 4) were analysed and showed similar results. SEM-EDX mapping for the different elements, including oxygen, showed even distribution throughout the sample. The two EDX spectra showed a lower oxygen content for high temperature porous BN, in good agreement with both XPS and FTIR analysis. A quantification was also performed from the EDX spectra and is reported in Table 5-1. The atomic percentages recorded were consistent within different particles of the same sample. The carbon content observed from EDX analysis likely derives from the carbon tape used to mount samples, rather than from the BN itself.

Table 5-1 Elemental atomic and weight percentages for porous BN sample BN-MU1:5 synthesised at low and high synthesis temperatures deriving from EDX analysis.

	Boron		**Carbon**		**Nitrogen**		**Oxygen**	
	wt. %	at. %	wt. %	at. %	wt. %	at. %	wt. %	at. %
BN-MU1:5 1050 ºC	37	43	11	12	41	40	11	9
BN-MU1:5 1500 ºC	37	43	16	16	43	38	4	3

Water vapour isotherms at 30 ºC were collected for high temperature porous BN samples (Figure 5-7a) and compared to those obtained for low temperature BN (Figure 5-7b). High temperature BN exhibited little/no water uptake at low relative pressures, indicating an increased hydrophobicity compared to low temperature porous BN, likely due to lower oxygen contents and/or less defects. All samples were characterised after water vapour sorption analysis and regeneration at 250 ºC and the characterisation is reported in Appendix 3. Porous BN synthesised at higher temperature exhibited improve stability when exposed to water vapour compared to low temperature BN.

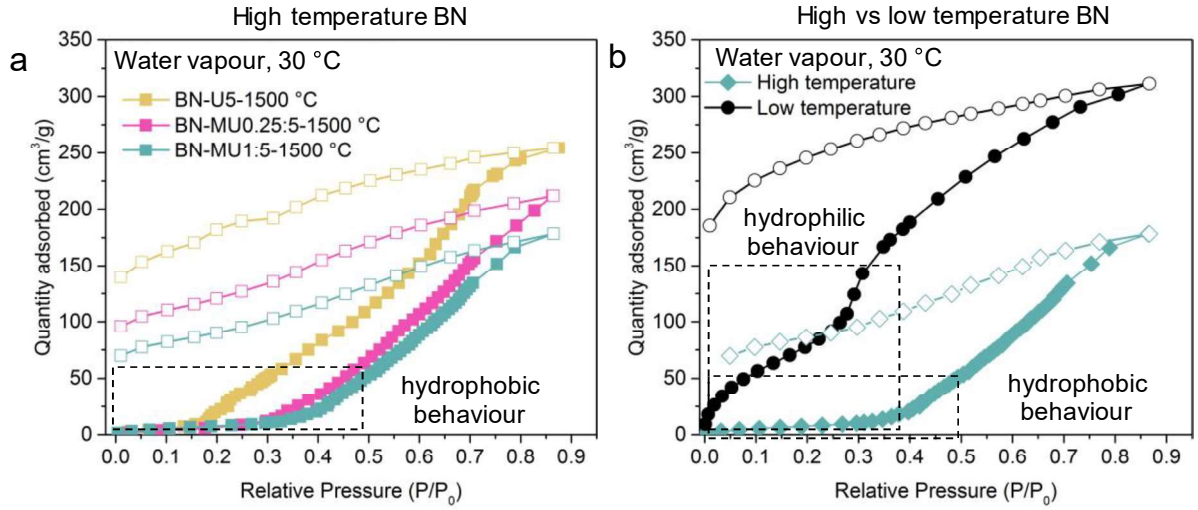


Figure 5-7 (a) Water vapour isotherms at 30 ºC measured with a volumetric analyser (3Flex) on three porous BN samples with different pore structures synthesised at 1500 ºC and (b) a comparison of water vapour isotherms collected for two samples with identical formulations but prepared at different synthesis temperatures (open symbols represent desorption).

5.4.2.2 Water stability evaluation for high temperature BN

In order to evaluate the aqueous stability of high temperature BN samples, the materials were exposed to water in dye sorption tests for RhB removal. The samples were then regenerated at

600 °C and fully characterised to evaluate their hydrolytic stability. The pore structure of the samples was characterised *via* nitrogen sorption and the results for BN before and after regeneration are shown in Figure 5-8a-d. Little/no difference was observed in the isotherms for BN-U5 and BN-MU0.25:5 samples, showing significantly improved aqueous stability compared to low temperature BN. BN-MU1:5-1500 ºC still showed a decrease in surface area (from 980 to 584 m^2/g) and total pore volume. However, this decrease is much less significant than those observed in low temperature BN samples (maximum decrease: 40 % in high temperature BN *vs* 98 % in low temperature BN). Finally XRD patterns for high temperature BN samples before and after exposure to water are reported in Figure 5-8e,f and show a slight increase in crystallinity after exposure to water, indicating a small degree of decomposition for the amorphous component of porous BN.

The chemistry of the samples after regeneration was also analysed using FTIR and XPS and the results reported in Figure 5-9. FTIR spectra for all samples after regeneration showed the appearance of a large shoulder at around 3250 cm^{-1}, which was assigned to the presence of B–OH groups.[197] The h-BN vibrational bands at ~1350 cm^{-1} and ~800 cm^{-1} for B-N-B stretching and B-N bending modes respectively, were still present. However, the width of the peaks increased, with an increase relative intensity of the band at ~800 cm^{-1} compared to the band at ~1350 cm^{-1}. This difference was likely associated to the incorporation of oxygen within the structure. However, despite the differences observed from FTIR in the chemistries of the samples, XPS relative atomic percentages (Figure 5-9d) did not show any major variations for two of the samples (BN-U5-1500 ºC and BN-MU0.25:5-1500 ºC), while for BN-MU1:5-1500 ºC a significant increase in oxygen content was observed. This was explained considering that the small degree of decomposition was likely localised inside the micropores of the samples and while FTIR is a bulk analysis technique, XPS only gives information about the surface of the samples. XPS core level spectra for high temperature BN after exposure to water are reported in Figure A3.12 in Appendix 3 and show similar features to untreated BN. The survey spectrum confirms that no residual dye was present on the sample, because no additional peaks other than N, C, B, O were observed.

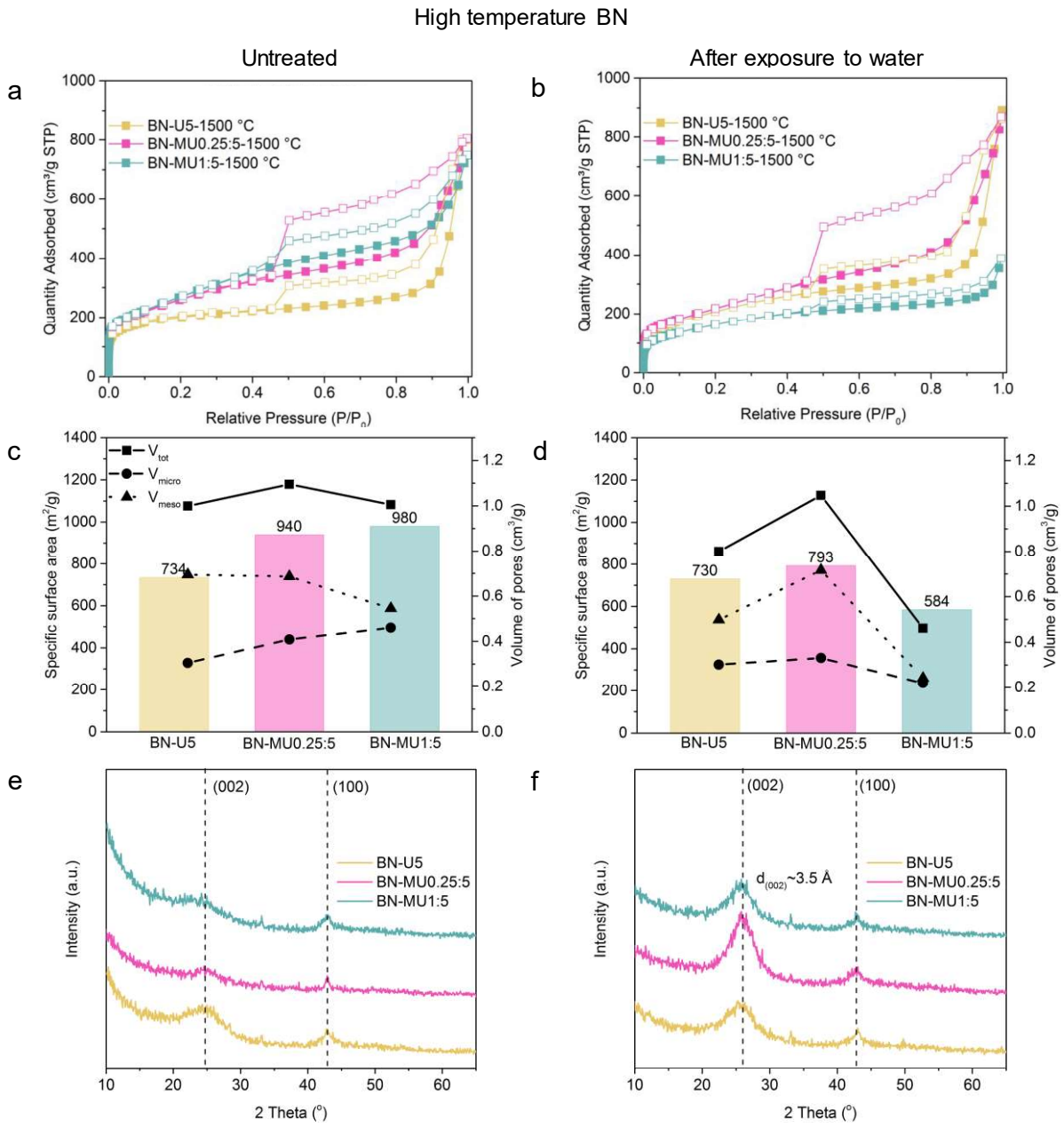


Figure 5-8 (a,b) Nitrogen sorption isotherms at -196 °C for high temperature BN before and after exposure to water (*via* RhB sorption) (open symbols represent desorption) and (c,d) textural parameters deriving from the same; (e,f) XRD patterns for high temperature BN before and after exposure to water.

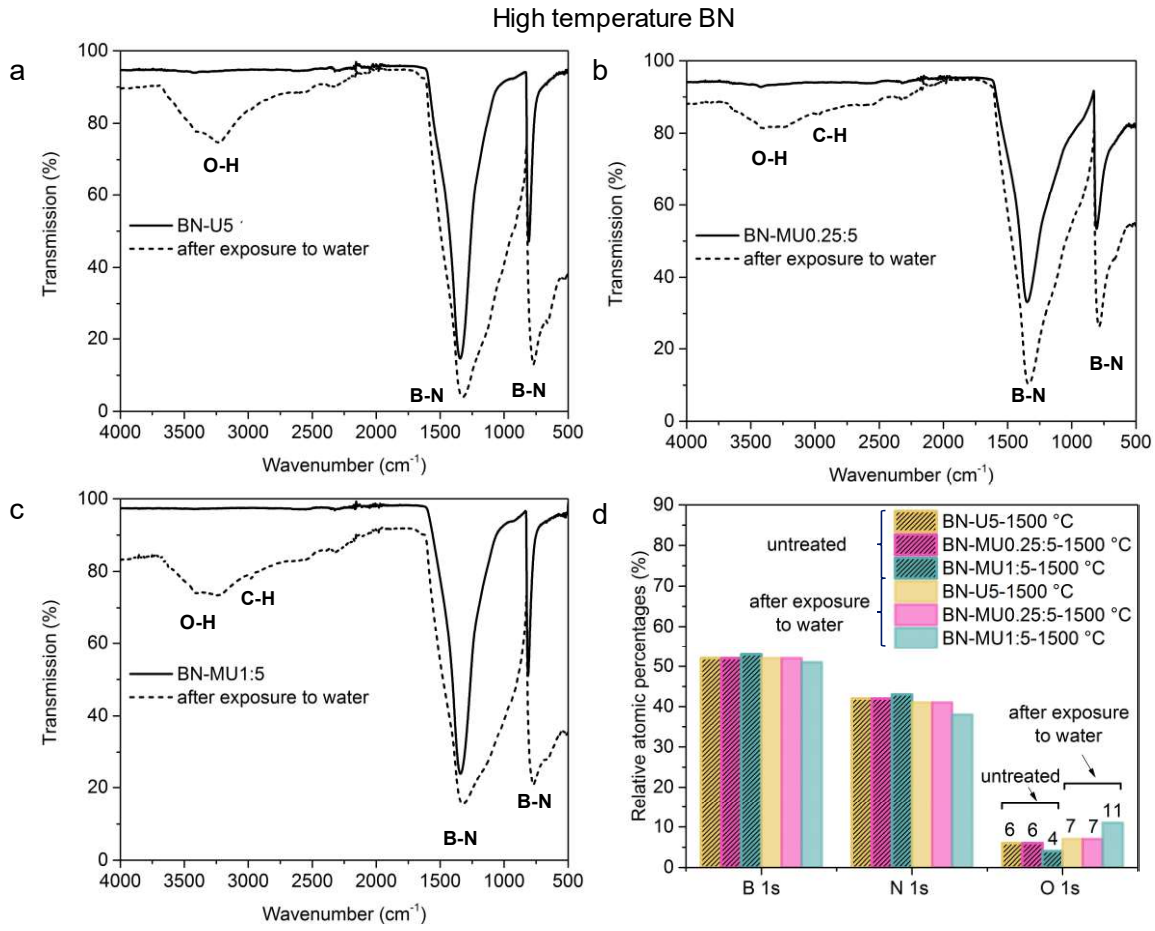


Figure 5-9 (a-c) FTIR spectra for high temperature BN before and after exposure to water (*via* RhB sorption) and regeneration: (d) XPS relative atomic percentages for all samples before and after RhB sorption and regeneration.

5.4.3 Organic solvent stability evaluation

In the previous section it was shown that low temperature porous BN samples were unstable in water. The most microporous sample (BN-M1:5) showed the highest susceptibility to hydrolytic attack. The stability of this sample in other solvents (n-heptane and ethanol) was, therefore, evaluated.

The pore structure of porous BN before and after exposure to solvents was analysed *via* nitrogen sorption at -196 °C (Figure 5-10) which showed little/no changes, indicating that the samples exhibited good stability. This was further confirmed with the analysis of the chemical structure using XPS analysis, as all samples exhibited similar features (O content ~ 10 at%).

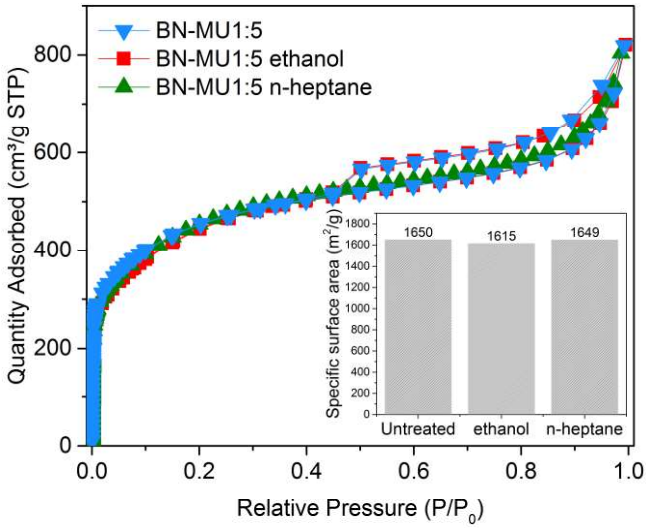


Figure 5-10 Nitrogen sorption isotherms at -196 °C for low temperature porous BN (BN-MU1:5) before and after exposure to ethanol and n-heptane (no desorption performed for 2 of the samples); the inset shows the surface areas deriving from BET analysis for all samples.

5.4.4 Thermal and oxidative stability evaluation

Porous BN's thermal and oxidative stability was evaluated for low temperature BN in order to confirm that the decomposition previously observed was related to hydrolysis and not to thermal oxidation. TGA analysis was performed in nitrogen and air for two porous BN samples (Figure 5-11). Porous BN showed little/no mass change up to 1050 °C under nitrogen atmosphere. On the other hand, when porous BN was heated in air, it showed good stability up to ~850 °C and then the mass of the material increased by about 32 wt%, which matches well with the formation of B_2O_3 from BN. This analysis confirmed that BN exhibited incredibly high thermal (>1000 °C) and oxidative (>800 °C) stabilities.

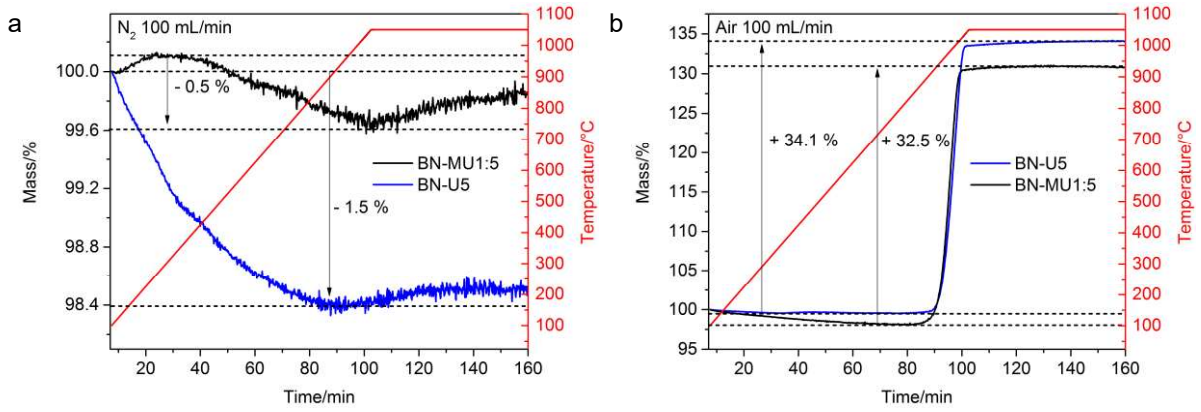


Figure 5-11 TGA analysis for low temperature porous BN under (a) nitrogen and (b) air.

5.5 Conclusions

This study provided greater insights into the stability of porous BN in water and the hydrolysis reaction mechanisms. A detailed investigation was conducted into the influence of water on chemistry and structure of BN materials and it was found that materials with higher micropore volumes and surface areas were more susceptible to hydrolysis reactions, independent of their d-spacing. This may be associated to the favourable adsorption of water inside the micropores and to the larger amount of defect sites likely present in those materials. It was therefore hypothesised that the instability of the material derives from a combination of large surface area, low crystallinity ad a large amount of oxygen impurities and defect sites.

Based on these findings, a strategy for the improvement of the stability in water was, proposed and it was demonstrated that by increasing the synthesis temperature, porous BN with significantly greater stability could be produced, while still maintaining surface areas of ~ 1000 m^2/g. This study highlighted the importance of testing porous BN materials for water stability and proposed a way to reduce the hydrolysis of BN in water. In addition to the hydrolysis stability, porous BN proved to be stable in select organic solvents, as no decrease in porosity or change in chemistry was observed and the material showed excellent thermal stability up to the testing temperature of 1050 °C and good oxidative stability up to ~850 °C

Chapter 6: Testing Porous BN for Gas and Liquid Separations

6.1 Introduction

Chemical separations (*e.g.* the extraction of hydrocarbons from crude oil, the sequestration of greenhouse gases from emission sources, etc.) account for more than half of the total energy consumed in industry as many of these processes are performed *via* distillation.[5] Adsorbent materials or membranes, which are able to separate molecules based on size exclusion principles and/or chemistries, offer an environmentally friendly alternative, however, currently their use at scale remains limited.[5] To try to improve the energy efficiency of separation processes, a global research effort into the production of novel adsorbents and/or membranes is underway, primarily focusing on materials such as metal-organic frameworks,[13] zeolites,[198] carbon-based materials[199] and covalent organic frameworks.[200]

Porous BN is a promising adsorbent due to its high thermal stability, "rich" chemistry, and high surface area. BN materials were tested for a range of different applications such as catalysis,[144] CO_2 capture, oil spill clean-up,[120] hydrogen storage[90, 92-93, 201] and water cleaning.[38, 74, 80, 90] However, the number of studies in which BN was tested for sorption applications remains limited and little is known on how to optimise the material's properties in order to improve its sorption capacity.

In CO_2 capture applications[87, 91, 109, 181] porous BN materials showed limited sorption capacities (18- 35 mg/g at 25 °C and 1 bar)[87, 114] , however, it was demonstrated that CO_2 sorption capacity did not directly correlate with BN surface areas, but pore size control was necessary in order to improve the adsorption.[87, 109] The presence of functional groups such as -NH_2 and -OH was also shown to affect CO_2 sorption.[114] Therefore, if a better control over BN structure

and chemistry were achieved, this could lead to a large improvement of BN capacity. In addition, little/no studies were published testing porous BN for high pressure CO_2 sorption applications, despite this material exhibiting high micropore volume.

Porous BN also showed promise is water cleaning applications, more specifically for the removal of organic molecules (*e.g.* dyes, pharmaceutical molecules, oils) from water.[38, 74, 80, 90] Different sorption mechanisms were proposed, including π-π stacking interactions, dipole-dipole interactions between the B-N bond and dyes, physisorption, hydrophobic/oleophilic interactions.[80, 123-125] Again, good control of porous BN chemistry and pore structure proved fundamental. Moreover, most of the porous BN materials used in these applications showed a turbostratic character, which is likely to confer to the material hydrolytic instability.[105-106] However, to the best of our knowledge, this instability issue was never considered in water-based applications, and needs to be carefully evaluated.

A novel synthesis method developed by our group (Chapter 5), provided a way to carefully tune BN pore structure, despite this material exhibiting poor crystallographic order. Moreover, BN water stability was greatly improved in Chapter 6, by producing BN samples with increased hydrophobicity, lower amount of defects and a different chemistry.

Herein, porous BN samples with different chemistries and pore structures were tested for gas sorption (CO_2, CH_4) at low (<1 bar) and high pressures (up to 20 bar), in order to understand and improve the adsorption capacity. Porous BN pellets were tested for CO_2 sorption showing similar sorption capacities to powder samples, indicating the potential for processability of this material.

Porous BN was also tested for the first time in the separation of organic solvents *via* vapour sorption isotherms and a clear correlation between both BN's pore structure and chemistry to the resulting sorption capacity of various solvents was shown.

Finally, porous BN was tested for water cleaning applications, *i.e.* oil spill clean-up and the removal of pollutant organics *via* performance in dye adsorption from aqueous solutions. It was demonstrated that porous BN samples with improved water stability removed over 80 % of Rhodamine B from water, even after regeneration, with no decrease in performance.

6.2 Materials testing

The selection of porous BN materials to test for potential applications is summarised in Table 6-1.

Table 6-1 Naming system for porous BN samples with molar ratios, synthesis temperatures and average surface areas.

Sample name	Melamine (mol)	Urea (mol)	Boric acid (mol)	Synthesis T (°C)	Surface area (m^2/g)
BN-U5 low temperature	0	5	1	1050	~ 1000
BN-MU0.25:5 low temperature	0.25	5	1	1050	~ 1350
BN-MU1:5 low temperature	1	5	1	1050	~ 1750
BN-U5 high temperature	0	5	1	1500	~ 700
BN-MU0.25:5 high temperature	0.25	5	1	1500	~ 1000
BN-MU1:5 high temperature	1	5	1	1500	~ 1000

Low temperature porous BN samples exhibited similar chemistries and different pore structures (as prepared in Chapter 5). In particular:

- BN-U5: exhibited large mesopore volume and relatively low micropore volume;
- BN-MU0.25:5: exhibited high mesopore and micropore volumes;
- BN-MU1:5: was mostly microporous;

A porous BN pellet was also prepared by simply compressing porous BN powder (BN-MU1:5 low temperature) by the applying of 5 tonnes (Chapter 5) and showed a small decrease in porosity ~15 %.

High temperature porous BN samples (Chapter 6) exhibited similar pore structures to low temperature samples (with reduced surface areas) but improved hydrophobicity, lower amount of oxygen atoms and higher in-plane crystallinity due to a reduction in defect amount.

All of these samples were tested here for different adsorption applications as described below.

6.2.1 Gas sorption

6.2.1.1 Low pressure gas sorption

Gas sorption tests at low pressure (up to 1 bar) were performed on a Micromeritics 3Flex sorption analyzer at 25 °C, using a water bath to control the temperature. The samples (~ 100 mg) were degassed overnight at 120 °C at a pressure of roughly 0.2 mbar before further degassing *in-situ* for 4 hours at around 0.0030 mbar, prior to analysis. Gases were tested in the following order: nitrogen, methane, carbon dioxide; and an additional *in-situ* degas step was repeated between each measurement.

6.2.1.2 High pressure gas sorption

Gas sorption tests at high pressures (up to 20 bar) were performed gravimetrically on an IGA-200 from Hiden Isochema. The sample (~ 30 mg) was added to a porous sample container,

connected to a high-precision balance (± 0.0001 mg). The sample was degassed *in-situ* prior to analysis at 120 ºC for 4 hours using a furnace attachment. An ultra-high vacuum of down to 10^{-6} mbar can be created inside the chamber. Nitrogen and carbon dioxide sorptions were performed at different temperatures (10, 25, 40 °C) and the sample was degassed at 120 °C for 3 h between each run. The temperature was controlled using a water/ethylene glycol bath.

6.2.1.3 Heat of adsorption calculation

The heat of adsorption (Q_{st}) and entropy (ΔS) for CO_2 were calculated by fitting the gas sorption isotherms, collected at 3 different temperatures (10, 25, 40 °C), using a Langmuir-Freudlich equation[202] (1):

$$y = \frac{abx^{1-c}}{1 + bx^{1-c}} \quad (1)$$

The fitting was used to calculate the pressures (P) at desired CO_2 loadings (0.1-5). ln(P) was then plotted against $\frac{1}{T}$ for each selected loading and fitted with a linear fit. Based on the van't Hoff equation,[203] the heat of adsorption and entropy were finally calculated from equations (2,3).

$$Q_{st} = -mR \quad (2)$$

$$\Delta S = -cR \quad (3)$$

Where m is the slope, c is the intercept and R is the universal gas constant.

6.2.1.4 Temperature swing adsorption

Temperature swing CO_2 adsorption/desorption cycles (10 cycles) were performed on a TGA Netzsch TG209 F1 Libra. A buoyancy was performed with an empty crucible with the same conditions as used during the analysis. The samples were first pre-degassed in a vacuum oven at 120 °C and then degassed *in-situ* at 120 °C for 2 hours at atmospheric pressure. Adsorption was performed at 30 °C by flowing CO_2 (80 mL/min) and N_2 (20 mL/min) gases for 2 hours. Desorption was performed by increasing the temperature to 120 °C (10 °C/min) under N_2 gas flow (100 mL/min) for 2 hours. CO_2 sorption and desorption capacities were measured by the change in mass of the sample.

6.2.2 Organic vapour sorption

Vapour sorption experiments were performed on an IGA gravimetric analyser. The samples (~30 mg) were degassed *in-situ* at 120 ºC for 4 hours using a furnace attachment, prior to analysis. An ultra-high vacuum of up to 10^{-6} mbar could be created inside the chamber. The solvents were vaporised and dosed up to 90 % of their saturation pressures at 25 °C: n-heptane (P_0: 61.12 mbar), 2,3-dymethylpentane (P_0: 91.82 mbar), toluene (P_0: 37.93 mbar), methylcyclohexane (P_0: 61.79 mbar), 1-butanol (P_0: 9.22 mbar), methanol (P_0: 169.24 mbar). All solvents were of analytical grade. *In situ*-degas was performed in between each experiment at 250 °C to regenerate porous BN.

6.2.3 Dye sorption

Dye sorption tests were performed by preparing 1 L stock solutions of dyes in DI water with concentration of 40 mg/L. The dyes used were Methyl Orange (ACS reagent, Sigma Aldrich) and Rhodamine B (HPLC, Sigma Aldrich). After complete dissolution of the dyes, 250 mL of solution were vigorously stirred and 100 mg of porous BN powder were added to the solution while stirring. After selected timings: 0, 5, 10, 30, 60, 120, 240 min, about 2 mL of solution were collected with a syringe and filtered with a syringe filter (0.45 μm) to remove BN powder. These solutions were then analysed using UV-Vis spectroscopy to calculate the dye concentration. After 240 min, BN samples were filtered using a Buchner filtration system, dried in the oven at 120 °C and then heated at 600 °C (10 °C/min) for 3 hours in a tubular furnace under air gas flow (50 mL/min) before being reused for a second adsorption cycle.

UV-Vis spectroscopy was performed in a Perkin Elmer Lambda 35 spectrometer with quartz cuvettes, 480 nm/min scan speed between different ranges of wavelengths: 200-700 nm for Methyl Orange (λ_{max} = 464 nm) and 400-650 for Rhodamine B (λ_{max} = 554 nm). Calibration was performed by preparing solution with decreasing concentrations and had a R^2 value larger than 0.99 (Figure-A4.3 Appendix 4).

After sorption, the BN samples were regenerated by heating in air at 600 ºC and reused for a second adsorption cycle. The regeneration temperature was selected based on the decomposition temperature of the dyes, as determined by TGA analysis (Figure A4.3e in Appendix 4). While RhB fully decomposed at 600 ºC, MO did not completely decompose even at temperatures up to 900 °C, which would explain a possible decrease in porosity and dye uptake after regeneration.

6.2.4 Oil spills cleanup

Samples were added to a weighing boat placed on top of an analytical balance. Two different types of crude oils with increasing viscosity (CrudeA and CrudeB, provided by BP were added dropwise until saturation was observed (oil not retained by the material but spread onto the weighing boat). The oil sorption capacity was estimated gravimetrically (rough estimate). A porous BN sample (20 mg) was added to an heterogenous mixture of crude oil (CrudeA, less viscous, 150 mg) in water. Oil sorption was monitored until full saturation and estimated gravimetrically by weighing the sample before and after the analysis.

6.3 Results and discussion

6.3.1 Gas sorption

6.3.1.1 Low pressure gas sorption

Porous BN materials with different pore structures and chemistries were tested for low pressure gas sorption. In particular, considering the high porosity and presence of N atoms, the materials were studied for CO_2/N_2 and CO_2/CH_4 separations (Figure 6-1). These separations are relevant to the energy sector in the context of carbon capture and natural gas processing, respectively. As expected, the microporosity enhanced the CO_2 gas sorption capacity, which reached a maximum uptake of 1.6 mmol/g of CO_2 (at 25 °C and 1 bar) for BN-MU1:5 low temperature, which is the sample with the highest surface area and micropore volume (Figure 6-1b). This is approximately four times higher than a porous BN material previously tested under the same conditions, which exhibited lower surface area and higher crystallinity.[87] However, more recently, a higher CO_2 sorption capacity was reported for carbon-doped porous BN materials (~4 mmol/g *vs* ~1.6 mmol/g for pure BN), by increasing ultramicropore volume (< 0.7 nm) and especially modifying the chemistry (carbon-doping).[88] Nevetherless, the sorption capacity of BN remained relatively low when compared to other porous materials.[204-205] This is explained by the fact that at low temperature chemisorption is key. Surprisingly, the CO_2 sorption capacity followed a linear trend with BN microporosity even for a high temperature porous BN sample (BN-MU0.25:5 high temperature), despite this sample having a different chemistry (lower oxygen content) and improved hydrophobicity (Figure 6-1b). The CO_2 sorption and desorption cyclability was also studied *via* temperature swing adsorption/desorption using TGA analysis in Figure 6-1d. The total sorption capacity for CO_2 from TGA analysis was calculated to be about 4 wt.% (0.9 mmol/g) per cycle and showed no decrease after 10 cycles.

The sorption capacity measured by TGA analysis was significantly lower than that previously measured *via* volumetric gas sorption. This was attributed to: i) inclomplete *in-situ* degas due to lack of vacuum, ii) higher analysis temperature (30 ºC instead of 25 ºC), and iii) non-equilibrium conditions. Nevetherless, the TGA gravimetric study showed a good CO_2 cyclability over 10 sorption-desorption cycles.

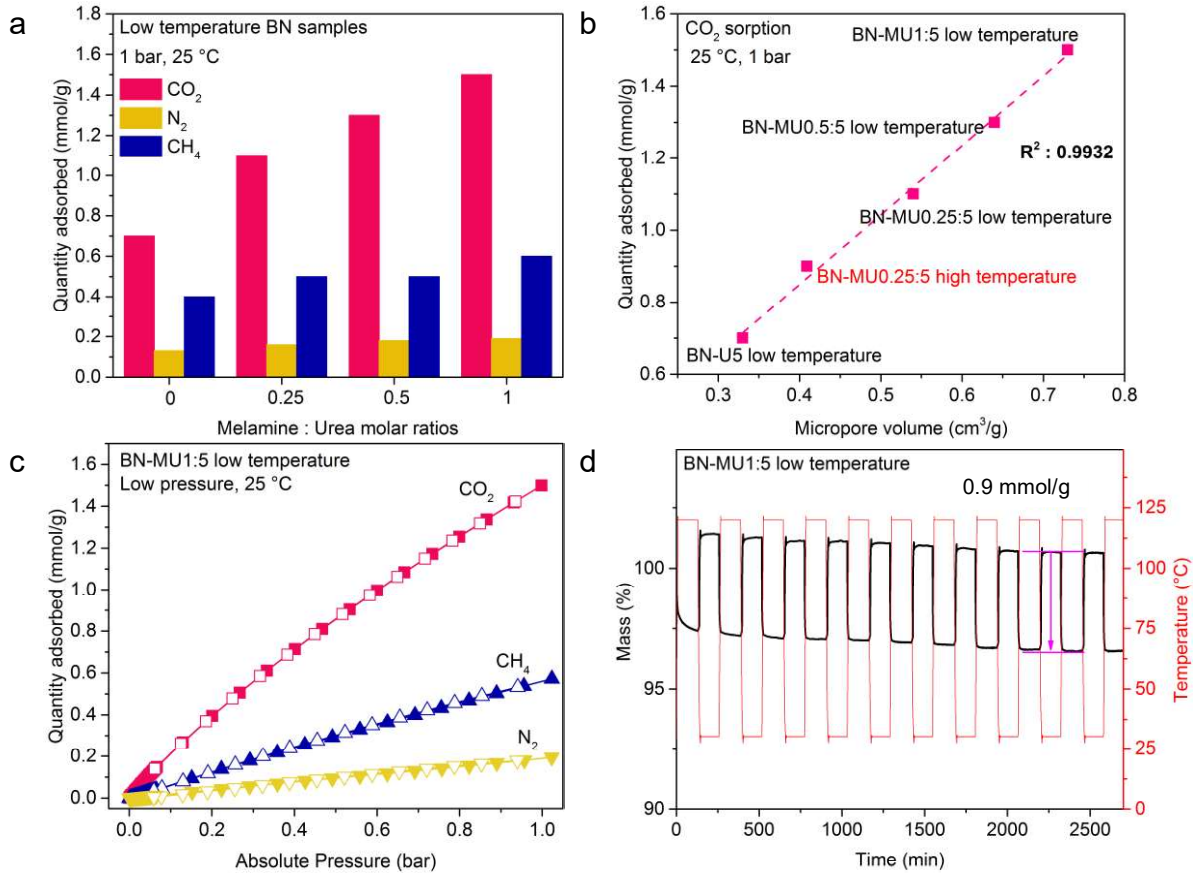


Figure 6-1 Gas sorption at low pressure: (a) CO_2, CH_4 and N_2 bar plots with maximum sorption capacities at 25 ºC and 1 bar for low temperature porous BN samples;(b) CO_2 sorption capacity *vs* micropore volume for low and high temperature porous BN; (c), Low pressure isotherms at 25 °C and up to 1 bar for BN-MU1:5 for CO_2, CH_4 and N_2, (d) gravimetric CO_2 sorption and desorption cycles with temperature swing desorption between 30 ºC and 120 ºC (1 bar) on BN-MU1:5.

6.3.1.2 High pressure gas sorption and heat of adsorption

Considering the high micropore volume of the BN produced, it was hypothesised that the material could perform well in gas sorption applications at high pressures. Therefore, the highest surface area BN sample (BN-MU1:5 low temperature) was tested for CO_2 sorption at high pressure (up to 20 bar) and various temperatures (10, 25 and 40 °C, Figure 6-2b). One possible application is pre-combustion CO_2 capture in powerplants. For this particular application, high pressure CO_2/H_2 mixtures need to be separated. However, the set-up available

did not allow for testing of H_2 sorption, therefore, N_2 and CO_2 sorption were compared instead. The CO_2 sorption capacity measured at 25 °C and 20 bar (8.3 mmol/g) is higher than the capacity of some commerial zeolites and similar to what is reported for commercial activated carbon under similar conditions.[206] Compared to other adsorbent materials, BN holds the advantage of increased thermal stability. The heat of adsorption for CO_2 was calculated from sorption isotherms at different temperatures (Figure A4.1, Appendix 4) and was approximately 19 kJ/mol (Figure 6-2c-f). This value is in good agreement with the theoretical calculation for CO_2 physisorption on a BN sheet.[207] This is also indicative that no chemisorption took place, which explains the low CO_2 sorption uptake at low pressures, as well as the good cyclability measured by temperature swing desorption. The high pressure CO_2 gas sorption capacity was compared for porous BN powder and pellet (Figure 6-2a). No differences in CO_2 sorption capacity were observed in the material after pelletisation, despite the reduced surface area of the pellet.

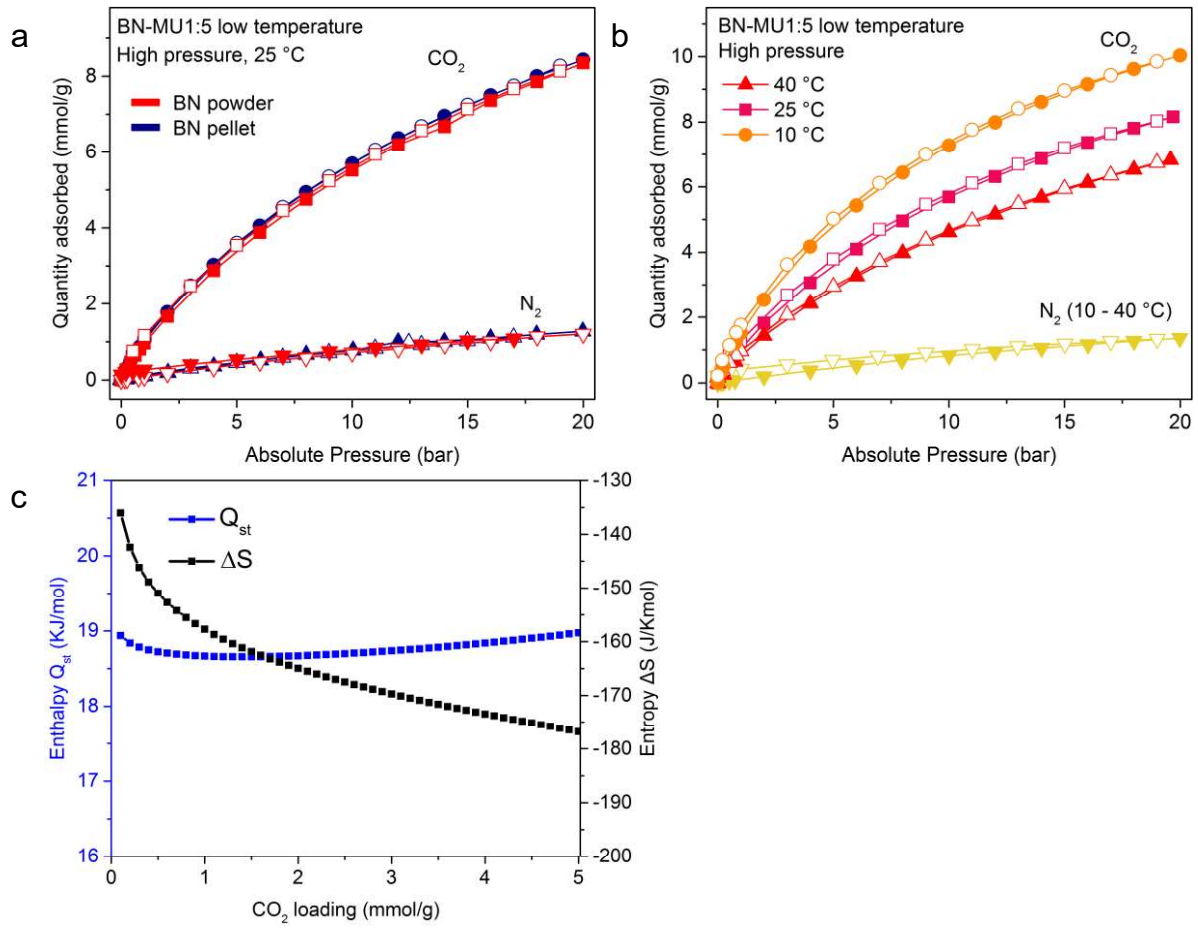


Figure 6-2 (a) High pressure CO_2 and N_2 sorption on porous BN powder and pellet (BN-MU1:5);(b) CO_2 and N_2 sorption on porous BN-MU1:5 at different temperatures;(c) entropy and heat of adsorption for CO_2.

In conclusion, porous BN materials showed relatively low CO_2 sorption capacities at low pressures due to weak chemical interactions between the adsorbent and this molecule. The CO_2 sorption capacity at low pressures was mainly correlated to the materials' micropore volumes and surface areas. At high pressures porous BN showed a higher CO_2 sorption capacity because of the high micropore volume present. The low heat of adsorption indicated that porous BN may be easily regenerated *via* pressure swing adsorption.

6.3.2 Organic vapour sorption

Adsorbent materials (*i.e.* porous BN) can potentially be employed for the separation of solvent mixtures based on their size/shape and/or chemistry. For example, the separation of aromatic and non-aromatic compounds *via* traditional methods, such as distillation, is challenging owing to their similar boiling points.[208] Therefore, porous materials with excellent sorbate selectivity need to be developed. Here, porous BN materials with a range of different pore structures and oxygen groups contents were selected for the removal of organic solvents with different properties. The selection of solvents used in this study is summarised in Figure 6-3 and spans from C-7 hydrocarbons with different sizes/shapes (*e.g.* linear n-heptane or branched 2,3-dimethylpentane) and/or chemistries (*e.g.* aromatic toluene or non-aromatic methylcyclohexane) to two different alcohols (methanol and 1-butanol).

Effect of BN porosity on the organic vapour adsorption

The organic vapour sorption capacity was studied for low temperature porous BN materials with different pore structures and similar chemistries. Nitrogen sorption isotherms at -196 °C for three porous BN materials (with BET surface areas) are plotted in Figure 6-4a. Typical vapour sorption isotherms at 30 °C for an organic (methylcyclohexane) for the same three materials are reported in Figure 6-5b. Analogous vapour isotherms were collected for other solvents (Figure 6-6c, d). The isotherms' shapes for nitrogen sorption at -196 °C and organic vapour sorption at 30 °C are alike, indicating an obvious correlation between the pore structure and organic sorption capacity of the materials. This is indicative that physisorption played a major role in organic vapours sorption. The total vapour sorption capacity increased with increasing surface areas and most of the vapours were adsorbed at low relative pressures, in the microporous regions. The presence of mesopores caused capillary condensation of the vapours (*e.g.* in BN-MU0.25:5) as indicated by the presence of hystereses in the desorption curves. Moreover, most of the vapour were desorbed (Figure 6-7b) when the pressure was lowered, indicating that little/no chemisorption occured.

Porous BN sorption capacity for different solvents was calculated at 0.6 P/P_0 (Figure 6-8e), as at higher relative pressures condensation readily occurred. At this relative pressure, organic vapour uptake had ceased and it appeared to have saturated the BN materials. The quantity of vapour adsorbed in low temperature porous BN samples increased with increasing surface areas (Figure 6-12a). An obvious linear correlation between BN micropore volume and sorption capacity was found among porous BN materials with similar chemistries (Figure 6-12b), which is similar to that previously discussed in the literature for activated carbons.[209] Porous BN showed a comparable vapour sorption capacity to activated carbons with similar surface areas for toluene and methanol.[210] All porous BN materials tested showed the highest adsorption capacity for toluene, amongst all of the solvents tested. This may be explained due of the presence of π-π interactions between the h-BN rings in porous BN and the aromatic rings in toluene, which contributed to improved physisorption and resulted in higher sorption capacities. However, the selectivity measured between different solvents remained relatively low for all porous BN materials (Figure A4.2 in Appendix 4).

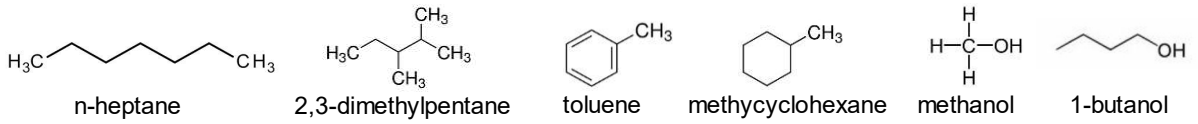


Figure 6-9 Organic solvents selection for vapour sorption.

Effect of BN chemistry on the organic vapour adsorption

A high temperature porous BN sample (BN-MU0.25:5 high T, BET SA: 940 m^2/g) was also tested for organic vapour sorption (Figure 6-10e) and surprisingly showed higher sorption capacities compared to a low temperature porous BN sample with similar surface area (BN-U5). As discussed in Chapter 6, high temperature BN exhibited lower oxygen content and fewer defects. The vapour sorption capacity plotted against surface areas and micropore volumes (Figure 6-12a, b) showed that high temperature BN exhibited higher sorption capacities for most of the solvents. For example, toluene sorption capacity was higher compared to similar low temperature porous BN samples (BN-U5). This result is indicative of the presence of a higher quantity of π electrons in high temperature BN, demonstrating that the material is more crystalline in the 2D plane and exhibits less defects, as previously discussed in Chapter 6. The sorption capacities for other solvents were also higher compared to low temperature porous BN materials with similar pore volumes. This behaviour was linked to the material's chemistry with lower oxygen content and a more hydrophobic and oleophilic nature.

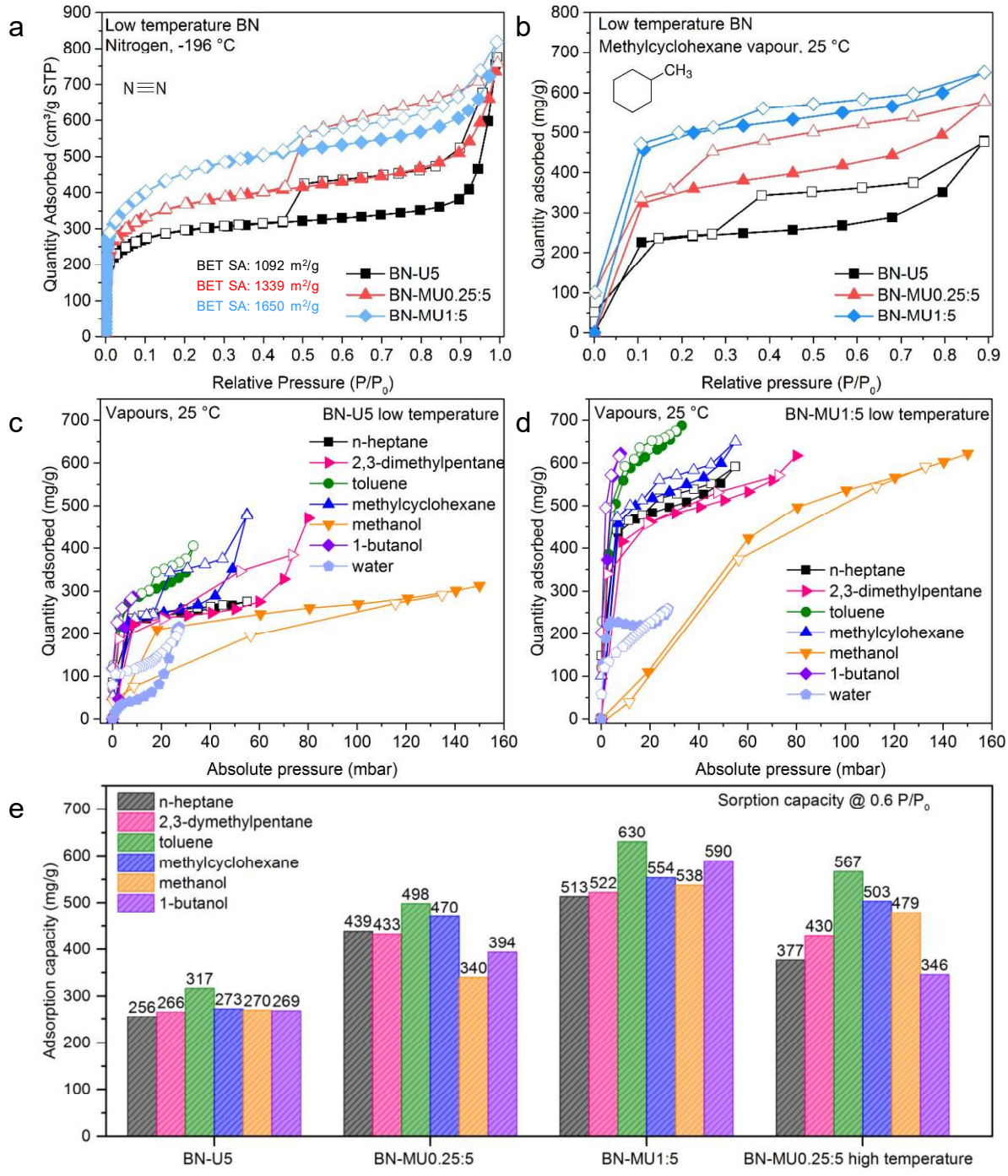


Figure 6-11 (a) Nitrogen sorption isotherms at -196 °C for three low temperature porous BN samples (b); Typical vapour sorption isotherms (for methylcyclohexane) measured at 25 ºC for the same three porous BN samples; (c, d) Vapour sorption isotherms for different organic solvents *vs* absolute pressures for two porous BN samples synthesised at low temperature (open symbols represent desorption); (e) Equilibrium vapour sorption capacity in mg/g for porous BN samples at 0.6 P/P_0.

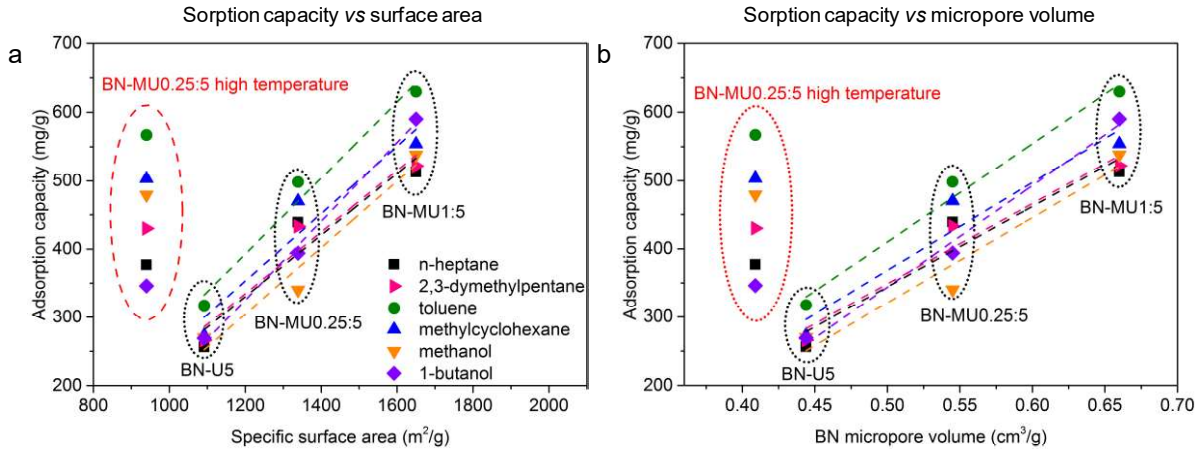


Figure 6-12 (a) Vapour sorption capacity at 0.6 P/P_0 *vs* BET surface areas calculated from nitrogen sorption analysis for three low temperature porous BN samples and one high temperature sample; (b) Vapour sorption capacity at 0.6 P/P_0 *vs* micropore volume derived from nitrogen sorption analysis for the same four BN samples.

In conclusion, organic vapour sorption strongly depended not only on the micropore volume of the porous BN, but also on its chemistry. Porous BN materials with lower oxygen content and higher hydrophobicity showed higher vapour adsorption capacities. The mechanisms of adsorption were identified as: i) physisorption, mainly depending on the surface area and micropore volume; ii) π-π interactions between porous BN and aromatic molecules, as indicated by the higher adsorption capacity for toluene; iii) hydrophobic/oleophilic interactions, as indicated by the higher capacity for high temperature BN.

6.3.3 Water cleaning

Dyes and oils are common contaminants present in water and their removal is of the utmost importance for water purification applications.[120, 211] Porous BN materials demonstrated higher affinity to aromatic solvents in the previous section, therefore it was hypothesised that porous BN would perform well in the removal of aromatic dyes from water. Here, porous BN materials with different porosity/chemistry were tested for dye sorption and oil/water separation.

6.3.3.1 Dye sorption

The dye removal capacity was evaluated at different times and curves representing concentration of dye in water *vs* time are reported in Figure 6-13 for both MO and RhB. Porous BN (BN-U5) removed up to 90 % of MO from water within 4 hours (Figure 6-13a), which is the highest sorption capacity among the BN samples studied, despite this sample exhibiting the lowest surface area and micropore volume. For short adsorption times, BN-MU1:5, with higher

micropore volume and surface area, exhibited the highest sorption capacity for MO, while for longer exposure times the trend was reversed (Figure 6-13a). It is hypothesised that this could be due to the higher instability of the high surface area BN (BN-MU1:5) in water, as discussed in Chapter 6, which may cause a reduction in surface area with time. Interestingly, porous BN samples exhibited a similar trend when used for the removal or RhB from water (Figure 6-13c). However, in this case, RhB was fully removed from water within 2 hours. The higher sorption capacity for RhB compared to MO could be attributed to stronger polar interactions between BN and RhB, which is a cationic dye, compared to MO which is anionic. This result suggested that porous BN materials had a basic surface character at the pH of the analysis (~7).[125]

The recyclability of porous BN was evaluated by regenerating the two best performing samples for MO and RhB adsorption and repeating the dye sorption tests in the same manner. The results of these recycling analyses are reported in Figure 6-13e. A decrease in dye uptake was observed (about 10 % for RhB and 20 % for MO). The higher decrease in dye uptake for MO was explained because of the incomplete decomposition of the dye at 600 °C. The dye sorption results for BN-U5 after regeneration are reported in Figure A4.3f Appendix 4. The general decrease in dye sorption capacity after regeneration was attributed to the decrease in surface areas and pore volumes because of BN decomposition in water *via* hydrolysis. Interestingly, regenerated BN-U5 showed higher removal capacity for MO at short adsorption times compared to the same sample prior to regeneration, which was attributed to finer particle sizes and therefore better dispersibility. Surprisingly, despite the huge decrease in surface area for BN-MU1:5 after regeneration (from ~1600 m^2/g to ~20 m^2/g, discussed in Chapter 6), the material could still adsorb up to 90 % of RhB (Figure 6-13e).

The sorption of RhB from water was tested also on high temperature porous BN materials, which exhibited lower oxygen content, increased water stability and hydrobophicity and a fewer defects (Chapter 6). The dye sorption results for all samples are shown in Figure 6-14a. Generally, samples synthesised at high temperature showed a higher removal capacity for RhB (Figure 6-14a). This result was attributed to both a higher water stability of high temperature BN (Chapter 6) and an increased amount of graphitic BN, improving the propensity for π-π stacking interactions with the dye. RhB was almost completely removed from water within 1 h when the highest surface area samples were employed (BN-MU0.25:5-1500 ºC or BN-MU1:5-1500 ºC). The lowest surface area sample, BN-U5-1500 ºC, also fully removed RhB from water, but at a decreased rate (2 h).

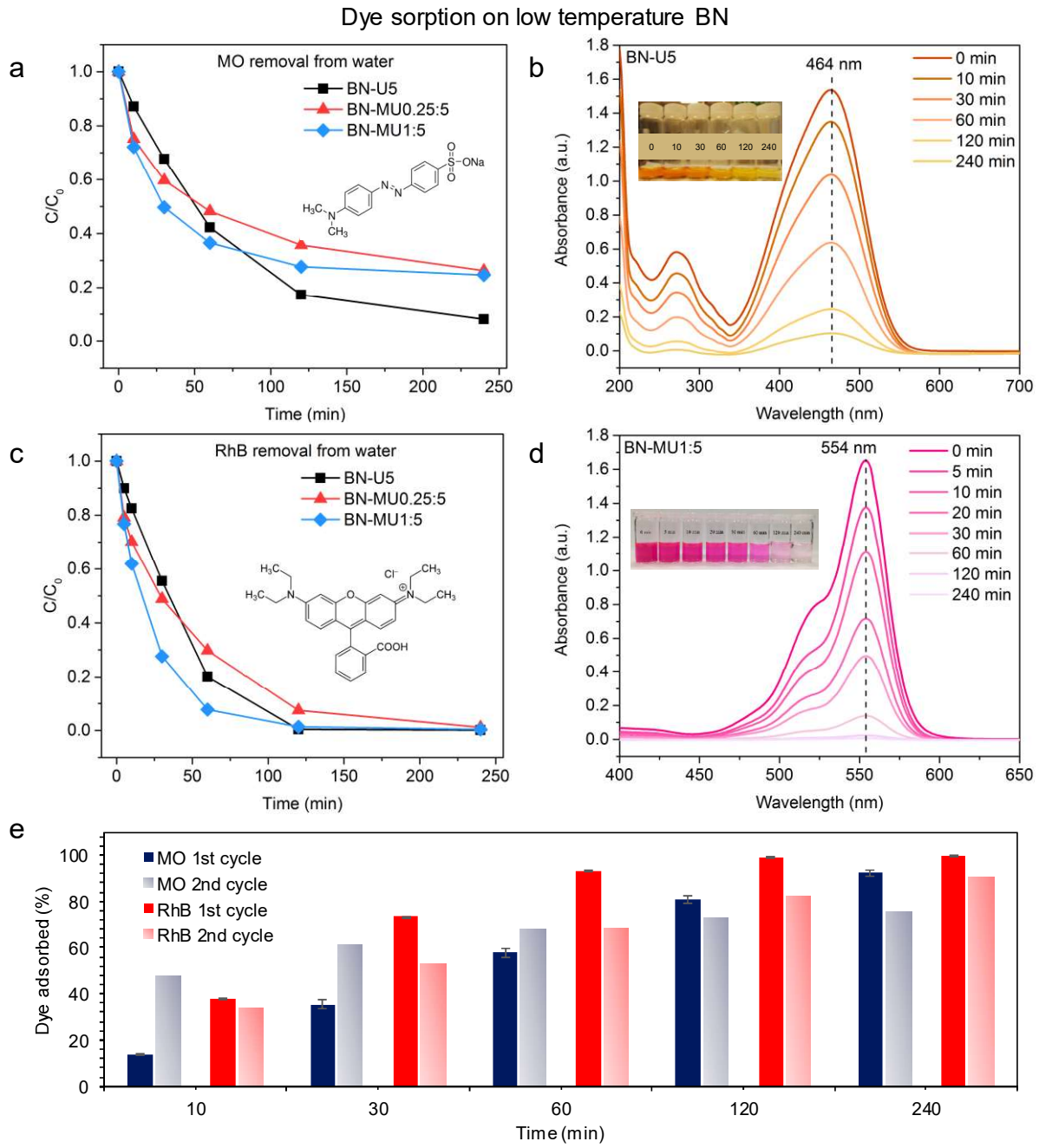


Figure 6-13 Dye sorption tests for porous BN samples with different pore structures for the removal of two different dyes: Methyl Orange (MO) and Rhodamine B (RhB).(a,c) Concentration of dye *vs* time,(b,d) UV-Vis spectra for the best performing samples and (e) dye removal performance before and after recycling the samples for the two best porous BN samples for RhB (BN-MU1:5) and MO (BN-U5).

The better performing high temperature sample (BN-MU0.25:5) was regenerated at 600 °C in air and employed for a second adsorption cycle. It must be noted that after regeneration the sample had the form of a very fine powder. The results for the 1st and 2nd sorption cycle on BN-MU0.25:5 at high temperature are reported in Figure 6-14c, d. After regeneration, porous BN

showed better adsorption performance at short exposure times, which was explained because of the better dispersibility of the fine powder in water (similarly to what was previously observed for BN-U5 synthesised at low temperatures, Figure 6-A3f). At higher exposure times, both samples completely removed RhB from water, with no decrease in adsorption capacity. This was attributed to the higher stability of high temperature BN samples in water, which showed little/no decrease of surface area after regeneration.

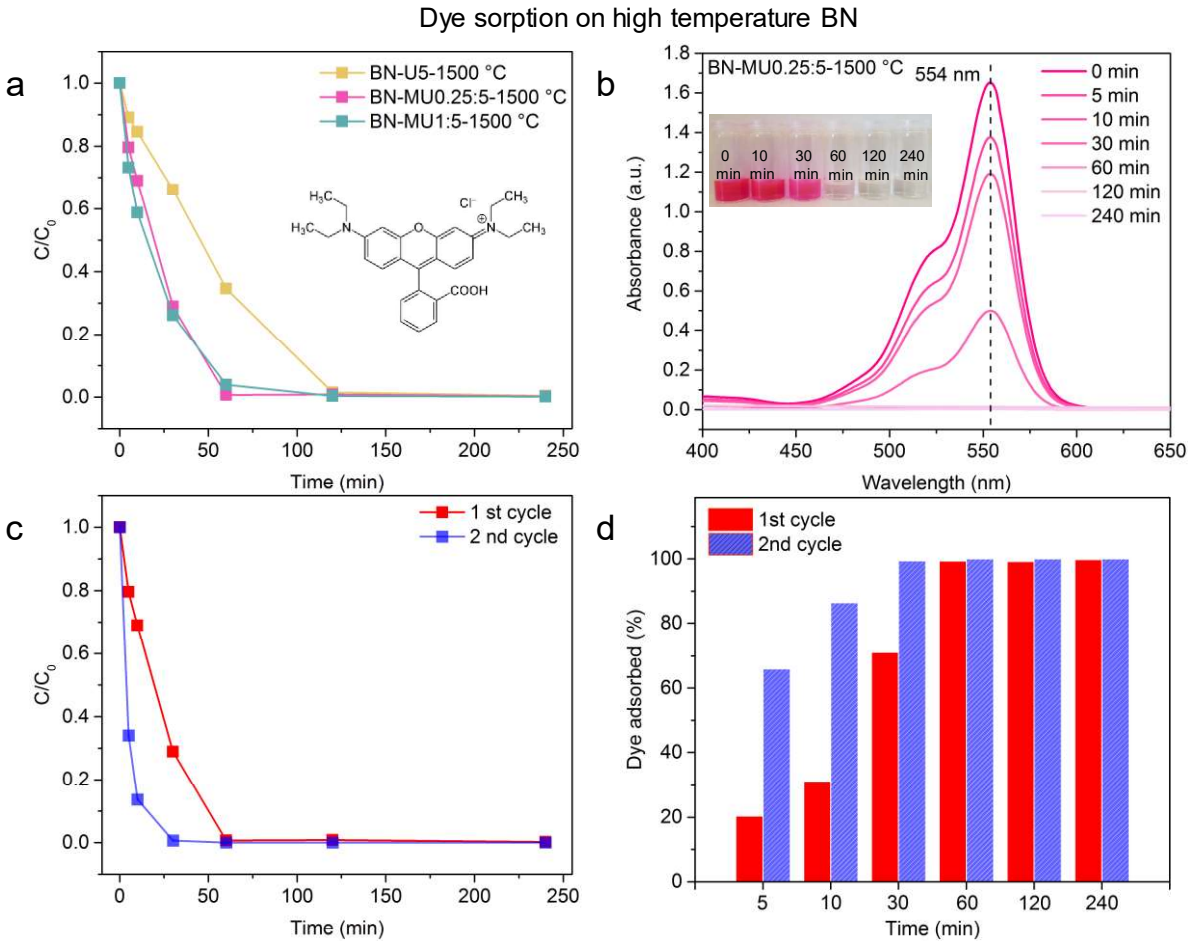


Figure 6-14 (a) RhB removal capacity *vs* time for *porous* BN samples synthesised at high temperature (1500 ºC);(b) UV-Vis absorption spectra for RhB solutions collected at different times from a sorption experiment performed with BN-MU0.25:5-1500 ºC.

In conclusion, dye sorption was attributed to multiple mechanisms: i) physisorption, as indicated by a higher sorption capacity for high surface area samples (when BN materials with higher water stability were employed); ii) π-π stacking between the dye molecules and the porous BN materials; iii) polar interactions between BN and the dyes, as indicated by a higher affinity for cationic RhB compared to anionic MO.

6.3.3.2 Oil spills cleanup

Porous BN samples with different pore structures and similar chemistries were tested for oil sorption (more or less viscous crude oils). It must be noted that when porous BN materials were employed for oil sorption in the literature, different sorption mechanisms were observed: i) adsorption (related to the surface area), ii) capillary effects, filling the larger pores and iii) filling of the spacing between the 2D sheets in BN, causing swelling of the material.[120] Porous BN materials with low surface areas and micropore volumes showed a high oil sorption capacity, suggesting micropores are not a necessity for oil sorption applications. [121-122]

A rough estimate of the gravimetric sorption capacities for porous BN samples is shown in Table 6-2. For CrudeA, with relatively low viscosity, higher surface area samples (BN-MU1:5> BN-MU0.25:5 > BN-U5) showed higher oil sorption capacities. However, when a higher viscosity crude oil was employed (CrudeB), little/no adsorption was observed for high surface area samples and the only sample which showed adsorption was BN-U5. This was attributed to the presence of a large amount of mesopores in the sample, which could adsorb the large hydrocarbon molecules present in the high viscosity crude.

Table 6-2 Gravimetric crude oil (with different viscosities) sorption capacities for three BN samples with different pore structures.

	BN-U5	*BN-MU0.25:5*	*BN-MU1:5*
CrudeA (low viscosity)	~ 600 wt. %	~ 780 wt. %	~1000 wt. %
CrudeB (high viscosity)	~ 650 wt. %	NA	NA

The best performing porous BN material for the removal of CrudeA (BN-MU1:5), was employed in a oil/water separation experiment (Figure 6-15). In less than 2 minutes roughly all of the oil was cleared from the water with a sorption capacity of ~750 wt%, which is slightly lower than the estimate shown in Table 6-2. This was attributed to competitive adsorption with water.

These results allowed us to conclude that porous BN materials could potentially be employed in the removal of crude oil from water. However, the removal efficiency strongly depended upon the type of crude oil and regeneration tests need to be performed. In order to optimise porous BN materials for crude oil sorption, macro- and mesopores should be introduced into porous BN materials in order to allow for better diffusion of the oils into the BN samples.

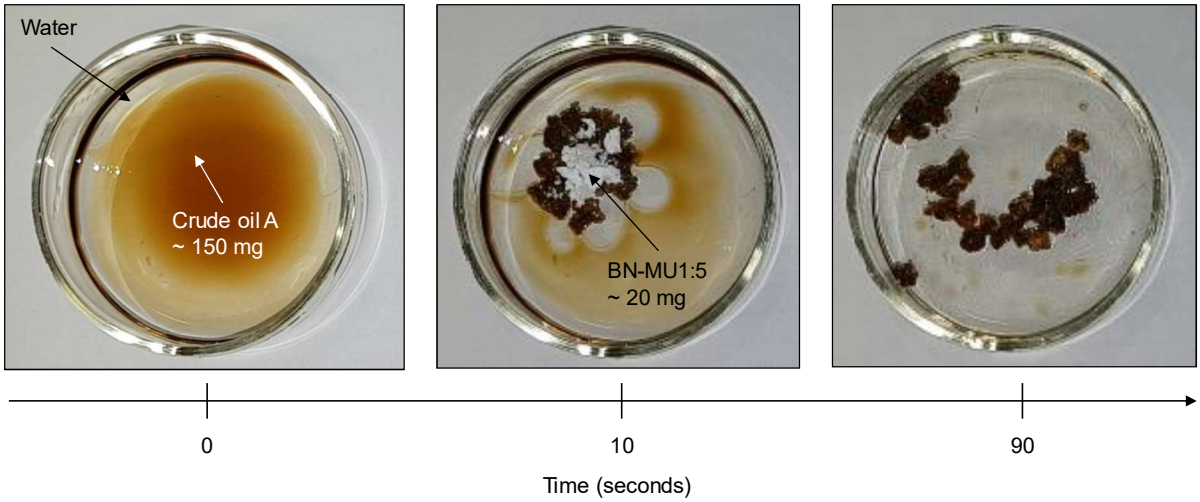


Figure 6-15 Crude oil (CrudeA) sorption from water using porous BN (BN-MU1:5).

6.4 Conclusions

Porous BN materials showed relatively low CO_2 and CH_4 sorption capacities at low pressures (< 1 bar). The CO_2 sorption mechanism was mainly attributed to physisorption and linearly increased with the materials' micropore volumes (highest sorption capacity of 1.6 mmol/g at 25 °C and 1 bar);

Porous BN was also tested for CO_2 sorption at high pressures (up to 20 bar). The capacity of BN was comparable to other commercial adsorbent materials (~8.3 mmol/g at 20 bar and 25 °C), even after pelletisation. The heat of adsorption for BN was calculated to be ~19 kJ/mol and matched well with simulations found in the literature.

Porous BN materials showed high sorption capacities for organic solvents, comparable to commercial activated carbons in the case of toluene adsorption. However, low selectivity between organic solvents was observed. All types of BN materials showed higher sorption capacity for toluene, likely due to BN's ability to form π-π interactions. High temperature porous BN materials showed higher organic solvent sorption capacities, which was attributed to higher hydrophobicity/oleophilicity, less defects and lower oxygen content.

Following on from the organic vapour tests, porous BN materials were tested for the removal of aromatics from water (dye removal of RhB and MO) and showed a stronger affinity for cationic dyes. High temperature porous BN samples showed higher dye sorption capacity and cyclability, with no decrease in removal capacity after regeneration. This was attributed to the

higher water stability of the materials. After regeneration, porous BN performed better at low adsorption times, suggesting that grinding the materials into fine powders helped the kinetics of adsorption;

Finally, porous BN materials showed promise in crude oil removal tests, although the results were preliminary and a more in-depth investigation is necessary in order to draw further conclusions.

Chapter 7: Conclusions and Future Plans

7.1 Findings and achievements

In Chapter 4, the synthesis parameters of porous BN were studied and their impact on BN structure, porosity and chemistry investigated. These parameters include: nature of precursors, molar ratios of precursors, intermediate of reaction preparation, synthesis temperature and synthesis ramp rate. A systematic variation of the synthesis parameters resulted in porous BN materials with different structure and/or chemistry.

In Chapter 5, a method to obtain highly porous BN with tuneable micro- and mesoporosity was described. This method was based on the use of an additional N-containing precursors which acts as a porogen during decomposition. By employing precursors in a variety of molar ratios and ensuring they had different decomposition temperatures, the fine-tuning of BN textural properties was achieved. This new method was reported in *ACS Nano* and a corresponding patent was filed. A scale-up of this synthesis method (up to ~gram-scale) is currently in development with a third-party company and BP are interested in testing the porous BN for various applications in separations and catalysis.

The stability of porous BN was evaluated in Chapter 6. While the material exhibited good mechanical and thermal stabilities in comparison to carbon-based equivalents (*e.g.* activated carbons), it was found to be sensitive to the presence of water and moisture, leading to its degradation. The water-instability of BN was shown to depend upon its chemistry, the presence of defects and the porosity of the material. Porous BN materials with significantly higher stability were produced by synthesising the material at higher temperatures (1500 °C). A manuscript is currently being reviewed by industrial partners.

In Chapter 7, preliminary sorption tests were conducted in gas phase, vapour phase and liquid phase. Porous BN proved promising for high pressure CO_2 adsorption applications and it was shown that CO_2 sorption capacity increased with increasing micropore volumes. Porous BN

also performed well in oil removal from water. Finally, porous BN was also tested for the first time for organic vapour sorption with distinct, albeit low, selectivity between different solvents. The sorption capacities for organic solvents were linked to both: i) BN pore structure; and ii) BN chemistry. Porous BN synthesised at higher temperatures showed increased uptake capacity for organics compared to those produced at lower temperatures, attributed to higher hydrophobicity/oleophilicity and higher crystallinity. This study allowed us to better describe the mechanisms of adsorption and link them to the material's properties. A manuscript is currently in preparation.

Overall, the porous nature and water stability of BN were improved during this research project, taking BN one step closer to successful industrial implementation. The method to fine-tune porous BN opens the door to tailored adsorbents analogous to successful carbonaceous materials and begins to make BN a competitive alternative to many leading porous materials.

7.2 Future plans

7.2.1 To produce stable BN materials via control of structure and chemistry

It was previously demonstrated that porous BN contains oxygen atoms within the structure (5-10 at.%). An increasing oxygen content can potentially reduce BN's chemical stability (in aqueous environments) and affect its adsorption and catalytic performance. Hence the reduction/elimination of the oxygen content is of key interest. The oxygen content can potentially be reduced *via* careful selection of precursors, molar ratios and synthesis temperatures. Alternatively, porous BN hydrophobicity may be increased *via* chemical routes for "blocking" the oxygen atoms. Porous BN hydrolytic stability and adsorption performance needs to be studied for all of the samples produced. A gravimetric analyser can be used to study the chemical stability of porous BN under different conditions (*i.e.* different relative humidity/ temperatures) by monitoring the change in sample mass and its full characterisation before and after analysis. This will allow for a better understanding of porous BN stability for use in specific applications.

7.2.2 To structure porous BN into valuable products.

Formation of pellets is a requirement for industrial utilisation of powder adsorbents, in order to avoid pressure drops in adsorption columns and to allow for easy handling. Porous BN powders can be structured into bulk materials (*i.e.* pellets as demonstrated in Chapter 5)

exhibiting hierarchical pore structures and high mechanical stability. Furthermore, pellets can be formed both with and without the use of binders. The mechanical stability of the pellets needs further evaluation in order to establish how well pellets maintain their structural integrity with subsequent adsorption-desorption cycles. Moreover, the pore structure of porous BN both before and after pelletisation need to be evaluated. Finally, porous BN pellets need to be tested for industrial applications to identify potential in the areas of separations and catalysis, in which BN may have the potential to surpass existing technologies.

7.2.3 To scale-up the synthesis of porous BN

The initial scale-up of BN production (to 10-100 g) is already underway with a third-party company in collaboration with BP. The material will need to be fully-characterised after scaling-up in order to demonstrate the successful synthesis of porous BN at scale, while still maintaining its desirable porous properties.

References

1. Jiuhui, Q., Research progress of novel adsorption processes in water purification: a review. *Journal of environmental sciences* **2008,** *20* (1), 1-13.
2. Choi, S.; Drese, J. H.; Jones, C. W., Adsorbent materials for carbon dioxide capture from large anthropogenic point sources. *ChemSusChem: Chemistry & Sustainability Energy & Materials* **2009,** *2* (9), 796-854.
3. Zhang, Y.; Riduan, S. N., Functional porous organic polymers for heterogeneous catalysis. *Chemical Society Reviews* **2012,** *41* (6), 2083-2094.
4. Zhao, M.; Ou, S.; Wu, C.-D., Porous metal–organic frameworks for heterogeneous biomimetic catalysis. *Accounts of chemical research* **2014,** *47* (4), 1199-1207.
5. Sholl, D. S.; Lively, R. P., Seven chemical separations: to change the world: purifying mixtures without using heat would lower global energy use, emissions and pollution--and open up new routes to resources. *Nature* **2016,** *532* (7600), 435-438.
6. Jiang, X.-F.; Weng, Q.; Wang, X.-B.; Li, X.; Zhang, J.; Golberg, D.; Bando, Y., Recent progress on fabrications and applications of boron nitride nanomaterials: a review. *Journal of Materials Science & Technology* **2015,** *31* (6), 589-598.
7. Rouquerol, J.; Rouquerol, F.; Llewellyn, P.; Maurin, G.; Sing, K. S., *Adsorption by powders and porous solids: principles, methodology and applications*. Academic press: 2013.
8. Brunauer, S.; Emmett, P. H.; Teller, E., Adsorption of gases in multimolecular layers. *Journal of the American chemical society* **1938,** *60* (2), 309-319.
9. Sing, K. S., Reporting physisorption data for gas/solid systems with special reference to the determination of surface area and porosity (Recommendations 1984). *Pure and applied chemistry* **1985,** *57* (4), 603-619.
10. Cox, D. M., High surface area materials. In *Nanostructure Science and Technology*, Springer: 1999; pp 49-66.
11. Ramesha, G.; Kumara, A. V.; Muralidhara, H.; Sampath, S., Graphene and graphene oxide as effective adsorbents toward anionic and cationic dyes. *Journal of colloid and interface science* **2011,** *361* (1), 270-277.
12. Wang, S.; Peng, Y., Natural zeolites as effective adsorbents in water and wastewater treatment. *Chemical Engineering Journal* **2010,** *156* (1), 11-24.
13. James, S. L., Metal-organic frameworks. *Chemical Society reviews* **2003,** *32* (5), 276-288.
14. Feng, X.; Ding, X.; Jiang, D., Covalent organic frameworks. *Chemical Society reviews* **2012,** *41* (18), 6010-6022.
15. Dawson, R.; Stöckel, E.; Holst, J. R.; Adams, D. J.; Cooper, A. I., Microporous organic polymers for carbon dioxide capture. *Energy & Environmental Science* **2011,** *4* (10), 4239-4245.
16. Jiang, J.-X.; Cooper, A. I., Microporous organic polymers: design, synthesis, and function. In *Functional Metal-Organic Frameworks: Gas Storage, Separation and Catalysis*, Springer: 2009; pp 1-33.
17. Radosz, M.; Hu, X.; Krutkramelis, K.; Shen, Y., Flue-gas carbon capture on carbonaceous sorbents: toward a low-cost multifunctional carbon filter for "green" energy producers. *Industrial & Engineering Chemistry Research* **2008,** *47* (10), 3783-3794.
18. Force, C. A. T., Advanced Post-Combustion CO2 Capture. **2009**.

19. Mueller, U.; Schubert, M.; Teich, F.; Puetter, H.; Schierle-Arndt, K.; Pastre, J., Metal–organic frameworks—prospective industrial applications. *Journal of Materials Chemistry* **2006,** *16* (7), 626-636.
20. Davis, M. E., Ordered porous materials for emerging applications. *Nature* **2002,** *417* (6891), 813.
21. Ma, Y.; Wang, Z.; Xu, X.; Wang, J., Review on porous nanomaterials for adsorption and photocatalytic conversion of CO 2. *Chinese Journal of Catalysis* **2017,** *38* (12), 1956-1969.
22. Otowa, T.; Nojima, Y.; Miyazaki, T., Development of KOH activated high surface area carbon and its application to drinking water purification. *Carbon* **1997,** *35* (9), 1315-1319.
23. Shi, Y.; Hamsen, C.; Jia, X.; Kim, K. K.; Reina, A.; Hofmann, M.; Hsu, A. L.; Zhang, K.; Li, H.; Juang, Z.-Y., Synthesis of few-layer hexagonal boron nitride thin film by chemical vapor deposition. *Nano letters* **2010,** *10* (10), 4134-4139.
24. Pakdel, A.; Bando, Y.; Golberg, D., Nano boron nitride flatland. *Chemical Society Reviews* **2014,** *43* (3), 934-959.
25. Lin, Y.; Connell, J. W., Advances in 2D boron nitride nanostructures: nanosheets, nanoribbons, nanomeshes, and hybrids with graphene. *Nanoscale* **2012,** *4* (22), 6908-6939.
26. Lee, K. H.; Shin, H.-J.; Lee, J.; Lee, I.-y.; Kim, G.-H.; Choi, J.-Y.; Kim, S.-W., Large-scale synthesis of high-quality hexagonal boron nitride nanosheets for large-area graphene electronics. *Nano letters* **2012,** *12* (2), 714-718.
27. Warner, J. H.; Rummeli, M. H.; Bachmatiuk, A.; Büchner, B., Atomic resolution imaging and topography of boron nitride sheets produced by chemical exfoliation. *Acs Nano* **2010,** *4* (3), 1299-1304.
28. Liu, Z.; Gong, Y.; Zhou, W.; Ma, L.; Yu, J.; Idrobo, J. C.; Jung, J.; MacDonald, A. H.; Vajtai, R.; Lou, J.; Ajayan, P. M., Ultrathin high-temperature oxidation-resistant coatings of hexagonal boron nitride. *Nat Commun* **2013,** *4*.
29. Zhu, Y.; Murali, S.; Cai, W.; Li, X.; Suk, J. W.; Potts, J. R.; Ruoff, R. S., Graphene and graphene oxide: synthesis, properties, and applications. *Advanced materials* **2010,** *22* (35), 3906-3924.
30. Novoselov, K.; Jiang, D.; Schedin, F.; Booth, T.; Khotkevich, V.; Morozov, S.; Geim, A., Two-dimensional atomic crystals. *Proceedings of the National Academy of Sciences of the United States of America* **2005,** *102* (30), 10451-10453.
31. Pacile, D.; Meyer, J. C.; Girit, C. O.; Zettl, A., The two-dimensional phase of boron nitride: Few-atomic-layer sheets and suspended membranes. *Applied Physics Letters* **2008,** *92* (13), 133107-133107-3.
32. Meyer, J. C.; Chuvilin, A.; Algara-Siller, G.; Biskupek, J.; Kaiser, U., Selective sputtering and atomic resolution imaging of atomically thin boron nitride membranes. *Nano letters* **2009,** *9* (7), 2683-2689.
33. Alem, N.; Erni, R.; Kisielowski, C.; Rossell, M. D.; Gannett, W.; Zettl, A., Atomically thin hexagonal boron nitride probed by ultrahigh-resolution transmission electron microscopy. *Physical Review B* **2009,** *80* (15), 155425.
34. Li, L. H.; Chen, Y.; Cheng, B.-M.; Lin, M.-Y.; Chou, S.-L.; Peng, Y.-C., Photoluminescence of boron nitride nanosheets exfoliated by ball milling. *Applied Physics Letters* **2012,** *100* (26), 261108.
35. Li, L. H.; Glushenkov, A. M.; Hait, S. K.; Hodgson, P.; Chen, Y., High-Efficient Production of Boron Nitride Nanosheets via an Optimized Ball Milling Process for Lubrication in Oil. *Scientific reports* **2014,** *4*.
36. Yao, Y.; Lin, Z.; Li, Z.; Song, X.; Moon, K.-S.; Wong, C.-p., Large-scale production of two-dimensional nanosheets. *Journal of Materials Chemistry* **2012,** *22* (27), 13494-13499.

37. Liu, L.; Xiong, Z.; Hu, D.; Wu, G.; Liu, B.; Chen, P., Solid exfoliation of hexagonal boron nitride crystals for the synthesis of few-layer boron nitride nanosheets. *Chemistry Letters* **2013,** *42* (11), 1415-1416.
38. Lei, W.; Liu, D.; Chen, Y., Highly Crumpled Boron Nitride Nanosheets as Adsorbents: Scalable Solvent-Less Production. *Advanced Materials Interfaces* **2015**.
39. Lin, Y.; Williams, T. V.; Cao, W.; Elsayed-Ali, H. E.; Connell, J. W., Defect functionalization of hexagonal boron nitride nanosheets. *The Journal of Physical Chemistry C* **2010,** *114* (41), 17434-17439.
40. HuaáLi, L., Large-scale mechanical peeling of boron nitride nanosheets by low-energy ball milling. *Journal of materials chemistry* **2011,** *21* (32), 11862-11866.
41. Lee, D.; Lee, B.; Park, K. H.; Ryu, H. J.; Jeon, S.; Hong, S. H., Scalable Exfoliation Process for Highly Soluble Boron Nitride Nanoplatelets by Hydroxide-assisted Ball Milling. *Nano letters* **2015**.
42. Chen, X.; Dobson, J. F.; Raston, C. L., Vortex fluidic exfoliation of graphite and boron nitride. *Chemical Communications* **2012,** *48* (31), 3703-3705.
43. Yurdakul, H.; Göncü, Y.; Durukan, O.; Akay, A.; Seyhan, A. T.; Ay, N.; Turan, S., Nanoscopic characterization of two-dimensional (2D) boron nitride nanosheets (BNNSs) produced by microfluidization. *Ceramics International* **2012,** *38* (3), 2187-2193.
44. Zhi, C.; Bando, Y.; Tang, C.; Kuwahara, H.; Golberg, D., Large-scale fabrication of boron nitride nanosheets and their utilization in polymeric composites with improved thermal and mechanical properties. *Advanced Materials* **2009,** *21* (28), 2889-2893.
45. Coleman, J. N.; Lotya, M.; O'Neill, A.; Bergin, S. D.; King, P. J.; Khan, U.; Young, K.; Gaucher, A.; De, S.; Smith, R. J.; Shvets, I. V.; Arora, S. K.; Stanton, G.; Kim, H.-Y.; Lee, K.; Kim, G. T.; Duesberg, G. S.; Hallam, T.; Boland, J. J.; Wang, J. J.; Donegan, J. F.; Grunlan, J. C.; Moriarty, G.; Shmeliov, A.; Nicholls, R. J.; Perkins, J. M.; Grieveson, E. M.; Theuwissen, K.; McComb, D. W.; Nellist, P. D.; Nicolosi, V., Two-Dimensional Nanosheets Produced by Liquid Exfoliation of Layered Materials. *Science* **2011,** *331* (6017), 568-571.
46. Lian, G.; Zhang, X.; Tan, M.; Zhang, S.; Cui, D.; Wang, Q., Facile synthesis of 3D boron nitride nanoflowers composed of vertically aligned nanoflakes and fabrication of graphene-like BN by exfoliation. *Journal of Materials Chemistry* **2011,** *21* (25), 9201-9207.
47. Huang, C.; Chen, C.; Ye, X.; Ye, W.; Hu, J.; Xu, C.; Qiu, X., Stable colloidal boron nitride nanosheet dispersion and its potential application in catalysis. *Journal of Materials Chemistry A* **2013,** *1* (39), 12192-12197.
48. Zhou, K. G.; Mao, N. N.; Wang, H. X.; Peng, Y.; Zhang, H. L., A Mixed-Solvent Strategy for Efficient Exfoliation of Inorganic Graphene Analogues. *Angewandte Chemie International Edition* **2011,** *50* (46), 10839-10842.
49. Marsh, K.; Souliman, M.; Kaner, R., Co-solvent exfoliation and suspension of hexagonal boron nitride. *Chemical Communications* **2015,** *51* (1), 187-190.
50. Lin, Y.; Williams, T. V.; Xu, T.-B.; Cao, W.; Elsayed-Ali, H. E.; Connell, J. W., Aqueous dispersions of few-layered and monolayered hexagonal boron nitride nanosheets from sonication-assisted hydrolysis: critical role of water. *The Journal of Physical Chemistry C* **2011,** *115* (6), 2679-2685.
51. Wang, Y.; Shi, Z.; Yin, J., Boron nitride nanosheets: large-scale exfoliation in methanesulfonic acid and their composites with polybenzimidazole. *Journal of Materials Chemistry* **2011,** *21* (30), 11371-11377.
52. Morishita, T.; Okamoto, H.; Katagiri, Y.; Matsushita, M.; Fukumori, K., A high-yield ionic liquid-promoted synthesis of boron nitride nanosheets by direct exfoliation. *Chemical Communications* **2015,** *51* (60), 12068-12071.
53. Štengl, V.; Henych, J.; Slušná, M.; Ecorchard, P., Ultrasound exfoliation of inorganic analogues of graphene. *Nanoscale research letters* **2014,** *9* (1), 1-14.

54. Wang, Y.; Zhou, C.; Wang, W.; Zhao, Y., Preparation of two dimensional atomic crystals BN, WS2, and MoS2 by supercritical CO2 assisted with ultrasound. *Industrial & Engineering Chemistry Research* **2013,** *52* (11), 4379-4382.
55. Zeng, Z.; Yin, Z.; Huang, X.; Li, H.; He, Q.; Lu, G.; Boey, F.; Zhang, H., Single-Layer Semiconducting Nanosheets: High-Yield Preparation and Device Fabrication. *Angewandte Chemie International Edition* **2011,** *50* (47), 11093-11097.
56. Zeng, Z.; Sun, T.; Zhu, J.; Huang, X.; Yin, Z.; Lu, G.; Fan, Z.; Yan, Q.; Hng, H. H.; Zhang, H., An Effective Method for the Fabrication of Few-Layer-Thick Inorganic Nanosheets. *Angewandte Chemie International Edition* **2012,** *51* (36), 9052-9056.
57. Han, W.-Q.; Wu, L.; Zhu, Y.; Watanabe, K.; Taniguchi, T., Structure of chemically derived mono-and few-atomic-layer boron nitride sheets. *Applied Physics Letters* **2008,** *93* (22), 223103.
58. Lin, Y.; Williams, T. V.; Connell, J. W., Soluble, exfoliated hexagonal boron nitride nanosheets. *The Journal of Physical Chemistry Letters* **2009,** *1* (1), 277-283.
59. Cao, L.; Emami, S.; Lafdi, K., Large-scale exfoliation of hexagonal boron nitride nanosheets in liquid phase. *Materials Express* **2014,** *4* (2), 165-171.
60. Du, M.; Wu, Y.; Hao, X., A facile chemical exfoliation method to obtain large size boron nitride nanosheets. *CrystEngComm* **2013,** *15* (9), 1782-1786.
61. Li, X.; Hao, X.; Zhao, M.; Wu, Y.; Yang, J.; Tian, Y.; Qian, G., Exfoliation of hexagonal boron nitride by molten hydroxides. *Advanced Materials* **2013,** *25* (15), 2200-2204.
62. Cui, Z.; Oyer, A. J.; Glover, A. J.; Schniepp, H. C.; Adamson, D. H., Large Scale Thermal Exfoliation and Functionalization of Boron Nitride. *Small* **2014**.
63. Yu, B.; Xing, W.; Guo, W.; Qiu, S.; Wang, X.; Lo, S.; Hu, Y., Thermal exfoliation of hexagonal boron nitride for effective enhancements on thermal stability, flame retardancy and smoke suppression of epoxy resin nanocomposites via sol–gel process. *Journal of Materials Chemistry A* **2016,** *4* (19), 7330-7340.
64. Zhu, W.; Gao, X.; Li, Q.; Li, H.; Chao, Y.; Li, M.; Mahurin, S. M.; Li, H.; Zhu, H.; Dai, S., Controlled Gas Exfoliation of Boron Nitride into Few-Layered Nanosheets. *Angewandte Chemie International Edition* **2016,** *55* (36), 10766-10770.
65. Zeng, H.; Zhi, C.; Zhang, Z.; Wei, X.; Wang, X.; Guo, W.; Bando, Y.; Golberg, D., "White graphenes": Boron nitride nanoribbons via boron nitride nanotube unwrapping. *Nano letters* **2010,** *10* (12), 5049-5055.
66. Erickson, K. J.; Gibb, A. L.; Sinitskii, A.; Rousseas, M.; Alem, N.; Tour, J. M.; Zettl, A. K., Longitudinal splitting of boron nitride nanotubes for the facile synthesis of high quality boron nitride nanoribbons. *Nano letters* **2011,** *11* (8), 3221-3226.
67. Wang, X.; Zhi, C.; Li, L.; Zeng, H.; Li, C.; Mitome, M.; Golberg, D.; Bando, Y., "Chemical Blowing" of Thin-Walled Bubbles: High-Throughput Fabrication of Large-Area, Few-Layered BN and Cx-BN Nanosheets. *Advanced Materials* **2011,** *23* (35), 4072-4076.
68. Wang, X.; Pakdel, A.; Zhi, C.; Watanabe, K.; Sekiguchi, T.; Golberg, D.; Bando, Y., High-yield boron nitride nanosheets from 'chemical blowing': towards practical applications in polymer composites. *Journal of Physics: Condensed Matter* **2012,** *24* (31), 314205.
69. Rand, M. J.; Roberts, J. F., Preparation and properties of thin film boron nitride. *Journal of the Electrochemical Society* **1968,** *115* (4), 423-429.
70. Dibandjo, P.; Chassagneux, F.; Bois, L.; Sigala, C.; Miele, P., Comparison between SBA-15 silica and CMK-3 carbon nanocasting for mesoporous boron nitride synthesis. *Journal of Materials Chemistry* **2005,** *15* (19), 1917-1923.
71. Rushton, B.; Mokaya, R., Mesoporous boron nitride and boron-nitride-carbon materials from mesoporous silica templates. *Journal of Materials Chemistry* **2008,** *18* (2), 235-241.

72. Schlienger, S.; Alauzun, J.; Michaux, F.; Vidal, L.; Parmentier, J.; Gervais, C.; Babonneau, F.; Bernard, S.; Miele, P.; Parra, J., Micro-, mesoporous boron nitride-based materials templated from zeolites. *Chemistry of Materials* **2011,** *24* (1), 88-96.
73. Dibandjo, P.; Bois, L.; Chassagneux, F.; Miele, P., Thermal stability of mesoporous boron nitride templated with a cationic surfactant. *Journal of the European Ceramic Society* **2007,** *27* (1), 313-317.
74. Li, J.; Xiao, X.; Xu, X.; Lin, J.; Huang, Y.; Xue, Y.; Jin, P.; Zou, J.; Tang, C., Activated boron nitride as an effective adsorbent for metal ions and organic pollutants. *Scientific reports* **2013,** *3*.
75. Zhang, N.; Liu, H.; Kan, H.; Wang, X.; Long, H.; Zhou, Y., The preparation of high-adsorption, spherical, hexagonal boron nitride by template method. *Journal of Alloys and Compounds* **2014,** *613*, 74-79.
76. Maleki, M.; Beitollahi, A.; Shokouhimehr, M., Simple Synthesis of Two-Dimensional Micro/Mesoporous Boron Nitride. *European Journal of Inorganic Chemistry* **2015**.
77. Xiong, J.; Zhu, W.; Li, H.; Yang, L.; Chao, Y.; Wu, P.; Xun, S.; Jiang, W.; Zhang, M., Carbon-Doped Porous Boron Nitride: Metal-Free Adsorbents for Sulfur Removal from Fuels. *Journal of Materials Chemistry A* **2015**.
78. Han, W.-Q.; Brutchey, R.; Tilley, T. D.; Zettl, A., Activated boron nitride derived from activated carbon. *Nano Letters* **2004,** *4* (1), 173-176.
79. Vinu, A.; Terrones, M.; Golberg, D.; Hishita, S.; Ariga, K.; Mori, T., Synthesis of mesoporous BN and BCN exhibiting large surface areas via templating methods. *Chemistry of materials* **2005,** *17* (24), 5887-5890.
80. Zhang, X.; Lian, G.; Zhang, S.; Cui, D.; Wang, Q., Boron nitride nanocarpets: controllable synthesis and their adsorption performance to organic pollutants. *CrystEngComm* **2012,** *14* (14), 4670-4676.
81. Fu, M.; Xing, H.; Chen, X.; Chen, F.; Wu, C.-M. L.; Zhao, R.; Cheng, C., Ultrathin-shell boron nitride hollow spheres as sorbent for dispersive solid-phase extraction of polychlorinated biphenyls from environmental water samples. *Journal of Chromatography A* **2014,** *1369*, 181-185.
82. Hagio, T.; Nonaka, K.; Sato, T., Microstructural development with crystallization of hexagonal boron nitride. *Journal of materials science letters* **1997,** *16* (10), 795-798.
83. Zhao, Z.; Yang, Z.; Wen, Y.; Wang, Y., Facile synthesis and characterization of hexagonal boron nitride nanoplates by two-step route. *Journal of the American Ceramic Society* **2011,** *94* (12), 4496-4501.
84. Ansaloni, L. M. S.; de Sousa, E. M. B., Boron Nitride Nanostructured: Synthesis, Characterization and Potential Use in Cosmetics. *Materials Sciences and Applications* **2013,** *4*, 22.
85. Li, J.; Jia, H.; Ding, Y.; Luo, H.; Abbas, S.; Liu, Z.; Hu, L.; Tang, C., NaOH-embedded three-dimensional porous boron nitride for efficient formaldehyde removal. *Nanotechnology* **2015,** *26* (47), 475704.
86. Hubáček, M.; Sato, T.; Ishii, T., A coexistence of boron nitride and boric oxide. *Journal of Solid State Chemistry* **1994,** *109* (2), 384-390.
87. Xiao, F.; Chen, Z.; Casillas, G.; Richardson, C.; Li, H.; Huang, Z., Controllable synthesis of few-layered and hierarchically porous boron nitride nanosheets. *Chemical Communications* **2016,** *52* (20), 3911-3914.
88. Chen, S.; Li, P.; Xu, S.; Pan, X.; Fu, Q.; Bao, X., Carbon doping of hexagonal boron nitride porous materials toward CO 2 capture. *Journal of Materials Chemistry A* **2018,** *6* (4), 1832-1839.

89. Li, Q.; Yang, T.; Yang, Q.; Wang, F.; Chou, K.-C.; Hou, X., Porous hexagonal boron nitride whiskers fabricated at low temperature for effective removal of organic pollutants from water. *Ceramics International* **2016,** *42* (7), 8754-8762.
90. Li, J.; Lin, J.; Xu, X.; Zhang, X.; Xue, Y.; Mi, J.; Mo, Z.; Fan, Y.; Hu, L.; Yang, X., Porous boron nitride with a high surface area: hydrogen storage and water treatment. *Nanotechnology* **2013,** *24* (15), 155603.
91. Nag, A.; Raidongia, K.; Hembram, K. P.; Datta, R.; Waghmare, U. V.; Rao, C., Graphene analogues of BN: novel synthesis and properties. *ACS nano* **2010,** *4* (3), 1539-1544.
92. Weng, Q.; Wang, X.; Bando, Y.; Golberg, D., One-Step Template-Free Synthesis of Highly Porous Boron Nitride Microsponges for Hydrogen Storage. *Advanced Energy Materials* **2014,** *4* (7).
93. Lei, W.; Zhang, H.; Wu, Y.; Zhang, B.; Liu, D.; Qin, S.; Liu, Z.; Liu, L.; Ma, Y.; Chen, Y., Oxygen-doped boron nitride nanosheets with excellent performance in hydrogen storage. *Nano Energy* **2014,** *6*, 219-224.
94. Weng, Q.; Wang, X.; Zhi, C.; Bando, Y.; Golberg, D., Boron nitride porous microbelts for hydrogen storage. *ACS nano* **2013,** *7* (2), 1558-1565.
95. Liu, Z.; Fang, Y.; Jia, H.; Wang, C.; Song, Q.; Li, L.; Lin, J.; Huang, Y.; Yu, C.; Tang, C., Novel multifunctional cheese-like 3D carbon-BN as a highly efficient adsorbent for water purification. *Scientific reports* **2018,** *8* (1), 1104.
96. Wu, P.; Zhu, W.; Chao, Y.; Zhang, J.; Zhang, P.; Zhu, H.; Li, C.; Chen, Z.; Li, H.; Dai, S., A template-free solvent-mediated synthesis of high surface area boron nitride nanosheets for aerobic oxidative desulfurization. *Chemical Communications* **2016,** *52* (1), 144-147.
97. Alkoy, S.; Toy, C.; Gönül, T.; Tekin, A., Crystallization behavior and characterization of turbostratic boron nitride. *Journal of the European Ceramic Society* **1997,** *17* (12), 1415-1422.
98. Zeng, X.; Ye, L.; Yu, S.; Sun, R.; Xu, J.; Wong, C.-P., Facile preparation of superelastic and ultralow dielectric boron nitride nanosheet aerogels via freeze-casting process. *Chemistry of Materials* **2015,** *27* (17), 5849-5855.
99. Zeng, X.; Yao, Y.; Gong, Z.; Wang, F.; Sun, R.; Xu, J.; Wong, C. P., Ice-Templated Assembly Strategy to Construct 3D Boron Nitride Nanosheet Networks in Polymer Composites for Thermal Conductivity Improvement. *Small* **2015,** *11* (46), 6205-6213.
100. Zeng, X.; Ye, L.; Sun, R.; Xu, J.; Wong, C.-P., Observation of viscoelasticity in boron nitride nanosheet aerogel. *Physical Chemistry Chemical Physics* **2015,** *17* (26), 16709-16714.
101. Sudeep, P. M.; Vinod, S.; Ozden, S.; Sruthi, R.; Kukovecz, A.; Konya, Z.; Vajtai, R.; Anantharaman, M.; Ajayan, P.; Narayanan, T. N., Functionalized boron nitride porous solids. *RSC Advances* **2015,** *5* (114), 93964-93968.
102. Zhao, H.; Song, X.; Zeng, H., 3D white graphene foam scavengers: vesicant-assisted foaming boosts the gram-level yield and forms hierarchical pores for superstrong pollutant removal applications. *NPG Asia Materials* **2015,** *7* (3), e168.
103. Ashton, T. S.; Moore, A. L., Foam-like hierarchical hexagonal boron nitride as a non-traditional thermal conductivity enhancer for polymer-based composite materials. *International Journal of Heat and Mass Transfer* **2017,** *115*, 273-281.
104. Pham, T.; Goldstein, A. P.; Lewicki, J. P.; Kucheyev, S. O.; Wang, C.; Russell, T. P.; Worsley, M. A.; Woo, L.; Mickelson, W.; Zettl, A., Nanoscale structure and superhydrophobicity of sp2-bonded boron nitride aerogels. *Nanoscale* **2015,** *7* (23), 10449-10458.
105. Motojima, S.; Tamura, Y.; Sugiyama, K., Low temperature deposition of hexagonal BN films by chemical vapour deposition. *Thin Solid Films* **1982,** *88* (3), 269-274.

106. Cofer, C. G.; Economy, J., Oxidative and hydrolytic stability of boron nitride—a new approach to improving the oxidation resistance of carbonaceous structures. *Carbon* **1995,** *33* (4), 389-395.
107. Streletskii, A.; Permenov, D.; Bokhonov, B.; Kolbanev, I.; Leonov, A.; Berestetskaya, I.; Streletzky, K. A., Destruction, amorphization and reactivity of nano-BN under ball milling. *Journal of Alloys and Compounds* **2009,** *483* (1-2), 313-316.
108. Florent, M.; Bandosz, T. J., Irreversible water mediated transformation of BCN from a 3D highly porous form to its nonporous hydrolyzed counterpart. *Journal of Materials Chemistry A* **2018,** *6* (8), 3510-3521.
109. Janik, J. F.; Ackerman, W. C.; Paine, R. T.; Hua, D.-W.; Maskara, A.; Smith, D. M., Boron nitride as a selective gas adsorbent. *Langmuir* **1994,** *10* (2), 514-518.
110. Owuor, P. S.; Park, O.-K.; Woellner, C. F.; Jalilov, A. S.; Susarla, S.; Joyner, J.; Ozden, S.; Duy, L.; Villegas Salvatierra, R.; Vajtai, R., Lightweight hexagonal boron nitride foam for co2 absorption. *ACS nano* **2017,** *11* (9), 8944-8952.
111. Marchesini, S.; Regoutz, A.; Payne, D.; Petit, C., Tunable porous boron nitride: Investigating its formation and its application for gas adsorption. *Microporous and Mesoporous Materials* **2017,** *243*, 154-163.
112. Ye, J.; Zhu, X.; Cheng, B.; Yu, J.; Jiang, C., Few-layered Graphene-like Boron Nitride: A Highly Efficient Adsorbent for Indoor Formaldehyde Removal. *Environmental Science & Technology Letters* **2016**.
113. Saha, D.; Orkoulas, G.; Yohannan, S.; Ho, H. C.; Cakmak, E.; Chen, J.; Ozcan, S., Nanoporous Boron Nitride as Exceptionally Thermally Stable Adsorbent: Role in Efficient Separation of Light Hydrocarbons. *ACS Applied Materials & Interfaces* **2017**.
114. Chen, Y.; Wang, J.; Chen, Y.; Liu, D.; Huang, S.; Lei, W., One-step template-free synthesis of 3D functionalized flower-like boron nitride nanosheets for NH3 and CO2 adsorption. *Nanoscale* **2018**.
115. Wang, Q.; Luo, J.; Zhong, Z.; Borgna, A., CO2 capture by solid adsorbents and their applications: current status and new trends. *Energy & Environmental Science* **2011,** *4* (1), 42-55.
116. Lian, G.; Zhang, X.; Zhang, S.; Liu, D.; Cui, D.; Wang, Q., Controlled fabrication of ultrathin-shell BN hollow spheres with excellent performance in hydrogen storage and wastewater treatment. *Energy & Environmental Science* **2012,** *5* (5), 7072-7080.
117. Yu, S.; Wang, X.; Pang, H.; Zhang, R.; Song, W.; Fu, D.; Hayat, T.; Wang, X., Boron nitride-based materials for the removal of pollutants from aqueous solutions: a review. *Chemical Engineering Journal* **2017**.
118. Li, J.; Jin, P.; Tang, C., Cr (III) adsorption by fluorinated activated boron nitride: a combined experimental and theoretical investigation. *RSC Advances* **2014,** *4* (29), 14815-14821.
119. Xue, Y.; Dai, P.; Jiang, X.; Wang, X.; Zhang, C.; Tang, D.; Weng, Q.; Wang, X.; Pakdel, A.; Tang, C., Template-free synthesis of boron nitride foam-like porous monoliths and their high-end applications in water purification. *Journal of Materials Chemistry A* **2016**.
120. Lei, W.; Portehault, D.; Liu, D.; Qin, S.; Chen, Y., Porous boron nitride nanosheets for effective water cleaning. *Nature communications* **2013,** *4*, 1777.
121. Zhao, H.; Song, X.; Zeng, H., 3D white graphene foam scavengers: vesicant-assisted foaming boosts the gram-level yield and forms hierarchical pores for superstrong pollutant removal applications. **2015**.
122. Maleki, M.; Shokouhimehr, M.; Karimian, H.; Beitollahi, A., Three-dimensionally interconnected porous boron nitride foam derived from polymeric foams. *RSC Advances* **2016,** *6* (56), 51426-51434.

123. Liu, D.; Lei, W.; Qin, S.; Chen, Y., Template-free synthesis of functional 3D BN architecture for removal of dyes from water. *Scientific reports* **2014,** *4*.
124. Liu, D.; He, L.; Lei, W.; Klika, K. D.; Kong, L.; Chen, Y., Multifunctional polymer/porous boron nitride nanosheet membranes for superior trapping emulsified oils and organic molecules. *Advanced Materials Interfaces* **2015,** *2* (12).
125. Lin, J.; Xu, L.; Huang, Y.; Li, J.; Wang, W.; Feng, C.; Liu, Z.; Xu, X.; Zou, J.; Tang, C., Ultrafine porous boron nitride nanofibers synthesized via a freeze-drying and pyrolysis process and their adsorption properties. *RSC Advances* **2016,** *6* (2), 1253-1259.
126. Singla, P.; Goel, N.; Singhal, S., Boron nitride nanomaterials with different morphologies: Synthesis, characterization and efficient application in dye adsorption. *Ceramics International* **2015**.
127. Li, J.; Huang, Y.; Liu, Z.; Zhang, J.; Liu, X.; Luo, H.; Ma, Y.; Xu, X.; Lu, Y.; Lin, J., Chemical activation of boron nitride fibers for improved cationic dye removal performance. *Journal of Materials Chemistry A* **2015,** *3* (15), 8185-8193.
128. Liu, D.; Lei, W.; Qin, S.; Klika, K. D.; Chen, Y., Superior adsorption of pharmaceutical molecules by highly porous BN nanosheets. *Physical Chemistry Chemical Physics* **2016,** *18* (1), 84-88.
129. Lin, Y.; Xu, S.; Li, J., Fast and highly efficient tetracyclines removal from environmental waters by graphene oxide functionalized magnetic particles. *Chemical Engineering Journal* **2013,** *225*, 679-685.
130. Dai, P.; Xue, Y.; Wang, X.; Weng, Q.; Zhang, C.; Jiang, X.; Tang, D.; Wang, X.; Kawamoto, N.; Ide, Y., Pollutant capturing SERS substrate: porous boron nitride microfibers with uniform silver nanoparticle decoration. *Nanoscale* **2015,** *7* (45), 18992-18997.
131. Song, Y.; Li, B.; Yang, S.; Ding, G.; Zhang, C.; Xie, X., Ultralight boron nitride aerogels via template-assisted chemical vapor deposition. *Scientific reports* **2015,** *5*.
132. Gautam, C.; Tiwary, C. S.; Jose, S.; Brunetto, G.; Ozden, S.; Vinod, S.; Raghavan, P.; Biradar, S.; Galvao, D. S.; Ajayan, P. M., Synthesis of Low-Density, Carbon-Doped, Porous Hexagonal Boron Nitride Solids. *ACS nano* **2015,** *9* (12), 12088-12095.
133. Sudeep, P.; Vinod, S.; Ozden, S.; Sruthi, R.; Kukovecz, A.; Konya, Z.; Vajtai, R.; Anantharaman, M.; Ajayan, P.; Narayanan, T. N., Functionalized boron nitride porous solids. *RSC Advances* **2015,** *5* (114), 93964-93968.
134. Jia, S.; Wang, Z.; Ding, N.; Wong, Y.-L. E.; Chen, X.; Qiu, G.; Chan, T.-W. D., Hexagonal boron nitride nanosheets as adsorbents for solid-phase extraction of polychlorinated biphenyls from water samples. *Analytica Chimica Acta* **2016**.
135. Li, T.; Wang, L.; Zhang, K.; Xu, Y.; Long, X.; Gao, S.; Li, R.; Yao, Y., Freestanding Boron Nitride Nanosheet Films for Ultrafast Oil/Water Separation. *Small* **2016**.
136. Feng, Y.; Zhou, Y.; Lee, P.-H.; Shih, K., Mineralization of perfluorooctanesulfonate (PFOS) and perfluorodecanoate (PFDA) from aqueous solution by porous hexagonal boron nitride: adsorption followed by simultaneous thermal decomposition and regeneration. *RSC Advances* **2016,** *6* (114), 113773-113780.
137. Xue, Y.; Dai, P.; Zhou, M.; Wang, X.; Pakdel, A.; Zhang, C.; Weng, Q.; Takei, T.; Fu, X.; Popov, Z. I., Multifunctional Superelastic Foam-Like Boron Nitride Nanotubular Cellular-Network Architectures. *ACS nano* **2016**.
138. Xue, L.; Lu, B.; Wu, Z.-S.; Ge, C.; Wang, P.; Zhang, R.; Zhang, X.-D., Synthesis of mesoporous hexagonal boron nitride fibers with high surface area for efficient removal of organic pollutants. *Chemical Engineering Journal* **2014,** *243*, 494-499.
139. Liu, F.; Yu, J.; Ji, X.; Qian, M., Nanosheet-structured boron nitride spheres with a versatile adsorption capacity for water cleaning. *ACS applied materials & interfaces* **2015,** *7* (3), 1824-1832.

140. Wu, J. C.-S.; Lin, Z.-A.; Pan, J.-W.; Rei, M.-H., A novel boron nitride supported Pt catalyst for VOC incineration. *Applied Catalysis A: General* **2001,** *219* (1), 117-124.
141. Lin, C.-A.; Wu, J. C.; Pan, J.-W.; Yeh, C.-T., Characterization of boron-nitride-supported Pt catalysts for the deep oxidation of benzene. *Journal of Catalysis* **2002,** *210* (1), 39-45.
142. Jacobsen, C. J., Boron nitride: a novel support for ruthenium-based ammonia synthesis catalysts. *Journal of Catalysis* **2001,** *200* (1), 1-3.
143. Postole, G.; Caldararu, M.; Ionescu, N.; Bonnetot, B.; Auroux, A.; Guimon, C., Boron nitride: A high potential support for combustion catalysts. *Thermochimica acta* **2005,** *434* (1), 150-157.
144. Venegas, J. M.; Grant, J. T.; McDermott, W. P.; Burt, S. P.; Micka, J.; Carrero, C. A.; Hermans, I., Selective Oxidation of n-Butane and Isobutane Catalyzed by Boron Nitride. *ChemCatChem* **2017,** *9* (12), 2118-2127.
145. Grant, J. T.; Carrero, C. A.; Goeltl, F.; Venegas, J.; Mueller, P.; Burt, S. P.; Specht, S. E.; McDermott, W. P.; Chieregato, A.; Hermans, I., Selective oxidative dehydrogenation of propane to propene using boron nitride catalysts. *Science* **2016,** *354* (6319), 1570-1573.
146. Shi, L.; Wang, D.; Lu, A.-H., A viewpoint on catalytic origin of boron nitride in oxidative dehydrogenation of light alkanes. *Chinese Journal of Catalysis* **2018,** *39* (5), 908-913.
147. Tian, J.; Lin, J.; Xu, M.; Wan, S.; Lin, J.; Wang, Y., Hexagonal boron nitride catalyst in a fixed-bed reactor for exothermic propane oxidation dehydrogenation. *Chemical Engineering Science* **2018,** *186*, 142-151.
148. Sing, K., The use of nitrogen adsorption for the characterisation of porous materials. *Colloids and Surfaces A: Physicochemical and Engineering Aspects* **2001,** *187*, 3-9.
149. Chen, S.; Yang, R., Theoretical basis for the potential theory adsorption isotherms. The Dubinin-Radushkevich and Dubinin-Astakhov equations. *Langmuir* **1994,** *10* (11), 4244-4249.
150. Vernon-Parry, K., Scanning electron microscopy: an introduction. *III-Vs Review* **2000,** *13* (4), 40-44.
151. Whittig, L., X-ray diffraction techniques for mineral identification and mineralogical composition. *Methods of Soil Analysis. Part 1. Physical and Mineralogical Properties, Including Statistics of Measurement and Sampling* **1965,** (methodsofsoilana), 671-698.
152. Ding, J.; Yan, W.; Xie, W.; Sun, S.; Bao, J.; Gao, C., Highly efficient photocatalytic hydrogen evolution of graphene/YInO 3 nanocomposites under visible light irradiation. *Nanoscale* **2014,** *6* (4), 2299-2306.
153. Williams, D. B.; Carter, C. B., The transmission electron microscope. In *Transmission electron microscopy*, Springer: 1996; pp 3-17.
154. Pennycook, S. J.; David, B.; Williams, C. B., Transmission electron microscopy: a textbook for materials science. *Microscopy and Microanalysis* **2010,** *16* (1), 111.
155. Rueden, C. T.; Schindelin, J.; Hiner, M. C.; DeZonia, B. E.; Walter, A. E.; Arena, E. T.; Eliceiri, K. W., ImageJ2: ImageJ for the next generation of scientific image data. *BMC bioinformatics* **2017,** *18* (1), 529.
156. Midgley, P.; Weyland, M., 3D electron microscopy in the physical sciences: the development of Z-contrast and EFTEM tomography. *Ultramicroscopy* **2003,** *96* (3-4), 413-431.
157. Kübel, C.; Voigt, A.; Schoenmakers, R.; Otten, M.; Su, D.; Lee, T.-C.; Carlsson, A.; Bradley, J., Recent advances in electron tomography: TEM and HAADF-STEM tomography for materials science and semiconductor applications. *Microscopy and Microanalysis* **2005,** *11* (5), 378-400.
158. Van Grieken, R.; Markowicz, A., *Handbook of X-ray Spectrometry*. CRC press: 2001.

159. O'Connor, T., Synthesis of boron nitride. *Journal of the American Chemical Society* **1962,** *84* (9), 1753-1754.
160. Thomas, J.; Weston, N.; O'connor, T., Turbostratic1 Boron Nitride, Thermal Transformation to Ordered-layer-lattice Boron Nitride. *Journal of the American Chemical Society* **1962,** *84* (24), 4619-4622.
161. Hagia, T.; Kobayashi, K.; Sato, T., Formation of Hexagonal BN by Thermal Decomposition of Melamine Diborate. *Journal of the Ceramic Society of Japan* **1994,** *102* (11), 1051-1054.
162. Gao, R.; Yin, L.; Wang, C.; Qi, Y.; Lun, N.; Zhang, L.; Liu, Y.-X.; Kang, L.; Wang, X., High-yield synthesis of boron nitride nanosheets with strong ultraviolet cathodoluminescence emission. *The Journal of Physical Chemistry C* **2009,** *113* (34), 15160-15165.
163. Wu, P.; Zhu, W.; Chao, Y.; Zhang, J.; Zhang, P.; Zhu, H.; Li, C.; Chen, Z.; Li, H.; Dai, S., A template-free solvent-mediated synthesis of high surface area boron nitride nanosheets for aerobic oxidative desulfurization. *Chemical Communications* **2016**.
164. Geick, R.; Perry, C.; Rupprecht, G., Normal modes in hexagonal boron nitride. *Physical Review* **1966,** *146* (2), 543.
165. Wang, D.; Hui, S.; Liu, C., Mass loss and evolved gas analysis in thermal decomposition of solid urea. *Fuel* **2017,** *207*, 268-273.
166. Kurakevych, O. O.; Solozhenko, V. L., Rhombohedral boron subnitride, B13N2, by X-ray powder diffraction. *Acta Crystallographica Section C: Crystal Structure Communications* **2007,** *63* (9), i80-i82.
167. Cholet, V.; Vandenbulcke, L.; Rouan, J.; Baillif, P.; Erre, R., Characterization of boron nitride films deposited from BCl3-NH3-H2 mixtures in chemical vapour infiltration conditions. *Journal of materials science* **1994,** *29* (6), 1417-1435.
168. Ciofani, G.; Genchi, G. G.; Liakos, I.; Athanassiou, A.; Dinucci, D.; Chiellini, F.; Mattoli, V., A simple approach to covalent functionalization of boron nitride nanotubes. *Journal of colloid and interface science* **2012,** *374* (1), 308-314.
169. Nazarov, A. S.; Demin, V. N.; Grayfer, E. D.; Bulavchenko, A. I.; Arymbaeva, A. T.; Shin, H. J.; Choi, J. Y.; Fedorov, V. E., Functionalization and Dispersion of Hexagonal Boron Nitride (h-BN) Nanosheets Treated with Inorganic Reagents. *Chemistry–An Asian Journal* **2012,** *7* (3), 554-560.
170. Park, K.; Lee, D.; Kim, K.; Moon, D., Observation of a hexagonal BN surface layer on the cubic BN film grown by dual ion beam sputter deposition. *Applied physics letters* **1997,** *70* (3), 315-317.
171. Riviere, J.; Pacaud, Y.; Cahoreau, M., Spectroscopic studies of BN films deposited by dynamic ion mixing. *Thin Solid Films* **1993,** *227* (1), 44-53.
172. Gouin, X.; Grange, P.; Bois, L.; L'Haridon, P.; Laurent, Y., Characterization of the nitridation process of boric acid. *Journal of alloys and compounds* **1995,** *224* (1), 22-28.
173. Worsham, J.; Levy, H.; Peterson, S., The positions of hydrogen atoms in urea by neutron diffraction. *Acta Crystallographica* **1957,** *10* (4), 319-323.
174. Shuvalov, R. R.; Burns, P. C., A new polytype of orthoboric acid, H3BO3-3T. *Acta Crystallographica Section C: Crystal Structure Communications* **2003,** *59* (6), i47-i49.
175. Schaber, P. M.; Colson, J.; Higgins, S.; Thielen, D.; Anspach, B.; Brauer, J., Thermal decomposition (pyrolysis) of urea in an open reaction vessel. *Thermochimica acta* **2004,** *424* (1-2), 131-142.
176. Sevim, F.; Demir, F.; Bilen, M.; Okur, H., Kinetic analysis of thermal decomposition of boric acid from thermogravimetric data. *Korean Journal of Chemical Engineering* **2006,** *23* (5), 736-740.

177. Highfield, J.; Lim, H.; Fagerlund, J.; Zevenhoven, R., Mechanochemical processing of serpentine with ammonium salts under ambient conditions for CO 2 mineralization. *Rsc Advances* **2012,** *2* (16), 6542-6548.
178. Bai, H.; Yeh, A. C., Removal of CO2 greenhouse gas by ammonia scrubbing. *Industrial & Engineering Chemistry Research* **1997,** *36* (6), 2490-2493.
179. Fauzi, F.; Suzue, M.; Tani, M., Process for producing boron nitride. Google Patents: 2001.
180. Roy, A.; Choudhury, A.; Rao, C. N. R., Supramolecular hydrogen-bonded structure of a 1: 2 adduct of melamine with boric acid. *Journal of molecular structure* **2002,** *613* (1), 61-66.
181. Marchesini, S.; McGilvery, C. M.; Bailey, J.; Petit, C., Template-Free Synthesis of Highly Porous Boron Nitride: Insights into Pore Network Design and Impact on Gas Sorption. *ACS nano* **2017,** *11* (10), 10003-10011.
182. Parlett, C. M.; Wilson, K.; Lee, A. F., Hierarchical porous materials: catalytic applications. *Chemical Society Reviews* **2013,** *42* (9), 3876-3893.
183. Weng, Q.; Wang, B.; Wang, X.; Hanagata, N.; Li, X.; Liu, D.; Wang, X.; Jiang, X.; Bando, Y.; Golberg, D., Highly water-soluble, porous, and biocompatible boron nitrides for anticancer drug delivery. *ACS nano* **2014,** *8* (6), 6123-6130.
184. Adebajo, M. O.; Frost, R. L.; Kloprogge, J. T.; Carmody, O.; Kokot, S., Porous materials for oil spill cleanup: a review of synthesis and absorbing properties. *Journal of Porous materials* **2003,** *10* (3), 159-170.
185. Li, J.; Xiao, X.; Xu, X.; Lin, J.; Huang, Y.; Xue, Y.; Jin, P.; Zou, J.; Tang, C., Activated boron nitride as an effective adsorbent for metal ions and organic pollutants. *Scientific reports* **2013,** *3*, 3208.
186. Grant, J.; Carrero, C.; Goeltl, F.; Venegas, J.; Mueller, P.; Burt, S.; Specht, S.; McDermott, W.; Chieregato, A.; Hermans, I., Selective oxidative dehydrogenation of propane to propene using boron nitride catalysts. *Science* **2016,** *354* (6319), 1570-1573.
187. Venegas, J. M.; Grant, J. T.; McDermott, W. P.; Burt, S. P.; Micka, J.; Carrero, C. A.; Hermans, I., Selective Oxidation of n-Butane and Isobutane Catalyzed by Boron Nitride. *ChemCatChem* **2017**.
188. Economy, J.; Anderson, R. In *Boron nitride fibers*, Journal of Polymer Science: Polymer Symposia, Wiley Online Library: 1967; pp 283-297.
189. Eichler, J.; Lesniak, C., Boron nitride (BN) and BN composites for high-temperature applications. *Journal of the European Ceramic Society* **2008,** *28* (5), 1105-1109.
190. Chen, Y.; Zou, J.; Campbell, S. J.; Le Caer, G., Boron nitride nanotubes: pronounced resistance to oxidation. *Applied physics letters* **2004,** *84* (13), 2430-2432.
191. Lipp, A.; Schwetz, K. A.; Hunold, K., Hexagonal boron nitride: fabrication, properties and applications. *Journal of the European Ceramic Society* **1989,** *5* (1), 3-9.
192. Lavrenko, V.; Alexeev, A., High-temperature oxidation of boron nitride. *Ceramics international* **1986,** *12* (1), 25-31.
193. Cao, F.; Liu, K.; Fang, Z.; Wang, S., Hydrolysis mechanism of borazine-derived boron nitride pyrolysized below 1200 C. *Journal of Materials Science & Technology* **2012,** *28* (10), 956-960.
194. Weng, Q.; Kvashnin, D. G.; Wang, X.; Cretu, O.; Yang, Y.; Zhou, M.; Zhang, C.; Tang, D. M.; Sorokin, P. B.; Bando, Y., Tuning of the optical, electronic, and magnetic properties of boron nitride nanosheets with oxygen doping and functionalization. *Advanced materials* **2017,** *29* (28).
195. Joyner, D. J.; Hercules, D. M., Chemical bonding and electronic structure of B2O3, H3BO3, and BN: An ESCA, Auger, SIMS, and SXS study. *The Journal of Chemical Physics* **1980,** *72* (2), 1095-1108.

196. Kasten, L.; Grant, J.; Grebasch, N.; Voevodin, N.; Arnold, F.; Donley, M., An XPS study of cerium dopants in sol–gel coatings for aluminum 2024-T3. *Surface and Coatings Technology* **2001,** *140* (1), 11-15.
197. Baraton, M.; Merle, T.; Quintard, P.; Lorenzelli, V., Surface activity of a boron nitride powder: a vibrational study. *Langmuir* **1993,** *9* (6), 1486-1491.
198. Misaelides, P., Application of natural zeolites in environmental remediation: A short review. *Microporous and Mesoporous Materials* **2011,** *144* (1-3), 15-18.
199. Dias, J. M.; Alvim-Ferraz, M. C.; Almeida, M. F.; Rivera-Utrilla, J.; Sánchez-Polo, M., Waste materials for activated carbon preparation and its use in aqueous-phase treatment: a review. *Journal of environmental management* **2007,** *85* (4), 833-846.
200. Cote, A. P.; Benin, A. I.; Ockwig, N. W.; O'keeffe, M.; Matzger, A. J.; Yaghi, O. M., Porous, crystalline, covalent organic frameworks. *science* **2005,** *310* (5751), 1166-1170.
201. Portehault, D.; Giordano, C.; Gervais, C.; Senkovska, I.; Kaskel, S.; Sanchez, C.; Antonietti, M., High-surface-area nanoporous boron carbon nitrides for hydrogen storage. *Advanced Functional Materials* **2010,** *20* (11), 1827-1833.
202. Umpleby, R. J.; Baxter, S. C.; Chen, Y.; Shah, R. N.; Shimizu, K. D., Characterization of molecularly imprinted polymers with the Langmuir− Freundlich isotherm. *Analytical chemistry* **2001,** *73* (19), 4584-4591.
203. Chaires, J. B., Possible origin of differences between van't Hoff and calorimetric enthalpy estimates. *Biophysical chemistry* **1997,** *64* (1-3), 15-23.
204. Aijaz, A.; Fujiwara, N.; Xu, Q., From metal–organic framework to nitrogen-decorated nanoporous carbons: high CO2 uptake and efficient catalytic oxygen reduction. *Journal of the American Chemical Society* **2014,** *136* (19), 6790-6793.
205. Li, J.-R.; Kuppler, R. J.; Zhou, H.-C., Selective gas adsorption and separation in metal–organic frameworks. *Chemical Society Reviews* **2009,** *38* (5), 1477-1504.
206. Millward, A. R.; Yaghi, O. M., Metal-organic frameworks with exceptionally high capacity for storage of carbon dioxide at room temperature. *Journal of the American Chemical Society* **2005,** *127* (51), 17998-17999.
207. Sun, Q.; Li, Z.; Searles, D. J.; Chen, Y.; Lu, G.; Du, A., Charge-controlled switchable CO2 capture on boron nitride nanomaterials. *Journal of the American Chemical Society* **2013,** *135* (22), 8246-8253.
208. Arce, A.; Earle, M. J.; Rodríguez, H.; Seddon, K. R., Separation of aromatic hydrocarbons from alkanes using the ionic liquid 1-ethyl-3-methylimidazolium bis {(trifluoromethyl) sulfonyl} amide. *Green Chemistry* **2007,** *9* (1), 70-74.
209. Lillo-Ródenas, M.; Cazorla-Amorós, D.; Linares-Solano, A., Behaviour of activated carbons with different pore size distributions and surface oxygen groups for benzene and toluene adsorption at low concentrations. *Carbon* **2005,** *43* (8), 1758-1767.
210. Xu, F.; Tang, Z.; Huang, S.; Chen, L.; Liang, Y.; Mai, W.; Zhong, H.; Fu, R.; Wu, D., Facile synthesis of ultrahigh-surface-area hollow carbon nanospheres for enhanced adsorption and energy storage. *Nature communications* **2015,** *6*, 7221.
211. Ge, J.; Zhao, H. Y.; Zhu, H. W.; Huang, J.; Shi, L. A.; Yu, S. H., Advanced sorbents for Oil-Spill cleanup: Recent advances and future perspectives. *Advanced materials* **2016,** *28* (47), 10459-10490.

Appendix 1

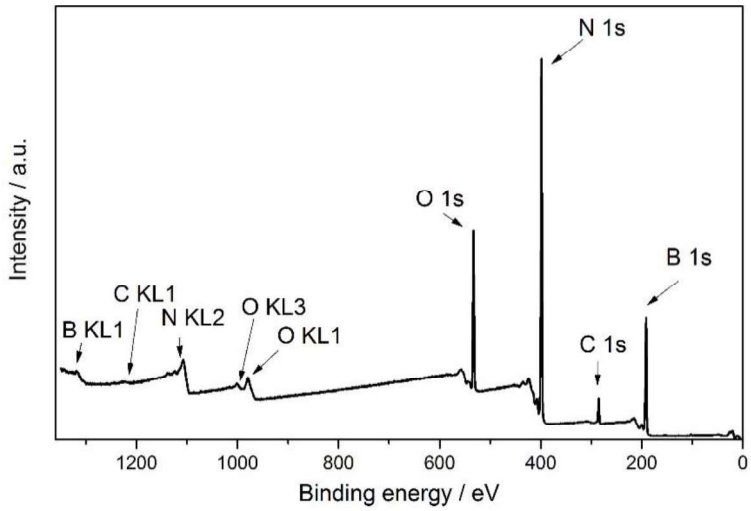


Figure A1.1 XPS survey spectrum for BN-U5-phys mix.

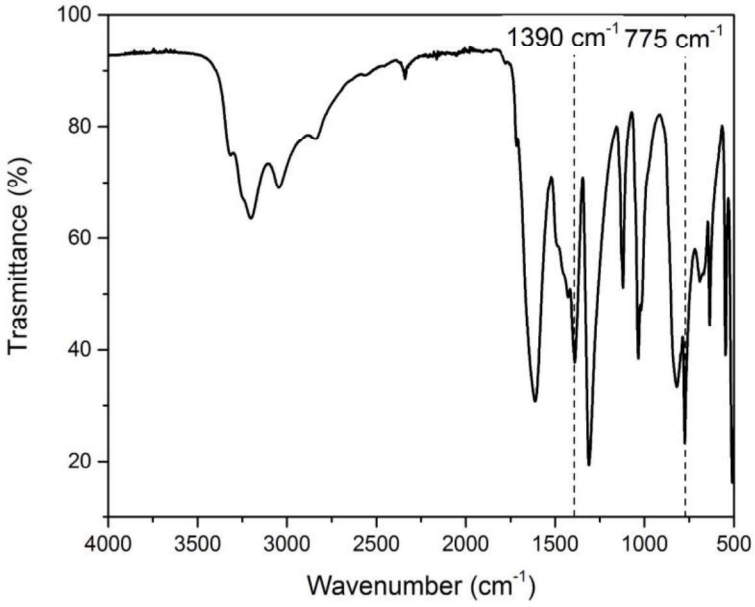


Figure A1.2 FTIR spectrum of INT-U5-0-250.

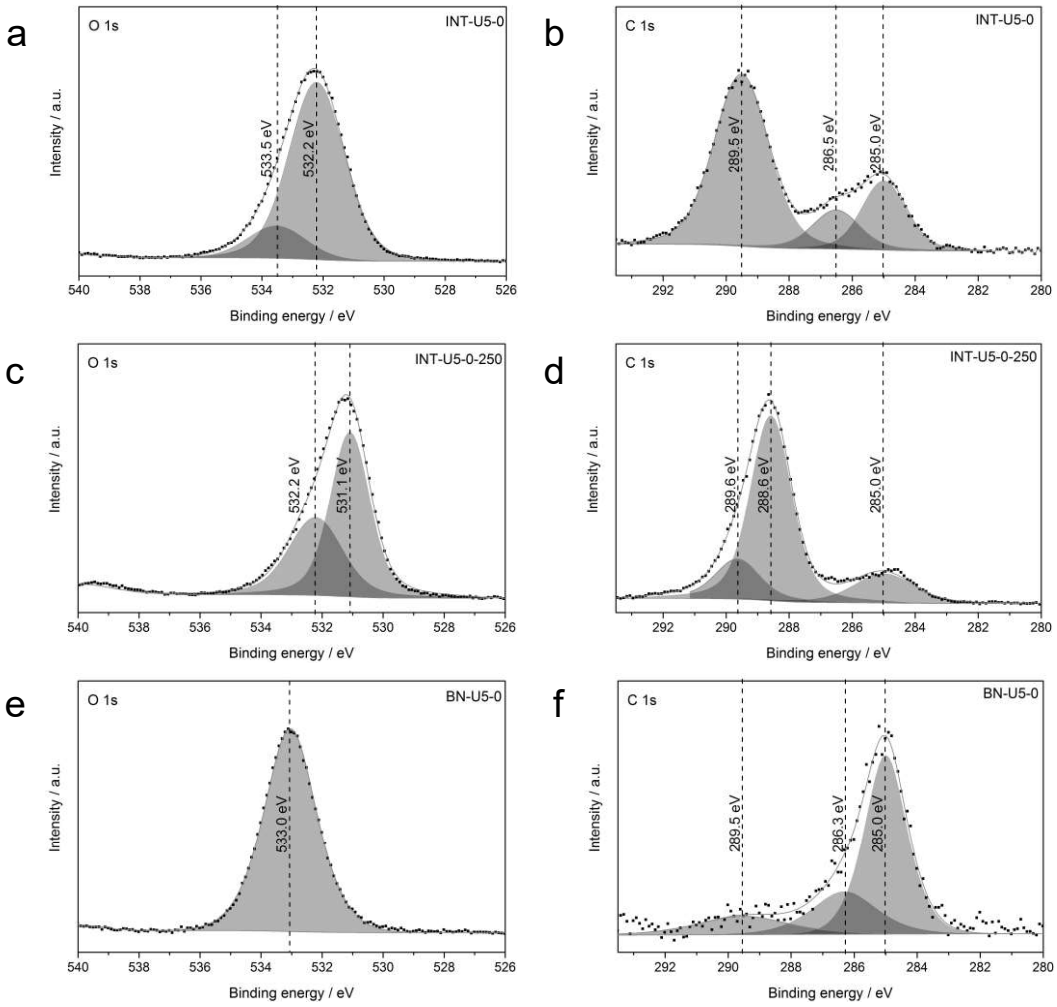


Figure A1.3 (a, b)XPS High-resolution core level spectra with peak fitting for O 1*s* and C 1*s* for intermediates deriving from urea and boric acid mixtures, (c, d) intermediates treated at 250 ℃ under nitrogen,(e, f) porous BN derived from the same intermediate treated at 1050 ℃ under nitrogen.

Study of the effect of ramp rate on porous BN: synthesis procedure

BN-MU1:5 was prepared *via* a multiple N-precursor method, whch will be described in detail in Chapter 5. Melamine:urea: boric acid in a 1:5:1 molar ratios were mixed and ground. The precursors where then heat-treated at 1050 °C under nitrogen gas flow 50 cc/min for 3.5 h and the temperature ramp rate was varied: 2.5, 5, 10, 15 °C/min.

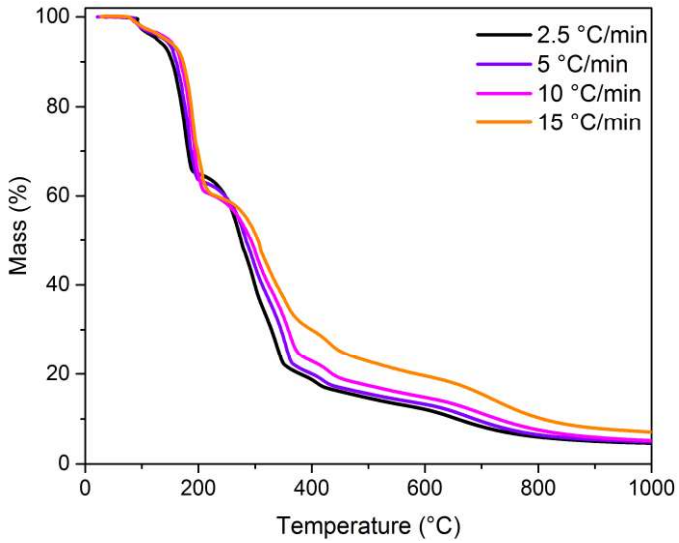


Figure A1.4 TGA curves with thermal decomposition of BN-MU1:5 precursors at different temperature ramp rates under nitrogen gas flow.

Appendix 2

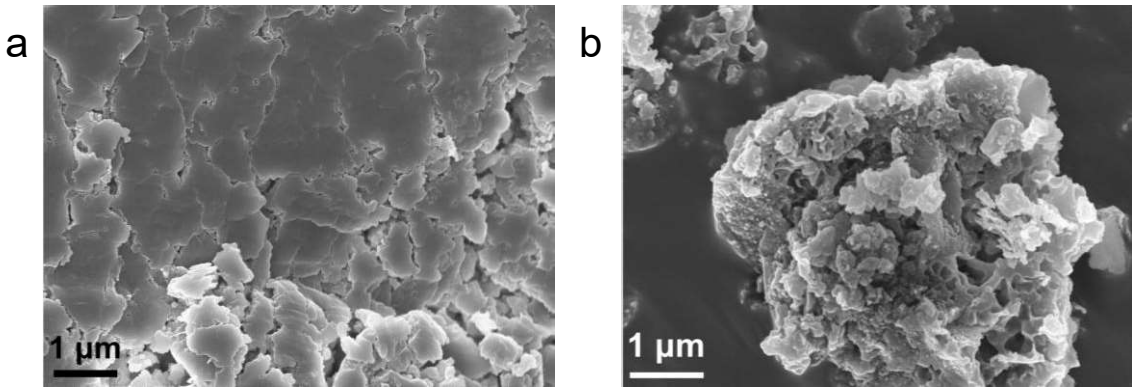


Figure A2.1 SEM images of (a) porous BN pellet (BN-MU1:5) and (b) porous BN (BN-MU1:5) powder.

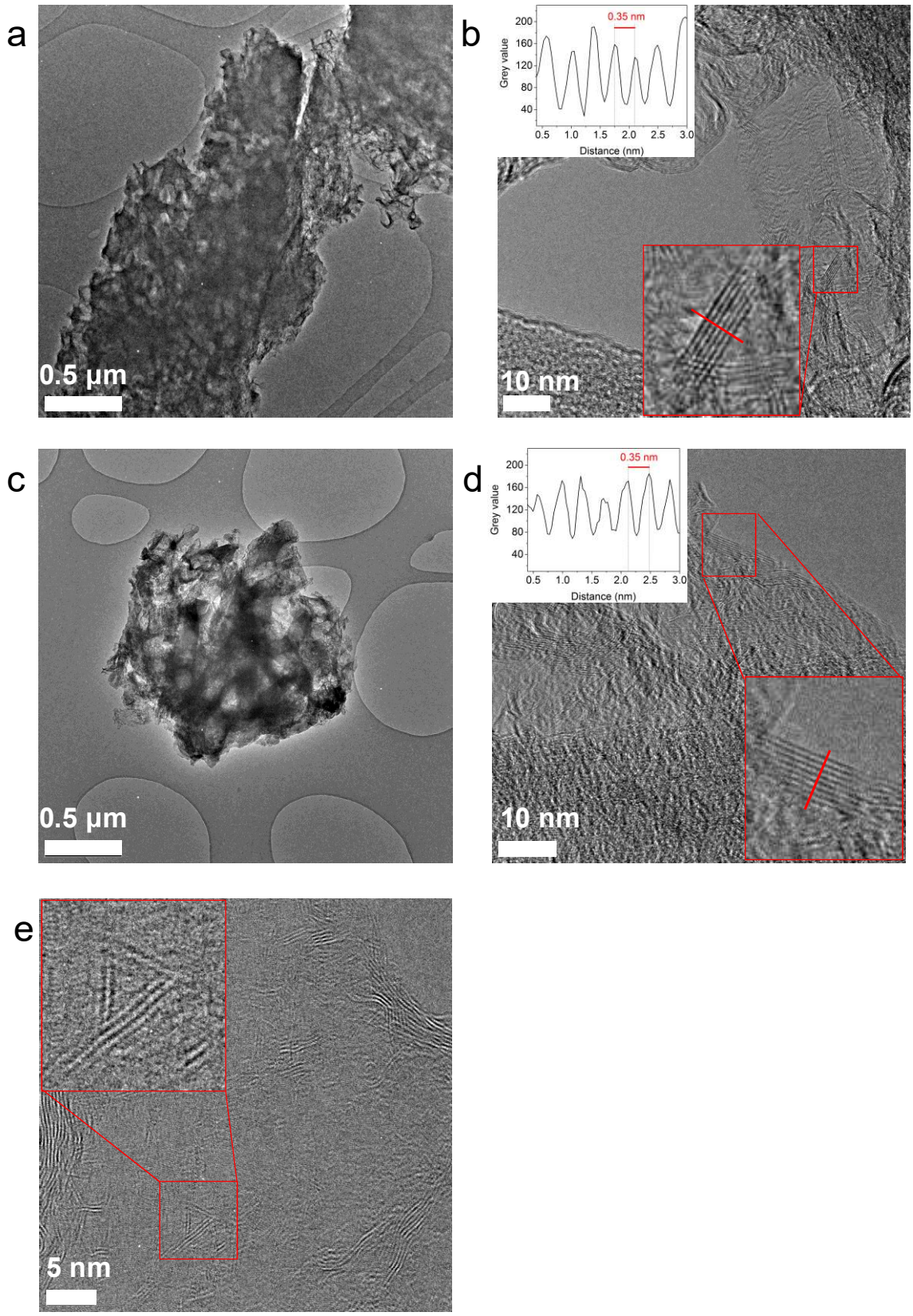


Figure A2.2 (a,b) TEM images for porous BN pellet after grinding it; (c-e) TEM images for porous BN powder. The inset in Figure e shows a typical triangular vacancy for h-BN.

Appendix 3

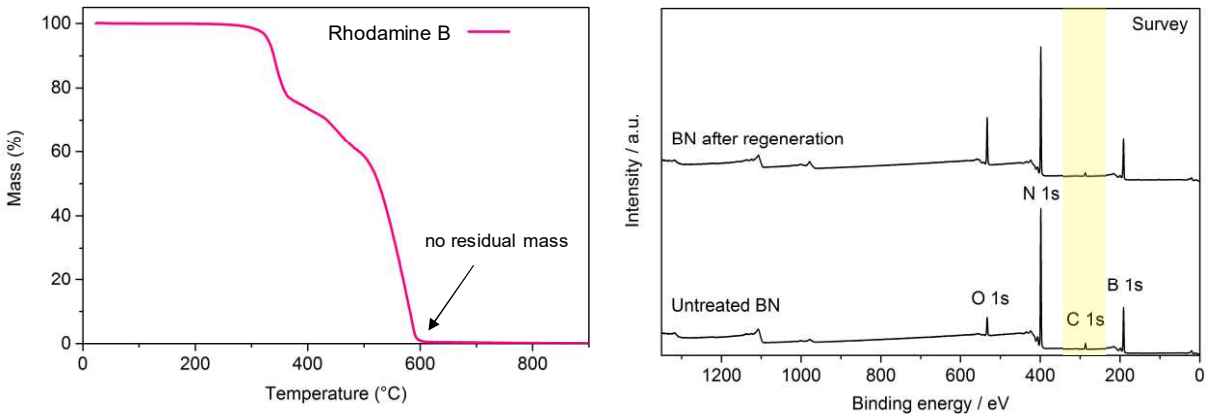


Figure A3.1 (a) TGA thermal decomposition pattern for Rhodamine B in air up to 900 °C (10 °C/min); (b) XPS survey spectrum for a typical porous BN sample (BN-MU1:5-1500 °C) before and after RhB exposure and regeneration at 600 °C in air.

Exposure to water via sonication and full evaporation

Methods

Low temperature porous BN (BN-U5, 500 mg) was dispersed in 50 mL of DI water and sonicated in an ultrasonic bath at 37 KHz in pulse mode for 7 hours. After 7 hours the water was fully evaporated at 65 °C on a hotplate and further dried in the oven overnight at the same temperature. The product obtained was then characterised with XPS analysis (Figure A3.2) to confirm the decomposition reaction.

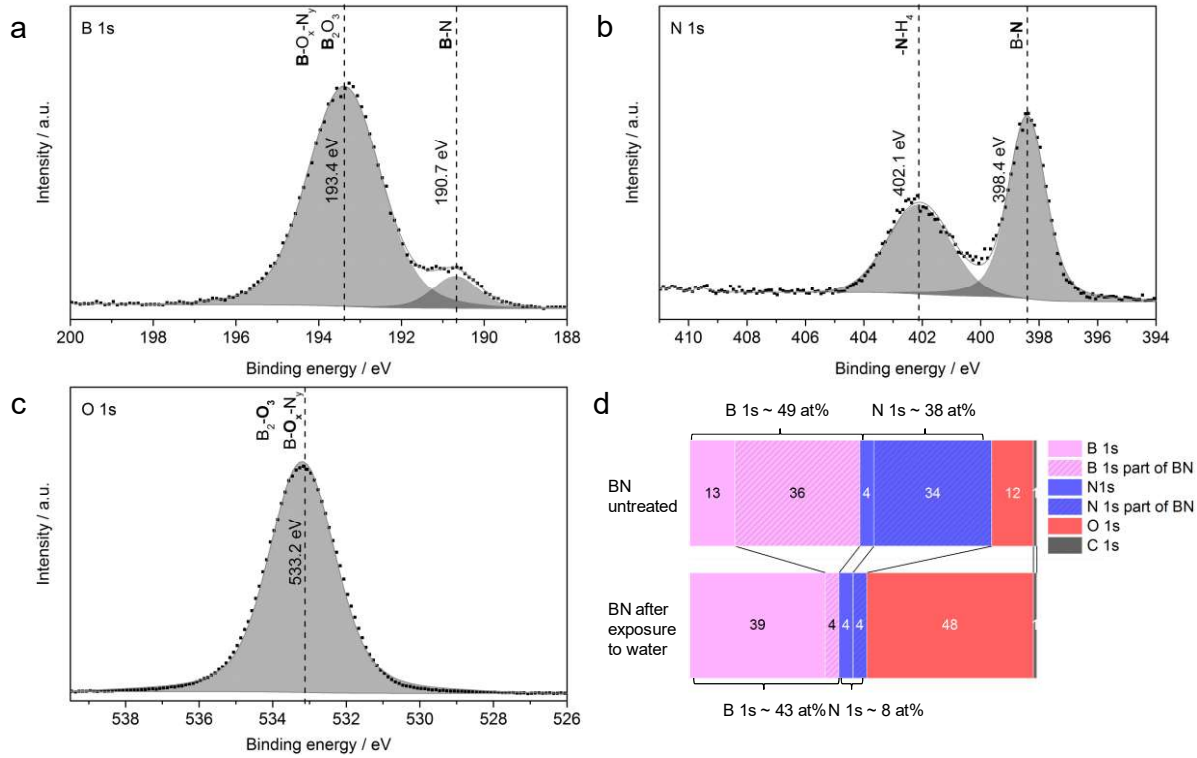


Figure A3.2 (a-c) XPS high resolution spectra for porous BN (BN-U5) after exposure to water *via* sonication and full evaporation, (d) relative atomic percentages deriving from XPS analysis.

Low temperature BN after humidity exposure

All low temperature BN samples were characterised with nitrogen sorption isotherms at -196 ºC (Figure A3.3) after exposure to water vapour. Similarly to what was observed after exposure to liquid water, the sample with higher micropore volume and surface area (BN-MU1:5) showed more significant decreases in nitrogen uptake at low pressure. The textural parameters for all samples are reported in Table A3.1 and show a decrease in BET surface areas and micropore volumes upon exposure to moisture. Although the degree of hydrolysis is much smaller when samples are exposed to water vapour rather than aqueous solutions, BN still exhibits a degree of instability. It must be noted that the analysis time was about 50 h for all samples during water vapour sorption. Interestingly, the mesopore volume increased slightly after exposure to moisture. It is hypothesised that degradation of the fine structure of micropores leads to the formation of larger mesopores, resulting in increases in mesopore volume. The crystalline structure of the samples before and after exposure to moisture was analysed *via* XRD (Figure A3.4), which showed little/no changes. Finally, the chemistry of the samples was analysed after exposure to moisture using XPS analysis. Relative atomic percentages deriving from XPS are reported in Figure A3.5. Little/no chemical changes were

again detected, which is attributed to the low extent of decomposition of the samples, and their localisation inside the micropores.

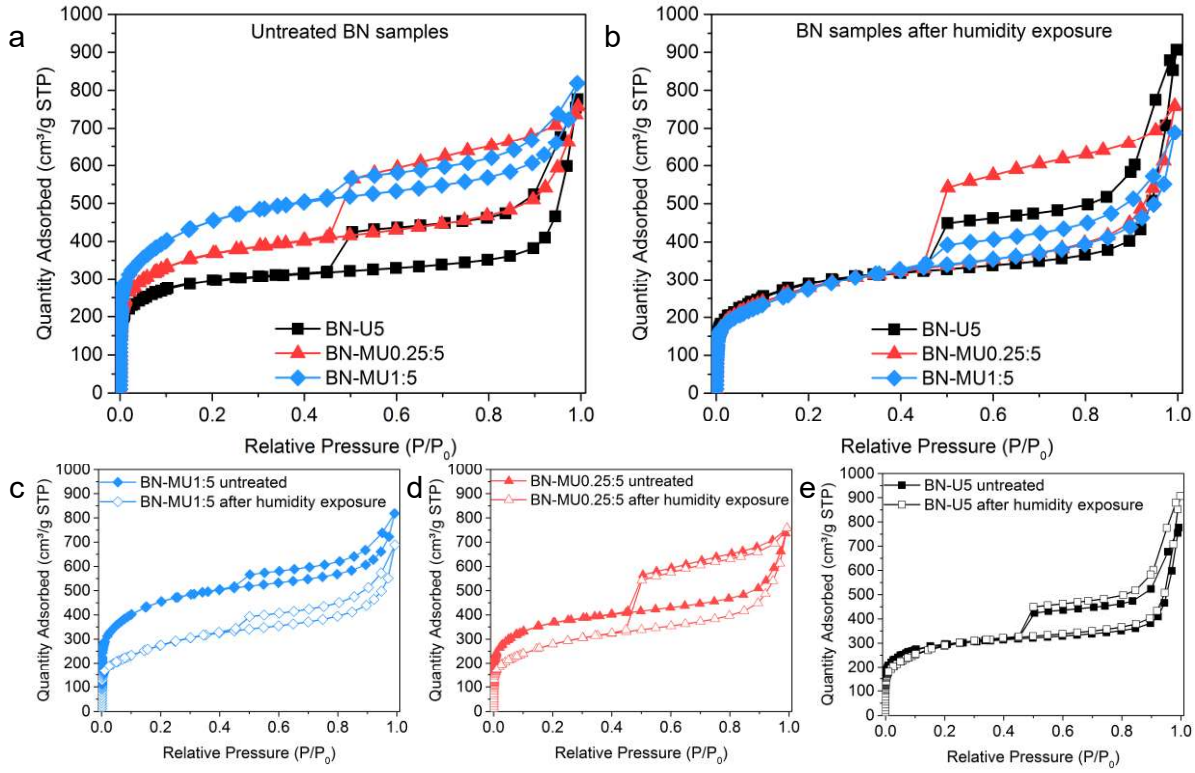


Figure A3.3 Nitrogen sorption isotherms at -196 °C for low-synthesis temperature BN: (a) untreated, (b) after exposure to water vapour and regeneration, (c-e) untreated and after humidity exposure.

Table A3.1 Textural parameters deriving from nitrogen sorption isotherms at -196 ºC for porous BN samples before and after exposure to water vapour at 30 ºC and regeneration at 250 °C (*).

Sample	S_{BET} (m^2/g)	V_{tot} (cm^3/g)	V_{micro}(cm^3/g)	V_{meso}(cm^3/g)	%mic
BN-U5	1092	0.927	0.444	0.483	48
BN-MU0.25:5	1339	1.026	0.545	0.481	53
BN-MU1:5	1650	1.120	0.660	0.460	59
BN-U5 *	1048	1.096	0.404	0.692	37
BN-MU0.25:5 *	1006	0.948	0.395	0.553	42
BN-MU1:5 *	988	0.854	0.383	0.471	45

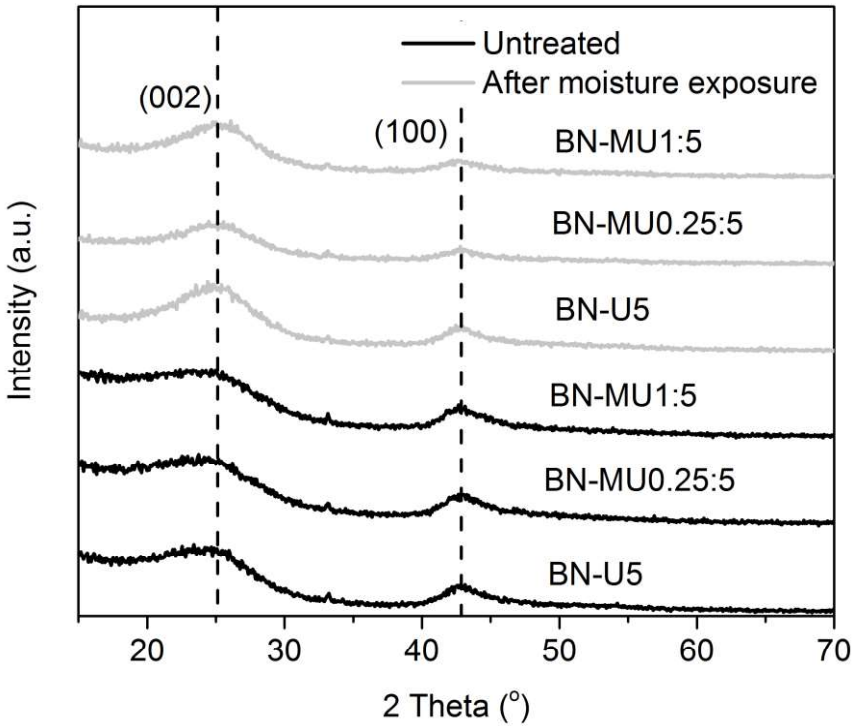


Figure A3.4 Crystalline structure of porous BN before and after exposure to moisture. XRD patterns for porous BN samples synthesised after exposure to water vapour at 30 ºC and regeneration at 250 ºC.

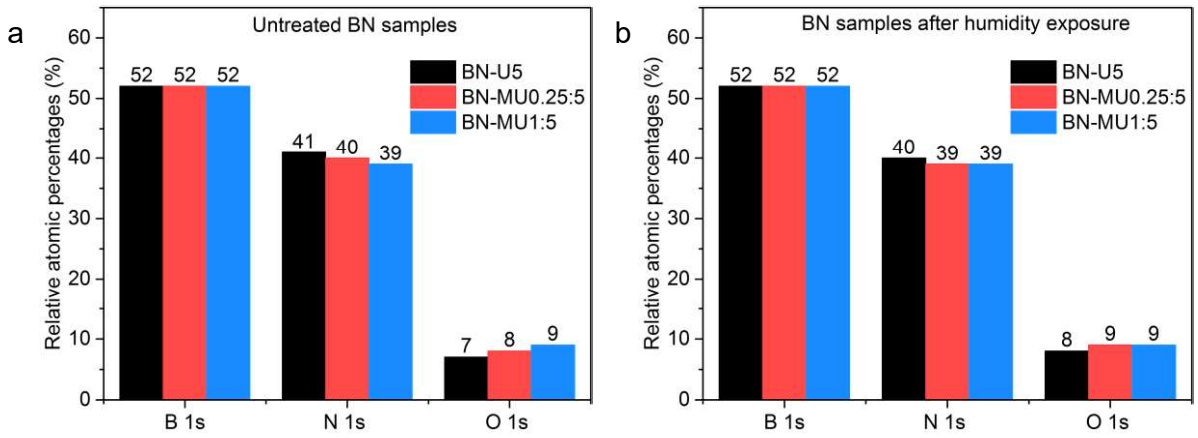


Figure A3.5 XPS relative atomic percentages for B 1*s*, N 1*s* and O 1*s* for 3 low-synthesis temperature BN (a) untreated and (b) after exposure to humidity at 30 °C and regeneration.

High temperature BN

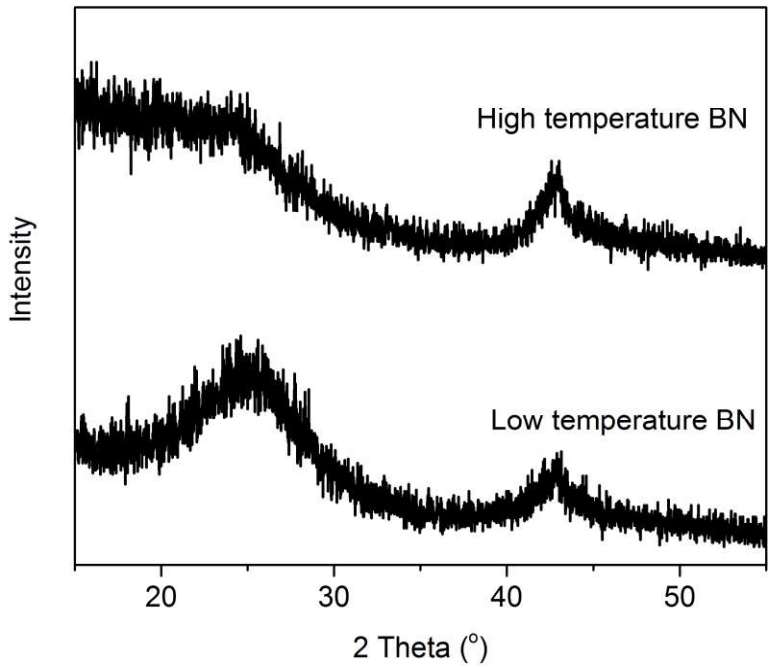


Figure A3.6 XRD patterns for two porous BN samples (BN-MU1:5) synthesised at low (1050 ºC) and high (1500 ºC) temperatures.

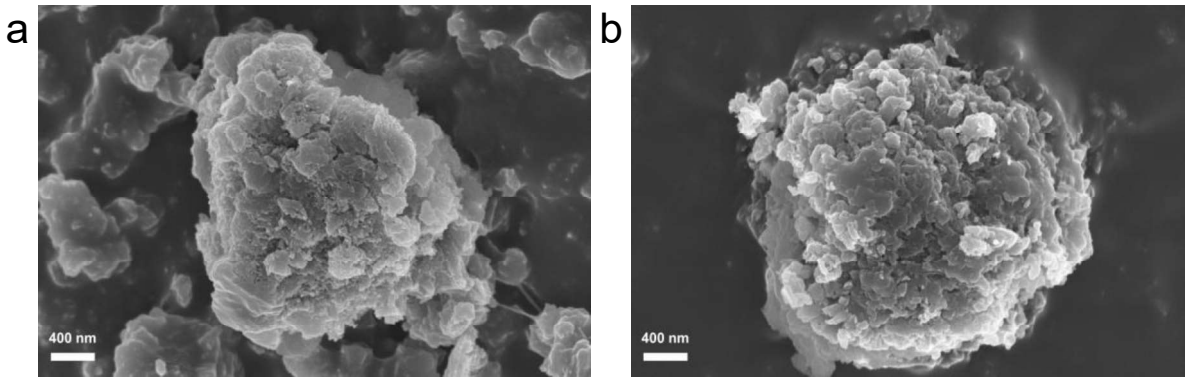


Figure A3.7 High resolution SEM images of porous BN BN-MU1:5 synthesised at low (1050 ºC) (a) and high temperatures (1500 ºC) (b). Scale bars represent 400 nm.

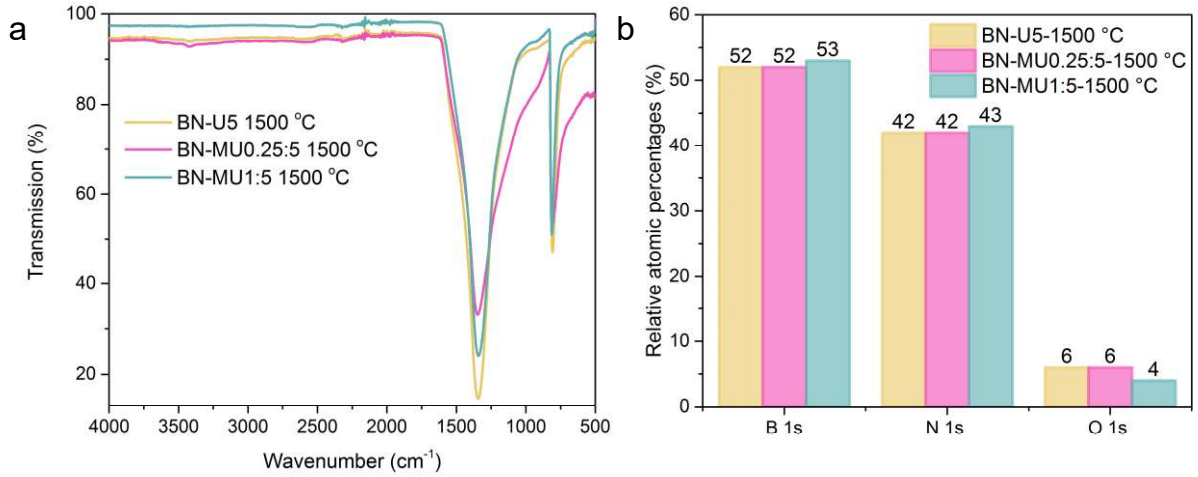


Figure A3.8 (a) FTIR spectra for all high temperature BN samples, (b) XPS relative atomic percentages for all high temperature BN samples.

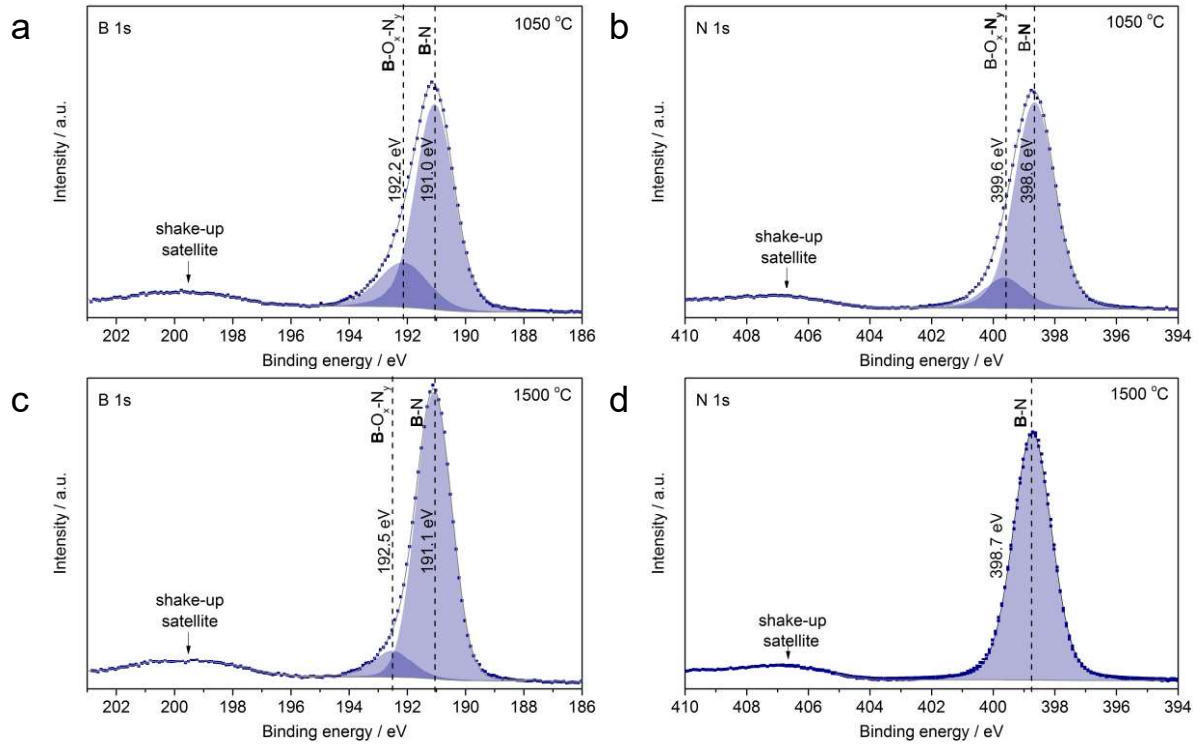


Figure A3.9 (a,b) XPS high resolution spectra for low temperature BN and (c,d) high temperature BN

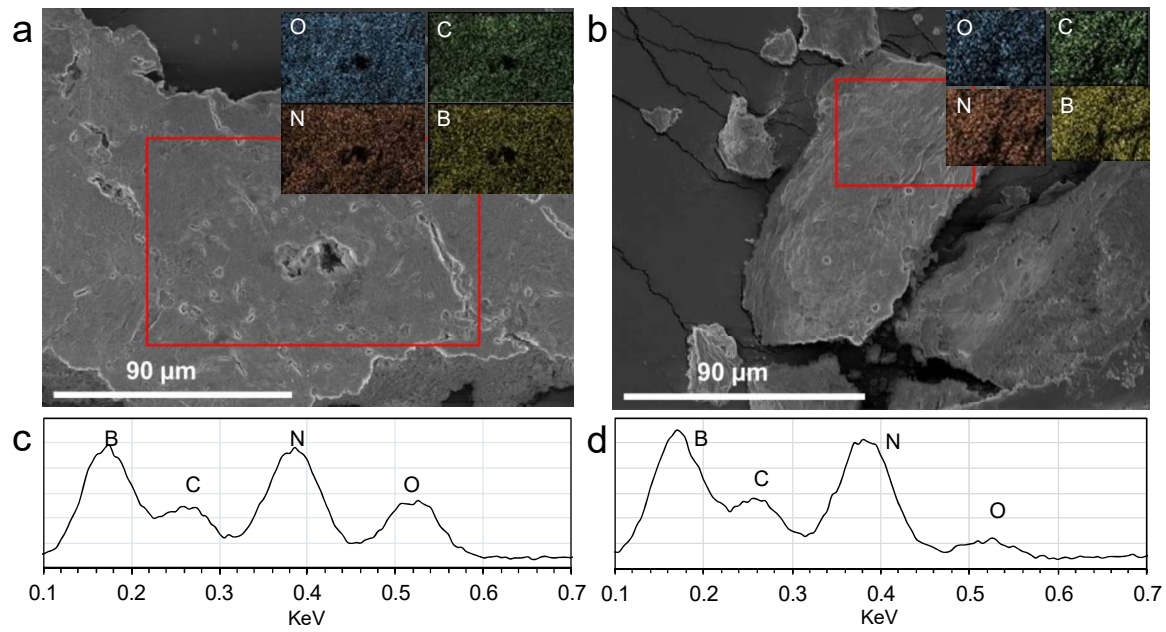


Figure A3.10 SEM-EDX images and spectra for porous BN-MU1:5 synthesised at (a,c) 1050 ºC and (b,d) at 1500 ºC.

High temperature BN after humidity exposure

Nitrogen sorption at -196 ºC were collected on high temperature BN samples after exposure to moisture to see if any structural changes occurred and XPS analysis to see if any chemical changes occurred (Figure A3.11). In general, despite the long analysis times >100 h, high temperature BN samples exhibited significantly improved stability to moisture, compared to low temperature BN, despite the analysis time for vapour sorption being longer. The sample exposed to water vapour for the longest amount of time (BN-U5-1500 ºC, >200 h) showed higher decrease in surface area and higher increase in oxygen content. This could be explained by a change in the samples chemistry, such as the formation of –OH groups with increasing moisture exposure time, gradually increasing the sample's hydrophilicity.

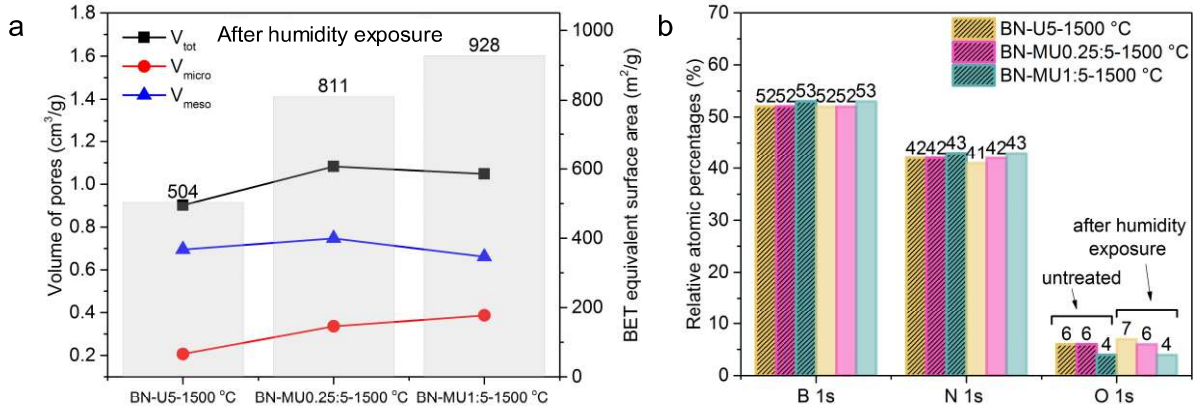


Figure A3.11 Textural parameters deriving from nitrogen sorption isotherms at -196 ºC for porous BN samples synthesised at high temperature (1500 ºC) after water vapour sorption and regeneration (a), XPS atomic percentages for the same samples before and after water vapour sorption and regeneration (dense patterns for samples regenerated).

High temperature BN after water exposure

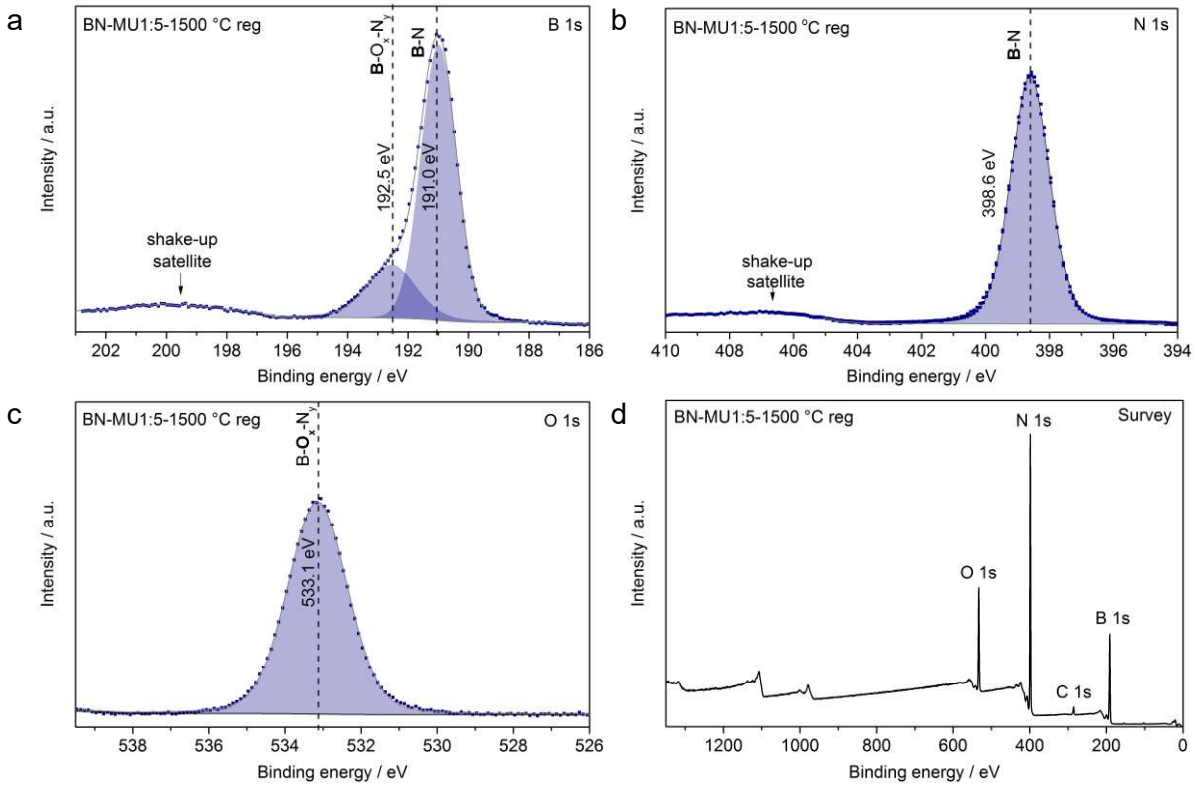


Figure A3.12 XPS core level peak fitted high resolution spectra and survey collected for BN-MU1:5-1500 ºC after RhB sorption and regeneration.

Appendix 4

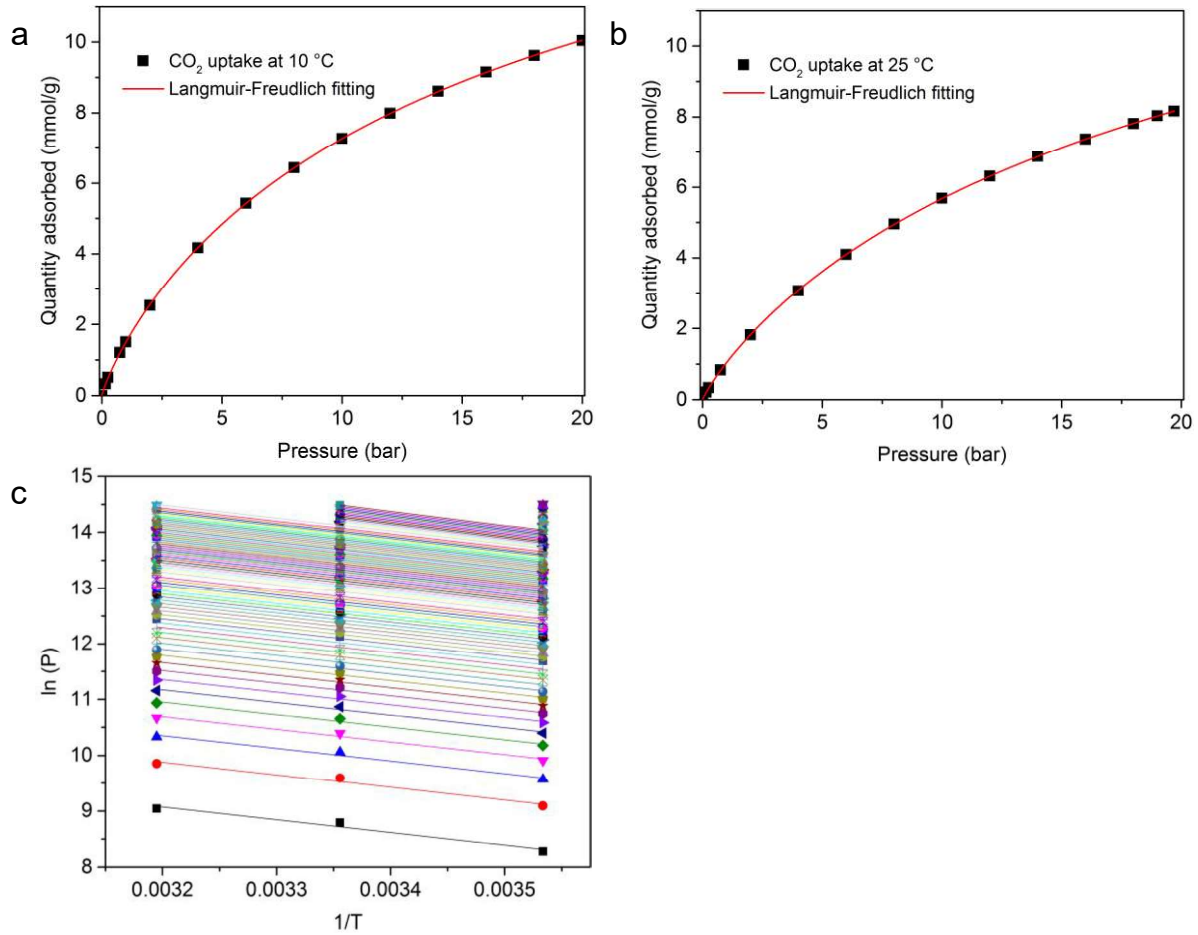


Figure A4.1 (a,b) CO_2 sorption isotherms with Langmuir-Freudlich fittings for 2 different temperatures;(c) plot of ln(P) *vs* 1/T for selected CO_2 loadings, fitted with linear fit and used to calculate heat of adsorption and entropy.

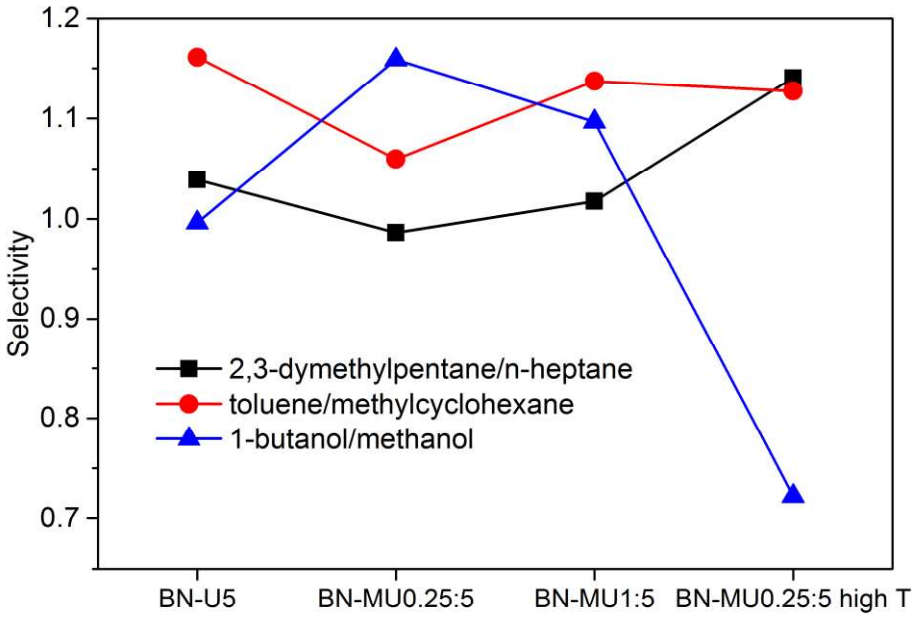


Figure A4.2 Selectivity values derived from the ratio of adsorption capacity for different solvents.

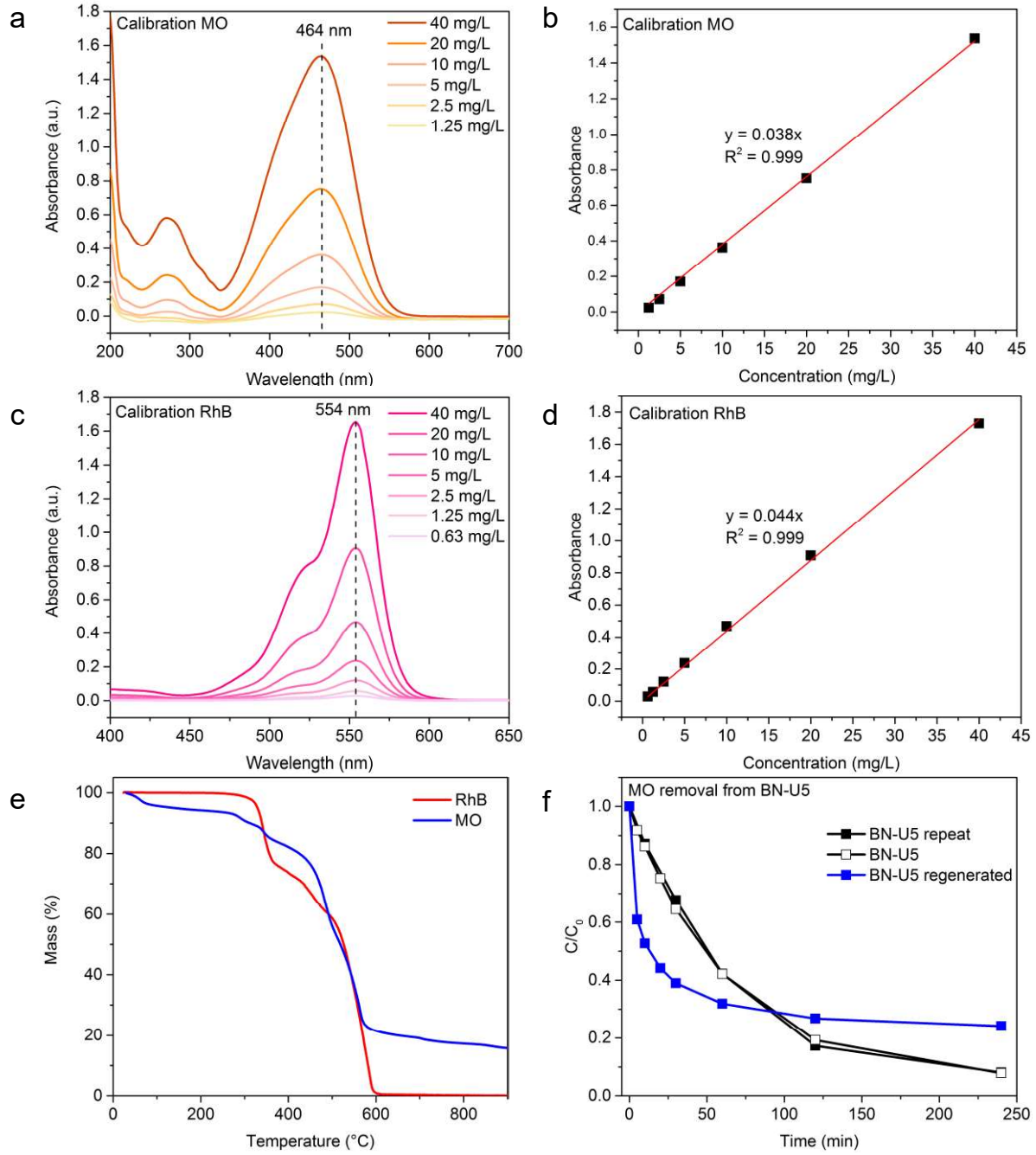


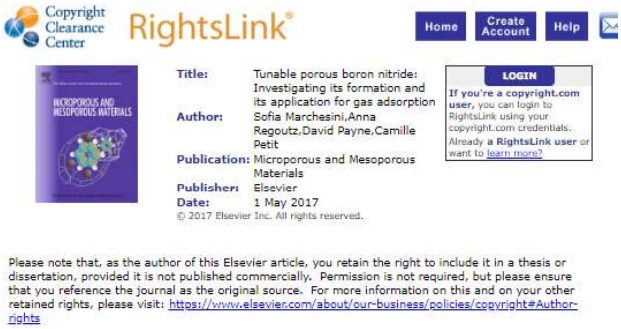
Figure A4.3 Calibration UV-Vis spectra and plots for Methyl Orange (MO) and Rhodamine B (RhB) (a-d), TGA analysis in air of RhB and MO, to show their decomposition profile in air (e); MO removal from BN-U5 with a repeat and regeneration (f).

Rights and Permissions

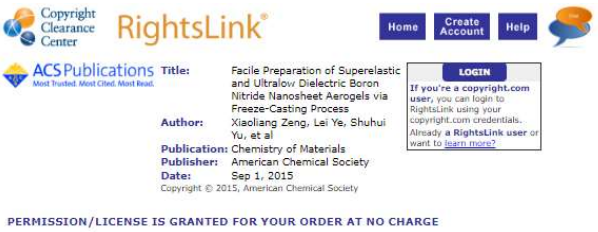
- Marchesini, S.; McGilvery, C. M.; Bailey, J.; Petit, C., Template-Free Synthesis of Highly Porous Boron Nitride: Insights into Pore Network Design and Impact on Gas Sorption. *ACS nano* **2017,** *11* (10), 10003-10011.



- Marchesini, S.; Regoutz, A.; Payne, D.; Petit, C., Tunable porous boron nitride: Investigating its formation and its application for gas adsorption. *Microporous and Mesoporous Materials* **2017,** *243*, 154-163.



- Zeng, X.; Ye, L.; Yu, S.; Sun, R.; Xu, J.; Wong, C.-P., Facile preparation of superelastic and ultralow dielectric boron nitride nanosheet aerogels via freeze-casting process. *Chemistry of Materials* **2015,** *27* (17), 5849-5855.



- Zhao, H.; Song, X.; Zeng, H., 3D white graphene foam scavengers: vesicant-assisted foaming boosts the gram-level yield and forms hierarchical pores for superstrong pollutant removal applications. *NPG Asia Materials* **2015,** *7* (3), e168.


3D white graphene foam scavengers: vesicant-assisted foaming boosts the gram-level yi

Rights and permissions

This work is licensed under a Creative Commons Attribution 4.0 International License. The images or other third party material in this article are included in the article's Creative Commons license, unless indicated otherwise in the credit line; if the material is not included under the Creative Commons license, users will need to obtain permission from the license holder to reproduce the material. To view a copy of this license, visit http://creativecommons.org/licenses/by/4.0/

- Ashton, T. S.; Moore, A. L., Foam-like hierarchical hexagonal boron nitride as a non-traditional thermal conductivity enhancer for polymer-based composite materials. International Journal of Heat and Mass Transfer 2017, 115, 273-281.


Copyright Clearance Center RightsLink

Home | Account Info | Help

Title: Foam-like hierarchical hexagonal boron nitride as a non-traditional thermal conductivity enhancer for polymer-based composite materials
Author: Taylor S. Ashton,Arden L. Moore
Publication: International Journal of Heat and Mass Transfer
Publisher: Elsevier
Date: December 2017
© 2017 Elsevier Ltd. All rights reserved.

Logged in as: Sofia Marchesini
Account #: 3001339057
LOGOUT

Order Completed

Thank you for your order.

This Agreement between Miss. Sofia Marchesini ("You") and Elsevier ("Elsevier") consists of your license details and the terms and conditions provided by Elsevier and Copyright Clearance Center.

- Zhu, W.; Gao, X.; Li, Q.; Li, H.; Chao, Y.; Li, M.; Mahurin, S. M.; Li, H.; Zhu, H.; Dai, S., Controlled Gas Exfoliation of Boron Nitride into Few-Layered Nanosheets. *Angewandte Chemie International Edition* **2016,** *55* (36), 10766-10770.


Copyright Clearance Center RightsLink

Home | Account Info | Help

Title: Controlled Gas Exfoliation of Boron Nitride into Few-Layered Nanosheets
Author: Wenshuai Zhu, Xiang Gao, Qian Li, et al
Publication: Angewandte Chemie International Edition
Publisher: John Wiley and Sons
Date: Jul 22, 2016
Copyright © 2016, John Wiley and Sons

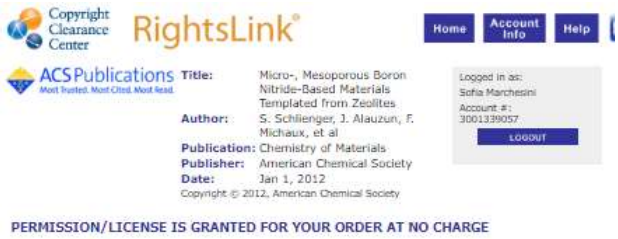
Logged in as: Sofia Marchesini
Account #: 3001339057
LOGOUT

Order Completed

Thank you for your order.

This Agreement between Miss. Sofia Marchesini ("You") and John Wiley and Sons ("John Wiley and Sons") consists of your license details and the terms and conditions provided by John Wiley and Sons and Copyright Clearance Center.

- Schlienger, S.; Alauzun, J.; Michaux, F.; Vidal, L.; Parmentier, J.; Gervais, C.; Babonneau, F.; Bernard, S.; Miele, P.; Parra, J., Micro-, mesoporous boron nitride-based materials templated from zeolites. *Chemistry of Materials* **2011,** *24* (1), 88-96.


Copyright Clearance Center RightsLink

Home | Account Info | Help

ACS Publications Most Trusted. Most Cited. Most Read.

Title: Micro-, Mesoporous Boron Nitride-Based Materials Templated from Zeolites
Author: S. Schlienger, J. Alauzun, F. Michaux, et al
Publication: Chemistry of Materials
Publisher: American Chemical Society
Date: Jan 1, 2012
Copyright © 2012, American Chemical Society

Logged in as: Sofia Marchesini
Account #: 3001339057
LOGOUT

PERMISSION/LICENSE IS GRANTED FOR YOUR ORDER AT NO CHARGE